The μ-calpain-ezrin axis: a potential target for therapy in inflammatory disease

by

Rhiannon Emma Roberts

A thesis submitted for the degree

DOCTOR OF PHILOSOPHY

Institute of Molecular and Experimental Medicine

Wales Heart Research Institute

Cardiff University School of Medicine

2017

To my parents, Cathy and Martin, for your constant love, support and encouragement

Acknowledgements

Firstly, my greatest thanks go to my supervisor Professor Maurice Hallett. I cannot express how much I have valued your support. Thank you for your continuous guidance and encouragement, for allowing me to go to Belgium, and for remaining the most outstanding supervisor, despite the changing times. Thanks also to Dr Sharon Dewitt and Mr Iraj Laffafian for your valued help and advice. My thanks also go to Professor Jan Parys and his lab at KU Leuven, with special thanks to Dr Tim Vervliet, for their warm welcome and advice (and for introducing me to ribs!).

A big thank you to my colleagues; Dr Katherine Connolly, thanks for your help (both in science and in baking!), and for being a true friend, you've made these last few weeks considerably more enjoyable; Mr Nicholas Burnley-Hall, thanks for your comradery when the going got tough, and also for your endless list of jokes (we laughed even though we groaned!); Mr Alberto Coccarelli, thanks for introducing me to proper Italian coffee, the long discussions about language, culture, politics and also how to write a thesis! Thanks also to Dr Justyna Witzcak and Miss Samantha Jennings. It's been a pleasure to share an office with you all.

Another massive thank you to my friends; Miss Shayda Maleki-Toyserkani – one of the last two standing! Thank you for listening to me ramble at the end of long days alone in the lab/office. Thank you for your moral support before (and during!) presentations, and for the celebrations afterwards! Thanks for always being there for me. I've been so lucky to have you as a housemate these past three years, I wish you all the best in your own doctoral studies, I'm so proud to call you my friend; Miss Bethany Burns and Miss Angharad Weatherall, who knew that attending that house hunting event would be one of the best things I ever did?! Thank you for all the laughs and for making Cardiff a 'home away from home'; Miss Katherine Marsay, thank you for being my voice of reason, and for your unwavering love and support. I have a new motto: "What would Kat do?" I wouldn't have taken this path had I not known you. Thank you for proving that distance doesn't affect true friendships; Miss Bryony Ackroyd and Miss Kerrie McNally, thanks for keeping me going when I couldn't see the light! You've been my role models and I'm so lucky we've been friends for the past 7 years. Thank you to Miss Katy Morrison, Miss Helena Nowak and Miss Rachel Pollitt for your friendship and for the much needed weekends away.
Finally, to Mr Pierre-Luc Escoubet, thanks for the adventures. Thank you all.

“In the fields of observation, chance favours only the prepared mind.”

Louis Pasteur

“When you are about to give up, you don’t know how far you are from success.”

Unknown via Iraj Laffafian

Summary

Neutrophils are the most abundant class of white blood cell in humans. They are among the first inflammatory cells to respond during infection or tissue damage, and their excessive recruitment to synovial joints in rheumatoid arthritis has been implicated in the progression of the disease. The process of neutrophil extravasation from blood vessels involves a rapid expansion of the available cell surface area. This ~200% increase is facilitated by the release of cell membrane microridges. As ezrin forms crucial cross-links between the plasma membrane and cortical F-actin, in neutrophils and other myeloid cells, it is thought to maintain the structure of these microridges, which act as a reservoir of plasma membrane for spreading. It has been suggested that elevating the cytosolic Ca^{2+} concentration, thereby activating the Ca^{2+}-activated cysteine protease μ-calpain, would break the ezrin link and permit cell spreading. This thesis has investigated the relationship between, μ-calpain, ezrin and Ca^{2+} concentration.

Through immunocytochemistry, confocal microscopy of live phagocytosis and chemotaxis experiments, observations in neutrophils have been complemented by investigations in a RAW 264.7 model cell line, amenable to transfection. By generating the novel genetically encoded Ca^{2+} indicator EPIC (Ezrin Peripheral Indicator of Ca^{2+}), it has been possible to experimentally measure the cytosolic Ca^{2+} concentration in ezrin-rich microdomains beneath plasma membrane microridges, in transfected myeloid cells, during Ca^{2+} influx. It has thus been found that sub-membranous cytosolic Ca^{2+} in these microridges reaches high-micromolar concentrations, well within the range required to activate μ-calpain and result in ezrin cleavage.

The work in this thesis contributes to the understanding of the molecular mechanisms which govern neutrophil morphological changes during events such as phagocytosis and extravasation. It is hoped that these findings will help contribute towards the body of research aimed at influencing the design of novel therapeutics to treat autoimmune conditions.

Publications

Roberts, R.E. and Hallett, M.B. (2016). Regulation of ezrin location in myeloid cells by threonine phosphorylation and elevation of cytosolic Ca^{2+}. Eur J Clin Invest, Volume: 46, Special Issue: SI, Supplement: 1, Meeting Abstract: 6.04, pp 69-69.

Roberts, R.E., Elumalai, G. and Hallett, M.B. Phagocytosis and motility in human neutrophils is competent but compromised by pharmacological inhibition of ezrin phosphorylation [in submission].

Roberts, R.E., Vervliet, T., Bultnyck, G., Parys, J.B. and Hallett, M.B. Locally elevated Ca^{2+} domains near plasma membrane microridges are revealed during phagocytosis by a novel ezrin-conjugated Ca^{2+} sensing probe [in preparation].

Prizes and competitions

Oct 2015 **Semi-finalist, Biotechnology Young Entrepreneurial Scheme (BiotechnologyYES),** University of Manchester, UK.

Dec 2015 **1st place prize for 3 minute oral presentation,** Cardiff School of Medicine 30th annual postgraduate research day, Cardiff University, UK.

Jan 2017 **1st place prize for 10 minute oral presentation,** Cardiff School of Medicine 31st annual postgraduate research day, Cardiff University, UK.

Awards

Apr 2016 **EFIS Young Investigator Travel Grant (450€) –** to present at ESCI 50th annual conference and Phagocyte Biology workshop, Institut Cochin, Paris, France.

May 2017 **EFIS Young Investigator Travel Grant (350€)** – to present at the ESCI 51st annual conference and Phagocyte Biology workshop, IRCCS San Martino Hospital – IST and University of Genoa, Genoa, Italy.

Conferences

May 2015 **Speaking of Science, Student-led conference,** Cardiff University, UK. (Oral presentation; Roberts, R.E. and Hallett, M.B.)

Dec 2015 **Cardiff School of Medicine 30th Annual postgraduate research day,** Cardiff University, UK. (Oral presentation; Roberts, R.E. and Hallett, M.B.)

Sept 2015 **Cardiff-KU Leuven Calcium Signalling Meeting,** Cardiff University, UK.

Apr 2016 **ESCI 50th annual conference and Phagocyte Biology workshop,** Institut Cochin, Paris, France. (Poster presentation; Roberts, R.E. and Hallett, M.B.)

Sept 2016 **SLB 49th annual conference and "Neutrophil 2016" meeting,** University of Verona Congress Centre, Verona, Italy. (Poster presentation; Roberts, R.E., Vervliet, T., Bultnyck, G., Parys, J.B. and Hallett, M.B.)

Jan 2017 **Cardiff School of Medicine 31st Annual postgraduate research day,** Cardiff University, UK. (Oral presentation; Roberts, R.E., Vervliet, T., Bultnyck, G., Parys, J.B. and Hallett, M.B.)

May 2017 **ESCI 51st annual conference and Phagocyte Biology workshop,** IRCCS San Martino Hospital – IST and University of Genoa, Genoa, Italy. (Poster presentation; Roberts, R. E., Vervliet, T., Bultnyck, G., Parys, J.B. and Hallett, M. B.)

Table of Contents

1. Chapter 1 - Introduction 4

1.1 The immune system 5

1.1.1 Innate immunity 5

1.1.2 Adaptive immunity 7

1.1.3 White blood cells 8

1.1.3.1 Phagocytes 10

1.2 Neutrophils 11

1.2.1 History of the neutrophil 11

1.2.1.1 Ilya Metchnikov (also written Elie Mechnikoff) (1845-1916) 12

1.2.1.2 Paul Ehrlich (1854-1915) 14

1.2.2 Lifecycle of a neutrophil 15

1.2.2.1 Myelopoiesis 16

1.3 Neutrophil morphology 19

1.3.1 Neutrophil granules 22

1.3.2 Neutrophil plasma membrane 24

1.4 Neutrophil behaviour 25

1.4.1 Response to inflammatory signals 27

1.4.2 Neutrophil Extravasation 29

1.4.3 Neutrophil phagocytosis 31

1.5 Neutrophils in disease 32

1.5.1 Rheumatoid arthritis 32

1.6 Ca^{2+} signalling 36

1.6.1 Ca^{2+} homeostasis in neutrophils 37

1.6.2 Ca^{2+} storage and distribution in human neutrophils 38

1.6.3 Ca^{2+} signalling in human neutrophils....41
1.6.3.1 G protein coupled receptors....42
1.6.3.2 Fc receptor and integrin mediated Ca^{2+} signalling....44
1.6.4 Ca^{2+} influx through plasma membrane channels....46
1.6.5 Measuring cytosolic Ca^{2+} levels....50
1.6.6 Ca^{2+}-regulated enzymes in neutrophils....51
1.7 μ-Calpain....52
1.7.1 Structure of μ-calpain....53
1.7.2 μ-calpain activation by Ca^{2+}....55
1.7.3 μ-calpain substrates....58
1.8 Ezrin....59
1.8.1 Structure and function of ezrin....59
1.8.2 Sensitivity to μ-calpain....64
1.9 Mechanisms of neutrophil spreading....66
1.9.1 A question of surface area....66
1.9.2 Plasma membrane microridges....68
1.9.3 Mechanisms of membrane expansion....71
1.10 Aims....72
2. Chapter 2 - General Methods....73
2. General methods....74
2.1 Preparation of Krebs and Krebs-BSA....74
2.2 Preparation of the balanced salt solution....74
2.3 Preparation of Dextran....74
2.4 Isolation of human neutrophils from peripheral blood....74
2.5 Isolation of normal human serum from whole blood....75
2.6 Immunocytochemistry....75

2.7 Protein extraction and preparation of cell lysates 76
2.8 Assessment of protein concentration.....76
2.9 Western blotting 76
2.10 Preparation of fMLP solution.....77
2.11 RAW cell culture, maintenance and storage 77
2.12 Plasmid amplification.....78
2.13 Preparation of Lysogeny broth 78
2.14 Preparation of agar plates 78
2.15 RAW 264.7 cell line transfection by nucleofection.....78
2.16 Opsonisation of zymosan particles 79
2.17 Confocal microscopy 79
2.18 Statistical analysis 80
33. Chapter 3 - Dynamic changes in subcellular ezrin location in myeloid cells .81
3.1 Introduction 82
3.1.1 Myeloid cell lines.....85
3.1.2 Aims and Objectives 86
3.2 Specific Materials and Methods 86
3.2.1 Immunocytochemistry 86
3.2.2 RAW 264.7 cell transfection 87
3.2.3 Confocal microscopy 87
3.2.4 Ezrin extraction from RAW 264.7 cells.....87
3.2.5 μ-calpain cleavage of ezrin constructs 88
3.3 Results 90
3.3.1 Native ezrin at the plasma membrane in neutrophils 90
3.3.2 Ezrin constructs at the plasma membrane of RAW 264.7 cells 90
3.3.3 Dynamic changes in ezrin during Ca^{2+} influx.....96

3.3.4 Dynamic changes in ezrin during myeloid phagocytosis.....98
3.3.5 Evaluation of ezrin GFPi as marker of ezrin cleavage 101
3.3.6 Ezrin cleavage during Ca^{2+} influx 102
3.3.7 Ezrin release during phagocytosis 106
3.4 Discussion.....111
3.4.1 Mechanisms of ezrin release.....113
3.4.2 Ca^{2+} hotspots in wrinkles and during phagocytosis 116
4. Chapter 4 - Generation of a novel genetically encoded Ca2+ indicator.....118
4.1 Introduction 119
4.1.2 CEPIA (calcium-measuring organelle-entrapped protein indicators) 120
4.2 Aims of this chapter 123
4.2.1 Cardiff-KU Leuven bilateral agreement.....123
4.3 Specific Materials and Methods 125
4.3.1 Generation of Ezrin-CEPIA conjugates for detection of localised calcium signalling.....125
4.3.1.1 Primer design.....125
4.3.1.2 PCR.....126
4.3.1.3 PCR clean-up.....128
4.3.1.4 Restriction and ligation of PCR products and pcDNA3.1(-) vector..128
4.3.1.5 Agarose gel electrophoresis 128
4.3.1.6 Transformation of DH5α cells.....132
4.3.1.7 Mini-preps.....132
4.3.1.8 Quantification of plasmid DNA.....133
4.3.2 Transfection of HeLa cells 133
4.4 Results.....133
4.4.1 Generation of EPIC2 and EPIC3 133

4.5 Discussion....134
5. Chapter 5 - Cytosolic microdomains of high Ca2+concnetration....145
5.1. Introduction....146
5.1.1 Microridge Ca^{2+} domains....147
5.1.2 Ezrin peripheral indicator of Ca^{2+} (EPIC)....150
5.1.3 Aims of this chapter....152
5.2 Specific Materials and Methods....153
5.2.1 Transfection of RAW 264.7 cells....153
5.2.2 Artificial elevation of Ca^{2+} concentration in RAW 264.7 cells....153
5.2.3 Physiological stimulation of RAW 264.7 cells (phagocytosis)....153
5.2.4 Measurement of dynamic changes in cytosolic Ca^{2+} as reported by novel EPIC3....154
5.2.4.1 Confocal microscopy....154
5.2.4.2 ImageJ EPIC3 image processing....154
A. EPIC3/ezrin-mCherry ratio....155
B. Dynamic mask using ezrin-mCherry and EPIC3 ratio....155
5.2.4.3 Calculating the Ca^{2+} concentration reported by EPIC3....156
A. The relationship between free Ca^{2+} + EPIC3 ↔ (Ca^{2+}EPIC3)....156
B. The relationship between EPIC3 fluorescence and f....156
C. The relationship between measured EPIC3 intensity and Ca^{2+} concentration....156
5.2.5 Calculating the cell footprint (2D area)....157
5.2.6 Calibrating the LUTs....157
5.3 Results....158
5.3.1 EPIC3 reports Ca^{2+} activity at the cell edge in myeloid cells....158
5.3.2 Dual expression ratio imaging of EPIC3 and ezrin-mCherry....164

5.3.3 Ca^{2+} responses during phagocytosis....172
5.4 Discussion....181
6.1 Introduction....187
6.1.1 Conformational states of ezrin....188
6.1.2 The ezrin inhibitor NSC668394....189
6.1.3 Aims of this chapter....189
6.2 Specific Materials and Methods....189
6.2.1 Immunocytochemistry....189
6.2.2 Plasmid amplification....190
6.2.3 RAW 264.7 cell transfection....190
6.2.4 Pre-treatment with NSC6683934 inhibitor of ezrin phosphorylation....190
6.2.5 Confocal microscopy....190
6.2.6 Protein extraction and preparation of cell lysates and Western blotting....191
6.2.7 Neutrophil Phagocytosis....191
6.2.8 Preparation of zymosan filled collagen beads....192
6.2.9 Neutrophil chemotaxis experiments....192
6.2.10 Imagestream....192
6.3 Results....193
6.3.1 Effect of NSC668394 on ezrin distribution at the plasma membrane in neutrophils....193
6.3.2 Effect of NSC668394 on ezrin cleavage....200
6.3.3 Effect of NSC668394 on neutrophil phagocytic ability....203
6.3.4 Effect of ezrin phosphorylation inhibition on neutrophil chemotactic ability....208
6.4 Discussion....212

7. General Discussion - General discussion: Synopsis, hypothesis and future work 217

7. General Discussion 218

7.1 Overall research strategy 219

7.2 Summary of progress made by this work 219

7.3 Hypothesis 222

7.4 Future work 223

7.4.1 Refined probe for *in vivo* ezrin cleavage 223

7.4.2 Refined probe for intra-microridge Ca^{2+} measurement and imaging 224

7.4.3 Interference of ezrin cleavage as a test of the hypothesis 225

7.5 Conclusions 226

8. References 227

Appendix I – Ezrin-GFPi sequencing results 247

Appendix II – Materials and Reagents 248

Appendix III – Buffers 251

Appendix IV – Equipment 252

Appendix V - Software 253

Abbreviations

7TM	7 Trans Membrane
AM	Acetoxymethyl esters
BSA	Bovine serum albumin
BSS	Balanced salt solution
CAPN1	80 kDa subunit of μ-calpain
CAPNS1	28 kDa regulatory subunit of μ-calpain
C3a	Complement component 3a
C3bi	Complement component 3bi
C5a	Complement component 5a
CD	Cluster of Differentiation
C-ERMAD	C-terminal, ERM-associated domain
CFU-G	Colony forming unit-granulocyte
CFU-GEMM	Colony forming unit-granulocyte, erythroid, monocyte, megakaryocyte
CFU-GM	Colony forming unit-granulocyte, macrophage
CNP	Circulating neutrophil pool
CSF	Colony stimulating factor
DAG	Diacylglycerol
dH_2O	Deionised water
DMEM	Dubecco's modified Eagle's medium
DMSO	Dimethyl sulphoxide
DNA	Deoxyribonucleic acid
EDTA	Ethylenediaminetetraacetic acid
EF-hand	E-helix-loop-F-helix motif
EGF	Epidermal growth factor
EGFP	Enhanced green fluorescent protein
EGTA	Ethylene glycol tetraacetic acid
ER	Endoplasmic reticulum
ERM	Ezrin, radixin, moesin
ERMBMPs	ERM binding membrane proteins

FBS	Foetal bovine serum
FcγRs	Fc portion of γ-Immunoglobulins
FERM	4.1 protein, ezrin, radixin and moesin
FITC	Fluorescein isothiocyanate
fMLP	N-Formylmethionyl-leucyl-phenylalanine
G-CSF	Granulocyte-colony stimulating
G-CSF	Granulocyte-colony stimulating factor
GDI	Guanidine dissociation
GFP	Green fluorescent protein
GM-CSF	Granulocyte monocyte-colony stimulating factor
GPCR	G protein coupled receptor
HEPES	2-[4-(2-Hydroxyethyl)piperazin-1-yl]ethanesulphonic acid
ICAM-1	Inter-cellular adhesion molecule 1
IgG	Immunoglobulin G
IL-1	Interleukin 1
IL-3	Interleukin 3
IL-8	Interleukin 8
IP_3	Inositol 1,4,5-trisphosphate
IP_3R	Inositol 1,4,5-trisphosphate receptor
ITAMs	Immunoreceptor tyrosine-based activation motifs
JAM	Junctional adhesion molecule
kDa	Kilodaltons
KO	Knock-out
LB	Lysogeny broth
LFA1	Lymphocyte function-associated antigen 1
LPS	Lipopolysaccharide
MNP	Marginal neutrophil pool
MW	Molecular weight
NADPH	Nicotinamide adenine dinucleotide phosphate
N-ERMAD	N-terminal ERM associated domain
ORAI1	ORAI1 protein
PAF	Platelet activating factor

PCR	Polymerase chain reaction
PI3K	Phosphoinositide 3-kinase
PIP	Phosphatidylinositol 4-phosphate
PIP_2	Phosphatidylinositol 4,5-bisphosphate
PIP_3	Phosphatidylinositol (3,4,5)-triphosphate
PKC	Protein kinase C
PLCβ	Phospholipase C beta
PMN/PMNL	Polymorphonuclear leukocytes
RA	Rheumatoid arthritis
Rf	Relative mobility
RPM	Revolutions per minute
SCF	Stem cell factor
SDS	Sodium dodecyl sulphate
SDS-PAGE	Sodium dodecyl sulphate-polyacrylamide gel electrophoresis
SEM	Standard error of the mean
SERCA	Sarco/endoplasmic reticulum Ca^{2+}-ATPase
SOCE	Store-operated Ca^{2+} entry
STIM1	Stromal interaction molecule 1
TBE	Tris/Borate/EDTA
TBS	Tris-buffered saline
TNF-α	Tumour necrosis factor alpha
TRIS	Tris(hydroxymethyl)aminomethane
UV	Ultra violet
WT	Wild type

Chapter 1: Introduction

1.1 The immune system

Humans, as with all higher order organisms, have developed immune systems as a means of protection from opportunistic invasion by micro-organisms including bacteria, viruses, fungi and parasites. The role of the immune system is to combat and destroy foreign pathogens entering the body, yet it must also recognise and remove host cells which have become damaged, senescent or cancerous. The ability of the immune system to be able to distinguish between self and non-self is critical to its success, and therefore to the survival of the organism.

Ilya Metchnikov (also written as Elie Mechnikoff), a Russian scientist credited as one of the forefathers of immunology, considered multicellular organisms to be intrinsically disharmonious, such that the state of 'physiological inflammation' involved the normal and regular activity of immune cells to restore 'harmony' (fig. 1.1). 'Pathological inflammation', he proposed, was due to the introduction of injury; infection and/or cell death in the organism. Immunity was therefore deemed to be the objective activity of an organism to defend itself from infection. Metchnikov speculated that phagocytic cells behave as the sentinel cells of the immune system, charged with effectively restoring harmony by patrolling the organism for foreign or dangerous bodies and removing them by a process called phagocytosis (Tauber, 1991; Tauber, 2003). It is crucial that every component of this very complex immune system is tightly regulated, to avoid the launch of an inappropriate or uncontrolled immune response, which may result in damage to the organism itself.

1.1.1 Innate immunity

Innate immunity, as the name suggests, is intrinsic to the organism. Humans are born with a complete innate immune system, and many other higher organisms also possess some components of it. Because it does not require the production of antibodies, the innate immune system is able to target a broad spectrum of pathogenic infections. It is composed of a very complex network of factors, both

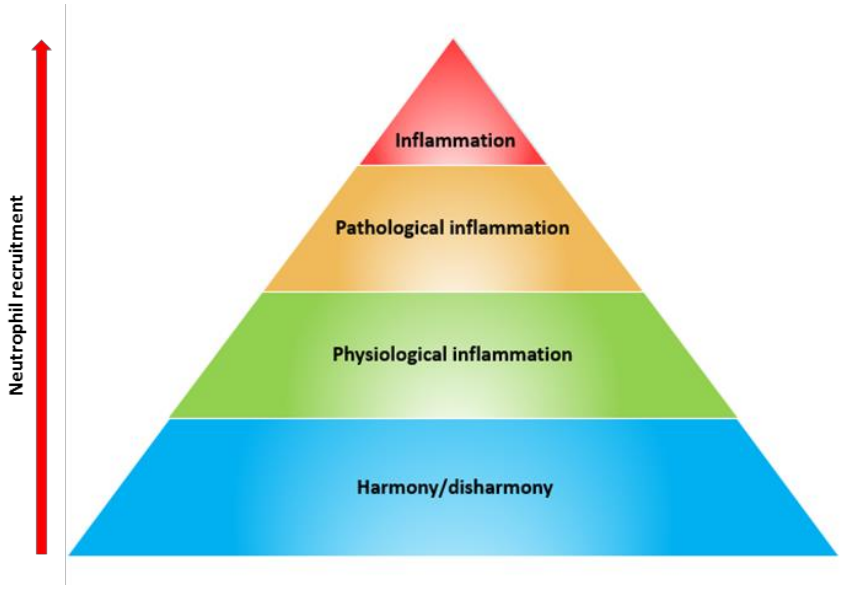

Figure 1.1: Metchnikov's pyramid of immunity
Metchnikov's hypothesis was that all organisms are intrinsically disordered, but striving to achieve harmony within their biological systems. Physiological inflammation is the typical condition of an organism as it aspires to reach harmony. The various states of disharmony increase towards the top of the pyramid, where pathological inflammation is the active restoration of imbalance, culminating in immunity, which is the specific resolution of disorder in the system, typically during tissue damage or infection. (Figure amended from Tauber, 1991).

cellular and molecular, that cooperate to counteract any invasion by pathogenic micro-organisms.

The cellular components of the innate immune system include phagocytic cells, of which neutrophils are the most abundant. The function of neutrophils in innate immunity will be discussed in this thesis.

The molecular aspect of the innate immune response is called complement. This is composed of a collection of proteins in the blood circulation, which work in a chain-like manner whereby each component interacts with the next in a cascade of proteolytic interactions to generate subsequently active molecules. The final result is the accumulation of complement components in the membrane of targeted cells to generate pores which kill the cell by causing lysis. Some members of the complement cascade also work together with cellular components and mark targeted cells (with complement component 3bi (C3bi)) for removal by phagocytic cells, in a process of opsonisation. Other complement components generate a chemotactic gradient (of complement component 5a (C5a)) which recruits phagocytic cells to the vicinity. In all instances, the resultant cell debris is swept away by the foot soldiers of the innate immune system – the phagocytic cells, including neutrophils.

1.1.2 Adaptive immunity

Vertebrates possess the unique ability to acquire immunity. That is to say that their immune systems have the ability to recognise and 'remember' a pathogen, in order to launch a faster and more accurate immune response upon re-infection with the same pathogen; this is called the adaptive immune response. By its nature it is a much more specific response, and as such it involves many different cellular and molecular components, some of which have a cross-talk relationship with those of the innate immune response.

Upon first infection with a micro-organism, a chain of events is started in which white blood cells (WBCs) generate antibodies specific to the invading pathogen.

These antibodies communicate with other cells of the adaptive immune system to label the micro-organism for destruction. Another function of the adaptive response is the maturation of memory B cells which retain a biological memory of the infection for the lifetime of the organism, thus giving the system the ability to launch a much more rapid and intensive response during subsequent encounters with the same pathogen. The blueprint of the adaptive immune system varies between individuals because its memory is continuously acquired throughout the lifetime of the organism, sculpted by an individual's exposure to various infectious agents.

1.1.3 White blood cells

Paul Ehrlich first divided WBCs into subpopulations based on differences in their morphologies (1898) (fig. 1.1.3). One subgroup, he noted, appeared to contain multiple clustered nuclei – two to five per cell – instead of a single nucleus. However, upon further inspection he observed the appearance of nuclear 'lobes', which were distinct but remained connected by fine tethers. He called them 'cells with polymorphous nuclei' (Ehrlich, 1898). This group of cells became the focus of much attention, and were later renamed in 1905, by the Russian scientist Ilya Mechnikov, as 'polymorphonuclear leukocytes' (PMNLs) to be a more accurate description. PMNLs (or PMNs) is the term still used to describe this subpopulation of WBCs.

PMNLs are also called granulocytes, because they contain granules within their cytoplasm. The differentiation of leukocytes into granulocytes is called granulopoesis, and occurs in the bone marrow. Figure 1.1.3 also shows the lineage of PMNL cells from pluripotent haemopoietic stem cells to granulocytes, of which there are three principle sub groups; eosinophils, basophils and neutrophils. The three subgroups were named accordingly based on their characteristic properties when stained with coal tar dyes. The differential staining technique was achieved using a mixture of acidic dyes which bind mainly to proteins, and basophilic dyes which bind mainly to negative charges, e.g. the phosphate backbone of deoxyribonucleic acid (DNA). Eosinophils were

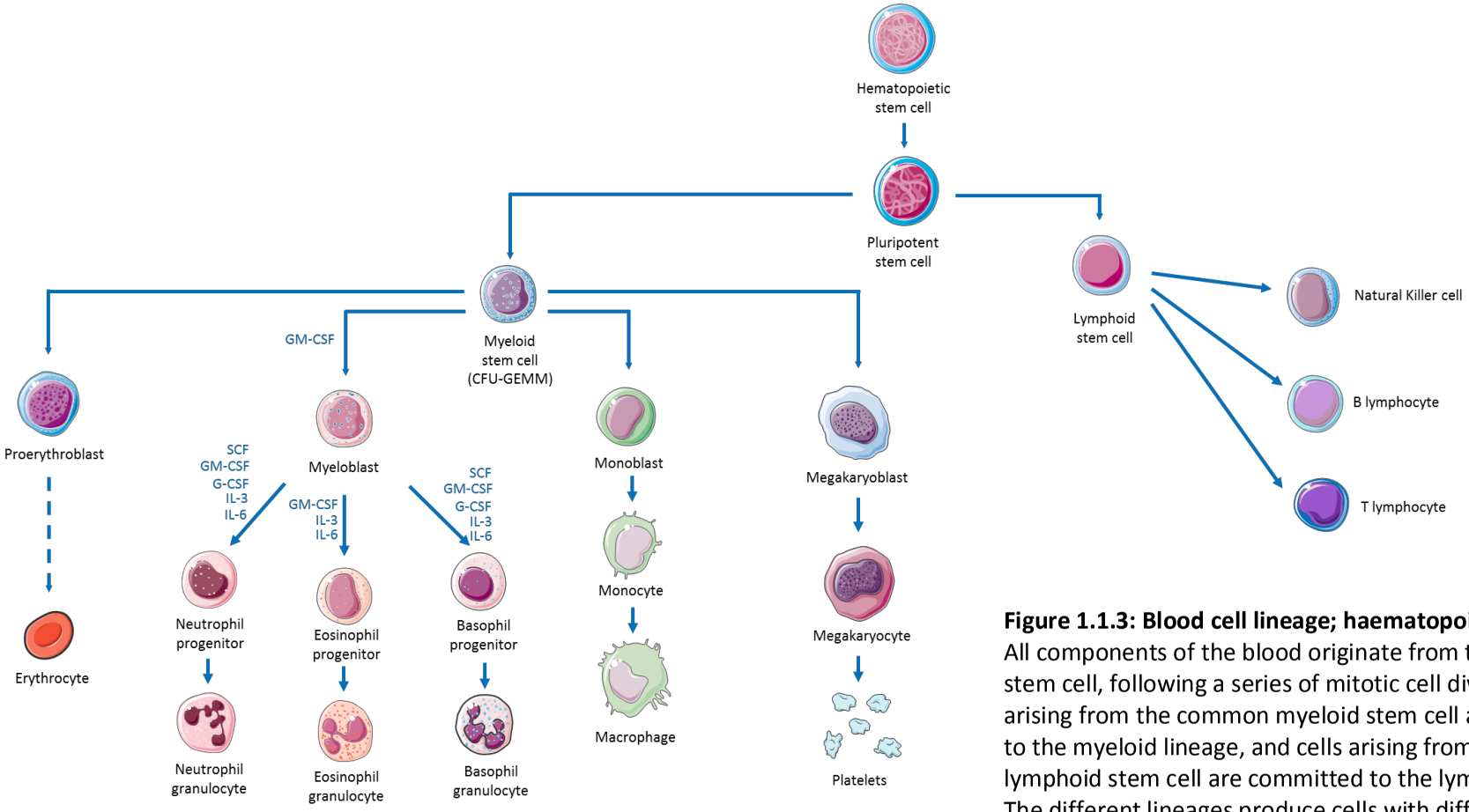

Figure 1.1.3: Blood cell lineage; haematopoiesis
All components of the blood originate from the pluripotent stem cell, following a series of mitotic cell divisions. Cells arising from the common myeloid stem cell are committed to the myeloid lineage, and cells arising from the common lymphoid stem cell are committed to the lymphoid lineage. The different lineages produce cells with different morphological phenotypes. Neutrophils result from mitotic divisions in the myeloid lineage and have a polymorphonuclear phenotype. Figure produced using Servier Medical Art.

found to stain strongly with the acidic dye eosin, basophils stained with the basic dye methylene blue. Neutrophils were so-called because of their propensity to stain with neutral dyes.

1.1.3.1 Phagocytes

Phagocytes (from the ancient Greek p*hagein,* meaning 'to devour' and *kytos,* meaning 'cell'), are a class of cells that act as the 'vacuum cleaners' of the immune system, by sweeping up any potentially dangerous cell debris and micro-organisms. Phagocytosis (from the ancient Greek *phagein*, *kytos* and *osis*, meaning 'process') is the mechanism by which cells, namely phagocytes, internalise foreign bodies within internal compartments known as phagosomes, and proceed to degrade them (Metchnikoff, 1893; 1901; 1905).

Vertebrates have well established phagocytic cells, which are crucial to their innate immune response to invading pathogens. The process of phagocytosis is notably similar to endocytosis, which is performed by many different cell types. Metchnikov proposed that the emergence of phagocytic cells occurred early on in evolution (Tauber, 1991; Tauber, 2003) and the process most likely first appeared in unicellular eukaryotes such as amoeba, which take up their nutrition by engulfing and digesting bacteria. For example the amoeba *Dictyostelium discoideum* captures the bacteria it feeds on through engagement of membrane proteins on its cell surface (Cosson & Soldati, 2008). The main adhesion receptor for this process is probably SibA on the *D. discoideum*, which also bears similarities to β-intergrins on the surface of neutrophils (Cornillon et al., 2006). Interaction of these receptors results in subsequent phagocytosis, and the bacteria are then digested within the cell and absorbed as nourishment.

Other lower organisms also utilise phagocytosis as a means of sustenance. For example, Coelenterates have inner cavities which are coated in phagocytic cells, and the organism derives its nutrition through the phagocytosis of the cavity's contents (McNeil, 1981; Bigger and Hildemann, 1982). Through evolution, higher organisms have moved away from phagocytosis as a means of sustenance and

developed more complex digestive systems. Phagocytic cells have not become redundant though, and are crucial for the maintenance of what Metchnikov referred to as the 'harmony' of the organism. Phagocytes remove harmful material from the organism, be it invasive extracellular pathogens or cell debris. Several different cell types are capable of performing phagocytosis, these are deemed 'professional' or 'non-professional' according to their capabilities (Rabinovitch, 1995). The principal 'professional' phagocytes include the subgroup of WBCs derived from the bone marrow; i.e. monocytes, macrophages and PMNLs, including neutrophils.

1.2 Neutrophils

Neutrophils are the most abundant type of WBC in whole blood, contributing approximately 40-80% of the WBCs in the circulation ($7x10^9$ cells/L) (Lewis et al., 2006). They are phagocytic cells, and form part of the first line of the innate immune response by removing invading extracellular pathogens, such as fungi and bacteria, through the process of phagocytosis (Metchnikoff, 1893; 1901; 1905) and proteolytic degradation following fusion with lysosomes (Coico and Sunshine, 2009).

1.2.1 History of the neutrophil

Throughout much of the 19th century there was significant confusion about the role of the neutrophil in infection and inflammation. Early observations of abundant neutrophils at inflamed sites in the body, and the high concentrations of neutrophils found in pus and mucus initially suggested a role for neutrophils as the agents of infection. It was speculated that neutrophils were spontaneously generated at sites of inflammation, and accumulated bacteria within themselves for the purpose of disseminating pathogens further around the body, thus propagating the infection. In 1846, drawing conclusions from his experiments in toads, Waller disproved this paradigm by discovering that neutrophils migrated out of blood vessels at sites of inflammation by

extravasation “de toute pièce” through the capillaries (Waller, 1846). He recognised that the WBCs exited the bloodstream without damage to or perforation of the blood vessel wall, but rather by the process of diapedesis – between endothelial cells of the blood vessel wall (Cohnheim, 1867a, b; 1967). However the role of neutrophils once at the site of infection and inflammation still remained in question until the late 19th and early 20th Centuries.

At the beginning of the 20th Century two leading researchers, Metchnikov and Ehrlich, were jointly awarded the 1908 Nobel Prize in Physiology or Medicine, in recognition of their enormous contribution towards the understanding of the immune system (and within that neutrophils); as such they are considered by many to be the Founding Fathers of immunology.

1.2.1.1 Ilya Metchnikov (also written Elie Mechnikoff) (1845-1916)

While working in a private laboratory in Messina, Russia in 1882, investigating comparative embryology, Metchnikov (fig. 1.2.1.1) conducted his now famous experiment on starfish larvae, that led to his discovery of the process of phagocytosis (Tauber 2003; Nobelprize.org). He had postulated that the mobile blood cells he had observed to extravasate (now understood to be neutrophils) may help to protect the organism from infection. This led him to perform the famous ‘thorn in the starfish’ experiment.

Metchnikov inserted a thorn from a rose bush (some sources describe a tangerine tree; from Metchnikov’s own account of events, it is understood that the tangerine tree had been ‘decorated’ for Christmas, and the rose thorns were taken from this (British Society for Immunology (2017); Desowitz, 1988)). The intention was to generate a wound that would render the starfish larvae vulnerable to infection. Upon inspecting the puncture caused by the thorn the next day, Metchnikov recognised an accumulation of cells around the wound.

Having already been impressed by Virchow and Cohnheim’s descriptions of diapedesis (Cohnheim, 1867a, b; 1967), and thus aware of the ability of

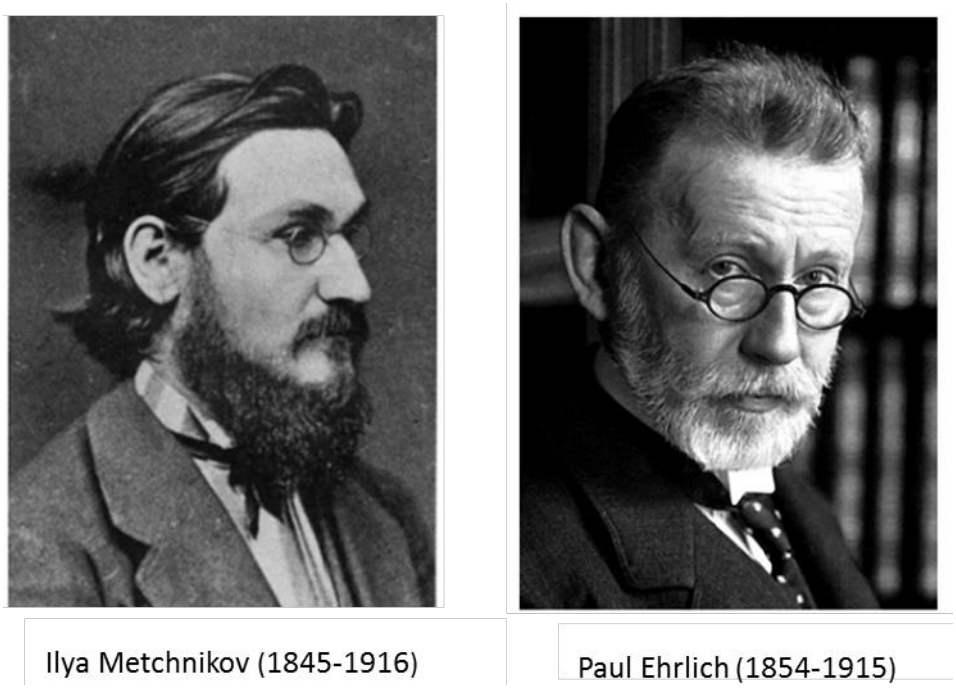

Figure 1.2.1.1: The Founding Fathers of immunology: Ilya Metchnikov and Paul Erhlich

Metchnikov Photographed circa 1875, aged ~30 years old. (Figure reprinted from Metchnikoff, O. N., Life of Ilya Ilyitch Metchnikoff, State Publishing House, Moscow, Leningrad 1926.) Ehrlich Photographed circa 1908, aged ~54 years old. (Figure reprinted from Kay AB. 2015. The early history of the eosinophil. Clin Exp Allergy 45:575–582.)

leukocytes to extravasate from the bloodstream in organisms with vasculature, he subsequently concluded that the observed accumulation of cells were leukocytes which had migrated from the blood towards the site of injury. It was this finding that led to his breakthrough discovery about the role of leukocytes in infection.

The previous paradigm had presumed that neutrophils were spontaneously generated at the site of infection, and Robert Koch had proposed that they served as agents of the infection by accumulating bacteria and transporting them to the inflamed area (Desowitz, 1988). In contrast, Metchnikov hypothesised that the role of these migratory cells was in fact to accumulate at the site of injury in response to infection, and to then digest invading pathogens in order to remove them from the body, in a process coined phagocytosis (Metchinkov 1893; 1901; 1905). In a paper he presented in Odessa in 1883, Metchnikov explained his theory of phagocytosis, after discussions with Claus, a Viennese professor of Zoology who was actually the first to propose the term phagocyte (Gordon, 2008). Metchnikov concluded that the cells he had observed were capable of carrying out phagocytosis, and named them macrophages and microphages, on account of their different cell sizes (from the Latin for 'big'-'eaters' and 'small'-'eaters' respectively). The terminology of microphages has since been changed to the cells we now know as neutrophils, however the term macrophages remains in use.

1.2.1.2 Paul Ehrlich (1854-1915)

Paul Ehrlich's (fig. 1.2.1.1) research in immunology began with an interest in the activity and production of antibodies, from his time working in Robert Koch's laboratory in 1890. Ehrlich was the first to propose "horror autotoxicus"; i.e. the possibility that the immune system can react "against the organism's own elements" (Tauber, 1991). This speculation was made with regard to the generation of autoantibodies which may attack the 'self'. However, it is at odds with Metchnikov's theory that the immune response was reactive to disharmony within the organism, without the potential to create it. Although Ehrlich and

Metchnikov had somewhat contrasting views on the function and purpose of the immune response, both were credited with their contributions towards the modern field of immunology.

Ehrlich first encountered neutrophils as part of his work developing staining techniques to differentiate between different cell types. Noticing that neutrophils did not stain with acidic or basic dyes (unlike eosinophils and basophils respectively) he developed triacid, a mixture of orange G, acid fuchsin and methyl green. He coined the term “epsilon” to describe those cells which stained with neutral dyes; the neutrophil (Kay, 2016). Ehrlich’s work developing techniques to stain blood films, and consequently his differential identification of blood cell types, paved the way for modern studies on blood leukocytes.

1.2.2 Lifecycle of a neutrophil

Neutrophils have three distinct stages in their lifecycle, associated with their abundance at different locations in the body. The transition between each stage involves significant dynamic changes within the cell; these occur in the bone, in circulation and finally also in tissues. Under resting basal conditions the main population of neutrophils reside in the bone marrow (approximately 2.3×10^9 cells per kg of body weight). However, in response to chemical inflammatory signals, indicative of infection or tissue damage, the pool of neutrophils can be rapidly mobilised and released into the blood. The number of neutrophils circulating the blood in a healthy individual is about 7×10^8 cells per kg (Athens et al., 1961).

Human neutrophils have a very short half-life in the circulation, approximately 6-8 hours (Summers et al., 2010), before they exit the circulation and undergo programmed cell death by apoptosis (Savill et al., 1989). In fact, in the time taken to read thus far into this section, some billions of the reader’s own neutrophils will have begun their departure from the circulation, by migrating between the endothelial cells of blood vessels and out into the extravascular space. Consequently, the population of neutrophils is in a state of constant

turnover throughout the lifetime of an individual. Because of the vital role they play in the innate immune system, it is important that neutrophil numbers in the blood remain consistently high enough to be able to quickly respond to an infection. The rate of neutrophil production in a healthy individual is typically 5-10 x 10^{10} cells/day, in order to replenish the pool of circulating neutrophils (Summers et al., 2010). During infection, and the resultant inflammatory cascade, neutrophils become activated and respond to chemical factors which increase their longevity, in order to provide enough primed neutrophils to be able to combat the infection (Summers et al., 2010).

It is likely that the unusually short life-span of neutrophils evolved as an inherently protective mechanism. Given the high reactivity of neutrophils, their accumulation in the blood stream without sufficient removal could lead to systemic propagation of the inflammatory response, and unregulated tissue damage. Furthermore, since a primary role of neutrophils is the ingestion of pathogenic extracellular micro-organisms, a rogue cell which was not itself readily disposed of (as neutrophils are by apoptosis and subsequent engulfment by macrophages) could become vulnerable to colonisation by invasive pathogens; which could lead to systemic dissemination of the infection.

1.2.2.1 Myelopoiesis

Neutrophils are generated from myeloid stem cells in the bone marrow by a differentiation process called myelopoiesis (fig. 1.2.2.1). Myelopoiesis also generates other granulocytes, such as eosinophils and basophils, as well as platelets, monocytes and erythrocytes. Each cell type arises from pluripotent stem cells in the bone marrow, which differentiate in successive mitotic divisions stimulated by a number of different chemical signals, to result in the variety of different cellular components of the blood. At each stage of mitotic division the cells become increasingly more distinct from each other. Together these cells are referred to as the myeloid progenitor pool, and thus each one gives rise to cells of distinct myeloid lineage. The process of neutrophil myelopoiesis is tightly regulated, and dependent on the timely recognition of several cytokines and

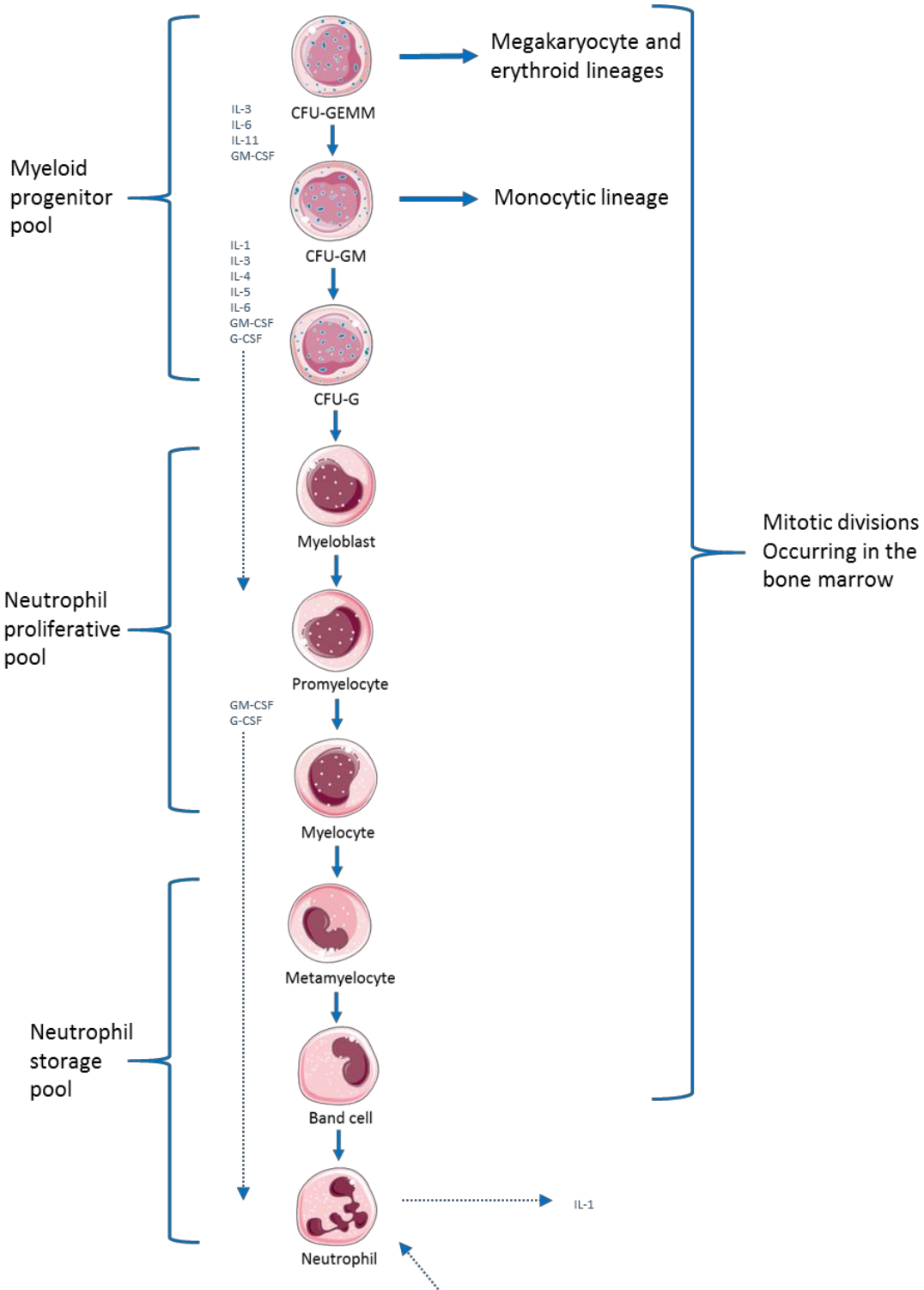

Figure 1.2.2.1: Neutrophil production by myelopoesis
In the myeloid lineage the CFU-GEMM gives rise to neutrophils through a series of mitotic divisions mostly occurring in the bone marrow. With each division the daughter cell becomes more committed to its fate. The commitment to become a neutrophil occurs at the division of the myeloblast, followed by subsequent divisions and maturation into a neutrophil (adapted from Arif and Mufti, 1998; drawn using Servier Medical Art.)

hematopoietic growth factors. There are three key stages beginning with the multiplication of progenitor cells, their maturation and finally functional differentiation. Multipotential hematopoietic stem cells in the bone marrow first lose their ability to self-replicate and differentiate into colony-forming unit-granulocyte, erythrocyte, monocyte, megakaryocytes (CFU-GEMMs). These are then known as the common myeloid progenitor cells, and are also found abundantly in the umbilical cord. The CFU-GEMMs can further differentiate to produce erythrocytes and megakaryocytes. The major growth factors responsible for CFU-GEMM maturation down the myeloid lineage are interleukin-1 (IL-1), interleukin-3 (IL-3), interleukin-6 (IL-6), granulocyte macrophage-colony stimulating factor (GM-CSF) and stem cell factor (SCF). In response to these factors CFU-GEMMs differentiate into colony forming unit-granulocyte macrophages (CFU-GMs). CFU-GMs mark the pivotal point between committed differentiation towards either granulocytes or macrophages. The decision to differentiate into colony forming unit-granulocytes (CFU-Gs) occurs in response to IL-3, adhesion Ig super family molecules (SF), GM-CSF and G-CSF. Together with the stem cells, CFU-Gs constitute the neutrophil progenitor pool (Kannwar and Cairo 1993; Wheeler 1993).

In response to GM-CSF, IL-6 and IL-3 the CFU-Gs further differentiate into myeloblasts (the earliest recognisable stage of myeloid lineage), promyelocytes and subsequently neutrophilic myelocytes via a series of mitotic divisions. Each of these three cell-stages is the product of consecutive mitotic divisions and take approximately one week to complete. The final stages of granulocyte maturation begin after these mitotic divisions. Cytokines, including GM-CSF, IL-6 and IL-3 promote the differentiation into monocytes and the PMNLs; neutrophils, basophils and eosinophils.

The neutrophil storage pool consists of neutrophils at varying stages of differentiation, following mitotic maturation from CFU-G progenitor cells and includes band cells, metamyelocytes and neutrophils. Factors such as GM-CSF, CSF and IL-3 regulate the final stages in neutrophil maturation, which involve dynamic changes in their cellular properties, when the cells acquire motility and

become deformable; characteristics which facilitate the exit of mature neutrophils from the bone marrow. Among these factors G-CSF interacts with Cluster of Differentiation 114 (CD114), a member of the family of hematopoietic cytokine receptors, on the surface of granulocytic precursors and promotes the release of neutrophils from the bone marrow. G-CSF/CD114 interaction also down-modulates CD114 expression on neutrophils and stimulates degranulation (Jilma et al., 2000).

Differentiation in the bone marrow takes about two weeks in total. Within the bone marrow there is a reserve pool of neutrophils which is about 20 times greater than the total population of circulating neutrophils. Mature neutrophils are released into the circulating blood via endothelial pores in sinusoids of the bone marrow. Upon entering the bloodstream the neutrophils become part of what is known as the circulating neutrophil pool (CNP). Regulation of neutrophil maturation and release is controlled by IL-3, GM-CSF and CSF (Okuda et al., 1992). Terminally differentiated neutrophils are unable to divide further. For a long time it was assumed that they also had little or no ability to perform *de novo* protein synthesis, because of their limited synthetic machinery. However, it is now understood that 'primed' neutrophils exposed to the stimulatory bacterial peptide N-Formylmethionine-leucyl-phenylalanine (fMLP), show increased protein synthesis via increased levels of both transcription and translation (Hughes et al., 1987; Humphreys et al., 1989).

1.3 Neutrophil morphology

Neutrophils belong to the class of PMNLs and granulocytes, on account of the multi-lobed appearance of their nucleus, and their numerous cytoplasmic granules respectively. They are of myeloid lineage, originating in the bone marrow, and have one of the shortest lifespans of any cell once in the circulation. As terminally differentiated cells their structure is specialised to suit their phagocytic functions. They are small, spherical cells in the circulation, with a diameter of approximately 9-10 µm (Wintrobe, 1967). Upon receiving a

chemical inflammatory signal they undergo a process called cell spreading, which sees their average diameter increase to approximately 20-30 µm. During cell spreading neutrophils assume a flattened and adherent morphology, in which the height of the cell is limited only by the volume of the nucleus (Dewitt et al. 2013) (fig. 1.3i).

Three distinct aspects of neutrophil morphology distinguish them from other types of WBC: (i) multi-lobed or segmented appearance of the nucleus, (ii) fewer than average mitochondria and (iii) numerous cytosolic granules.

(i) All PMNLs have a segmented nucleus, in which each lobe is connected via fine tethers. When stained with DAPI the nucleus occupies a significant 20% of the cytosol (Schmid-Schonbein et al., 1980), and is a distinguishable characteristic of these cells. The number of lobes increases from two up to five as the cell ages (Campbell et al., 1995; Olins and Olins, 2005; Fuchs et al., 2007; Hoffmann et al., 2007).

(ii) In neutrophils the mitochondria constitute only 0.6% of the total organelle volume, in comparison to hepatocytes in which the mitochondria make up approximately 20% of the entire cell volume (Hallett and Lloyds, 1997). They also lack substantial endoplasmic reticulum and golgi apparatus, making up less than 1% of the average volume of a cell (Hallett, 1989). This has indicated that mitochondria are not necessary for typical cellular functions in a neutrophil such as energy production, protein synthesis and storing Ca^{2+}. Instead, neutrophils employ glycolysis to produce energy, and Ca^{2+} is sequestered within other organellular structures resembling calciosomes (Krause et al., 1989). However more recently it has been found that neutrophils do possess an extensive intracellular network of mitochondria throughout their cytoplasm which is necessary for proper neutrophil functioning, but not required for acute bouts of

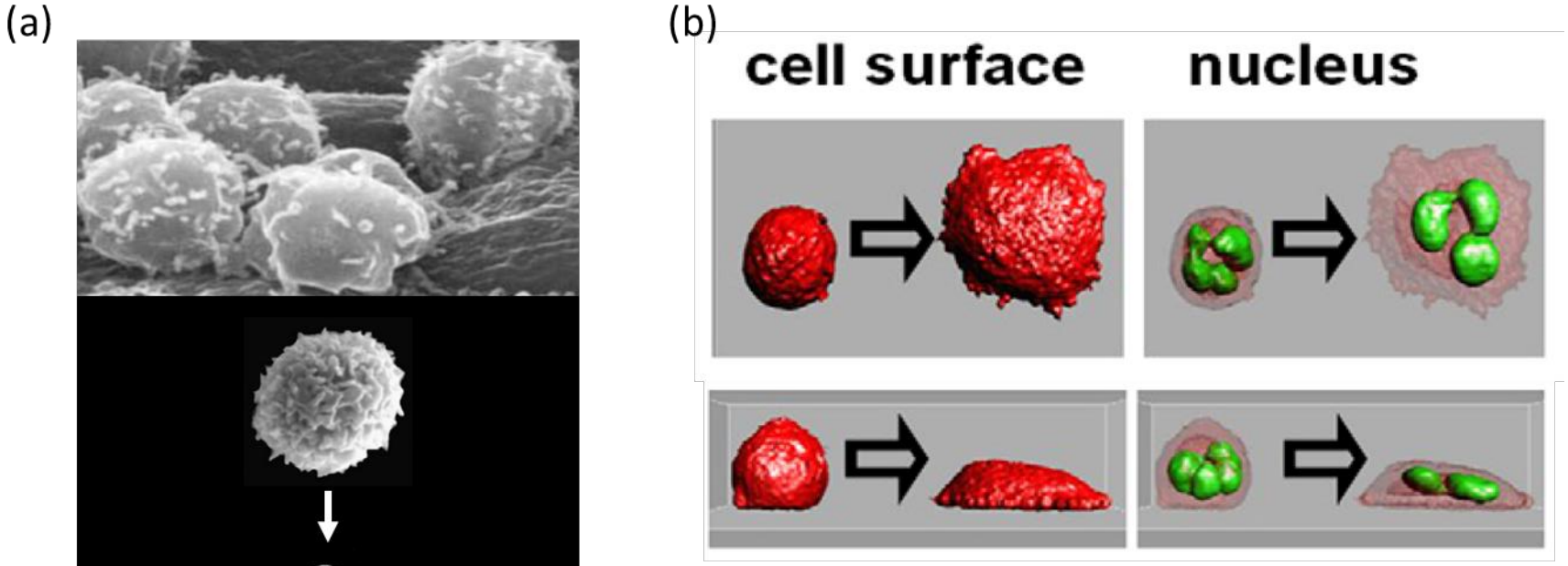

Figure 1.3i: The morphology of spreading neutrophils
(a) Scanning electron microscopy of neutrophils at different stages of cell spreading. As the neutrophil makes contact with a surface and begins to spread a skirt of plasma membrane appears, with visibly fewer wrinkles than the 'spherical' cell membrane. **(b)** The height of the spread neutrophil is limited only by the arrangement of the nuclear lobes (green) within the cell. This gives the 'fried egg' or 'lone mountain' appearance, as seen in (a). Figure amended from Hallett et al., 2008 and Dewitt et al., 2013.

activity such as phagocytosis or the respiratory burst (Fossati et al., 2003).

(iii) Neutrophils are a type of granulocyte, and contain abundant heterogeneous cytoplasmic granules. These are clearly visible in electron micrographs (fig. 1.3ii), occupying approximately 15-16% of the total cell volume (Schmid-Schonbein et al., 1980). They contain an arsenal of sequestered toxic host defence proteases (Borregaard and Cowland, 1997).

1.3.1 Neutrophil granules

Neutrophils have an average density of 1.08-1.09 g/mL (Clark and Nauseef, 2001), which is much denser than other WBCs, and this is largely due to the abundance of their cytoplasmic granules (Bretz and Baggionlini, 1974). Their characteristic density facilitates neutrophil isolation by dextran sedimentation. The contents of neutrophil granules can be released by controlled fusion with phagosomes, in order to destroy material that has been engulfed by the process of phagocytosis. The granular contents can also be released into the extracellular matrix, as in frustrated phagocytosis (Hallett and Lloyds, 1995). The latter can have damaging effects on other tissues, for example in the inflamed synovial junctions in rheumatoid arthritis (Edwards and Hallett, 1997).

Neutrophil granules can be divided into three categories based on their contents (Boxer and Smolen, 1988). The contents of the granules is dependent on at which stage of myeloid differentiation they were produced, and they are specialised to the functions of the cell at each stage of its life-cycle (Abramson and Wheeler, 1993). The three classes of granules are: azurophilic (primary), specific (secondary) and small (storage). The granules are dense intracellular structures (Bretz and Baggionlini, 1974) and occupy approximately 15-16% of the total cell volume (Schmid-Schonbein et al., 1980). They contain numerous cytotoxic enzymes for the purpose of digesting foreign pathogenic material and cell debris. Granule membranes are covered in signalling proteins, receptors and adhesion molecules (Borregaard and Cowland, 1997).

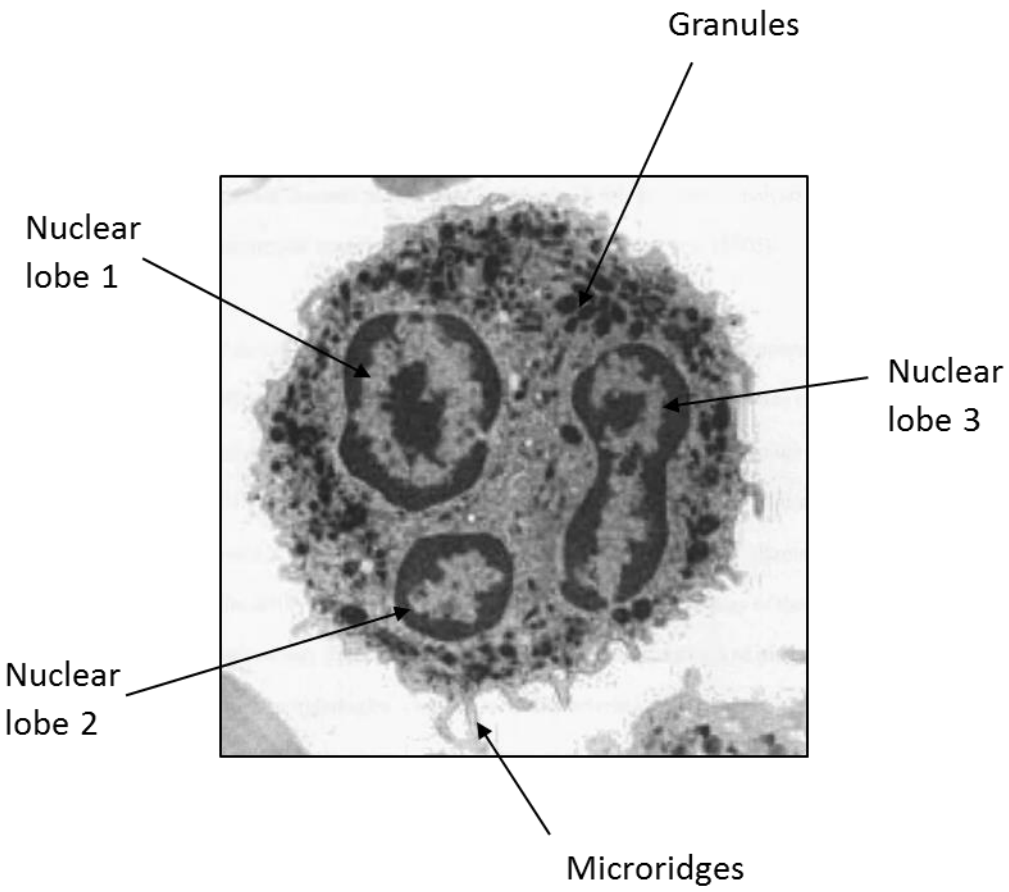

Figure 1.3ii: Neutrophil lobes and granules, viewed by electron microscopy
Three nuclear lobes and multiple cytoplasmic granules can be seen in the cell cytoplasm. Also of note is the absence of definable golgi apparatus, mitochondria or endoplasmic reticulum.
(Figure amended from Ohio State University, Microscopy and Imaging Facility.)

Granules mature along with progenitor cells in the stages of neutrophil development. The specific combination of enzymes and cytotoxic substances within the granules is dictated by the stage of myeloid cell differentiation at which protein synthesis occurs (Borregaard and Cowland, 1997), and not because of any specific granule sorting. This means there can be some similarity between the contents of granules. The primary azurophilic granules are first recognised in the promyelocyte. They make up approximately 1/3 of the granules in the mature neutrophil. Azurophilic granules contain the protease myeloperoxidase, which gives the neutrophils their characteristic green hue when viewed by bright field light microscopy. Myeloperoxidase is also responsible for breaking down bacterial cell walls during infection (Klebanoff et al., 2013), and its abundance in pus and mucus can give both a greenish appearance. The secondary, or specific granules are smaller in size and can be identified in both myelocytes and metamyelocytes. They form the basis of the neutrophilic bands observed in the final stages of maturation. The small storage granules contain gelatinases and cathepsins. A fourth subgroup of granules has also been identified as the secretory vesicles (Borregaard et al., 1987). They are formed by the process of endocytosis.

1.3.2 Neutrophil plasma membrane

The neutrophil plasma membrane has characteristics that distinguish it from any other cell type. Because neutrophils are able to both receive and relay signals to and from other cells of the immune response, they are equipped with a vast array of membrane receptors, between 0.5 and 1 million, to recognise a variety of inflammatory stimuli (Hallett, 1989). These receptors are sensitive to subtle chemical gradients in the extracellular matrix, and enable the neutrophil to detect and respond to inflammatory stimuli at considerable distances from the point of source, and as low as 0.1% over the length of the cell (Zigmond, 1977; Mak and Saunders, 2006). They recognise soluble inflammatory signals including: tumour necrosis factor-α (TNFα), cytokines, interleukins, bacterial components (formylated peptides and lipopolysaccharide endotoxin) and

members of the complement cascade (e.g. C5a). Ligation of these receptors, through specific ligand interaction, triggers a cascade of secondary intracellular messengers within the neutrophil (Hallett, 1989). The perceived signals from the neutrophil plasma membrane receptors may evoke a response in the cell to upregulate/downregulate other membrane receptors, or result in the degranulation and secretion of proteins sequestered within granules.

Neutrophils also have receptors which directly engage with the surface of other cells, including: selectins, integrins and immobilised C3bi (Lee et al., 2003), which assist neutrophil binding to the vascular endothelium, prior to extravasation; or the surface of opsonised material prior to phagocytosis.

The ability of a neutrophil to change morphology is crucial to its success at performing phagocytosis, extravasation and chemotaxis during inflammation. This morphology change from a 'spherical' neutrophil in circulation, to a 'flattened' adherent cell about to extravasate involves an apparent membrane expansion of about 200% (Hallett and Dewitt, 2007), much greater than the 4% expansion facilitated by the mechanics of the phospholipid membrane (Hamill and Martinac, 2001). During the process of extravasation the neutrophil makes several receptor-mediated interactions with endothelial cells of the blood vessel wall. A summary of the receptors involved in neutrophil adhesion to, and extravasation through, the endothelial layer is listed in table 1.3.2. The process of extravasation will be discussed in more detail in subsequent sections.

1.4 Neutrophil behaviour

Neutrophils are the first line of defence against bacterial and fungal infection within the innate immune system. Their primary function is phagocytosis and they have been nicknamed 'professional phagocytes' by Rabinovitch (1995). The circulating neutrophil pool constitutes only ~50% of neutrophils in the vascular compartment at any one time. The remaining 50% of neutrophils adhere to the

Cell	Receptor	Ligand	Ligand presented by	Response
Neutrophils	L-selectin	sLe^a and sLe^x	Endothelial cells	Weak adhesion of neutrophils to the endothelial wall of blood vessels; facilitates rolling
	CD11a/CD18	ICAM-1/2/3	Endothelial cells	Firm neutrophil adhesion to endothelium
	CD11b/CD18 (Mac-1)	ICAM-1, C3bi, fibrinogen, factor X	Endothelium and complement	Firm neutrophil adhesion to endothelium and phagocytosis
	PECAM-1	CD31/a_v	Leukocytes	Extravasation of neutrophils through endothelial lining of blood vessel
Endothelial cells	P-selectin	sLe^x and PSGL-1	Endothelial cells and neutrophils	Firm adhesion between neutrophils and endothelium
	E-selectin	sLe^x	Neutrophils	Firm adhesion of neutrophils to endothelium
	PECAM-1	CD31/a_v	Leukocytes	Extravasation of neutrophils through endothelial lining of blood vessel

Table 1.3.2: Receptors involved in neutrophil/endothelial cell interaction
The receptors and ligands involved specifically in neutrophil/endothelial cell adhesion and subsequent neutrophil extravasation through the endothelial lining of the blood vessel wall.

endothelial lining of small blood vessels, constituting the marginal neutrophil pool (MNP). Cells from the MNP are poised ready to respond to inflammation, and interact with endothelial cells via integrins and selectins, on their cell surface and on the surface of the neutrophil (Zarbock and Ley, 2008) (table 1.3.2). These interactions position the marginal neutrophils at the blood vessel wall so that they are ready to respond to inflammatory signals and exit the bloodstream via the process of extravasation, before migrating into tissues towards the source of inflammatory stimuli. This is a crucial, yet little understood, hurdle in the neutrophils' ability to respond to inflammation and accumulate at sites where they may be required to perform phagocytosis.

1.4.1 Response to inflammatory signals

Circulating neutrophils have an apparently spherical morphology, the smallest surface area to volume ratio to enclose any given volume (Hallett and Dewitt, 2007). Upon recognition of inflammatory chemical signals such as the chemokines (e.g. TNFα, IL-1, IL-6, IL-8 and C5a) through extracellular receptors (e.g. TNF-receptor (TNF-R), cytokine receptors and C5a receptor (C5aR)) (Futosi et al., 2013), neutrophils respond by migrating along the gradient of chemoattractant towards sites of infection and inflammation (fig 1.4.1).

Neutrophils play an active role in the propagation of the inflammatory cascade, as well as having a direct role in the resolution of inflammation. Migration from the blood into the surrounding issue involves the extravasation of neutrophils through junctions in the vascular endothelial layer (Ley et al., 2007). This process involves a dramatic change in cellular morphology, specifically from the apparently spherical morphology of circulating neutrophils to a flattened morphology of adherent neutrophils; the immediate prelude to neutrophil extravasation, which facilitates the exit of neutrophils from the vasculature (fig. 1.4.1). The mechanism of neutrophil spreading and extravasation will be discussed further in the context of Ca^{2+} signalling in later sections.

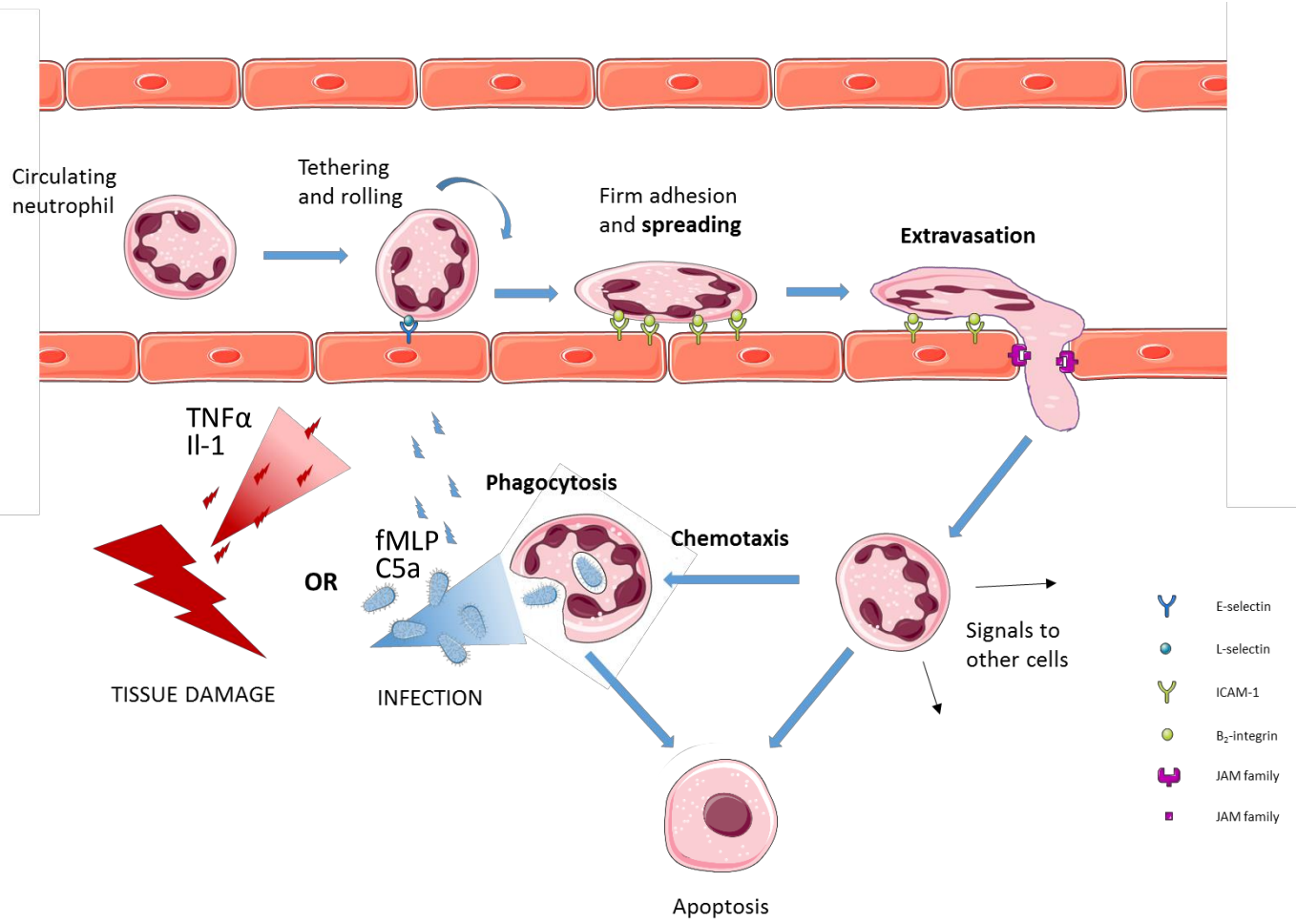

Figure 1.4.1: Neutrophil exit from the circulation
Rolling neutrophils form weak interactions between selectins (blue), followed by increasingly firm adhesions between β2-integrins on the neutrophil surface and upregulated ICAM-1 (green) on the surface of luminal endothelial cells. These interactions stimulate the neutrophil to arrest and assume a flattened morphology, the necessary prelude to extravasation. The cell squeezes between endothelial cell junctions, interacting with JAMS (violet), before following a chemotactic gradient (blue wedge) of inflammatory stimuli towards the site of infection or inflammation, where they perform phagocytosis of C3bi opsonised bacteria. The neutrophils also release chemoattractants, further recruiting immune cells to the area. Activated neutrophils are on a one way ticket to programmed cell death and ultimately complete apoptosis.

Upon leaving the bloodstream and entering the extravascular space, neutrophils continue to be guided towards sites of inflammation by interactions with the extracellular matrix (Hynes, 1992), and also by a chemotactic gradient of chemical inflammatory stimuli. These chemoattractants are generated by the organism ('self'), such as the complement component C5a and cytokines IL-8 and leukotriene B4 (LTB4), and also by pathogenic bacteria such as the bacterial peptide fMLP (Zigmond, 1977; Murphy, 1994; Gerard and Gerard, 1994).

The concentration gradient of these stimulants guide the neutrophils, like breadcrumbs, towards tissue damage and/or infection. Cell surface receptors on the neutrophil are able to detect concentrations of chemoattractant as low as 0.1% over the cell length (Zigmond, 1977; Mak and Saunders, 2006). It has also been suggested that presence of these agents may actively increase the neutrophil's life span up to 1-2 days (rather than the typical half-life of 6-8 hours). Neutrophils will continue to proceed in the direction of chemoattractant, by extending protrusions of the plasma membrane, called pseudopodia, and retracting their trailing edge, as long as they continue to sense further increases in chemoattractant concentration (Mak and Saunders, 2006). When they arrive at the source of inflammatory stimuli, neutrophil chemotaxis arrests. Neutrophils themselves secrete additional chemoattractants to recruit nearby lymphocytes, and also begin their primary job of clearing away any invading extracellular pathogens.

1.4.2 Neutrophil Extravasation

The first stage in neutrophil extravasation from the bloodstream involves recruitment of cells to begin the migration process. Neutrophils are alerted to the need to extravasate by receptor engagement with inflammatory stimuli. Within the circulation there exists two sub-populations of neutrophils; the CNP and the MNP. Cells move from the CNP to the MNP in response to inflammatory stimuli, and integrins and selectins on both the neutrophil and endothelial cell surfaces engage to tether the neutrophil at the vascular wall. The interactions are weak, e.g. hydrogen-bonds, and easily sheered by the exertive force of the

blood flow. Neutrophils in the MNP 'roll' along the vascular endothelial lining by forming and breaking interactions between selectins, under the flow pressure of the blood (McEver 1991; Bevilacqua et al, 1991).

The slow rolling enables the neutrophil to assess the environment next to the endothelial cells, and detect local inflammatory factors such as platelet activating factor (PAF), which alerts the cell to a state of inflammation (Lorani et al., 1995; Abbassi et al, 1993). Neutrophils may then increase the externalisation of integrin receptors CD11b/CD18 (Mac-1). Inflamed endothelial cells in the vicinity of underlying tissue inflammation respond to TNF generated locally by tissue macrophages in response to cell injury or infection (Macconi et al, 1995). Endothelial cells upregulate expression of intercellular adhesion molecule-1 (ICAM-1) on their luminal cell surface. The slow 'rolling' of neutrophils in the MNP, relative to those in the CNP, facilitate CD11b/CD18 integrins on the neutrophil cell surface to recognise and engage with ICAM-1 molecules on the endothelial cells. These interactions are much stronger than the hydrogen bonds formed by selectin interactions, and in combination with lipid mediators such as PAF, the adhesiveness of neutrophil cell surface receptors is increased to facilitate firm binding and neutrophil 'arrest' on the endothelial lining (Lawrence and Springer, 1991; Lorani et al., 1995).

Inflammatory mediators responsible for ICAM-1 upregulation include: LPS, TNF-α, IL-1 and PAF. These molecules act as signposts, leading the neutrophil to perform extravasation adjacent to the source of the inflammatory signal. The relatively high concentration of TNF-α also has a priming effect on neutrophils, which triggers a much greater oxidative response upon secondary stimulation (Hallett and Lloyds, 1995; Lloyds et al., 1995).

Key to neutrophils' functions outside of the bloodstream in the tissues, is their ability to exit from the bloodstream intact, and without causing damage or rupture to themselves, or to the blood vessel wall. This process of extravasation was first reported by Virchow and Cohnheim in 1867 (Cohnheim, 1867a). Once recruited to the inflammatory response, the neutrophils must undergo a

dramatic change in cell morphology which is the immediate prelude facilitating extravasation from the blood capillaries. The mechanism of neutrophil extravasation is the focus of the work presented in this thesis.

1.4.3 Neutrophil phagocytosis

Upon reaching their final destination, at the site of inflammation, neutrophils perform their 'professional duty' and go about the controlled removal and destruction of invading extracellular microbes, via the process of phagocytosis.

Neutrophils recognise the invading bacteria and fungi by their CD11b/CD18 (Mac-1) receptors engaging with the complement component opsonin C3bi, or via their Fc IIa and III receptors engaging with opsonising antibodies on the surface of microbes (Anderson and Looney, 1986; Fossati et al., 2002; van Spriel et al., 2001). This receptor engagement triggers a conformational change in neutrophil morphology, which enables them to perform phagocytosis. Cells extend pseudopods towards the particle and encircle it. The offending microbe is engulfed by the neutrophil and held within a newly formed intracellular vacuole called the phagosome (Thelen et al., 1993).

Neutrophils contain abundant cytoplasmic granules, as previously described. In a process called degranulation, the cytoplasmic granules fuse with the phagosome containing the foreign particle (Hirsch and Cohn, 1960; Zuckerfranklin and Hirsch, 1963; Pryzwansky et al., 1979). A change in pH within the phagosome creates an environment which activates the arsenal of toxic enzymes sequestered within the granules. The phagosomal membrane also has specific proteins which when activated aggregate to form non-mitochondrial NADPH oxidase, and produce reactive oxygen species (ROS) (Baggiolini and Wymann, 1990; Barbior, 1984; Segal and Jones, 1978). The combination of ROS and the arsenal of cytotoxic contents of neutrophil granules efficiently destroy the engulfed microorganism, without causing damage to surrounding host tissues.

Similarly to the membrane expansion required to perform phagocytosis, the process of neutrophil extravasation from the bloodstream also necessitates a dramatic change in cell surface morphology; more precisely an apparent ~200% expansion of the plasma membrane (Hallett and Dewitt, 2007). The apparent expansion of the plasma membrane will be discussed in the context of Ca^{2+} signalling in later sections, and phagocytosis will be used as a model of localised membrane expansion for some of the results presented in this thesis.

1.5 Neutrophils in disease

Whilst the primary role of neutrophils is to defend the host from disease caused by the infection of pathogenic microorganisms, there are some instances in which aberrant neutrophil behaviour makes them the causative factor in some disease conditions. For example, impaired neutrophil activity can be devastating, such as in chronic granulomatous disease where a genetic defect in the neutrophil oxidase pathway prevents neutrophils from functioning correctly (Segal, 1987; 1996). Conversely, over activation of neutrophils can cause damage to host tissue; such as during the inappropriate release of neutrophil elastase in chronic obstructive pulmonary disease (COPD) (Nadel, 2000), or the excessive infiltration of neutrophils into synovial junctions in rheumatoid arthritis (Edwards and Hallett, 1997).

1.5.1 Rheumatoid arthritis

Rheumatoid arthritis is a chronic inflammatory autoimmune disease, and one of the most prevalent autoimmune disorders in the world, affecting approximately 1% of the global population (Alamanos & Drosos, 2005; WHO 2017). It is a systemic condition and can also lead onto secondary disorders including pulmonary fibrosis and cardiovascular disease, with rheumatoid arthritis patients being two-fold more likely to suffer myocardial infarction, and having an increased incidence of mortality (Zegkos et al., 2016).

The most common and physically prominent symptoms of rheumatoid arthritis are presented in the joints, typically the hands, where inflammation causes debilitating pain and deformity (see fig. 1.5.1). Both environmental and genetic factors contribute to the disease prognosis in rheumatoid arthritis patients, with those patients presenting recognised risk factors such as Rheumatoid factor (RF) and genetic factors such as HLA-DRB1, being necessarily more susceptible to the cumulative effect of environmental factors. RF can be detected in the circulation of individuals many years before the onset of symptoms, yet there is still little understanding of the events triggering the pathophysiology of the disease, and none of the available medications prove effective at preventing the condition.

Rheumatic joints appear swollen due to the large infiltration of immune cells into the synovial junction, leading to inflammation of the synovial lining (fig. 1.5.1), which is typically only two to three cells thick in a healthy joint (Wright et al., 2014). There is also an excessive accumulation of synovial fluid, which can exceed 30 mL in volume, containing up to $5x10^9$ neutrophils (Edwards and Hallett, 1997). This not only contributes to the physical swelling of the joints, but a reduction in viscosity of the synovial fluid further decreases lubrication in the joint, contributing to difficulty in movement and ultimately further damage to the cartilage. The inflamed synovial lining also becomes enriched with new blood vessels and a new granular pannus tissue composed of macrophages, lymphocytes, activated synovial fibroblasts and neutrophils extends across the articular cartilage (Shiozawa et al., 1983; Wright et al., 2014). Invasion of these cells contributes to bone and cartilage damage due to the secretion of pro-inflammatory chemokines, cytokines and prostaglandins, and the high concentration of destructive collagenases and metalloproteases (Shiozawa et al., 1983; McCachren et al., 1990; Brinckerhoff, 1991; Wright et al., 2014). Neutrophil elastase, cathepsin G, proteinase 3 and some matrix metalloproteinases (namely MMP-8 and 9) are produced by neutrophils and further contribute to matrix degradation at the pannus-cartilage junction (Murphy et al., 2008).

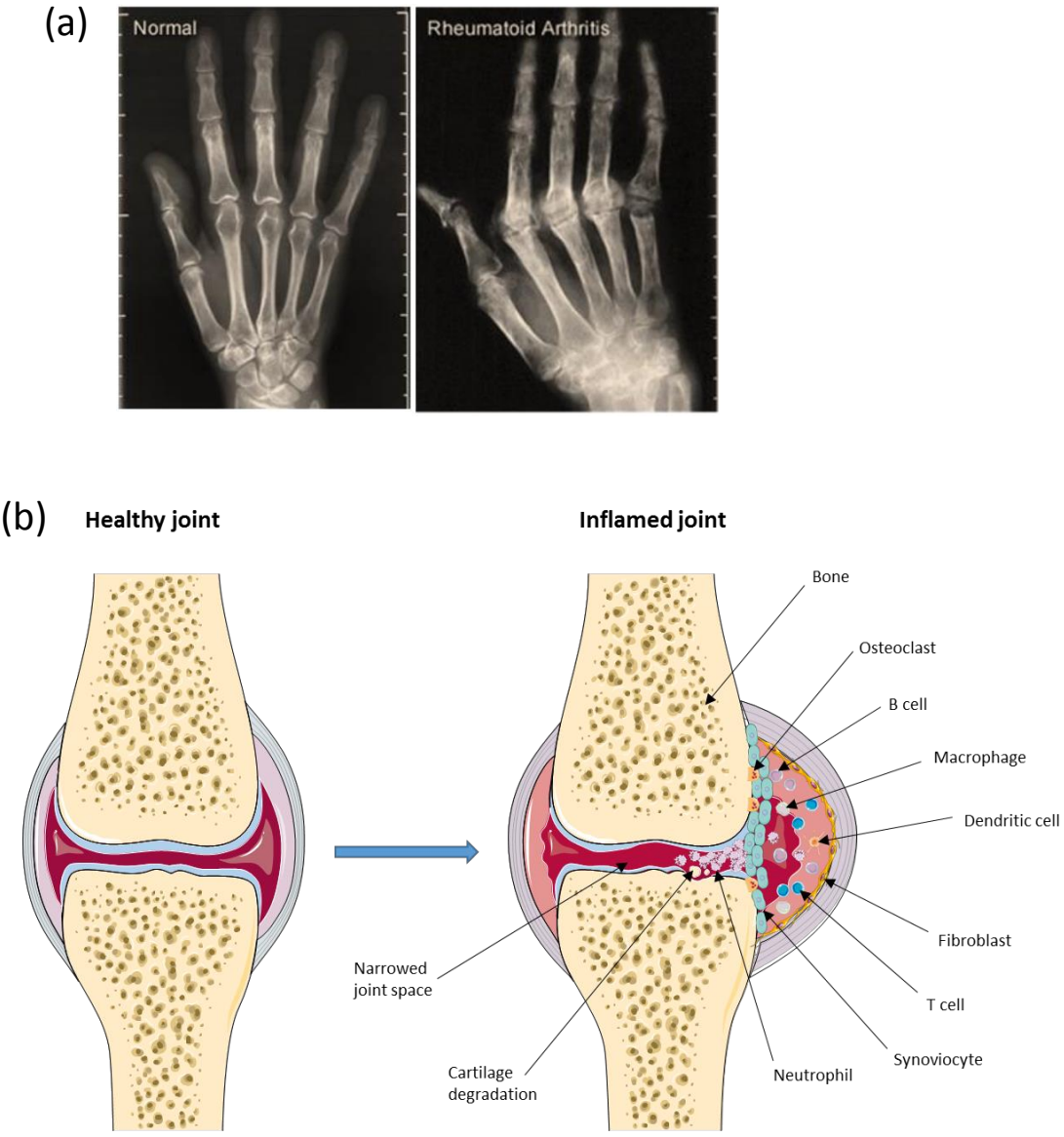

Figure 1.5.1: Damage to joints in rheumatoid arthritis
(a) X-ray images comparing a healthy hand (left) (Adams, 2013) with the distorted joints in a hand afflicted with rheumatoid arthritis (right). **(b)** Cross-section of a healthy joint showing progression to a rheumatic joint. The diseased joint is swollen and due to excessive synovial fluid, infiltration of immune cells and the growth of new pannus tissue. Bone and cartilage degradation occurs due to the release of damaging ROS and enzymes from neutrophils and other immune cells. Amended from Wright et al., 2014 – drawn using Servier Medical Art).

Neutrophils respond to chemical signals produced by immune cells at the site of inflammation and are recruited from the circulation to the joint, where they then exacerbate the inflammatory state. Upon arriving at the synovial junction, neutrophils become activated by immune complexes deposited locally by other cells as part of the inflammatory response. Neutrophils recognise the immune

complexes via engagement with their Fcγ receptors (FcγR) (Fossati et al., 2001; 2002) and react by releasing their arsenal of destructive enzymes and ROS from cytosolic granules, in a process termed 'frustrated phagocytosis', due to incomplete phagosome formation (Hallett & Lloyds, 1995). Release of these cytotoxic products directly onto the articular cartilage and bone causes erosion of the joint.

The effect of increased neutrophil recruitment to the inflamed joint is not limited to the destructive capabilities of their cytotoxic products. It is understood that neutrophils also play a regulatory role in the progression of inflammation, by orchestrating the activity of other immune cells in the vicinity, and coordinating the immune 'self-attack' (Mantovani et al., 2011). Neutrophil organisation of the other immune cells is achieved through several activities, including; (i) secretion of chemical factors such as cytokines and chemokines that stimulate and recruit immune cells to infiltrate the joint, (ii) release of some proteases which regulate the activity of the cytokines and chemokines, (iii) direct cell-cell interactions which activate cells such as natural killer cells, and (iv) upregulation of specific receptors on the neutrophil plasma membrane, such as the major histocompatibility class (MHC) II proteins, enabling antigen presentation to T cells in the matrix (Wright et al., 2014).

Neutrophils isolated from patients with rheumatoid arthritis also have different characteristics to those isolated from healthy individuals. Synovial fluid extracted from the joints of rheumatoid arthritis patients contains a larger majority of activated neutrophils, than in the synovial fluid of healthy individuals (Wittkowski et al., 2007). These neutrophils are primed for the release of ROS (Eggleton et al., 1995) and they secrete a number of cytokines and chemokines

which in turn regulate the activity of osteoclasts and B lymphocytes in the afflicted joint. Furthermore, the hypoxic environment of a rheumatic joint, in combination with the occurrence of antiapoptotic cytokines such as TNFα, IL-8 and GM-CSF, has the effect of prolonging the neutrophil's lifespan from the typical 24 hours up to several days (Raza et al., 2006; Weinmann et al., 2007). These factors make neutrophils both antagonists of the rheumatic condition, and also effectors of the tissue destruction; as such reducing neutrophil recruitment to the joints is a prominent target for developing novel therapies to treat rheumatoid arthritis.

1.6 Ca^{2+} signalling

Calcium is one of the most abundant elements on Earth, superseded only by silicon, aluminium, iron and oxygen (Case, 2007). As Ca^{2+} ions have a high affinity for electrostatic interaction with carboxylate oxygen (Jaiswal et al., 2001; Saris and Carafoli, 2005), this may have led to the evolution of Ca^{2+} binding proteins with 'effector functions'. Within cells, Ca^{2+} concentration is therefore tightly regulated. The Ca^{2+} ion is a ubiquitous signalling system in various cell types, and is involved in a vast range of cellular processes including fertilisation and smooth muscle contraction. Its tendency to interact with carboxyl groups, such as those on amino acids, means that high intracellular Ca^{2+} concentrations can lead to protein aggregation, disruption of the integrity of the plasma membrane, aggregation of nucleic acids and the precipitation of phosphates, sulphates and carbonates. As such, elevated concentrations of Ca^{2+}, if unregulated, are undesirable in biological systems. For example calcification, where the inappropriate deposition of insoluble calcium salts in soft tissues causes them to harden. High concentrations of aqueous Ca^{2+} will also react rapidly with phosphate, producing calcium phosphate (the main insoluble component in bone). Since the energy currency in most eukaryotic cells is ATP, there is an abundance of ATP in cellular systems (1-5mM) fuelling protein phosphorylation, which in turn is a substrate for phosphatases which liberate inorganic phosphate. This is an important reason for the tight regulation of Ca^{2+}, and it is

essential that the free Ca^{2+} concentration within the cell does not typically exceed 100 nM, to reduce the likelihood of Ca^{2+}/phosphate interaction. This is achieved via Ca^{2+} sequestering molecules and transmembrane Ca^{2+} pumps in the plasma membrane and the membrane of intracellular Ca^{2+} stores; which actively maintain a comfortable homeostasis, by expelling excessive Ca^{2+} into the extracellular milieu, or entrapping it within organelles.

Gradients of Ca^{2+} across the membrane of intracellular organelles, and across the plasma membrane, enable Ca^{2+} influx or efflux, thus generating a biological signal for the cell to react. The 'Ca^{2+} toolkit' refers to the numerous Ca^{2+} signalling mechanisms achievable in cellular systems, although not every cell has every component of the 'toolkit', suggesting that the Ca^{2+} signalling mechanisms of different cell types are tailored to suit their proper functions. The way the 'Ca^{2+} toolkit' is tailored to suit neutrophil function is not fully understood, and this thesis will discuss the relationship between Ca^{2+} influx and the localised activation of membrane-proximal cytosolic proteases.

1.6.1 Ca^{2+} homeostasis in neutrophils

The levels of cytosolic Ca^{2+} regulate important neutrophils behaviours, including extravasation, chemotaxis and phagocytosis. Ca^{2+} exists in the neutrophil cytosol, either free or bound to a Ca^{2+} chelator, and sequestered within intracellular Ca^{2+} storage organelles. The cytosolic free Ca^{2+} in healthy neutrophils is highly regulated both at rest and in the activated state. At rest, the concentration of free Ca^{2+} in the neutrophil cytosol is 100 nM (Hallett and Lloyds, 1997), whereas, extracellular Ca^{2+} concentrations exist in the milimolar range. This creates a concentration difference of 10,000-fold across the plasma membrane. This gradient is maintained by the active removal of Ca^{2+} from the cell by transmembrane Ca^{2+} pumps (Na^{2+}/Ca^{2+} exchangers (Reuter and Seitz, 1968; Blaustein and Hodgkin, 1968) and Ca^{2+}-ATPase pumps (Volpi et al., 1983), coupled with the relatively low permeability of the plasma membrane to extracellular Ca^{2+}.

Where acute fluctuations in cytosolic Ca^{2+} concentration across the cell membrane occur, they are buffered by soluble chelators sequestered within organelles such as calciosomes (Krause et al., 1989). Ca^{2+}-ATPase pumps are required to stabilise resting levels of intracellular Ca^{2+} concentration between 100-200 nM (Schatzmann, 1966). They are activated by the Ca^{2+} binding protein calmodulin (Larsen and Vincenzi, 1979; Vincenzi, 1979), which has a high affinity for Ca^{2+}. As a result of maintaining a low concentration of free Ca^{2+} in the global cytosol, Ca^{2+} that enters the cell has a significant effect on the free Ca^{2+} concentration, and thus serves as a signalling ion.

Upon neutrophil activation, the release of Ca^{2+} from intracellular Ca^{2+} stores, as well as Ca^{2+} influx across the plasma membrane, can cause the average concentration of the global cytosol to reach up to 1 µM (Demaurex et al., 1992). Because of the high Ca^{2+} buffering within the cytosol, Ca^{2+} elevations may be greatest in the subcellular domain immediately adjacent to the site of Ca^{2+} influx. Computer models by Brasen and colleagues (2010) have predicted that localised Ca^{2+} hotspots of 30 µM could exist within the cytosolic microdomains beneath neutrophil plasma membrane microridges (Brasen et al., 2010). This property means that Ca^{2+} signalling can be localised to parts of the cell periphery. This could be important in neutrophils, as they exhibit highly localised responses, such as pseudopodia extension and phagocytic cup formation. However, at the moment it is not possible to measure Ca^{2+} at this defined intra-wrinkle subdomain (see Chapter 5).

1.6.2 Ca^{2+} storage and distribution in human neutrophils

Neutrophils are anything but a 'typical' cell, particularly in regard to their Ca^{2+} signalling behaviours. The Ca^{2+} distribution in the human neutrophil is not yet fully understood, and is the subject of work presented in this thesis.

When the cytosolic Ca^{2+} level becomes high, Ca^{2+} is removed from the cytoplasm by the activity of Ca^{2+} pumps in the plasma membrane and across the membrane of intracellular organelles. Neutrophils appear to have more than

one site for storing intracellular Ca^{2+}, and these may be involved in different cellular functions, utilising different mechanisms to liberate their Ca^{2+} for secondary signalling (Pettit and Hallett, 1998). One site of high Ca^{2+} in the neutrophils is located at the perinuclear space. Typically 50% of the Ca^{2+} in an average cell is sequestered within the nucleus (Hallett and Campbell, 1983), and antimony staining of neutrophils has revealed that the nucleus is indeed a Ca^{2+} hotspot (Hoffstein 1979; Cramer and Gallin, 1979), with the juxtanuclear space implicated as a Ca^{2+} storage site. A second site of localised Ca^{2+} concentrations in neutrophils is in the peripheral cytosol beneath the plasma membrane. High levels of sub-membranous Ca^{2+} concentration were identified beneath the plasma membrane in neutrophils (Pettit and Hallett, 1996a, 1996b, 1995, 1997; Al-Mohanna et al., 1997) using the Ca^{2+} chelator chlortetracycline which binds to Ca^{2+} with a K_d of 0.4 mM (Caswell, 1979). When bound to Ca^{2+} it becomes membrane impermeable, and will accumulate within the cell where there is high Ca^{2+}. This sub-membranous location of high Ca^{2+} concentration may also play a role in the activation of β_2-integrins (Pettit and Hallett, 1998) during cell arrest and extravasation. Approximately 95% of the Ca^{2+} in the neutrophil can be accounted for in regions of high Ca^{2+} concentration at the cell periphery and the juxtanucelar site (fig. 1.6.2), which may function as physiological Ca^{2+} storage sites.

It is now also understood that neutrophils possess a much more substantial mitochondrial system than previously thought (Fossati et al., 2003), and these organelles may also act as conventional intracellular Ca^{2+} storage sites in neutrophils (Montero et al., 2004). Other small mobile organellular structures resembling the sarcoplasmic reticulum of muscle cells or calciosomes (Volpe et al., 1988; Krause et al., 1989; Favre et al., 1996a,b) are estimated to contain up to 5% of cellular Ca^{2+} concentration in neutrophils.

Where Ca^{2+} is sequestered within the cell for future signalling capabilities, it is sequestered into 'calciosomes', small Ca^{2+} storage organelles via the sarco-endoplasmic reticulum Ca^{2+}-ATPase (SERCA) pumps. Neutrophils express several isoforms of the SERCA proteins, including SERCA III (Lominadze et al., 2005) and

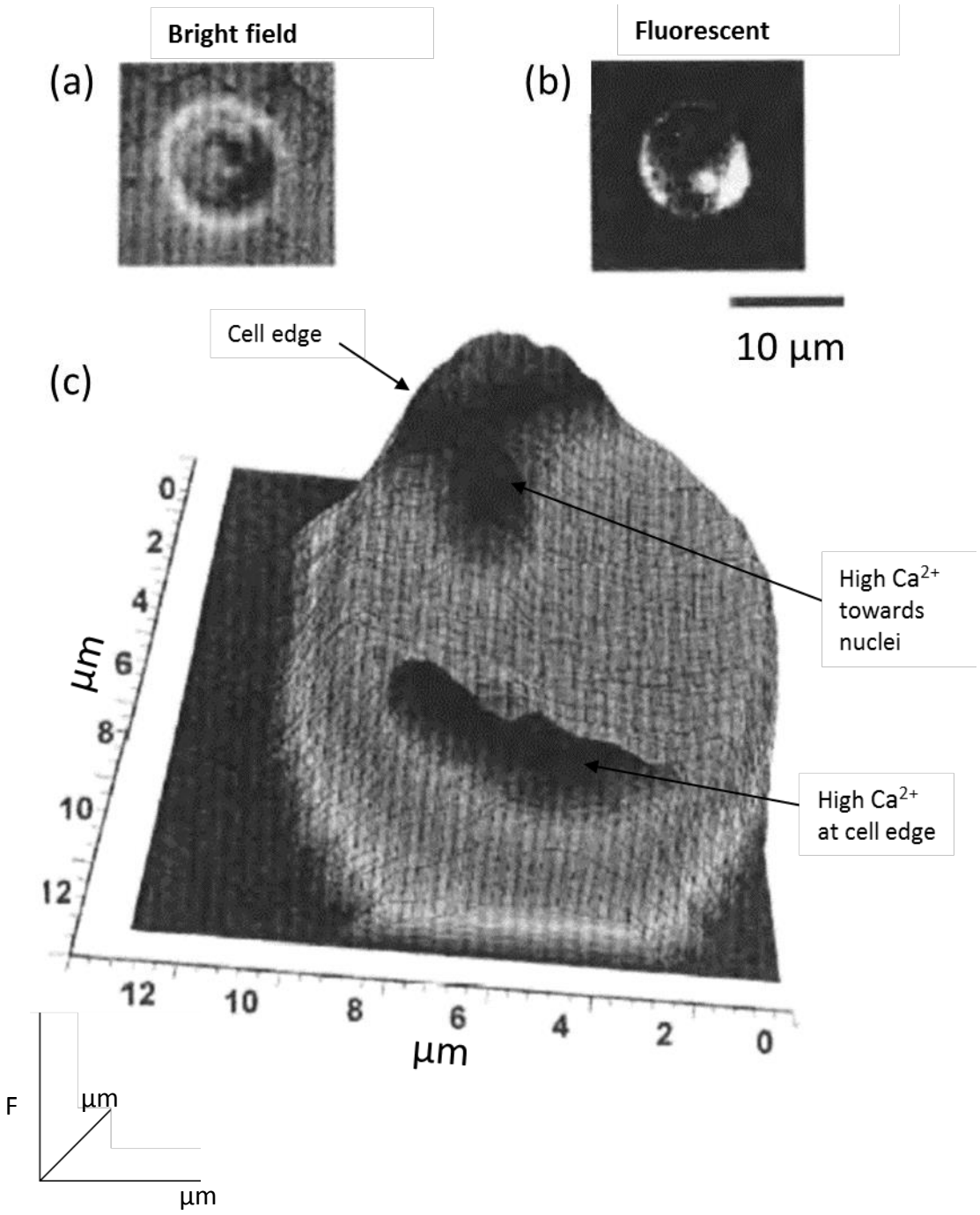

Figure 1.6.2: Ca^{2+} distribution in the neutrophil

Physiological Ca^{2+} stores in a resting neutrophil identified by chlortetracycline fluorescence (1:50 chlortetracycline in DMSO, 45 mins). **(a)** Bright-field and **(b)** fluorescent images. **(c)** Ca^{2+} intensity map across 2D image. Chlortetracycline distribution shows regions of high Ca^{2+} concentration at the cell edge and centrally close to nuclei. (Amended from Al-Mohanna, 1997).

SERCA IIb which was found to be specifically associated with 'calciosome' organelles (Favre et al., 1996a). The 'calciosome' storage organelles also contain abundant proteins with Ca^{2+} binding properties, such as calreticulin (Favre et al., 1996a; Krause et al., 1989; Stendahl et al., 1994; Volpe et al., 1988), for sequestering Ca^{2+} within the membrane-bound structures. They also have receptors for the soluble secondary messenger inositol 1,4,5-trisphosphate (IP_3), which is important in the signal transduction involved during the biphasic Ca^{2+} response in neutrophils.

1.6.3 Ca^{2+} signalling in human neutrophils

Neutrophils are autonomous cells. Therefore in order to coordinate a unified response amongst a population sensing the same chemical stimuli, the signalling cascade within each neutrophil must involve a multitude of complex interactions. Neutrophils are equipped with an array of cell surface receptors, and the way in which their activation brings about a secondary Ca^{2+} signalling response varies. It is worth exploring some of these behaviours in detail, since this will provide some background for the experimental approach and results presented in subsequent chapters.

Neutrophils are non-excitable cells and represent a specific niche of cell behaviour. They respond to a vast array of different stimuli via engagement with a number of different types of receptor. In the 1960s Woodin and Weineke demonstrated that neutrophils treated with Streptolysin A became activated. They concluded this was due to increased membrane permeability to Ca^{2+}, thus indicating an important role of cytosolic Ca^{2+} signalling in neutrophil signalling and activation (Woodin and Wieneke, 1963; 1964). Since then much work has been carried out to investigate the mechanisms of Ca^{2+} entry and Ca^{2+} store release in neutrophils.

Classically, the large rise in the cytosolic Ca^{2+} concentration of neutrophils, which occurs when they are stimulated, involves a biphasic Ca^{2+} response. An initial

rise in cytosolic Ca^{2+} is achieved by release from intracellular Ca^{2+} storage organelles, followed by an influx of Ca^{2+} ions from the extracellular milieu. The typical concentration of extracellular Ca^{2+} concentration is around 1 mM, which generates a 10,000 fold concentration gradient across the cell membrane, where the resting intracellular Ca^{2+} concentration is around 100 nM (Hallett and Lloyds, 1997). The result is an overall 10-fold increase in cytosolic Ca^{2+} concentration in the neutrophil cytosol (Demaurex et al., 1992). This is possibly the most dramatic change in intracellular chemical properties that the neutrophil experiences and is a significant event for the cell, being necessary for a number of neutrophil effector functions (Hallett and Campbell, 1984).

1.6.3.1 G protein coupled receptors

G protein coupled receptors (GPCRs) are a family of seven transmembrane (7TM) receptors on the surface of many different cell types. Neutrophils have a number of heterotrimeric pertussis toxin-sensitive GPCRs, of the $G_{i/o}$ family, which recognise a wide range of chemoattractants including: the bacterial peptide fMLP, LTB4, C5a and PAF (Futosi et al., 2013). Engagement of the receptors with their respective ligands causes a dissociation of the Gαβγ subunits on the inner leaflet of the plasma membrane.

GPCR activation in neutrophils triggers a biphasic Ca^{2+} signal (fig. 1.6.3.1). The first phase is mediated by activation of phospholipase C β (PLCβ), which cleaves phosphatidylinositol 4,5-bisphosphate (PIP_2) to produce IP_3 and diacylglycerol (DAG). DAG remains associated with plasma membrane phospholipids, whilst IP_3 translocates to intracellular Ca^{2+} stores where it engages with the IP_3 receptor (IP_3R) to release sequestered Ca^{2+} into the cytosol. There is a slight delay between GPCR activation by extracellular ligand, and the subsequent increase in cytosolic Ca^{2+} levels from both intracellular store release and from Ca^{2+} influx across the plasma membrane (Pettit and Hallett, 1998a,c; Favre et al., 1996b). This delay correlates with the diffusion of IP_3 signalling molecules from the plasma membrane to the Ca^{2+} stores (Hallett and Lloyds, 1997). The Ca^{2+} liberated from IP_3 sensitive Ca^{2+} stores can activate the plasma membrane

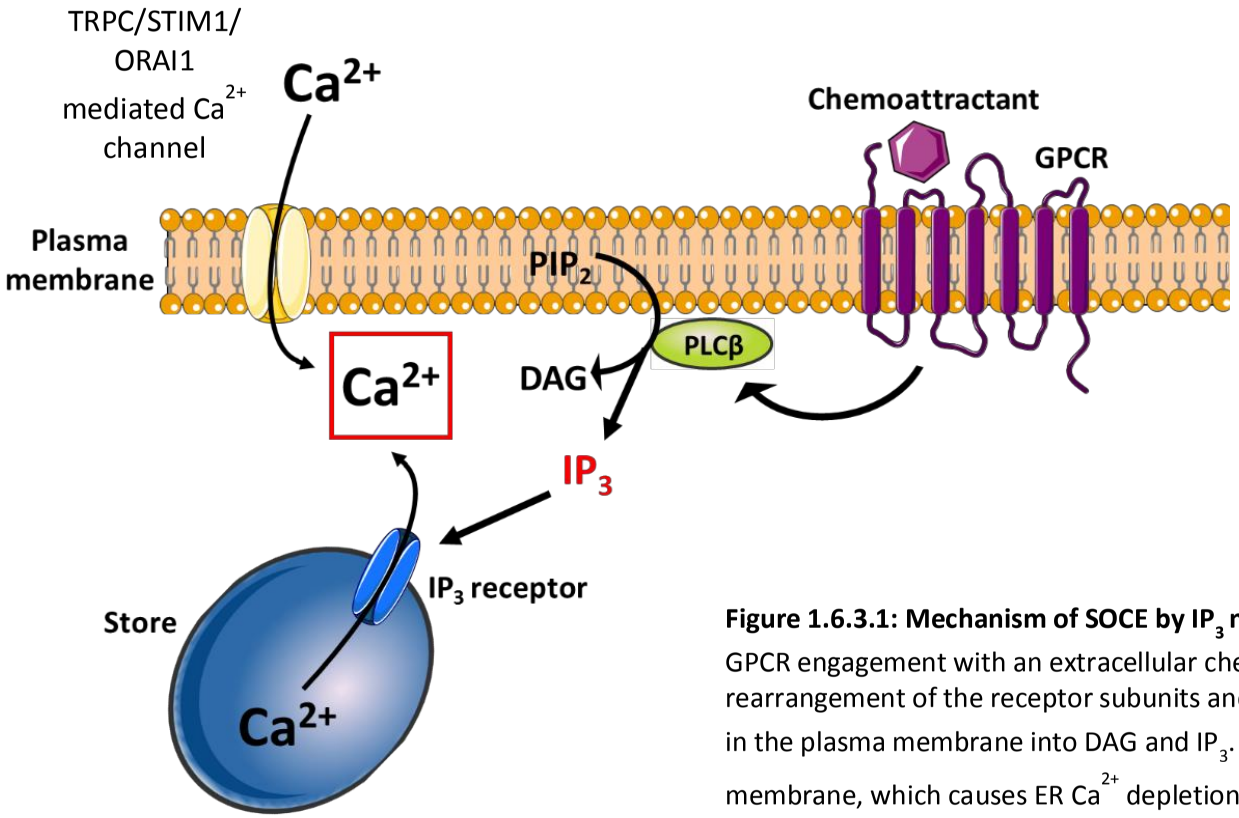

Figure 1.6.3.1: Mechanism of SOCE by IP_3 mediated Ca^{2+} signalling

GPCR engagement with an extracellular chemoattractant (e.g. IL-8) causes a rearrangement of the receptor subunits and activates PLCβ. PLCβ cleaves PIP_2 in the plasma membrane into DAG and IP_3. IP_3 activates the IP_3R on the ER membrane, which causes ER Ca^{2+} depletion and store operated Ca^{2+} influx (via SOCE) across the plasma membrane. SOCE may be mediated by functional interactions between TRPs and STIM1/ORAI1 forming Ca^{2+} channels in the plasma membrane (Liao et al., 2007). (Drawn using Servier Medical Art.)

channel Melastatin-related Transient Receptor Potential cation channel 2 (TRPM2) (Du et al., 2009). As such, it is suggested that this may be one mechanism that facilitates the secondary Ca^{2+} influx phase, which occurs after intracellular store release.

1.6.3.2 Fc receptor and integrin mediated Ca^{2+} signalling

Neutrophils have both FcRs, which recognise IgG-opsonised pathogens, and integrin receptors which recognise both molecules expressed on the surface of endothelial cells during transmigration, and C3bi-opsonised pathogens. Both types of receptor are activated by cross-linking, which generates an intracellular Ca^{2+} signal (Pettit and Hallett, 1998a,b, 1996a) through separate yet similar mechanisms to GPCR mediated Ca^{2+} release.

Neutrophils express a number of integrins which are involved in cell-cell adhesion and the process of transendothelial migration. The integrin family are a group of heterodimeric transmembrane glycoproteins, and are expressed on almost all mammalian cells, but the most important type expressed on the neutrophil cell surface is the β_2 integrin family member CD11b/CD18 (Hellberg et al., 1996), which is significant in neutrophil adhesion, migration and phagocytosis (Anderson and Springer, 1987). During inflammation, CD11b/CD18 on the neutrophil interacts with ICAM-1 on endothelial cells and C3bi opsonised pathogens (Plow et al., 2000). This stimulates downstream tyrosine kinase dependent release of Ca^{2+} from IP_3-sensitive intracellular stores, via Phospholipase C y2 (PLCy2) activity which in turn cleaves PIP_2 to generate DAG and IP_3 (Hellberg et al., 1996). A secondary global Ca^{2+} signal is achieved by Ca^{2+} influx through plasma membrane channels (Davies and Hallett, 1995a,b).

Neutrophils also have other classes of FcR on their surface, but the most important FcRs on neutrophils belong to the class of low affinity FcγRs (Bruhns, 2012). The primary role of these receptors (including FcγRIIA and FcγRIIIB) is the recognition of and engagement with IgG-opsonised pathogens for removal by phagocytosis. Upon activation by extracellular ligands, the receptors undergo

conformational changes. Cross-linking of the cytoplasmic tails of both FcγRs and integrins triggers the Src-family kinases to phosphorylate the immunoreceptor tyrosine-based activation motif (ITAM) domains, recruiting the Syk tyrosine kinase to the plasma membrane (Mocsai et al., 2002, 2010). Activation of Syk leads to further signalling pathways inside the cell, including activation of PLCγ2 (Jakus et al., 2009) and PI3K isoforms essential for neutrophil effector functions (Kulkarni et al., 2011), and also Ca^{2+} release from IP_3-sensitive intracellular stores (Davies and Hallett, 1995b).

Both mechanisms of activation display a lag time between receptor stimulation and the Ca^{2+} signal, which can be explained by the time taken for receptors to laterally diffuse along the plasma membrane in order to form aggregates which are able to generate the Ca^{2+} response (Roberts et al., 1997). There is a delay (~500 ms) in generating the Ca^{2+} signal by soluble stimuli, such as fMLP which also triggers IP_3-dependent Ca^{2+} release from intracellular Ca^{2} stores, and is followed by the larger Ca^{2+} influx across the plasma membrane (Pettit and Hallett, 1995). In contrast, when neutrophils are stimulated by the cross-linking of integrin receptors in the plasma membrane, the lag time in Ca^{2+} influx is longer, and a second Ca^{2+} influx occurs ~10-100 s after the initial liberation of Ca^{2+} from storage sites (Pettit and Hallett, 1996b). Therefore, it is possible that initial release of Ca^{2+} comes from different Ca^{2+} storage locations, depending on the mechanism of neutrophil activation, in order to achieve the desired effector function of the neutrophil, e.g. chemotaxis vs. cell arrest/spreading.

Downstream Ca^{2+} signals are inhibited in the presence of tyrosine phosphorylation inhibitors (Morgan et al., 1993) as well as small molecule inhibitors of protein L-plastin (Rosales et al., 1994) which suggests that the actin cytoskeleton also plays an important role in signal transduction from the plasma membrane.

1.6.4 Ca^{2+} influx through plasma membrane channels

Significant changes in cytosolic Ca^{2+} concentration occur when Ca^{2+} channels in the plasma membrane are opened. There are three main groups of Ca^{2+} channel, which can be categorised based on their mechanism of activation, they are: (i) receptor operated channels (ROCs), (ii) voltage operated channels (VOCs) and (iii) store operated channels (SOCs).

(i) ROCs are found in non-excitable cells, including endothelial cells. The receptors can be activated either by ligation of the extracellular domains (e.g. with ATP, glutamate and acetylcholine) or the intracellular domains (e.g. with aracadonic acid or DAG). Binding of a ligand with the ROC induces a conformational change in the tertiary structure of the receptor which causes the channel to open enough to enable Ca^{2+} ions to flow into the cell along a concentration gradient. The ROCs can also be coupled with downstream activator proteins, such as kinases and phosphatases, which also become activated upon ROC engagement with a ligand.

(ii) VOCs are expressed in excitable cells, such as muscle cells and neurons, which respond to a change in potential difference across the cell plasma membrane. Depolarisation of the plasma membrane in these cells causes a conformational change in the receptor, and facilitates Ca^{2+} entry into the cell. Neutrophils require voltage-gated proton channels to produce ROS via the electrogenic enzyme NADPH oxidase (Henderson et al., 1987), but not for global Ca^{2+} influx across the plasma membrane (Demaurex et al., 1994).

(iii) SOCs facilitate Ca^{2+} influx across the plasma membrane in coordination with Ca^{2+} release from intracellular stores, and are also known as Ca^{2+} release activated Ca^{2+} channels (CRACs). The interaction between the two Ca^{2+} release mechanisms is logical, since opening of Ca^{2+} channels in the plasma membrane, following the depletion of intracellular stores, is necessary to replenish the stores

for future activity. The mechanism of store operated Ca^{2+} entry (SOCE) is recognised as the primary mechanism of Ca^{2+} entry into neutrophils (Davies and Hallett, 1998).

Inhibition of VOCs does not prevent Ca^{2+} influx across the plasma membrane (Demaurex et al., 1994) therefore the predominant Ca^{2+} channels involved in influx across the plasma membrane are not thought to be voltage-gated. Furthermore, neutrophil Ca^{2+} channels are not activated by engagement with extracellular ligands. Instead, their activity is closely linked to the Ca^{2+} status of intracellular Ca^{2+} stores (von Tscharner et al., 1986). When stores are depleted, the channels open and Ca^{2+} ions flood into the cell down the concentration gradient (via SOCE). Inhibition of the Ca^{2+} influx through plasma membrane Ca^{2+} channels prevents neutrophils from carrying out downstream effector functions (Hallett and Campbell, 1984; Marks and Maxfield, 1990a,b).

While SOCE has long been recognised as the predominant mechanism of Ca^{2+} entry in neutrophil cell signalling (Pettit and Hallett, 1998a,b; Itagaki et al., 2002), unravelling the complexities of the mechanism has taken several years, mainly due to the lack of specific SOCE inhibitors and reliance on the artificial manipulation of external Ca^{2+} concentrations. Over the last two decades, significant advances have been made with the discovery of two Ca^{2+}-sensing proteins, Stromal interaction molecule 1 (STIM1) (Zhang et al., 2005) and ORAI Ca^{2+} release-activated Ca^{2+} modulator 1 (ORAI1) (Prakriya et al., 2006), and with them the ability to study the consequences of genetic mutations in these two molecules.

STIM1 is a Ca^{2+} sensing protein on the ER membrane, which undergoes a conformational change in low Ca^{2+} conditions. When Ca^{2+} stores are high, The N-terminal luminal EF-hand domain of STIM1 binds Ca^{2+}. Depletion of Ca^{2+} from intracellular stores causes dissociation of Ca^{2+} ions from the ER-luminal domains, and a clustering of STIM1 molecules at ER/plasma membrane proximal sites in the ER membrane (Soboloff et al., 2012) (fig. 1.6.4). This enables direct

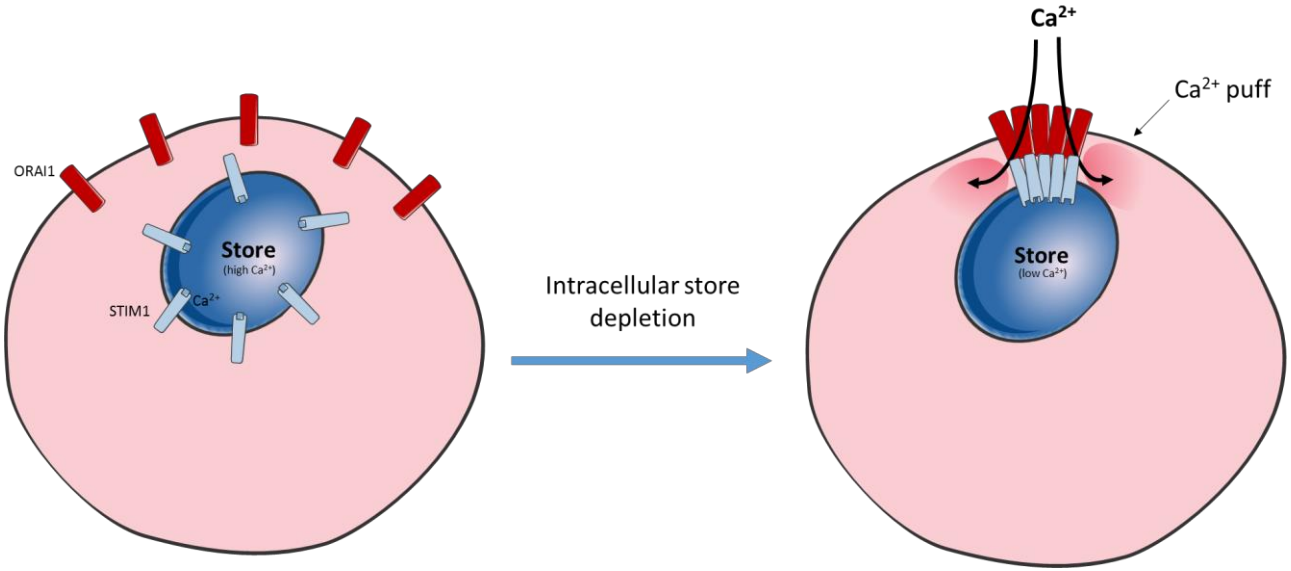

Figure 1.6.4: Schematic of STIM1/ORAI1 interaction

At rest the ER Ca^{2+} stores are full and the Ca^{2+}-sensing N-terminal domain of STIM1 is Ca^{2+} bound. Ca^{2+} saturated STIM1 molecules are evenly distributed across the ER membrane. Inactive ORAI1 channels are also evenly distributed across the plasma membrane. When the Ca^{2+} concentration within the ER lumen drops, due to Ca^{2+} release, Ca^{2+} dissociates from the ER-luminal Ca^{2+}-sensing EF-hand of STIM1, which causes it to move laterally within the ER membrane and form STIM1 aggregates at sites of ER-plasma membrane puncta. STIM1 aggregates interact with ORAI1 channels in the plasma membrane which cluster to facilitate Ca^{2+} influx into the cell, generating Ca^{2+} hotspots near sites of Ca^{2+} entry (Luik et al., 2006). (Adapted from Mancarella et al., 2011, drawn using Servier Medical Art.)

engagement between STIM1 and ORAI1 channels on the plasma membrane (Roos et al., 2005; Zhang et al., 2005). Clustered STIM1 molecules bind to the STIM1-binding site on the C-terminal domain of ORAI1, triggering a conformational change in the core of ORAI1 which is sufficient for channel gating (Zhou et al., 2016). This facilitates the formation of puncta sites between the ER membrane and the plasma membrane. Activation of ORAI1 by its intracellular ligand STIM1 plays a significant role in SOCE, triggering CRAC channels to open and facilitating Ca^{2+} influx (Zhang et al., 2005) to refill intracellular stores (Feske, 2007; Hogan et al., 2010).

Neutrophil activation and inflammatory response functions such as phagocytosis, neutrophil rolling arrest and transendothelial migration may be regulated by the activity of SOCE via ORAI1 and STIM1 interaction (Schaff et al., 2010; Steinckwich et al., 2011). Studies in mice have found that *Stim1*$^{-/-}$ knock-out neutrophils show almost complete inhibition of Ca^{2+} influx stimulated by receptor cross-linking, and displayed a 50-70% reduced ability to perform phagocytosis of opsonised *Staphylococcus aureus* (Zhang et al., 2014). This suggests that in mouse neutrophils, mutations in STIM1/ORAI have a significant effect on neutrophil function and therefore immunodeficiency (Clemens and Lowell, 2015).

Surprisingly, STIM1/ORAI1 deficient human neutrophils exhibit normal Ca^{2+} responses, chemotaxis, adhesion, ROS production and phagocytosis (Elling et al., 2016). Furthermore, STIM1/ORAI1 depletion only mildly diminishes the SOCE activity, but does not abrogate Ca^{2+} influx in the same way as Ca^{2+} chelators. Taken together, the implication is that an alternative Ca^{2+} channel may also be contributing to SOCE in neutrophils, and this suggests that neutrophils may have multiple mechanisms for generating intracellular Ca^{2+} signals. This is not unlikely since phagocytes are the first line of defence against invasive pathogens, neutrophils may have evolved mechanisms to circumnavigate the Ca^{2+} blocking activity of intracellular pathogens such as *Leishmania*, *Franciscella* and *Mycobacterium tuberculosis*, during phagocytosis (Demaurex and Nunes, 2016).

Mouse knock-out models have also revealed that the two proteins are both important but have different significances in conferring the ability of neutrophils to carry out typical cellular functions. For example ORAI1, but not STIM1, is necessary to achieve Ca^{2+} influx following ROC/agonist interaction during neutrophil migration; whilst STIM1 is crucial to SOCE (Zhang et al., 2014).

Prior to the identification of ORAI1, it was suggested that the TRP family of Ca^{2+} channels, including TRPM2 (Du et al., 2009), were responsible for CRAC. Indeed, more recently TRPM2 has been found to mediate the efflux of cations across the phagosomal membrane during phagosome maturation (Di et al., 2017). Thus TRPM2 is essential for the proper functioning of phagocytosis, and may also be an important key player together with STIM1/ORAI1, in mediated Ca^{2+} influx (Liao et al., 2007) involved in the second stage of the biphasic Ca^{2+} signal.

1.6.5 Measuring cytosolic Ca^{2+} levels

Cytosolic free Ca^{2+} is commonly measured in live cells using fluorescent calcium chelators conjugated to acetoxymethyl esters (AM), which make the probes lipid soluble, masking the Ca^{2+} binding site and enabling them to diffuse across the cell membrane. Non-specific esterases in the cell cytosol cleave the ester linkage, revealing the Ca^{2+} binding site and also rendering the probe hydrophilic. This effectively engineers the equilibrium of diffusion to favour movement of the probe across the plasma membrane and into the cell, where it then becomes trapped in the cytoplasm and can report Ca^{2+} concentration (Hallett and Lloyds, 1997). This also prevents the probe from being lost from the cell, enabling an accurate measurement of the Ca^{2+} within the cell.

Fura-2-AM is one such traditionally used probe, with a K_d of approximately 200 nM. Since the resting Ca^{2+} concentration in neutrophils is considered to be 100 nM, Fura-2-AM allows detection of Ca^{2+} fluctuations in the mid-physiological range. Extraction of data from Ca^{2+} measurements using Fura-2 requires ratiometric imaging, since both the bound and un-bound forms are fluorescent, and excited at different wavelengths (Tsein and Poenie, 1986). However, the

wavelengths for excitation are in the UV spectrum, which is problematic in neutrophils because they contain many small molecules which may become activated in response to UV light, such as NAD(P)H (Monsel et al., 2014).

An alternative probe which avoids this problem, is Fluo4. With a Ca^{2+} affinity of around 345 nM (Gee et al., 2000) its fluorescence increases around 100-fold in the Ca^{2+} bound form, making it useful to measure sensitive changes in Ca^{2+} concentration. Fluo4 is excited by longer wavelengths (488 nm), which also reduces the occurrence of auto fluorescence. Fluo4 does not induce a shift in the emission wavelength when binding Ca^{2+}, and therefore fluorescence must be visualised using confocal microscopy techniques and optical slicing (Hallett and Lloyds, 1997).

The probes described here diffuse through the cytosol, and therefore report the Ca^{2+} concentration across the global cytosol. However, it is known that some cell types display patterns of cytosolic Ca^{2+} signalling, including waves and oscillations (Rooney and Thomas, 1993), and the cytosolic Ca^{2+} concentration in cells is not uniform across the cytosol. Presently there is no established method for measuring changes in Ca^{2+} concentration at discrete sub-membranous cytosolic locations in single cells, which would be useful to identify the existence of transiently high Ca^{2+} concentrations which are important in the Ca^{2+}-regulated activity of some cytosolic enzymes.

1.6.6 Ca^{2+}-regulated enzymes in neutrophils

It has been highlighted that Ca^{2+} signalling is very important for enacting the appropriate response to extracellular stimuli. One possible effector of Ca^{2+} signalling in neutrophils, is the enzyme calpain. The calpain family of proteases become activated upon sensing high concentrations of cytosolic Ca^{2+}, and their engagement has been reported in the migration of neutrophils (Saez et al., 2006). It has been proposed that calpains may have important roles in regulating neutrophil behaviour; particularly in the morphological rearrangements that enable neutrophils circulating in a spherical shape to spread during adhesion to

endothelial cells during transendothelial migration, and the projection of pseudopodia during engulfment of foreign particles in phagocytosis. Calpains may also be involved in detachment of neutrophils from the extracellular matrix by lysis of adhesion complexes, and play a role in neutrophil apoptosis pathways. However, the role of Ca^{2+}-regulated calpain activity in neutrophil functions, specifically morphology changes, is not fully understood. Since this mechanism presents possibilities for small molecule therapeutic intervention to control neutrophil activity in autoimmune disease, it is important that calpain activity in neutrophils is explored.

1.7 μ-Calpain

The calpain family consists of several Ca^{2+} activated cysteine proteases, within the larger papain super-family (Murachi et al., 1980; Berti and Storer, 1995). The name calpain is derived from calmodulin and papain, in a nod to its Ca^{2+} interacting and proteolysing properties respectively. It was first purified from soluble fractions of rat brain in in the 1960s (Guroff, 1964). Although the calpains are a relatively large protein family, with 15 known isoforms, the two most studied members are μ-calpain (also known as calpain-1) and m-calpain (also known as calpain-2), which share 62% sequence similarity (Imajoh et al., 1988). The two calpains were named μ-calpain and m-calpain because of the differences in their sensitivity to Ca^{2+} concentration; ~20-60 μM and ~0.3-1.3 mM respectively (Goll et al., 2003). These concentrations were experimentally found to activate the two calpain isoforms *in vitro*, however, both concentrations exceed the levels of cytosolic free Ca^{2+} found *in vivo*, initially suggesting a role for other modulatory factors in the intracellular activation of calpains.

Both μ-calpain and m-calpain are ubiquitously expressed cytosolic proteases in vertebrates (Johnson, 1990; Hayashi et al., 1999), and are known as modulator proteases because of the way they alter the activity of their substrates. Unlike caspases and proteasomes, calpains do not hydrolyse their protein substrates to

destruction. Instead, they modify the activity or the behaviour of the protein, with consequences on cellular function (Ono and Sorimachi, 2012). This thesis will focus on the intracellular activity of μ-calpain, the predominant isotype of calpain found in neutrophils (Goll et al., 2003).

1.7.1 Structure of μ-calpain

μ-calpain is involved in many different physiological processes. However, elucidating its precise role in neutrophils has proved difficult to achieve experimentally, mainly because of the need for specific calpain inhibitors (Carafoli and Molinari, 1998), and the difficulty in generating crystals for structural determination by x-ray crystallography. To date, the structure of full length μ-calpain has not yet been solved by crystallography, however the structure of m-calpain and a μ-calpain/m-calpain hybrid have proved useful in the study of calpain domain interactions (Wendt et al., 2004).

μ-calpain is a heterodimeric protein composed of a large 80 kDa subunit (CAPN1), with proteolytic activity, encoded on chromosome 1, and a smaller 28 kDa regulatory subunit (CAPNS1) which is also common to m-calpain, encoded on chromosome 19 in humans (Aoki et al., 1986; Imajoh et al., 1988; Goll et al., 2003; Sorimachi et al., 2011) (fig. 1.7.1). The two subunits of μ-calpain are further sub-divided into smaller domains, with different properties (fig. 1.7.1). Presently, the only full-length calpain structures have been solved with m-calpain, although these have made the classification of common subdomains possible. For example the small regulatory subunit, common to both, contains domains V and VI, of which domain VI has a calmodulin-like domain consisting of five EF hand motifs which bind Ca^{2+} (Blanchard et al., 1997; Ohno et al., 1986).

Domain I of the larger proteolytic subunit does not have any sequence homology to any other protein. The catalytic activity of μ-calpain arises from its catalytic triad of histidine, asparagine and cysteine in domain II of the larger subunit, which together attack the carbonyl group of the targeted substrate peptide

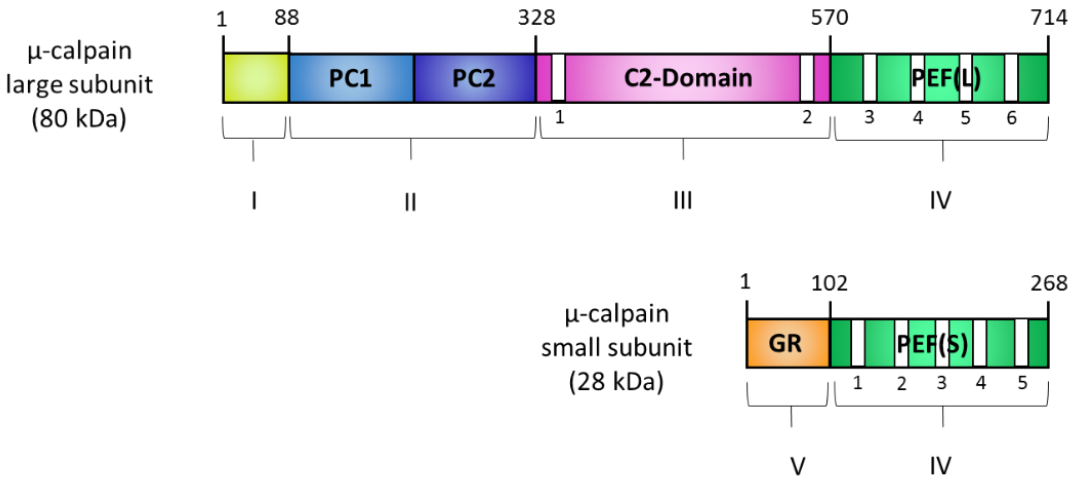

Figure 1.7.1: Structure of μ-calpain
Schematic diagram of the structure of human μ-calpain CAPN1 (large subunit) and CAPNS1 (small subunit), with domain regions predicted from its amino acid sequence. The large subunit is made up of three smaller subunits. The N terminal domain of CAPN1 (yellow) is an alpha helix; domain II forms the Proteolytic Core, known as CysPc, and is itself divided into two halves (PC1 and PC2); domain III resembles the C2 phospholipid binding domains of phospholipases; domain IV is the Ca^{2+} binding domain containing four of the six EF-hand motifs (white bars). The smaller subunit is made up of two subdomains. The N-terminal contains a glycine rich domain (GR), and another Ca^{2+} binding domain, with five EF-hand motifs. Figure adapted from Goll et al., 2003.

bond by hydrolysing it (Goll et al., 2003; Polgar, 1989). However, at present the preferred cleavage site among substrates of μ-calpain is unknown. Domain II is also the region that interacts with the endogenous calpain inhibitor, calpastatin. Domain III of the large subunit may have some regulatory function, as it resembles a C2-like domain and enables μ-calpain to translocate to the plasma membrane through binding to phosphatidylserine. This allows μ-calpain to associate with the plasma membrane in regions of elevated Ca^{2+} concentration (Tompa et al., 2001). The fourth domain of the large subunit, IV is partially homologous to the Ca^{2+} binding protein calmodulin, and contains four EF motifs (Goll et al., 2003), similar to domain VI of the smaller subunit.

The only characterised endogenous calpain inhibitor is calpastatin, which acts exclusively on both μ-calpain and m-calpain (Wendt et al., 2004; Saez et al., 2006). Inhibition of calpain by calpastatin is irreversible, and requires calpain to be in the active state bound to Ca^{2+} (Otsuka and Goll, 1987). This suggests that *in vivo* calpastatin mediated inhibition occurs to 'switch-off' or limit calpain activity once activated. This may be an important regulatory mechanism, since calpain is a cytosolic protein with multiple substrates, therefore unregulated calpain activation could prove detrimental to the cell. Indeed, calpain activity has been implicated in the process of apoptosis (Squier et al., 1994), and neuronal degeneration (Wingrave et al., 2003). Calpastatin is made up of five domains, which make up three regions of inhibitory activity. A number of peptide based inhibitors have been designed to inhibit calpains, based on the sequence of the inhibitory region B of calpastatin. The regulation of μ-calpain activation by Ca^{2+} will be explored in detail in this thesis.

1.7.2 μ-calpain activation by Ca^{2+}

Ca^{2+} signalling in neutrophils has previously been discussed. It is thought that μ-calpain is a key enzyme which is activated in neutrophils, upon Ca^{2+} influx. μ-calpain is involved in the mechanism which facilitates migration in many cells, including neutrophils (Saez et al., 2006), and there is convincing evidence that μ-

calpain activation is important in the morphological changes that neutrophils undergo during adhesion and detachment from the extracellular matrix. This has further suggested the involvement of μ-calpain in the regulation of neutrophil behaviour; to complete cellular functions such as phagocytosis, chemotaxis and cell spreading for extravasation. μ-calpain-mediated regulation of neutrophil function is therefore a possible target for therapeutic intervention. However, the question of μ-calpain activation in neutrophils remains. μ-calpain has a K_d of ~20-60 μM Ca^{2+}, which as previously discussed is much higher than the Ca^{2+} concentration of the global cytosol. With a broad range of many different substrates, it is therefore important that μ-calpain activation is tightly regulated, both spatially and temporally.

Both μ-calpain and m-calpain are found exclusively in the cell cytoplasm, although their distribution throughout the cytosol varies depending on the cell type and the nature of its activity. In unstimulated cells, calpains are found to be located in cytosolic regions close to the nucleus (Gil-Parrado et al., 2003). However, being cytosolic, calpains are able to move in response to soluble signals, and may coordinate translocation to peripheral regions of cytosol close to the plasma membrane in response to elevated Ca^{2+}, through their C2-like domains (Goll et al., 2003). This relocation is observed when cells are artificially stimulated with Ca^{2+} ionophores. This suggests that calpain activity is required at the cell periphery upon cell activation and during Ca^{2+} signalling. In human neutrophils, it has been predicted that the Ca^{2+} concentration during influx reaches high enough concentrations to activate μ-calpain located beneath plasma membrane microridges (Davies and Hallett, 1998; Brasen et al, 2010), although this has not been possible to measure experimentally. It seems likely that the location of Ca^{2+} hotspots may correlate with areas of μ-calpain activity during Ca^{2+} influx and neutrophil effector functions.

μ-calpain is inactive at cytosolic Ca^{2+} concentrations, in the range 50-100 nM (Pietrobon et al., 1990), and exists as a pro-enzyme. Under physiological conditions, μ-calpain becomes activated by transient cytosolic domains of high

Ca^{2+} concentration, which regulate its activity in cooperation with the endogenous inhibitor calpastatin, in regions of the cell where μ-calpain activity is required for appropriate cell function (Suzuki and Sorimachi, 1998). It is understood that Ca^{2+} binding to the calmodulin-like domain of μ-calpain reduces the Ca^{2+} concentration required for calpain activation, and can trigger autolysis of the N-terminal domains of both μ-calpain subunits. This causes dissociation of the subunits in the pro-enzyme, generating an active μ-calpain protein (Suzuki and Sorimachi, 1998). The proteolytic activity of μ-calpain is derived from its catalytic triad. In un-activated (i.e. unbound to Ca^{2+} calpain), the triad is not fully formed. Upon Ca^{2+} binding to the EF-hands, the protein undergoes a conformational change and reorganises the arrangement of the active site to assemble a functional catalytic triad (Hosfield et al., 1999a,b). The concept of calpain autolysis in calpain activation has been controversial. It is known that both m- and μ-calpain will perform autolysis when incubated with activating Ca^{2+} concentrations (Cong et al., 1993). However, oxidation of μ-calpain has been found to inhibit its proteolytic, but not its autolytic activity (Guttmann et al., 1997), suggesting that the two events are not connected and that autolytic calpain activity is not involved in the mechanism of calpain activation. Another two-step mechanism has been proposed, whereby Ca^{2+} binding to the EF motifs may bring about subtle conformational changes in domains IV and VI. This may promote disassociation of the larger and smaller subunits, leading to reorganisation of the catalytic site (Khorchid and Ikura, 2002). In either case, a two-step mechanism for μ-calpain activation introduces another safety measure to protect the cell against unregulated μ-calpain activity.

A second mechanism of calpain activation proposes that high cytosolic Ca^{2+} concentrations trigger inactive calpain to translocate to the cell edge, where it becomes activated by association with phospholipids in the cell membrane (Suzuki and Sorimachi, 1998). Furthermore, conversion of the 80 kDa proenzyme to a 76 kDa active enzyme occurs upon μ-calpain interaction with the cytoplasmic face of the cell membrane (Hayashi et al., 1999), suggesting that autolysis occurs during the process of calpain activation at the cell membrane. In

both instances a rise in cytosolic Ca^{2+} is involved in μ-calpain activation, and these activities place active μ-calpain in the vicinity of membrane-skeletal binding proteins which may be involved in enabling morphological changes. It is therefore of interest to investigate the relationship between Ca^{2+} concentration, μ-calpain activation and the downstream modification of μ-calpain substrates, in the regulation of neutrophil functions, which rely on morphological changes at the cell membrane.

1.7.3 μ-calpain substrates

More than 100 substrates of μ-calpain have been discovered and recorded following numerous *in vitro* assays. They can be broadly categorised into three main groups, including (i) transcription factors, (ii) kinases/phosphatases, (iii) cytoskeletal and membrane associated proteins (Goll et al., 2003). Of these groups, it is the relationship between μ-calpain and the cytoskeletal binding proteins that is of particular interest to the mechanism of neutrophil morphology change. Presently, there is no commonly recognised μ-calpain cleavage site among μ-calpain substrates.

The main role of μ-calpain activity in neutrophils appears to be associated with the cytoskeletal reorganisations that occur during cell shape changes. μ-calpain-mediated cleavage of the β-integrin family proteins is a prelude to disassembly of the focal adhesion molecule (Pfaff et al., 1999), and talin cleavage also seems to be important in their turnover, since μ-calpain deficiency decreases the number of focal adhesions (Lebart and Benyamin, 2006).

μ-calpain mediated cleavage of membrane-linker proteins is also significant in the context of cell spreading. Although there is currently no recognised μ-calpain cleavage site, μ-calpain cleaves the ezrin/radixin/moesin (ERM) family protein ezrin, but not moesin (Shcherbina et al., 1999). This displays a level of selectivity for ezrin as a substrate, rather than its structurally and functionally similar cousin moesin, which indicates that a sensitive mechanism to distinguish

between substrates does exist. This thesis will focus on the affects and regulation of Ca^{2+} mediated μ-calpain cleavage of the linker protein ezrin.

1.8 Ezrin

Ezrin is a member of the ERM family of membrane-cytoskeletal linker proteins. It was previously known as p81, the epidermal growth factor (EGF) receptor tyrosine kinase substrate, villin-2 and cytovillin. The name ezrin was coined in 1983 by Bretscher, which was derived from the name of the co-founder of the University in which it was first purified: Ezra Cornell, co-founder of Cornell University, in New York (Bretscher, 1983; 1991). It was first purified from the microvilli of epithelial cells in the intestinal brush border (Bretscher, 1983). Ezrin and moesin are the only members of the ERM family present in neutrophils.

1.8.1 Structure and function of ezrin

Ezrin has two main functional domains, located at the N and C termini (fig. 1.8.1i). The phosphorylation status of ERM proteins correlates with their functional activity as cross-linkers between the plasma membrane and the actin cytoskeleton (fig. 1.8.1ii). Where ERM proteins are phosphorylated, they are found associated with the cortical cytoskeleton. Where ERM dephosphorylation occurs, inactive ERM proteins are unstable and cytosolic (Grune et al., 2002), returning to the soluble monomeric form, concurrent with the disassembly of membrane and cytoskeletal interactions (Mackay et al., 1997; Tran Quang et al., 2000). ERM proteins can be directly phosphorylated by protein kinase C, MRCK and AKT (Ivetic and Ridley, 2004; Shiue et al., 2005) at tyrosine, serine and threonine residues.

Monomeric ezrin is found abundantly in the cell cytoplasm, where the N-terminal and C-terminal domains self-associate (Gary and Bretscher, 1995). This finding led to the suggestion that in unbound monomeric ezrin, head-to-tail association of the amino- and carboxy-terminal domains inhibits the binding

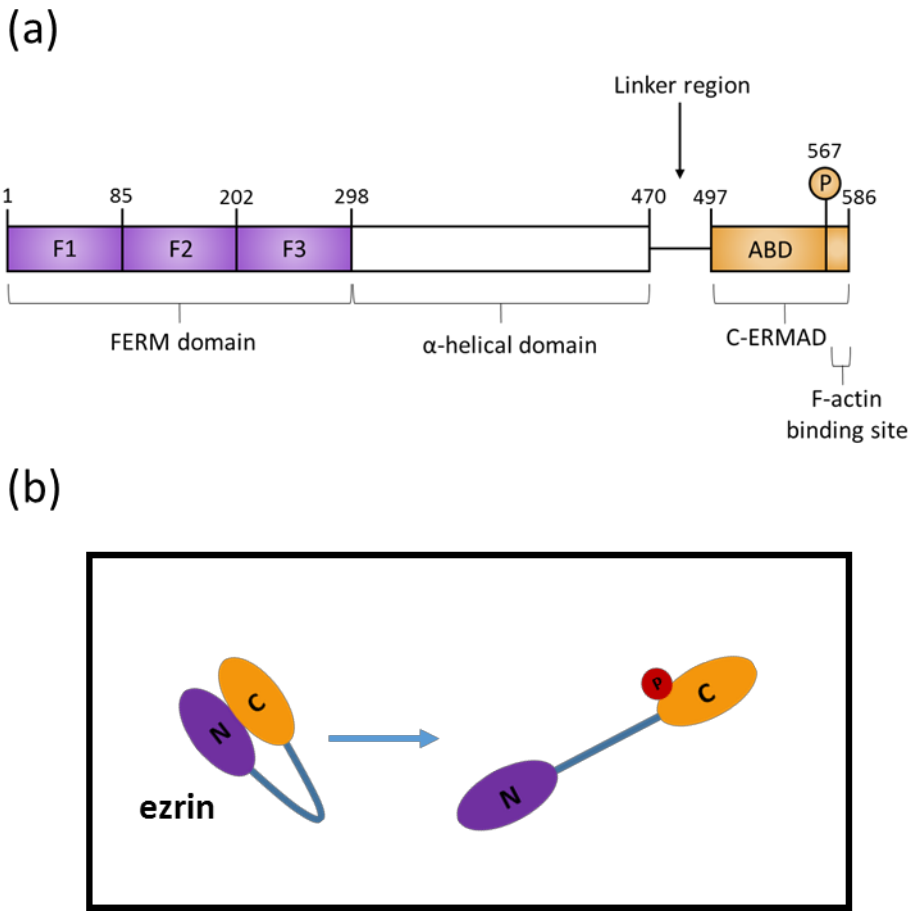

Figure 1.8.1i: Structure of ezrin
The structure of ERM family proteins is conserved, with all three having a similar structure. **(a)** The N-terminal FERM domain (purple) is made up of three smaller sub-domains (F1, F2, F3 or A, B, C (Hamada et al., 2000)). The C-terminal ABD (orange) contains the site of threonine phosphorylation responsible for the activation and self-dissociation of the molecule (Thr567), and also the F-actin binding site. The central region between these two functional domains is largely α-helical, forming a coiled coil, and is connected to the ABD via a proline rich linker region. Figure adapted from Fehon et al., 2010. **(b)** The two conformational states of ezrin Head-to-tail self-associated ezrin is inactive until phosphorylated at Thr567 in the C-terminal domain.

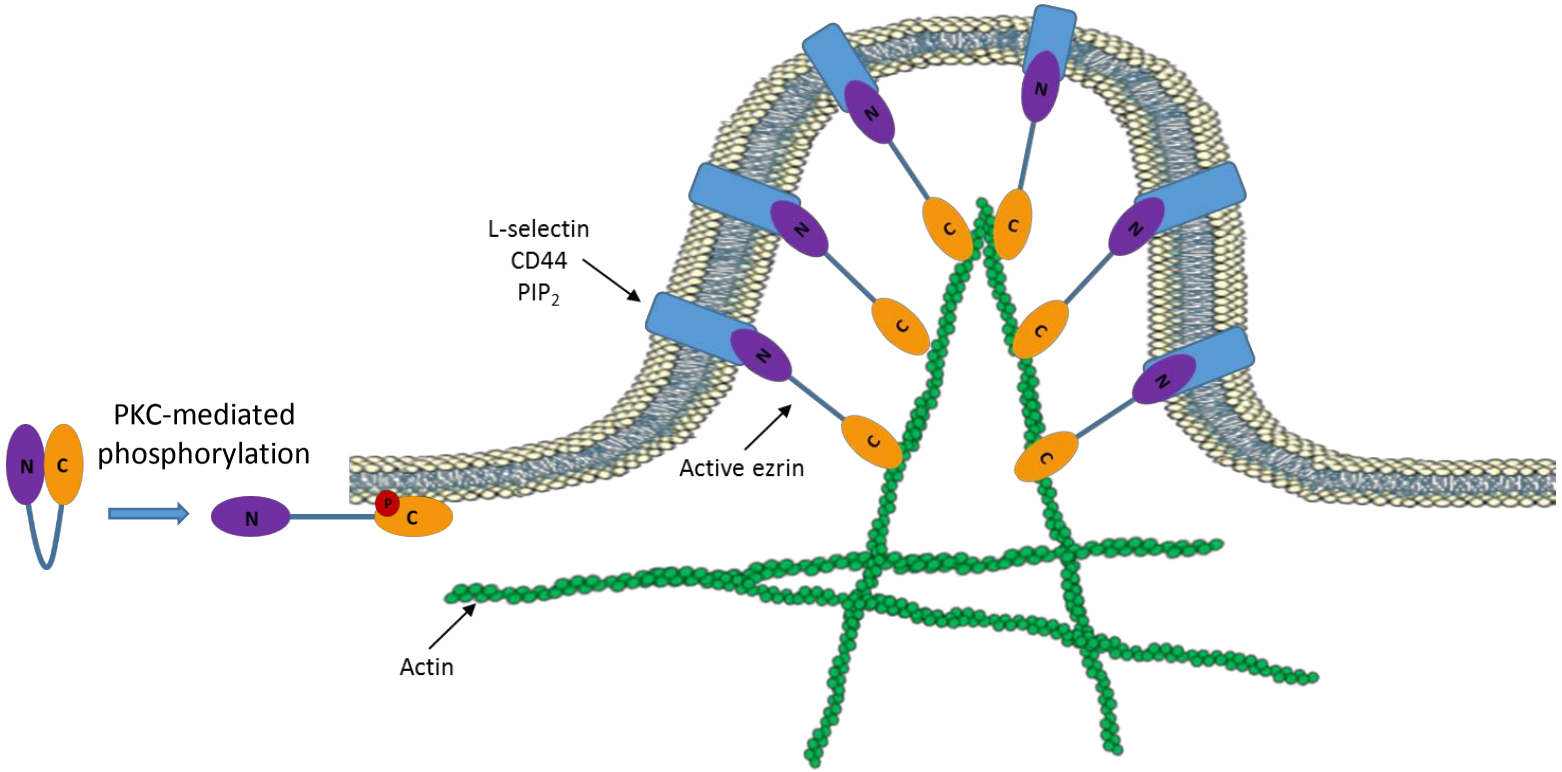

Figure 1.8.1ii: Schematic of neutrophil microridge structure
Phosphorylation on thr567 causes dissociation of ezrin's functional domains. The N-terminal FERM domain of active ezrin binds to the cytosolic tails of the plasma membrane proteins (blue). The C-terminal actin-binding domain binds to the F-actin cortical cytoskeleton. These ezrin bridges provide the crosstalk between the plasma membrane and the cortical F-actin cytoskeleton, which pushes the plasma membrane outwards forming microridges in the cell surface. These microridges serve as a reservoir of excess membrane storage, required for events which demand an apparent increase in cell surface area, such as phagocytosis and extravasation.

activity of either domain. In fact, ezrin exists in two conformational states, and conversion between the two is proposed to act as a switch to regulate ezrin activity (Bretscher et al., 1997). The first state is an unphosphorylated closed, inactive conformation where the N-terminal ERM domain self-associates with the C-terminal actin binding domain (ABD) (Ohtani et al., 2002), masking plasma membrane and actin binding sites. The second is an open, active conformation where the two domains are separate. The 'open' conformation is achieved through PIP_2 binding (Ivetic and Ridley, 2004) and phosphorylation at the conserved threonine 567 (Thr567) residue (Gautreau et al., 2000; Fievet et al. 2004; Shiue et al., 2005), which causes a change in the intramolecular binding properties between the two domains, facilitating ezrin self-dissociation and subsequent F-actin binding (Viswanatha et al., 2013) (fig. 1.8.1ib).

The ERM family of proteins associate with several ERM binding membrane proteins (EBMPs) at the plasma membrane via direct or indirect interactions (Yonemura et al., 1999). Ezrin was first suggested to play a role in crosslinking the plasma membrane to the F-actin cytoskeleton by Gould and colleagues (1989) on account of its similarity to talin and band 4.1, which binds to glycophyrin C (Correas et al., 1986). Algrain and colleagues (1993) performed transfection experiments which confirmed the interactions between the N-terminal FERM domain of ezrin and the plasma membrane. They found that the amino terminal domain localised to the dorsal plasma membrane, and was readily extracted following treatment with non-ionic detergents; suggesting interaction with the plasma membrane (Algrain et al., 1993). The ERM domain of ezrin also forms a complex with the cytosolic tail of L-selectin (Ivetic et al., 2002), which anchors ezrin at the plasma membrane. The C-terminal ABD of ezrin binds to the F-actin cytoskeleton at the carboxyl terminus, which co-localises with actin filaments beneath the plasma membrane, and remains associated with these following treatment with detergent (Algrain et al., 1993). This demonstrates a role of ezrin as a bridge between the cortical actin cytoskeleton and the plasma membrane, given the affinity of its functional domains to both structures. Furthermore, mutations in the ezrin-binding domain of L-selectin

impair neutrophil functions such as rolling, both *in vitro* and *in vivo* (Dwir et al., 2001; Kansas et al., 1993). This is further evidence to support the role of ezrin as an important linker protein between the plasma membrane and the cytoskeleton, specifically during morphological rearrangements of the cell cortex.

ERM proteins are known to bind phosphatidylinositol 4-phosphate (PIP) and PIP_2 (Barret et al., 2000; Gautreau et al., 2002; Ivetic and Ridley, 2004), increasing the affinity of ezrin for EBMPs in the plasma membrane (Gautreau et al., 2002), and enabling Thr567 phosphorylation (Fievet et al., 2004). Therefore the regulation of phosphoinositide phosphorylation is considered important in the relationship between plasma membrane associated EBMPs and the cortical F-actin cytoskeleton. Indeed, Rho, a small GTP-binding protein, has been associated with phosphatidylinositol turnover (Nakamura et al., 1999) and thus has been implicated in the activation of ERM protein cross-linking activity (Gautreau et al., 2002). Specific inhibition of Rho, by C3 toxin, suppresses ERM-EBMP interactions *in vitro* (Matsui et al., 1998), and Rho regulation by the Rho guanine nucleotide dissociation inhibitor (GDI) is closely involved in ERM protein complex interactions (Bretscher et al., 2002). Further evidence of Rho involvement comes from the observation that Myc-tagged Rho co-localises with ERM proteins in MSCK cells (Matsui et al., 1998). Rho has been found to regulate the activity of serine/threonine kinases (Nakamura et al., 1999), which may be involved in ERM protein phosphorylation at threonine residues, critical to ezrin domain interactions and conformational changes. It is not unlikely that Rho activity could play a role in mediating membrane-cytoskeletal interactions via regulation of ERM protein phosphorylation.

Within dynamic structures of the plasma membrane such as in microvilli and gastric parietal cells, the ezrin to actin ratio is almost 1:1 (Berryman et al., 1995). Given its relative abundance at sites proximal to dynamic cytoskeletal structures, it is likely that ezrin is involved in the mechanisms of actin/plasma membrane reorganisation. Ezrin also contains a G-actin binding site (Roy et al., 1997), which

loses actin binding activity when the N-terminal ERM domain is truncated (Martin et al., 1997), However, the isolated carboxyl terminal domain of ezrin is able to bind to filamentous actin with high affinity (Badour et al., 2003; Lee et al., 2003; Cao et al., 2005), suggesting that ERM binding to the plasma membrane is important for the F-actin cross-linking activity of full length ezrin.

Ezrin and ERM protein involvement in the mechanism of cell adhesion and morphogenesis, where the cross-linking interactions are necessarily altered, is not yet fully understood. It is likely that ezrin is involved in the molecular mechanism for releasing the membrane to perform cellular functions such as cell spreading and phagocytosis, both of which require enormous rearrangements of the cytoskeleton and plasma membrane.

1.8.2 Sensitivity to μ-calpain

Ezrin, but not the structurally similar ERM family protein moesin, is susceptible to cleavage by μ-calpain (Shcherbina et al., 1999). Although the exact cleavage site is not known, it is predicted to be in the linker region between the two functional binding domains (Dewitt and Hallett, 2007; Hallett and Dewitt, 2007). Therefore cleavage of ezrin would terminate its cross-linking activity and disrupt any relationship between the cytoskeleton and the plasma membrane (Algrain et al., 1993) (fig. 1.8.2). There is strong experimental evidence to support the hypothesis that selective sensitivity to μ-calpain serves as a discriminatory mechanism for specifically terminating ezrin linkage activity. In gastric parietal cells, μ-calpain-mediated cleavage of ezrin is associated with reduced ability to accumulate protons (Yao et al., 1993). More specifically related to cell morphological functions, endothelial cells have shown that ezrin cleavage by μ-calpain correlated with cellular locomotion, and completely disrupted ezrin-actin interaction (Shuster and Herman, 1995).

Ezrin and moesin are capable of forming heterodimers *in vivo* (Gary and Bretscher, 1993), and the two ERM proteins have been found to co-localise in

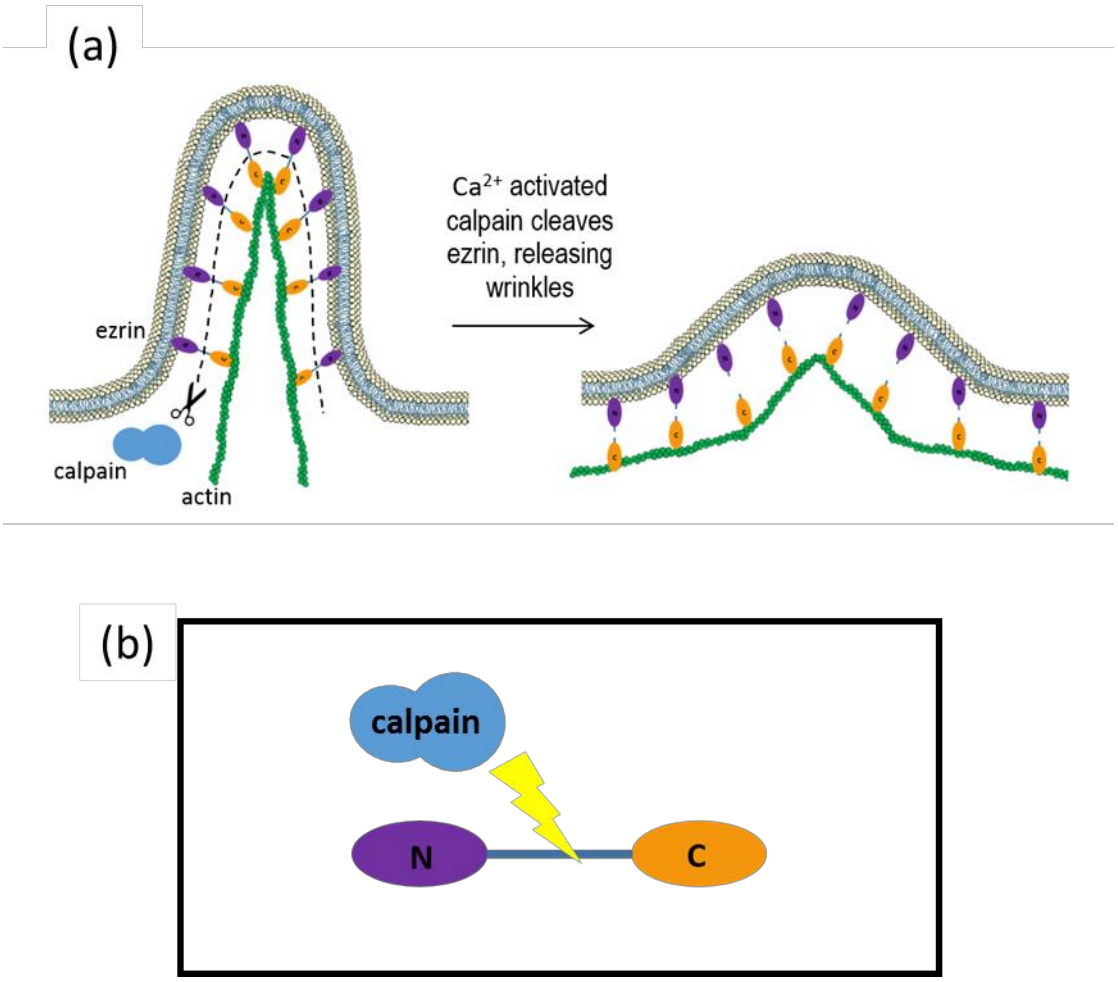

Fig. 1.8.2: Schematic of neutrophil microridge structure
(a) Phosphorylated ezrin in the 'open' active conformation forms a cross-link between the plasma membrane and the actin cytoskeleton. Ca^{2+}-activated calpain cleaves the active ezrin cross-link **(b)**, allowing the microridges to relax.

membrane structures such as microvilli in resting lymphocytes. Stimulated lymphocytes undergo extensive remodelling of their cytoskeleton during polarisation (Dustin et al., 1998; Stewart et al., 1998), and fluorescence microscopy of activated T-lymphoblasts has identified moesin as the only ERM protein in the uropods of polarised cells (Serrador et al., 1997). This suggests that although ezrin and moesin may function in a coordinated manner in the initial cross-linking interactions at the cell membrane, lymphocyte stimulation and μ-calpain activation disrupts only the ezrin linkages. In support of this, ezrin was also found evenly distributed in the cell cytosol of polarised lymphocytes (Serrador et al., 1997).

Ezrin and moesin constitute the only ERM family proteins expressed in cells of the blood. Although the exact cleavage site in ezrin is still unknown, it is a known substrate of Ca^{2+}-activated μ-calpain. Since μ-calpain displays selectivity for ezrin cleavage in lymphocytes during polarisation, it is likely that the μ-calpain-ezrin relationship is also important in the reorganisation of the cell membrane in neutrophils.

1.9 Mechanisms of neutrophil spreading

During important cellular functions such as extravasation prior to transmigration, chemotaxis and phagocytosis, the neutrophil undergoes dramatic changes in its morphology. As discussed, these events have complex regulatory mechanisms which govern their activity. Among these regulatory steps, there is one mechanism that has been overlooked, yet it is perhaps the most obvious hurdle in the process of neutrophil morphological changes. This is the apparent expansion of the plasma membrane.

1.9.1 A question of surface area

Circulating neutrophils have a ‘spherical’ morphology, which was initially thought to be a smooth surface area which could easily be calculated. However,

electron micrographs reveal a markedly contoured or 'ridged' surface (fig. 1.3i). Upon engagement with the endothelial cell surface during transendothelial migration, the neutrophil undergoes a massive change, assuming a flattened morphology as it spreads out onto the blood vessel wall. This activity is accompanied by an apparent surface area increase of about 200% (Dewitt and Hallett, 2007) (fig. 1.3i). A number of mechanisms which could provide additional plasma membrane for this process have been proposed. These include ER 'swallowing', endocytosis/exocytosis cycling and unravelling of plasma membrane microridges. The simplest assumption to explain this would be that the neutrophil membrane simply stretches, akin to the inflation of a balloon. However, biophysical characterisation of the lipid bilayer shows that the plasma membrane can only stretch by ~4% before lateral forces disrupt the hydrophobic interactions between fatty acids in the membrane, causing it to tear (Hamill and Martinac, 2001). Therefore it is not possible that membrane stretching accommodates the necessary 200% expansion observed in spreading neutrophils.

Whilst in macrophages there is evidence that the ER lies proximal to the plasma membrane and may be involved with phagosome formation (Gagnon et al., 2002), it is unlikely that the ER provides the additional membrane for neutrophil expansion. The reasons for this are two-fold: (i) neutrophils have markedly less ER than macrophages (Bessis, 1973), and (ii) the ER in neutrophils is not close enough to the plasma membrane to fuse with a new phagosome. Furthermore, unlike macrophages, neutrophil phagosomes do not display the ER marker glucose-6-phosphate (Gagnon et al., 2002), providing further evidence that membrane fusion does not occur.

Kay and colleagues have previously discussed the "surface-area problem" during chemotaxis (Kay et al., 2008), with a particular focus on the endocytic cycle as a mechanism for providing additional membrane. They dismissed a role of plasma membrane folds or microridge involvement in the mechanism of membrane expansion, citing that perturbation of the endocytic cycle consequently reduced

pseudopod formation and cell motility in *Dictyostelium*. However, this explanation significantly underestimates the apparent increase in cell surface observed in neutrophils changing morphology (~200% (Hallett and Dewitt, 2007). Observation of scanning electron micrographs of neutrophils reveals that neutrophil plasma membranes are far from smooth. Indeed, a striking feature of the neutrophil plasma membrane is their wrinkled structure (fig. 1.3i) (Bessis, 1973; Hallett et al., 2008). Upon osmotic swelling, and neutrophil spreading, these wrinkles in the membrane are reduced. Furthermore, quantification of the potential membrane stored in these microridge 'membrane reservoirs' indicates that they could contribute a further 100% to the cell surface area, when flattened (Ting-Beall et al., 1993). This suggests a mechanism for releasing folded plasma membrane within microridges may exist, in order for neutrophils to carry out the necessary morphological changes for them to perform phagocytosis, chemotaxis and extravasation.

1.9.2 Plasma membrane microridges

Neutrophil plasma membrane 'microridges' are suggested to play a role in the neutrophil's ability to change morphology, necessary for processes such as phagocytosis, chemotaxis and extravasation. It has been estimated that the surface of a neutrophil contains approximately 85% more plasma membrane than is required to enclose the cell volume (Hogg, 1987), and it is possible that this excess membrane serves as a reservoir for the necessary membrane expansion required for neutrophils to perform proper cellular functions. Rather than stretching the membrane, with the risk of shearing the phospholipid barrier and lysing the cell, the excess membrane stored in the wrinkles is proposed to be released by way of a molecular 'Velcro' mechanism (Dewitt and Hallett, 2007; Hallett and Dewitt, 2007), thus facilitating the apparent membrane expansion required for the cells to squeeze between the vascular endothelium, and also to project pseudopodia and engulf particles by phagocytosis.

A number of elegant characterisations of the biophysical properties of the neutrophil plasma membrane have been performed using micropipettes attached to a vacuum pump at moderate power. When it was drawn up into the pipette tip under suction, there was a measurable 5% expansion of the neutrophil membrane (Evans et al., 1993; Herant et al., 2005; 2006), but significantly further expansion of the membrane could be achieved under greater suction pressure (Herant et al., 2003; Dewitt and Hallett 2007; Hallett and Dewitt 2007). These findings were consistent with the works of Hamill and Martinac (2001) who calculated an approximate 4% slack in the plasma membrane was available under moderate suction. However, this suggests an additional mechanism is required to release 'stored' membrane from 'Velcro-like' microridges (Herant et al., 2003, Hallett and Dewitt, 2007), which must also be strong enough to resist osmotic pressure.

During neutrophil phagocytosis, the amount of force required to 'undo' the 'Velcro-like' microridges is considerably reduced, and the amount of available slack in the plasma membrane increases (Herant et al., 2005). This slack membrane, visibly devoid of microridges, can be seen in classic SEMs of neutrophils (fig. 1.3i), and is conceivably enough to enable the morphological changes that the neutrophil exhibits during cell spreading (Hallett and Dewitt, 2007).

Although this perceived membrane reservoir would provide the material to enable expansion, it does not in itself elicit any directionality over the membrane protrusions. During phagocytosis or chemotaxis, neutrophils project discrete pseudopodia, thus relying on a mechanism for selecting which areas of the membrane should expand. The underlying cortical actin cytoskeleton provides a scaffold beneath the plasma membrane, which is able to push/pull the membrane into different morphologies as necessary. The cytoskeleton is composed primarily of actin (Stossel, 1989), one of the most abundant proteins found in mammalian leukocytes (Southwich and Stossel, 1983). Actin assembly into the cytoskeleton requires polymerisation of G-actin into F-actin, and is a

dynamic process within the cell. The ratio of G-actin to F-actin can be influenced by recognition of extracellular stimuli. Neutrophil activation can shift the equilibrium towards F-actin, and increase the polymerisation of G-actin to F-actin by up to 4-fold (Stossel, 1989), thereby enabling the neutrophil to rapidly respond to external stimuli and prompt dramatic changes in cell morphology.

Crawling neutrophils exhibit two distinct protrusions of the cell membrane: lamellipodia and filopodia. Both formations are supported by a network of polarised F-actin, which forms a broad mesh beneath lamellipodia, and focal bundles in filopodia (Atilgan et al., 2006). The cortical F-actin network is organised by members of the WASP and WAVE protein families which bind to G-actin through VCA regions and generate points of F-actin nucleation (Takenawa and Miki, 2001). F-actin polymerisation in pseudopodia is restricted by the presence of the plasma membrane, and protrusions are achieved via the Brownian Ratchet model of unidirectional filament growth (Peskin et al., 1993). Dynamic fluctuations within the cell membrane and between surrounding proteins create opportunities for F-actin polymerisation, enabling filament extension which would be otherwise restricted by the tension of the plasma membrane (Peskin et al., 1993). Therefore the 'stretchiness' of the plasma membrane influences the extent of actin polymerisation that the cell is capable of. If plasma membrane tension were to be relaxed, the dynamic fluctuations would favour continued F-actin polymerisation in the direction of the 'slack' membrane. It has been suggested that plasma membrane microridges contain the membrane 'reservoirs' (Hallett and Dewitt, 2007) required for large scale changes in cell morphology. Therefore disruption of the mechanism which holds these microridges intact would provide the membrane slack which is favourable for F-actin polymerisation, via the Brownian Ratchet model.

The intracellular molecular mechanisms responsible for maintaining, and also liberating, neutrophil microridge structures are not completely established, but two models have been proposed, which connect the plasma membrane to the cytoskeleton via the linker proteins talin or ezrin (Dewitt and Hallett, 2007;

Hallett and Dewitt, 2007). In the first model the plasma membrane is linked to the cytoskeleton via talin, at the base of microridges. In the second ezrin connects the two within microridges, along the length of the structure. The two models may cooperate to regulate microridge structure, depending on L-selectin (in the protrusion) and β_2-integrin (at the base) linkages to the plasma membrane. This is also a reasonable explanation for their unequal distribution across the neutrophil surface (Dewitt and Hallett, 2007; Hallett and Dewitt, 2007).

1.9.3 Mechanisms of membrane expansion

Large rises in global cytosolic-free Ca^{2+} have long been associated with neutrophil and macrophage spreading (Kruskal et al., 1986; Jaconi et al., 1991). The rate of neutrophil spreading has also been found to accelerate upon manipulations of Ca^{2+} elevation, resulting from the controlled uncaging of cytosolic Ca^{2+} (Pettit and Hallett, 1998b) or uncaging of cytosolic IP_3 (Dewitt et al, 2013). Lymphocyte spreading upon β_2-integrin adhesion depends on μ-calpain activity (Stewart et al., 1998; Leitinger et al., 2000). Similarly, in pseudopod extension around a selected particle for phagocytosis, acceleration of μ-calpain activity and membrane expansion has been connected to Ca^{2+} elevation (Dewitt and Hallett, 2002; Carafoli and Molinari, 1998). μ-calpain has been implicated in the mechanism of neutrophil membrane expansion and spreading because it lists among its substrates a number of cytoskeletal linker proteins (Franco and Huttenlocher, 2005). Therefore Ca^{2+}-mediated μ-calpain activation could provide the trigger to release the 'Velcro-like' structure of plasma membrane microridges, to enable changes in neutrophil morphology. Given that cell spreading represents a major hurdle in neutrophil extravasation, from the blood towards sites of inflammation, the μ-calpain-ezrin axis may provide a potential target to interfere with and disrupt this mechanism. Investigating this may be of great interest to the development of novel pharmaceuticals to target key cellular processes involved in the exaggerated immune responses seen in rheumatoid arthritis patients.

1.10 Aims

This study aims to unravel a key intracellular molecular mechanism governing neutrophil morphology change in response to Ca^{2+}, namely the relationship between μ-calpain and ezrin. It is hoped that by further understanding the interactions between these proteins within the cell at the molecular level, we will be better placed to inform the directed development of novel therapeutics to target autoimmune conditions.

The primary objectives of the work presented in this thesis are:

1. To investigate the effect of Ca^{2+} influx on ezrin distribution in myeloid cells.
2. To develop novel techniques of measuring peripheral cytosolic Ca^{2+} concentrations.
3. To probe the relationship between Ca^{2+} concentration, and the Ca^{2+}-mediated cleavage of ezrin.
4. To determine the importance of plasma membrane microridges in this relationship.

Freshly isolated neutrophils are notoriously problematic to study experimentally, owing to their short half-life, tendency to become activated, and also their predisposition to spontaneously perform apoptosis. However, their involvement in both the resolution and instigation of disease states makes any advance in our understanding of their function, however incremental, very valuable. In the approach to tackle any disease indication, a clear understanding of the biological system is first necessary. The work presented in this thesis has used a RAW 264.7 cell line to compliment neutrophil studies, to overcome some of the challenges faced when working with freshly isolated human neutrophils.

Chapter 2:
General Methods

2. General methods

The materials and methods described in this section are non-specific and relevant to the results presented in multiple chapters in this thesis. Descriptions of the materials and methods specific to individual chapters will be given at the start of each chapter.

2.1 Preparation of Krebs and Krebs-BSA

Hepes buffered Krebs [120 mM NaCl, 25 mM Hepes, 4.8 mM KCl, 1.2 mM KH_2PO_4, 1.2 mM $MgSO_4 \bullet 7H_20$, 1.3 mM $CaCl_2 \bullet 2H_20$] was prepared in dH_20 and adjusted to pH 7.4 with NaOH. The buffer was stored at 4°C. Krebs-BSA was prepared by adding 0.1% (w/v) BSA.

2.2 Preparation of the balanced salt solution

The balanced salt solution (BSS) [130 mM NaCl, 2.6 mM KCl, 8 mM Na_2HPO_4 and 1.83 mM KH_2PO_4] was prepared in dH_20 and adjusted to pH 7.4 with NaOH.

2.3 Preparation of Dextran

6g of Dextran (Mr 70,000) was dissolved in 100 mL of BSS at room temperature on a magnetic mixer.

2.4 Isolation of human neutrophils from peripheral blood

Human neutrophils were isolated from blood donated by healthy volunteers, as described by (Davies and Hallett, 1998). 10 mL of blood was collected into a universal container containing 100 µL of Heparin (CP Pharmaceuticals). Dextran (6%) was added at one quarter the volume of blood taken (typically 2.5 mL of Dextran to 10 mL of whole blood). The suspension was gently inverted and allowed to sediment at room temperature for approximately 30 minutes

(sedimentation times varied between donor samples). The whole blood separated into three layers, and the middle 'buffy coat' layer containing the white blood cells (WBC) was carefully aspirated using a Pasteur pipette, and centrifuged at 1,400 x *g* for 1 minute at room temperature. The supernatant was discarded and red blood cell lysis was carried out by re-suspending the cell pellet in 1 mL of dH2O for 10 seconds, before the osmolarity was recovered by the addition of 20 mL of balanced salt solution (BSS).

The cells were centrifuged at 1,400 x *g* for a further 2 minutes, and the supernatant was discarded and the resultant pellet was re-suspended in 1 mL of bovine serum albumin (BSA) supplemented Krebs (Krebs-BSA). The cleanness of the prep was checked by observing the cell population on a bright field microscope, and the number of cells was assessed with a Nexcelom Cellometer (Nexcelom Bioscience). The typical neutrophil count from this isolation procedure was around $1x10^6$ cells/mL.

2.5 Isolation of normal human serum from whole blood

Blood was taken from healthy donors as previously described. 1 mL of whole blood was collected into a glass vial without heparin and left to clot at room temperature for 30 minutes, before centrifuging at 700 x *g* for 10 minutes to pellet the clot. Normal human serum was aspirated from the supernatant using a Pasteur pipette, and kept on ice until use the same day. Every effort was made to ensure serum and neutrophils from the same donors were used in experiments, although sometimes serum from another donor was used.

2.6 Immunocytochemistry

100 µL of isolated neutrophils ~10^6 cell/mL were pipetted onto glass slides and left to settle for 10 mins at 37°C. The cells were fixed and permeabilised in 4% formalin and 0.1% Triton respectively. 4% goat serum was used to block non-specific antibody binding, prior to overnight incubation with 1:100 primary

antibody at 4°C, and subsequently 1:20 secondary antibody, for 1 hour at room temperature. Slides were imaged on the Leica SP5 confocal inverted microscope (Leica Microsystems, Heidelberg) with resonance scanner, laser scanning, [63x immersion objective; 488 nm argon laser].

2.7 Protein extraction and preparation of cell lysates

Isolated neutrophils were spun down and re-suspended in neutrophil lysis buffer (50 mM HEPES, 150 mM NaCl, 10% Glycerol, 1% Triton X100, 5 mM EDTA, 5 mM EGTA, 1 mM Na_3VO_4, 1.5 mM NaF, 0.1% SDS, 1.5 mM $MgCl_2$) and PIC was added at 1:1000. Samples were incubated on ice for 1 hour and vortexed every 15 minutes to increase the efficacy of cell lysis. If used for Western Blotting the samples were boiled for 10 minutes and then centrifuged for 5 minutes at 13,000 x *g*.

2.8 Assessment of protein concentration

Protein concentration was assessed using the Pierce™ BCA Protein Assay Kit (Life Technologies), according to manufacturer's protocol, or using the NanoDrop™ Lite.

2.9 Western blotting

10 µg protein was loaded per well of the pre-cast 7% NuPAGE® Tris-Acetate Gel (Life Technologies), and the gel was run at constant 150 V for 1 hour in the NuPAGE Tris-Acetate buffer system (Invitrogen). A test gel was run and stained with InstantBlue (Expedon) to check for the presence of protein bands.

Electroblotting to a PVDF membrane (GE Healthcare Life Sciences) was carried out at constant 350 mA for 1 hour. The PVDF membrane was stained with Ponseau S (Sigma-Aldrich) to assess the success of the electroblotting procedure. Blocking was performed in 5% milk (Marvel) or BSA, in TBS-T for 2

hours at RT prior to incubation with 1:1000 primary antibody overnight at 4°C, and subsequently 1:1000 secondary antibody for 2 hours at RT. Protein bands were detected using the SuperSignal™ West Dura Extended Duration Substrate (Life Technologies) and the G:BOX imager (Syngene), at five 30 second intervals to achieve the best exposure.

2.10 Preparation of fMLP solution

The bacterial peptide fMLP was purchased from Sigma-Aldrich in powder form. A 1 mM stock solution was made by diluting 1 mg of powder in 2.3 mL DMSO. In neutrophil experiments the stock solution was further diluted to 1 µM in Krebs-BSA.

2.11 RAW cell culture, maintenance and storage

RAW 264.7 cells, originally from American Type Culture Collection, were cultured in Dulbecco's Modified Eagle's Medium (DMEM) supplemented with 10% heat inactivated foetal bovine serum (FBS) and 1% Penicillin and Streptomycin. Cells were incubated at 37°C in 5% CO_2.

Aliquots were routinely frozen for long-term storage in liquid nitrogen, to maintain cell stocks. Cells were harvested from culture flasks at about 70% confluence, by cell scraping. The cells were then centrifuged at 2000 rpm for 2 minutes, and re-suspended in 90% DMEM, 10% DMSO. One cryovial was frozen from each confluent T25 flask (approximately $5x10^6$ cells).

Cells were defrosted from long-term storage by rapid thawing in a water bath at 37°C, then immediately transferred to 15 mL of pre-warmed supplemented DMEM. The cells were left to recover for 20 minutes in an incubator at 37°C with 5% CO_2, then centrifuged at 2000 rpm for 2 minutes. The cells were then re-suspended in 15 mL of fresh pre-warmed and supplemented DMEM and put into T25 culture flasks, to incubate at 37°C with 5% CO_2.

2.12 Plasmid amplification

Plasmids were purchased from Addgene (Michael Davidson lab), gifted (from Sabrina Marion) or novel (Chapter 4). In order to amplify stocks for mammalian transfection experiments in RAW 264.7 cells, the plasmids were amplified via bacterial transformation. One Shot™ TOP10 Chemically Competent *E. coli* were chemically transformed according to the manufacturer's protocol. Transformed bacteria were streaked out onto agar plates with appropriate antibiotic, at 3 different dilutions (200 µL, 50 µL and 20 µL), because the competency of the bacteria was unknown.

2.13 Preparation of Lysogeny broth

The lysogeny broth (LB) was made by dissolving 10 g Lennox powder (Sigma-Aldrich) in 500 mL dH_20. The solution was sterilised in a benchtop autoclave, and left to cool before the addition of appropriate antibiotics.

2.14 Preparation of agar plates

LB broth was prepared as described and supplemented with 3.75 g agar powder (Sigma-Aldrich) prior to autoclaving. 30 mL of warm agar was transferred to labelled sterile petri dishes and left to set at room temperature for at least 30 mins. The plates were then inverted and stored at 4°C until needed. When they were to be used, the plates were removed from the fridge 30 mins before plating bacteria, to allow the temperature of the agar to come up to room temperature.

2.15 RAW 264.7 cell line transfection by nucleofection

RAW cells were cultured to approximately 70% confluence and transfected using the Cell Line Nucleofector™ Device (Lonza), according to the manufacturer's protocol. $2x10^6$ cells were harvested by scraping, and centrifuged at 750 rpm for

10 minutes, then re-suspended in 100 µL Amaxa® Cell Line Nucleofector® Kit V (Lonza). 2-4 µg of plasmid DNA was added to the suspension, which was transferred to the electroporation cuvette. The cells were electroporated using programme D-032 on the nucleofector device, quickly recovered in 500 µL pre-warmed DMEM, then transferred to 5 mL warm DMEM. 0.9 mL of recovered cell suspension was transferred to glass-bottomed petri dishes and supplemented with an additional 1.1 mL of pre-warmed DMEM. The cells were left to incubate at 37°C in 5% CO_2 for 3-4 hours, before imaging.

2.16 Opsonisation of zymosan particles

Zymosan were opsonised by incubation with excess NHS (prepared as described section 2.5), at 37°C for 30 mins. The zymosan were then spun down and re-suspended in 1 mL Krebs-BSA. 100 µL zymosan suspension was added to the cells on the cover slide and allowed to 'rain down' onto the cells. Cells within proximity of the opsonised zymosan (i.e. <5 µm) were imaged on the Leica SP5 confocal inverted microscope, using the 488 nm laser to record changes in Ca^{2+} concentration.

2.17 Confocal microscopy

Confocal images were taken using the Leica SP5 confocal inverted microscope (Leica Microsystems, Heidelberg) with resonance scanner, equipped with a 543 nm, 633nm and argon 488 nm lasers. The fluorescent photo multiplier tubes were set to the maximum gain of approximately 1200, and the phase contrast (PC) gain was set to approximately 300. Laser intensities were adjusted accordingly to achieve the optimum signal from fluorescent probes. For some experiments more than one fluorophore was imaged at the same time, in this instance sequential imaging was used. This allowed for fluorescent emissions at each appropriate wavelength to be detected simultaneously, with minimal interference between channels.

2.18 Statistical analysis

Neutrophil experiments were carried out on at least three occasions and with blood from different healthy donors in the lab. All data shown is representative of at least three similar results, with standard error of the mean (SEM). Statistical analysis was performed using GraphPad Prism 5 for Windows, Version 5.00.

Chapter 3:

Dynamic changes in subcellular ezrin location in myeloid cells

3.1 Introduction

Ezrin is an important cross-linking protein in the architecture of plasma membrane structures (Gould et al., 1989). Its two functional domains, the N-ERMAD and C-ERMAD, bind to the plasma membrane and cortical F-actin respectively (Algrain et al., 1993; Ivetic et al., 2002; Badour et al., 2003; Lee et al., 2003; Cao et al., 2005), thus stabilising the connection between the bi-lipid boundary of the cell, and the internal cytoskeleton. The regulation of ezrin cross-links are therefore important in the morphological rearrangements undergone by cells which receive signals to spread, such as neutrophils during an inflammatory response. Disruption of the ezrin tether would release the plasma membrane from cytoskeletally orchestrated microridge structures, and this release of membrane 'reservoir' has been suggested as the mechanism by which cells such as neutrophils are able to drastically alter their morphology in processes such as extravasation, which may require up to an approximate 200% apparent expansion in plasma membrane area (Dewitt and Hallett, 2007).

Since proteolytic cleavage of ezrin would serve to sever the link between the plasma membrane and the cortical F-actin cytoskeleton, it is possible that the activity of ezrin is disrupted by μ-calpain activation (Dewitt and Hallett, 2013). The relationship between ezrin and μ-calpain may therefore be important in maintaining surface membrane microridges in the plasma membrane of neutrophils, and other myeloid cells. The hypothesis to be tested in this chapter is that elevating cytosolic Ca^{2+} will activate μ-calpain, thereby liberating its proteolytic capabilities in regions of high cytosolic Ca^{2+} concentration, such as the ezrin-rich microdomains beneath plasma membrane microridges.

In order to investigate the relationship between ezrin, μ-calpain activation and the dynamic maintenance of cell surface membrane microridges in a myeloid cell plasma membrane, some novel approaches will be adopted. Previously, the link between the location of ezrin and μ-calpain activity has been shown in biochemical studies in neutrophils, by Western blotting of extracted proteins

(Fehon et al, 2010). Ezrin is a known neutrophil substrate of the cytosolic protease, μ-calpain (Shcherbina et al., 1999), and is known to be localised to microvilli in a number of cell types. Knocking out ezrin expression has shown that ezrin is clearly required for the assembly and maintenance of cell surface structures (Morales et al., 2004), such as microvilli on brush boarder cells (Bretscher, 1983). It for these reasons that ezrin was originally named cytovillin. In neutrophils however, it is proposed that the cell surface microridges are dynamic structures which can be 'released' when there is a requirement to produce additional cell surface area (Dewitt and Hallett, 2007). This proposal requires that ezrin is initially located within microridges at the cell surface of resting neutrophils, holding the plasma membrane and cortical actin network together, thus maintaining the plasma membrane in a 'wrinkled' topography. Furthermore, this would suggest that the ezrin cross-link is disrupted during, and for the purpose of, membrane expansion. This process may be driven by the Ca^{2+}-activated cleavage of ezrin by μ-calpain (Shcherbina et al., 1999; Dewitt and Hallett, 2007; Hallett and Dewitt, 2007).

In order to test these hypotheses a methodology which explores both the subcellular location of ezrin and, ideally, its cleavage state is required. It has been shown that by attaching a fluorophore to ezrin, it is possible to monitor the dynamics of ezrin localisation and re-distribution, in live cells. The fluorescent domain can be conjugated to ezrin either at the N-terminal ERMAD, the C-terminal ERMAD or at an intra-domain position (fig. 3.1). The approach that has been adopted in the work presented in this chapter is therefore based on fluorescent ezrin which can be imaged microscopically, as a surrogate marker of the dynamic activities of endogenous ezrin. However, the major disadvantage of this approach is that it cannot be applied directly to neutrophils, because as terminally differentiated cells they cannot be transfected to produce the required fluorescent proteins. A myeloid cell line with the required characteristics will therefore be used.

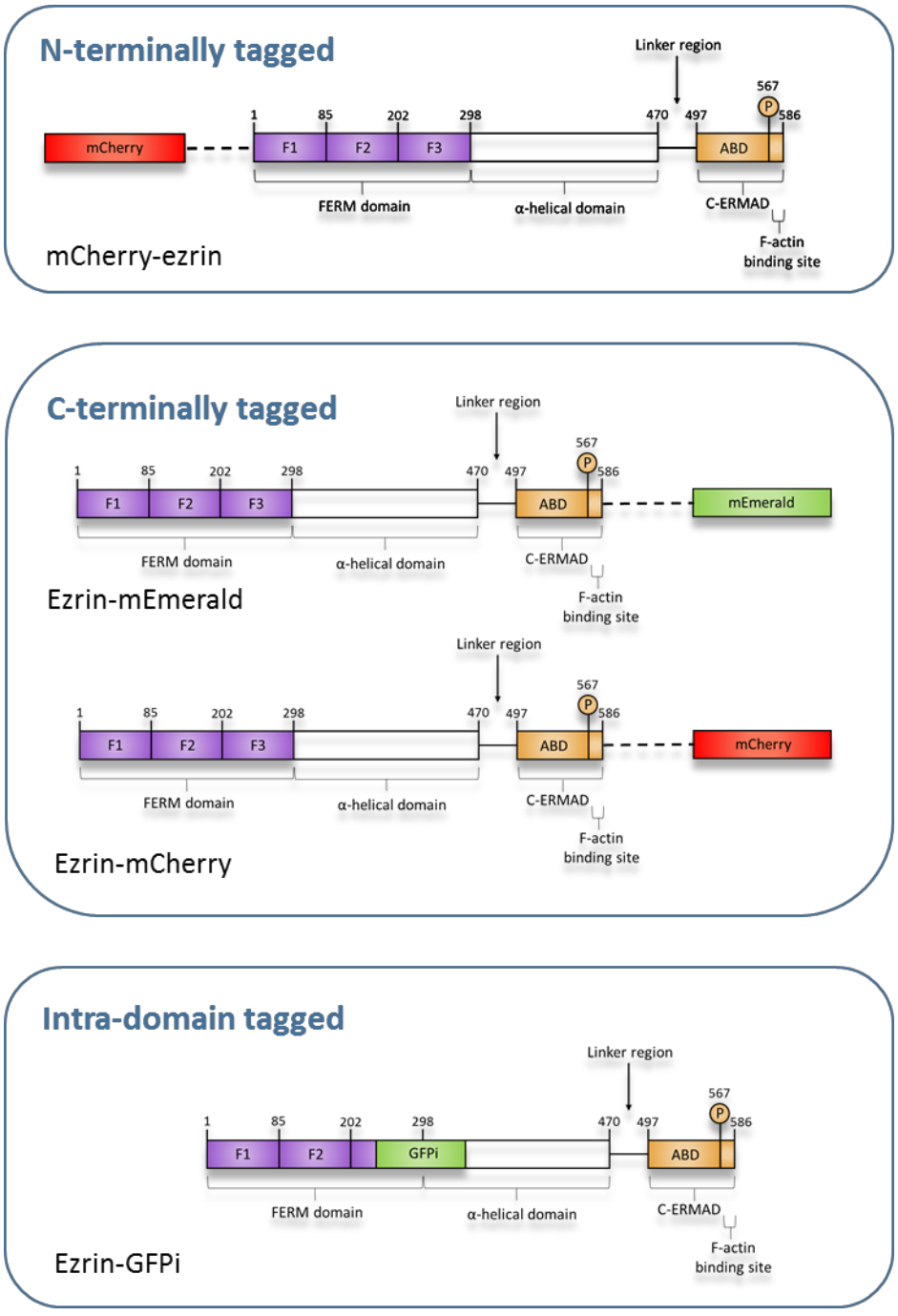

Figure 3.1: Fluorescently tagged ezrin
Structures of the fluorescently-tagged ezrin constructs used in this thesis.

3.1.1 Myeloid cell lines

A number of myeloid cell lines could be considered, in which to investigate the dynamics of fluorescently-tagged ezrin constructs. An important characteristic to note is the ability of cells to perform phagocytosis. The most widely used myeloid cell line in this regard has perhaps been the HL60 cell line, or its subclone PLB-985 (Pivot-Pajot et al., 2010). After appropriate differentiation these cells readily perform phagocytosis of C3bi-opsonised zymosan particles (Tohyama and Yamamura, 2006), whereas the undifferentiated cells do not. As a consequence of this, the 'differentiated' cell populations invariably contain a mixture of (i) un-differentiated non-phagocytic cells, (ii) newly differentiated phagocytic cells, and (iii) older differentiated but non-phagocytic cells which are progressing towards apoptosis. In addition, the differentiation of HL60s usually also corresponds to a marked decrease in their novel protein synthetic capability. Therefore, it is difficult to achieve cells with adequately high expression of the fluorescent protein constructs, but that are also phagocytic.

For these reasons, a cell line which is phagocytic without the need for differentiation has been used: RAW 264.7 cells. These cells are murine and were derived from the ascites infiltrate of a tumour in a male mouse, induced by intraperitoneal injection of Abelson Leukaemia Virus (ECACC Data base). RAW 264.7 cells are capable of antibody-dependent phagocytosis of sheep erythrocytes and tumour targets. They will also perform phagocytosis of zymosan, and their phagocytic capabilities are especially apparent when the zymosan has already been opsonised with C3bi, from mouse serum. RAW 264.7 surface membranes are also covered in microscopic surface microridges, which resemble the microridges seen in neutrophils. Fluorescent protein expression can be detected about 1 hour post transfection by electroporation, but is optimal at about 4 hours after transfection. Furthermore, the RAW 264.7 cell line is semi-adherent, therefore cells can be harvested from culture flasks mechanically, and without the need for additional extracellular proteases; thus avoiding the potential of degrading cell surface receptors important for

phagocytosis. For these reasons, the RAW 264.7 cell line is an ideal model for these studies.

3.1.2 Aims and Objectives

The aim of the work presented in this chapter is to express fluorescent constructs of ezrin in a myeloid cell line (RAW 264.7); in order to document ezrin subcellular location in resting cells, and also in dynamic cells during an experimentally induced elevation of Ca^{2+} influx, and phagocytosis. A further aim is to establish whether cleavage of ezrin by μ-calpain occurs, by using constructs that place the fluorescent marker either side of the predicted μ-calpain cleavage site. In this way, ezrin cleavage within the cell would be detectable. As this is a novel approach, it will be necessary to establish the methodology.

The specific objectives of the work in this chapter are therefore:

1. To compare the subcellular location of fluorescent ezrin constructs expressed in RAW 264.7 cells.
2. To establish the dynamic changes in subcellular location of ezrin using fluorescent constructs expressed in RAW 264.7 cells.
3. To establish a new methodology to monitor ezrin cleavage within living cells.
4. To use this new methodology to investigate whether ezrin cleavage occurs during experimentally induced Ca^{2+} influx and phagocytosis events.

3.2 Specific Materials and Methods

3.2.1 Immunocytochemistry

Human neutrophils were isolated from healthy donor blood, as previously described in Chapter 2. Fixed and permeabilised neutrophils were stained with mouse anti-ezrin primary antibody (Santa Cruz (3C12)) and goat anti-mouse FITC

conjugated secondary antibody (Santa Cruz IgG1-FITC). Cell staining was analysed using the Leica SP5 confocal microscope with 488 nm argon laser.

3.2.2 RAW 264.7 cell transfection

RAW 264.7 cells were electroporated to introduce ezrin plasmids: mCherry-ezrin, ezrin-mEmerald, ezrin-mCherry and ezrin-GFPi (3 µg plasmid DNA/ $2x10^6$ cells) using the Cell Line Nucleofector™ Device (Lonza) as previously described (Chapter 2). The novel ezrin-GFPi plasmid (Marion et al., 2011) was verified by sequencing, which showed the intra-domain location of the GFP insert within the N-terminal FERM domain. This was before the linker region in ezrin, which is postulated to be the µ-calpain cleavage site. Cells were incubated at 37°C in 5% CO_2 for 3-4 hours to enable expression of the newly introduced DNA, before imaging on the Leica SP5 confocal microscope.

3.2.3 Confocal microscopy

Confocal images were taken using the Leica SP5 confocal inverted microscope (Leica Microsystems, Heidelberg) with resonance scanner, laser scanning [63x objective; 633 nm and 488 nm argon laser] in a perfusion chamber at 37°C. Images were acquired from the two lasers by sequentially scanning alternate lines with each laser. In this way each image line was from a single laser excitation and there was no possibility of cross-over (by inadvertent excitation of both fluorophores). Sequential line imaging also gave simultaneous images from each laser excitation, as previously described in Chapter 2.

3.2.4 Ezrin extraction from RAW 264.7 cells

Transfected RAW 264.7 cells were harvested by scraping and DMEM growth medium was removed by centrifugation at 100 x *g* for 10 mins. The cell pellet was washed by resuspension in 1 mL BSS, and re-centrifuged to re-pellet the cells. Cell lysis was performed in the absence of free Ca^{2+} ions (10 mM EGTA) to avoid activation of µ-calpain, using ice cold Pierce™ IP Lysis Buffer (from the

Pierce™ Co-Immunoprecipitation Kit) with additional PIC (1:1000), and kept on ice for 5 mins, with pipetting. The lysates were centrifuged at 14, 000 rpm for 10 mins. Supernatant was aspirated and the pellets containing the extracted protein were retained for immunoprecipitation. Ezrin was extracted from the RAW 264.7 lysates by co-immunoprecipitation with a rabbit anti-ezrin polyclonal antibody (Cell Signalling, 3145), using the Pierce™ Co-Immunoprecipitation Kit, according to the manufacturer's instructions.

3.2.5 μ-calpain cleavage of ezrin constructs

The anti-ezrin antibody (RabMAb EP924Y) to residues surrounding Tyrosine 145 in the N-terminal domain of ezrin, was plated onto a Greiner flat-bottomed high and medium binding 96-well plate (Sigma) at a 1:10 dilution in 50 μL BSS, and left overnight at 4°C to adhere (fig. 3.2.5). Non-adhered antibody was removed by aspiration and the plate was washed twice in BSS. 50 μL RAW 264.7 cell lysate containing ezrin-mCherry or ezrin-GFPi (prepared as previously described) was loaded per well, in triplicate, and left overnight at 4°C. Unbound lysate was removed by aspiration and the plate was washed twice in BSS.

Neutrophil lysate (prepared as described in Chapter 2) was used as the source of μ-calpain. 40 μL of neutrophil lysate plus 10 μL of either Ca^{2+} (final concentration 1.65 mM) or dH_20 (Ca^{2+}-free) water as a control. The reaction was allowed to proceed for 2 mins before the supernatant was extracted from the wells and placed in a flat clear-bottomed microtiter plate for further analysis. The Pierce™ IP Lysis Buffer was used as a blank.

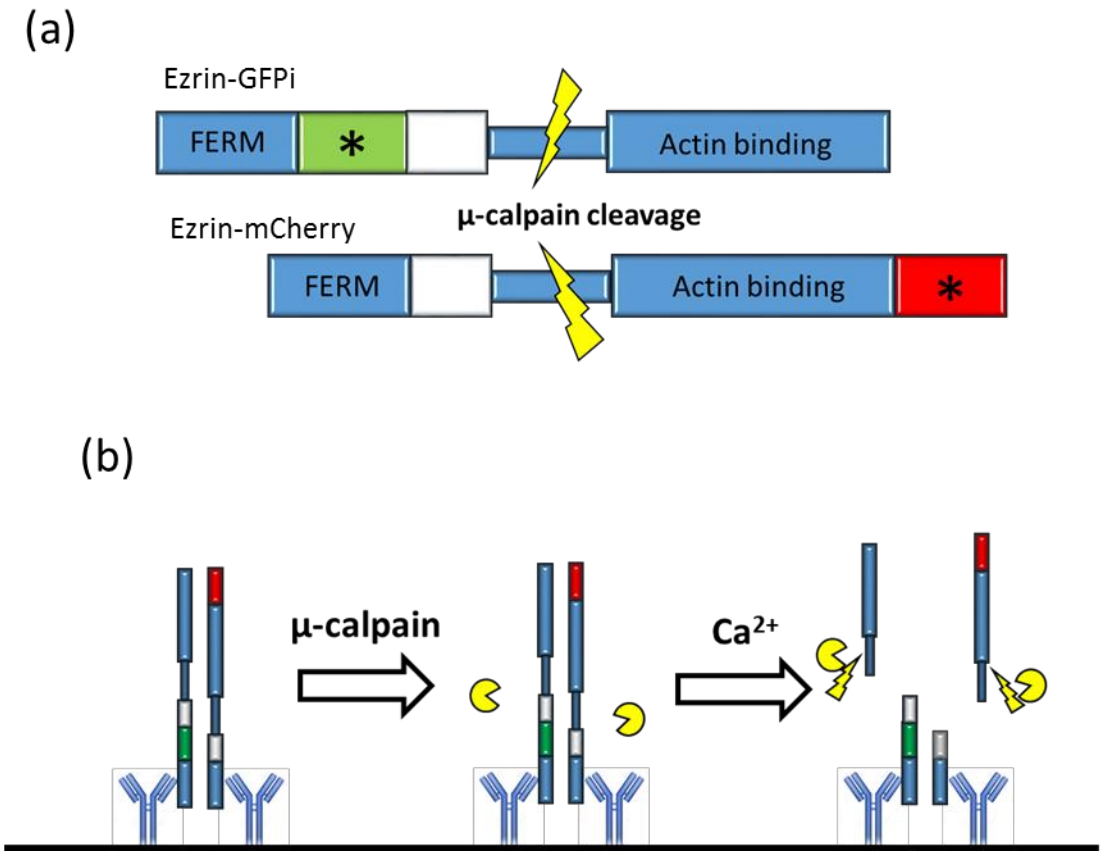

Figure 3.2.5: Principle of differential fluorophore release following μ-calpain cleavage of ezrin-GFPi and ezrin-mCherry
(a) The simplified structures of ezrin-GFPi and ezrin-mCherry are shown with the μ-calpain cleavage site indicated. **(b)** Schematic of ezrin immobilisation by antibodies to the FERM domain of ezrin. Following addition of μ-calpain and its activation by Ca^{2+}, the ezrin fragment containing the mCherry is released, whereas the GFPi containing ezrin fragment remains attached to the antibody.

Fluorescence was recorded on the BMG FLUOstar OPTIMA. For ezrin-GFPi the excitation/emission settings used were 485 nm/520 nm, and using the top optics gave the highest reading. For ezrin-mCherry the excitation/emission settings used were 544 nm/590 nm, and bottom optics were selected to give the highest reading. The maximum value attainable was 65,000 (fig. 3.2.4).

3.3 Results

3.3.1 Native ezrin at the plasma membrane in neutrophils

Immunocytochemistry of fixed human neutrophils shows that ezrin in the resting 'spherical' neutrophil is located at the cell periphery (fig 3.3.1). However, when undergoing phagocytosis, ezrin is absent from the base of the phagocytic cup and also from the phagosome membrane. These data show that ezrin is lost and must translocate away from the plasma membrane during phagocytosis (fig 3.3.1).

3.3.2 Ezrin constructs at the plasma membrane of RAW 264.7 cells

In order to visualise the dynamics of changes in the subcellular location of ezrin, fluorescent ezrin constructs were expressed in the RAW 264.7 model myeloid cell line. Nucleofection using the Cell Line Nucleofector™ Device (Lonza) has previously been found to be the most effective method for successful transfection in our lab, and was therefore the chosen method of transfection in these experiments. RAW 264.7 cells were harvested by scraping and transfected with either mCherry-ezrin or ezrin-mEmerald alone, or co-transfected with both. Transfected cells were inspected and imaged using the Leica SP5.

Constructs with the fluorophore at the plasma membrane binding N-terminus (e.g. mCherry-ezrin) remained free in the cytosol, but were excluded from the nucleus (fig. 3.3.2i), whereas constructs with the fluorophore attached at the C-terminus (e.g. ezrin-mEmerald) were clearly located at the cell periphery

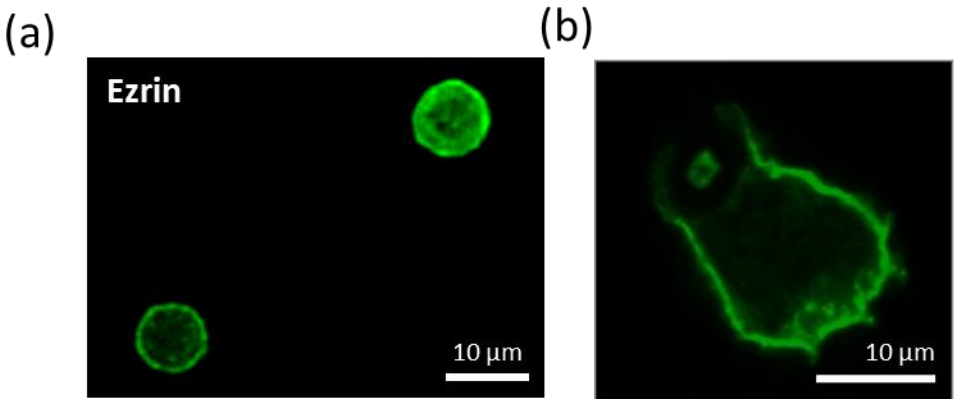

Figure 3.3.1i: Native ezrin location in human neutrophils
Immunocytochemical detection of ezrin in **(a)** unstimulated human neutrophils, and **(b)** a human neutrophil performing phagocytosis of a zymosan particle (Roberts et al., 2017 – unpublished).

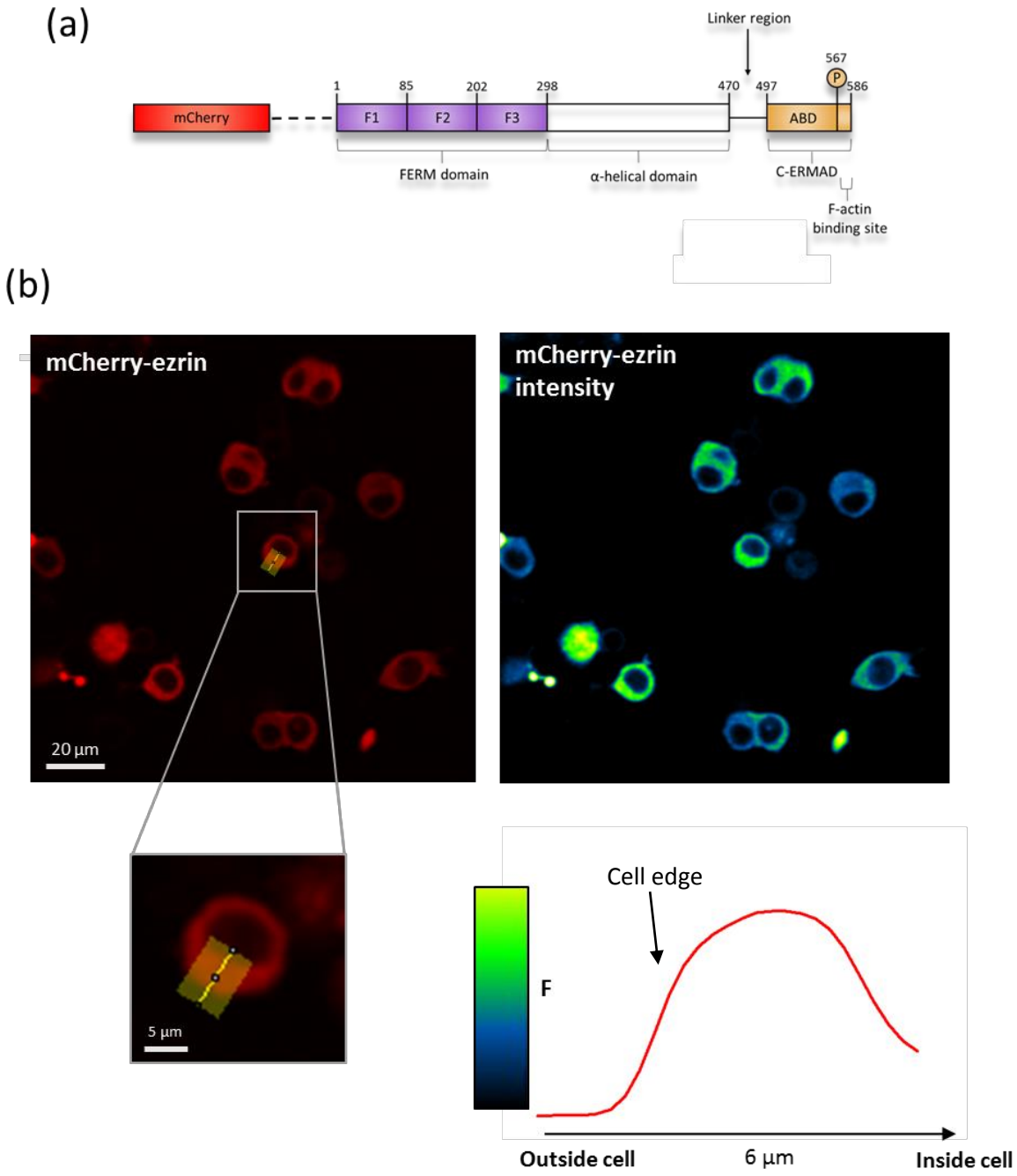

Figure 3.3.2i: mCherry-Ezrin expression in RAW 264.7 cells
(a) Structure of mCherry-Ezrin. The fluorophore is attached to ezrin at the N-terminal FERM plasma membrane binding domain. **(b)** First panel: RAW 264.7 cells expressing cytosolic mCherry-Ezrin (red). Insert: Relative fluorescence quantification of mCherry-ezrin distribution in a single RAW 264.7 cell, within a defined region of interest at the cell edge (yellow shaded box). Fluorescence intensity increases towards the cytosol and plateaus. Second panel: Pseudo coloured look-up table (LUT) applied to the same cells. Most ezrin reports uniform fluorophore intensity across the cytoplasm. Scale bar 20 µm; insert 5 µm. Representative of at least 20 cells.

(fig.3.3.2ii). This difference in subcellular location was further demonstrated by expressing the proteins simultaneously within individual cells, and was made strikingly apparent by overlaying images of both fluorophores (fig. 3.3.2iii). Therefore, the observed difference in subcellular location was not due to a competition between the two constructs, because the same pattern of localisation was observed in cells transfected with either construct, in the absence of the other.

It was found that plasma membrane binding of ezrin via the FERM domain at the N-terminus was disrupted by the attachment of the fluorophore (e.g. mCherry). Since ezrin-mCherry remained cytosolic, it was concluded that the C-terminal domain actin binding activity alone was insufficient to maintain ezrin at the cell edge. This is in keeping with findings by Fritzsche and colleagues, whose work on the dynamics of ezrin turnover demonstrated that the N-FERM domain interaction is dynamically more important than the actin binding relationship, in ezrin localisation to the plasma membrane (Fritzsche et al., 2014).

This may be in part be due to the dynamic nature of the cortical actin network, which is not a static molecular structure. The actin cytoskeleton undergoes monomeric actin (G-actin) additions and removals (known as 'treadmilling'). This is in combination with the long length of F-actin, relative to its diameter, which makes it subject to Brownian perturbations. In contrast, placing the fluorophore at the C-terminus (e.g. ezrin-mEmerald or ezrin-mCherry) would have no effect of the FERM binding activity at the N-terminus, as shown here (fig. 3.3.2 ii). This configuration was presumably stable, because the FERM binding locks the N-terminus to the plasma membrane, which holds the ezrin molecule in close enough proximity for it to bind F-actin with a lower affinity (Algrain et al., 1993; Fritzsche et al., 2014). Ezrin expressed in RAW 264.7 cells which is fluorescently-tagged at the C-terminal domain, therefore gives the best representation of the ezrin location observed in unstimulated human neutrophils.

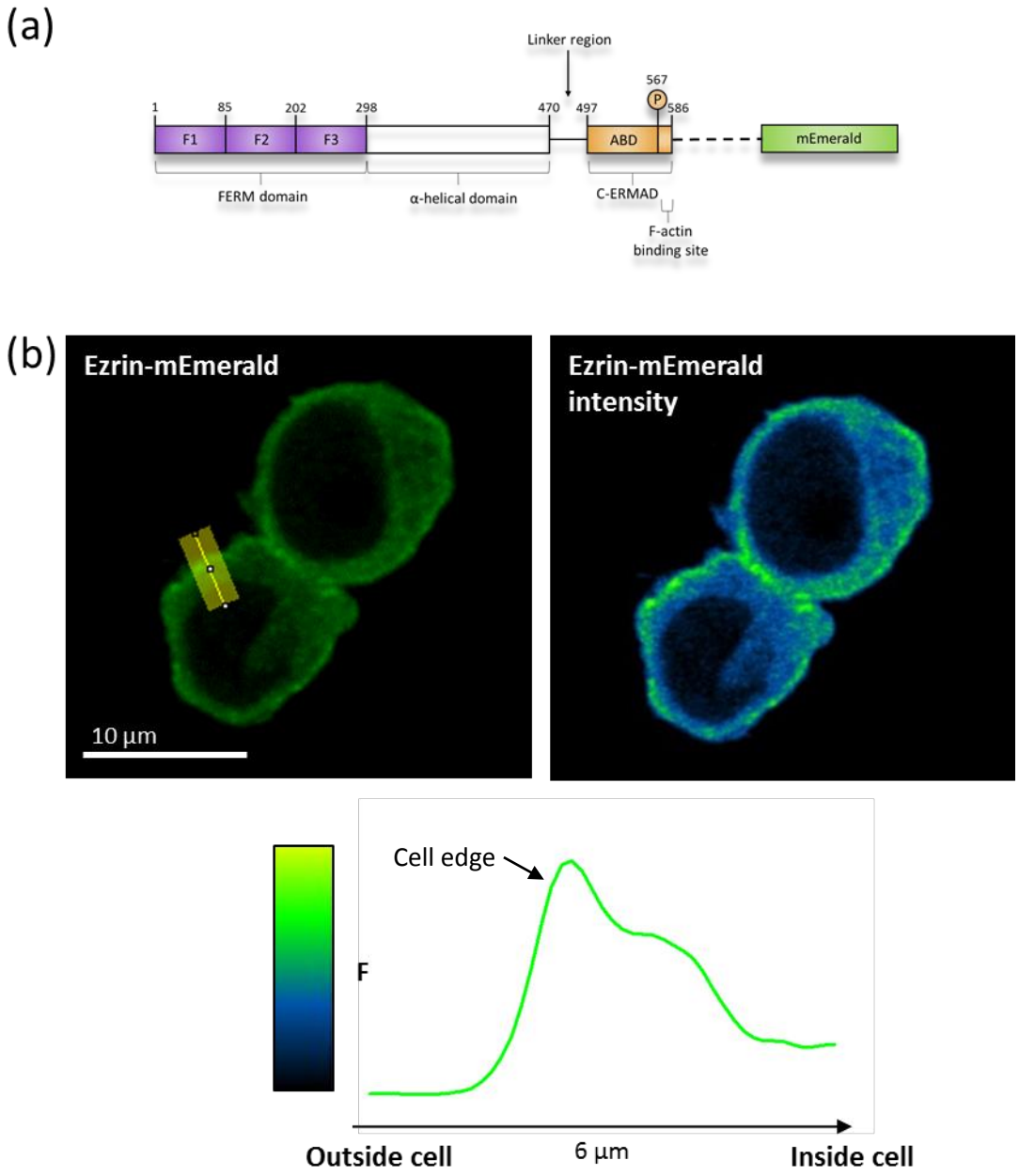

Figure 3.3.2ii: Ezrin-mEmerald expression in RAW 264.7 cells
(a) Structure of Ezrin-mEmerald. The fluorophore is attached to ezrin at the C-terminal actin binding domain. **(b)** First panel: RAW 264.7 cells expressing Ezrin-mEmerald (green) at the cell edge. Relative fluorescence quantification of Ezrin-mEmerald distribution in a single RAW264.7 cell, within a defined ROI at the cell edge (yellow shaded box). Fluorescence intensity is highest at the cell edge, and decreases towards the cytosol. Second panel: LUT applied to the same cells. Ezrin is primarily located at the cell edge. Scale bar 10 µm. Representative of at least 20 cells.

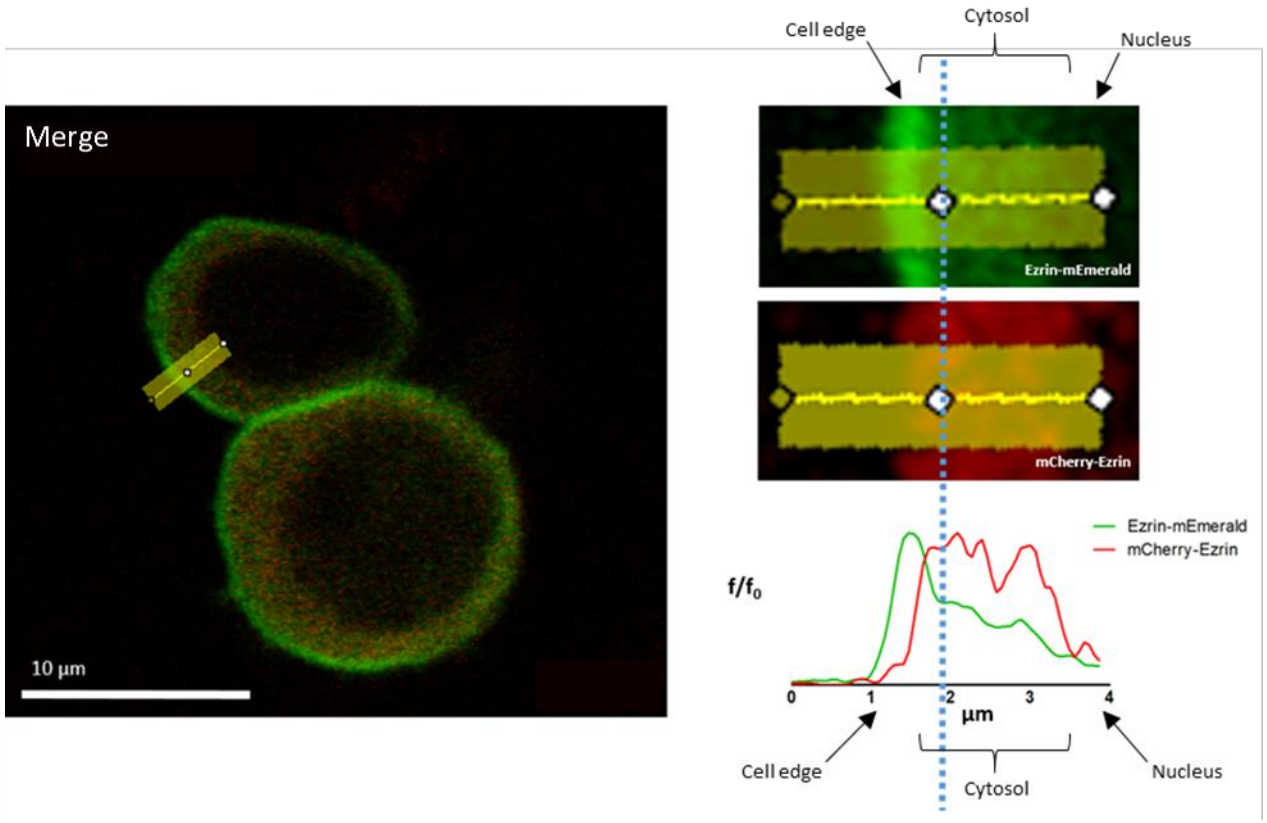

Figure 3.3.2iii: Co-expression of mCherry-Ezrin and Ezrin-mEmerald in RAW 264.7 cells

First panel: RAW 264.7 cells co-expressing cytosolic mCherry-Ezrin (red) in the cytosol, and Ezrin-mEmerald (green) at the cell edge. Relative fluorescence quantification of mCherry-Ezrin and Ezrin-mEmerald distribution in a single RAW264.7 cell, within a defined ROI at the cell edge (yellow shaded box). Ezrin-mEmerald fluorescence intensity is higher than mCherry-ezrin intensity within the first 0.5 µm of the cell edge. Ezrin-mEmerald intensity decreases towards the cytosol. mCherry-ezrin fluorescence intensity increases 0.5 µm into the cytosol and remains higher than ezrin-mEmerald. Both fluorophores show low intensity at the juxtanucelar position. Scale bar 10 µm. Representative of at least 10 cells.

3.3.3 Dynamic changes in ezrin during Ca^{2+} influx

The next consideration to explore, was whether or not the ezrin localisation at the cell periphery was disrupted by Ca^{2+} influx. Since RAW 264.7 cells do not have well-defined Ca^{2+} influx channels or receptor agonists which are linked to Ca^{2+} channel opening, it was necessary to employ a pharmacological approach.

In most cells, Ca^{2+} channels can be opened by the SOCE system, whereby depletion of intracellular Ca^{2+} stores lead to the opening of Ca^{2+} channels at the plasma membrane. In order to deplete the Ca^{2+} stores experimentally, it is necessary to inhibit the ATP-driven SERCA pumps which pull Ca^{2+} into the stores. If this is done in the absence of extracellular Ca^{2+}, there is a resultant 'trickle' of Ca^{2+} out of the stores (which can also not be replaced, due to the lack of extracellular Ca^{2+}) and the stores will become depleted of Ca^{2+} over a period of 2-5 mins. The intracellular stores can be made even 'leakier' to Ca^{2+} (as can the plasma membrane) by the application of a Ca^{2+} specific ionophore, such as ionomycin. When extracellular Ca^{2+} is reintroduced there will be a short pulse of Ca^{2+} influx, when the Ca^{2+} channels are open but the stores have not yet refilled, up to a point that causes closure of the plasma membrane Ca^{2+} channels. In order to maximise the amount of influx, a steeper inward gradient of Ca^{2+} concentration can be achieved through supraphysiological extracellular Ca^{2+} concentrations. This tactic was therefore employed to induce a large Ca^{2+} influx in RAW 264.7 cells expressing the fluorescent ezrin constructs. A 'cocktail' of thapsigargin (an inhibitor of SERCA pumps); ionomycin (a Ca^{2+}-specific ionophore) and EGTA (to chelate extracellular Ca^{2+}) was administered, followed after a few minutes by Ca^{2+}. When the cocktail was applied to RAW 264.7 cells expressing ezrin-mCherry or ezrin-mEmerald, there was a time dependent release of fluorophore from the cell periphery (fig. 3.3.3), accompanied by an expansion of the cell area (bloating) and sometimes blebbing. This demonstrated that the ezrin location at the cell edge could be disrupted by a Ca^{2+} influx, and a consequence of the loss of peripheral ezrin was morphological change in the cell, as a result of membrane expansion.

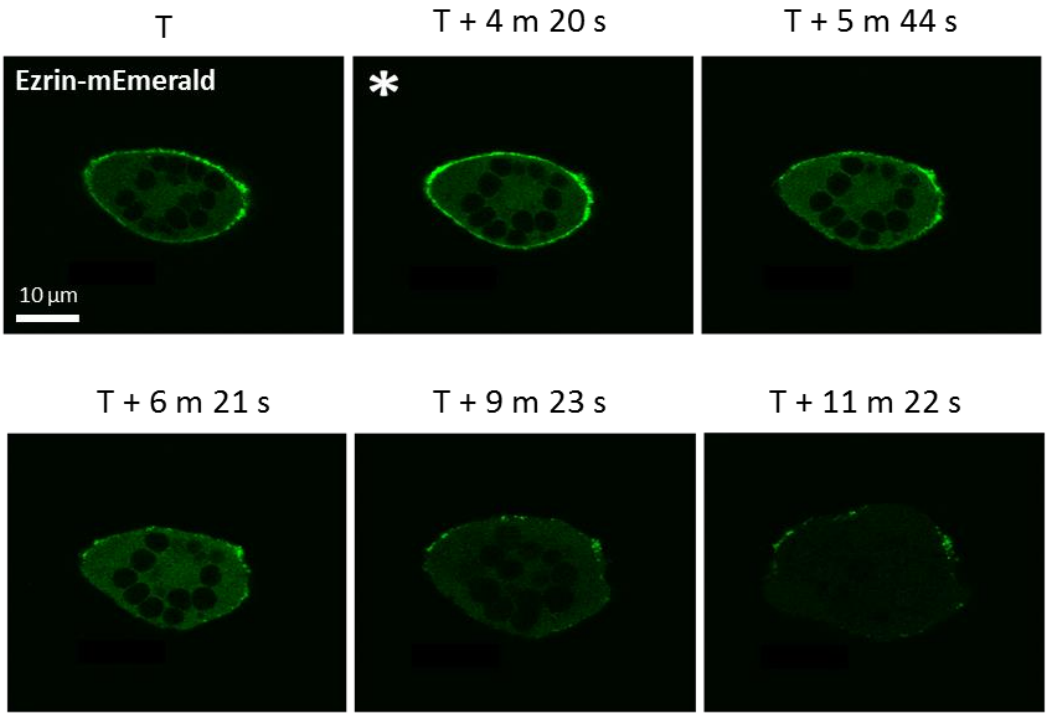

Figure 3.3.3: Ezrin location in RAW 264.7 cells treated with a high Ca^{2+} cocktail
RAW 264.7 expressing C-terminal tagged ezrin-mEmerald. A high Ca^{2+} cocktail (40 µM thapsigargin, 20 µM ionomycin) was administered, and extracellular Ca^{2+} was elevated to 65 mM at the (*). Ezrin is lost from the cell edge concurrent with cell spreading. Representative of at least 3 cells. Scale bar 10 µm.

3.3.4 Dynamic changes in ezrin during myeloid phagocytosis

In order to establish whether ezrin translocation away from the phagosomal membrane occurred in RAW 264.7 cells, in a similar way to that seen in neutrophils (fig. 3.3.1), RAW 264.7 cells expressing ezrin with a fluorophore attached at the C-terminal domain were challenged with C3bi-opsonised zymosan particles. The kinetics of ezrin re-distribution was monitored by imaging live cells performing phagocytosis. In all cells in which live phagocytosis events were captured (12 cells), there was a total loss of ezrin from the base of the phagocytic cup, before completion of phagocytosis (fig. 3.3.4i). No C-terminally-tagged ezrin was present at phagosomes containing zymosan particles (31 phagosomes), despite clear peripheral ezrin located at the rest of the plasma membrane. When an individual cell attempted or completed two separate phagocytic events, loss of ezrin was observed at both phagocytic cups independently, at the time of cup formation (fig. 3.3.4ii). Thus, the loss of peripheral ezrin was both temporally and spatially synchronised with the onset of phagocytosis. These data show that ezrin (C-terminal region, at least) is released from the plasma membrane during periods of high cytosolic Ca^{2+}; consistent with Ca^{2+}-mediated cleavage by μ-calpain.

Following proteolysis by μ-calpain, it is possible that the N-terminal domain of ezrin remains attached to the plasma membrane, via the N-terminal FERM domain. However, experiments with N-terminally tagged mCherry-ezrin have shown that ezrin-actin binding alone, via the C-terminus of ezrin, was not sufficient to maintain peripheral ezrin (section 3.3.2). Following cleavage of ezrin in the linker region, between the two functional domains, the downstream C-terminal fragment of ezrin would no longer have sufficient binding strength to remain at the cell periphery. The C-terminal fragment, along with the attached fluorophore, would be lost from its location at the cell edge.

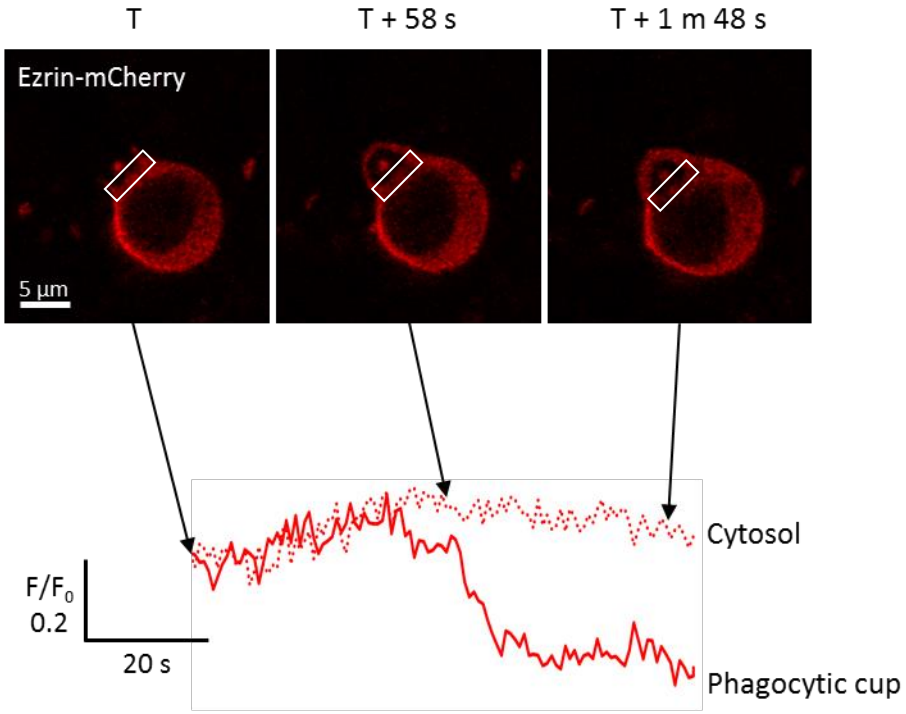

Figure 3.3.4i: Ezrin location in RAW 264.7 cells during phagocytosis
RAW 264.7 cell expressing ezrin-mCherry, performing phagocytosis of a single zymosan particle. Ezrin is lost from the phagocytic cup at the onset of phagocytosis. ROI: white box. Scale bar 5 µm.

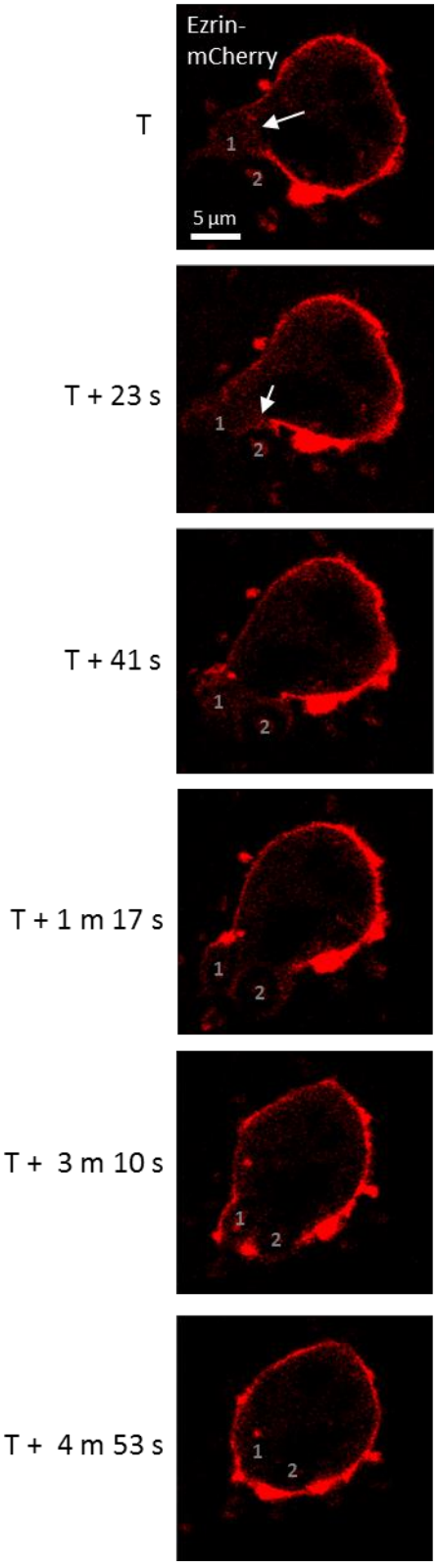

Figure 3.3.4ii: Ezrin loss is temporally and spatially synchronised with the onset of phagocytosis
RAW 264.7 cell expressing ezrin-mCherry, performing phagocytosis of two zymosan particles (1 and 2). Ezrin is lost from the phagocytic cup of each phagocytosis event independently (white arrows). Scale bar 5 µm.

3.3.5 Evaluation of ezrin GFPi as marker of ezrin cleavage

Although the global release of ezrin from the cell periphery, following global Ca^{2+} influx, was consistent with its cleavage by μ-calpain, other explanations of this re-distribution are possible. For example, elevated Ca^{2+} influx could activate processes which reduce either actin polymerisation (e.g. via gelsolin), or the PIP_2 content in the membrane (e.g. via activation of PLCβ), both of which would have an impact on ezrin localisation at the cell periphery. It was therefore important to seek further evidence for ezrin cleavage within the cell.

A novel approach was adopted based on the knowledge that ezrin preferentially binds to the plasma membrane via its N-terminal FERM domain. Therefore, it is possible that when ezrin cleavage occurs, the N-terminal FERM fragment may persist at the plasma membrane, whereas the C-terminal actin binding domain would be released into the global cytosol. If fluorophores of different excitation/emission wavelengths were attached at either side of the μ-calpain cleavage site in ezrin, separation of the two signals may occur following ezrin cleavage. While it has been established that C-terminally tagged ezrin constructs display the membrane localising properties of endogenous ezrin, it has also been found that fluorophores located at the N-terminal domain inhibit typical ezrin behaviours. Therefore a fluorophore attached to the N-terminal end of ezrin would be no use, since it fails to locate at the cell periphery (section 3.3.2)

One solution to this would be to use a fluorescent construct which does not mask the N-terminal binding domain, yet still marks the first half of the ezrin fragment (i.e. before the linker region). An ezrin construct with GFP inserted within lobe F3 of the FERM domain has previously been reported: ezrin-GFPi (GFP-intra) (fig. 3.1) (Marion et al., 2011). In order for ezrin-GFPi to be a useful tool for monitoring the cleavage of ezrin, two conditions must first be satisfied, these are: (i) ezrin-GFPi must behave as endogenous ezrin and localise to the cell edge of RAW 264.7 cells, and (ii) the GFPi fluorophore must be retained with the N-terminal fragment of ezrin, following proteolytic cleavage.

The first condition was satisfied by showing that in all RAW 264.7 cells expressing ezrin-GFPi, the fluorescent signal came from the cell edge (fig. 3.3.5i), and the location of ezrin-GFPi coincided with other fluorescently-tagged ezrin constructs. Furthermore, sequencing analysis of the ezrin-GFPi construct (a gift from Sabrina Marion), confirmed the location of GFPi in the N-FERM domain of ezrin (at position 234) (fig. 3.3.5ii – full sequence alignment in Appendix I).

In order to test the second condition, namely that the C-terminal fluorophore but not the GFPi would be released by μ-calpain activity, *ex vivo*, the probes were extracted from RAW 264.7 cells expressing them, and subjected to Ca^{2+}-activated μ-calpain. Human neutrophil lysate was used to supply the μ-calpain. The ezrin-mCherry and ezrin-GFPi were immobilised by antibody capture directed to the FERM domain, in plastic wells, and μ-calpain was added in the absence of Ca^{2+}. The addition of Ca^{2+} to the well, to activate μ-calpain, resulted in a full release of fluorophore from the C-terminus. However only 64% ± 4.37% of the GFPi was released (fig. 3.3.5iii). It is possible that under these *in vitro* conditions μ-calpain, which is remarkably non-specific (Goll et al., 2003), was able to cleave ezrin at other sites, albeit with slower kinetics and with lower affinity. The GFPi fluorophore may therefore have been released by cleavage at non-preferential sites in ezrin within the FERM domain, between the N-terminus and the GFPi insert site. While it was unclear as to why some GFPi was releasable in the in vitro assay, even under these severe proteolytic conditions, there was a clear distinction between the releases of the two fluorophores.

3.3.6 Ezrin cleavage during Ca^{2+} influx

As the Ca^{2+} conditions necessary to release ezrin from the cell periphery had been established (section 3.3.3), the question then arose as to whether this release was by ezrin cleavage of some other (perhaps non-physiological) mechanism. The 'dual fluor' approach, shown in section 3.3.5, was therefore applied to the RAW 264.7 cells expressing ezrin-mCherry and ezrin-GFPi.

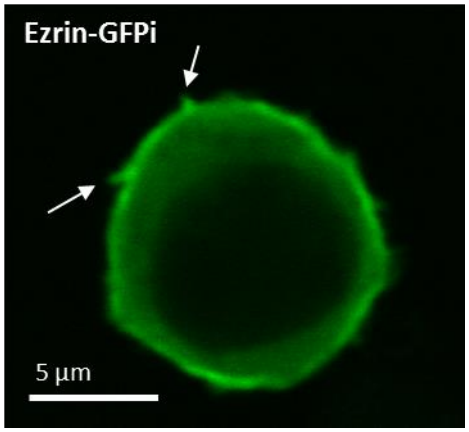

Figure 3.3.5i: Ezrin-GFPi distribution in RAW264.7 cells
RAW 264.7 cell expressing ezrin-GFPi, visible even in microridge structures (arrows). Scale bar 5 µm.

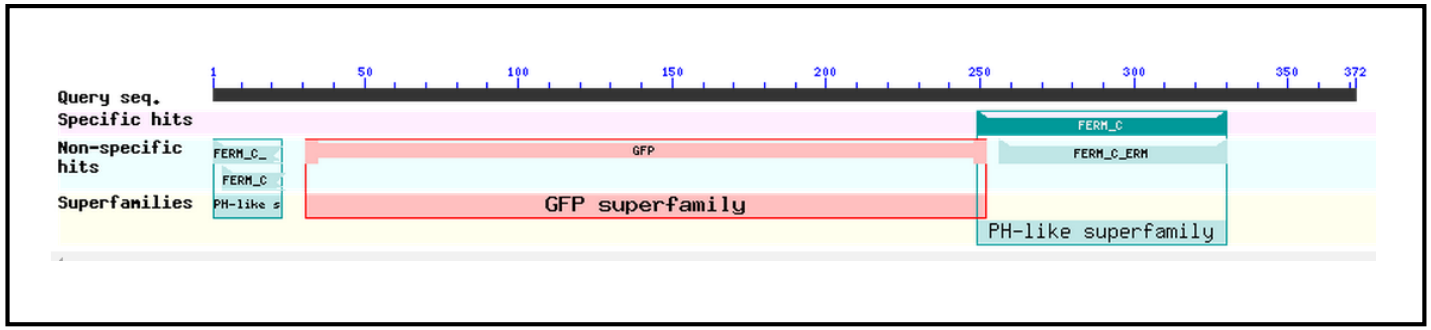

Figure 3.3.5ii: BLAST search of sequenced ezrin-GFPi
372 amino acids returned from Sanger sequencing results were entered as query in NCBI Protein Blast. Residues 4-24 align with FERM C-terminal PH-like domain (88% Identity, E-value 2.41e-03). Residues 31-252 align with GFP (E-value 3.72e-105). Residues 256-330 align with FERM domain C-lobe/F3 of the ERM family (76% Identity, E-value 4.72e-44). (Detailed alignment in Appendix.)

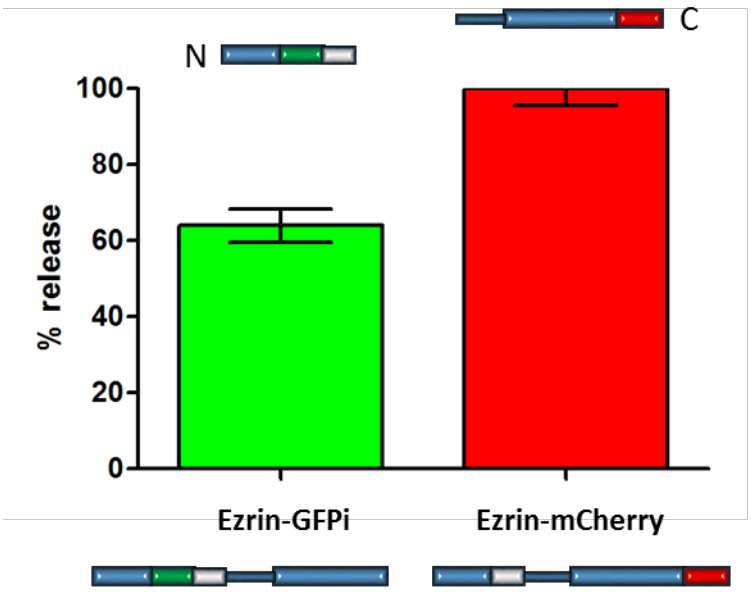

Figure 3.3.5iii: Differential fluorophore release following μ-calpain cleavage of ezrin-GFPi and ezrin-mCherry

The percentage (±SEM) Ca^{2+}-activated *ex vivo* release of ezrin fragments containing either the GFPi fluorophore (ezrin-GFPi) or mCherry (ezrin-mCherry). $P<0.05$ (two-tailed, un-paired T-test with equal variance), n=3.

In RAW 264.7 cells co-expressing both probes, both signals were found to come from the cell edge, and cells which expressed both probes at approximately comparable intensity levels were selected for further experimentation. When the Ca^{2+} influx strategy was applied, as before, cells often responded by bloating and assuming the maximal surface area to volume morphology (i.e. spherical) (fig. 3.3.6i). In these cells no ezrin-mCherry was detectable at the cell edge, but there was a delay in release of the ezrin-GFPi fragment, relative to the ezrin-mCherry fragment, and some ezrin-GFPi remained located at the cell edge (fig. 3.3.6ii). This was often at localised regions, associated with non-smooth zones e.g. small wrinkles (fig. 3.3.6i). When titrating the Ca^{2+} influx by two extracellular Ca^{2+} additions, so that Ca^{2+} influx was doubled at the second addition, it could be seen that the milder Ca^{2+} influx caused significant release of the mCherry fluorophore, without any release of GFPi (fig. 3.3.6iii). The subsequent larger Ca^{2+} influx caused both probes to be released. This was consistent with initial ezrin cleavage between the loci of the two fluorophores, i.e. the linker region; but that higher Ca^{2+} influx had an additional effect. The additional effect may have been caused by ezrin cleavage at other sites (such as before the GFPi insertion site, as seen in the *in vitro* assay (section 3.3.5)). Alternatively, the additional effect of the high level Ca^{2+} influx was unrelated to μ-calpain activity, and caused by an alternative mechanism which liberated ezrin from the cell edge.

3.3.7 Ezrin release during phagocytosis

Unlike the Ca^{2+} influx 'cocktail' approach, phagocytosis was shown to cause a localised and precisely timed release of ezrin from the base of phagocytic cups. In order to establish whether this was caused by ezrin cleavage, phagocytosis of C3bi zymosan particles was induced in cells co-expressing both ezrin-GFPi and ezrin-mCherry. In 7 out of 8 cells, in which live phagocytosis was observed, there was no measurable difference in the release of either fluorophore from the cell edge (fig. 3.3.7i). This suggested that ezrin was either: (i) released by the high influx mechanism identified in section 3.3.6, which may involve multiple

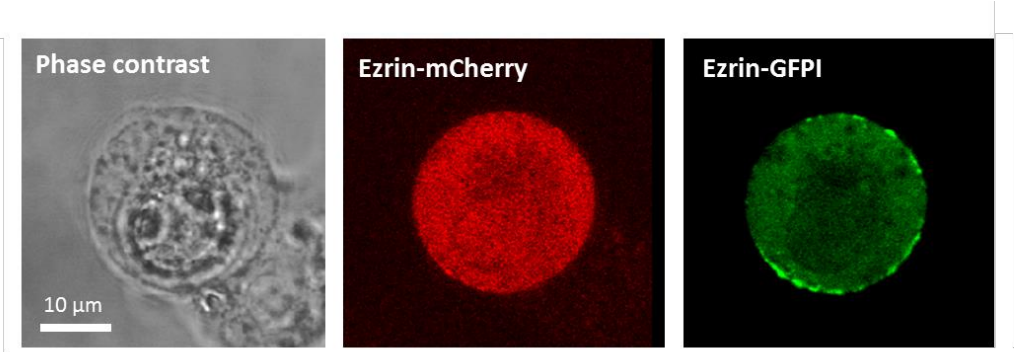

Figure 3.3.6i: Ezrin cleavage in RAW 264.7 cells treated with a high Ca^{2+} cocktail
RAW 264.7 cell co-expressing both C-terminally tagged ezrin-mCherry and ezrin-GFPi were exposed to a high Ca^{2+} cocktail (40 µM thapsigargin, 20 µM ionomycin and 65 mM Ca^{2+}). Ezrin-mCherry was lost from the cell edge, whereas ezrin-GPFi remained at the edge in some locations, despite cell bloating. Scale bar 10 µm.

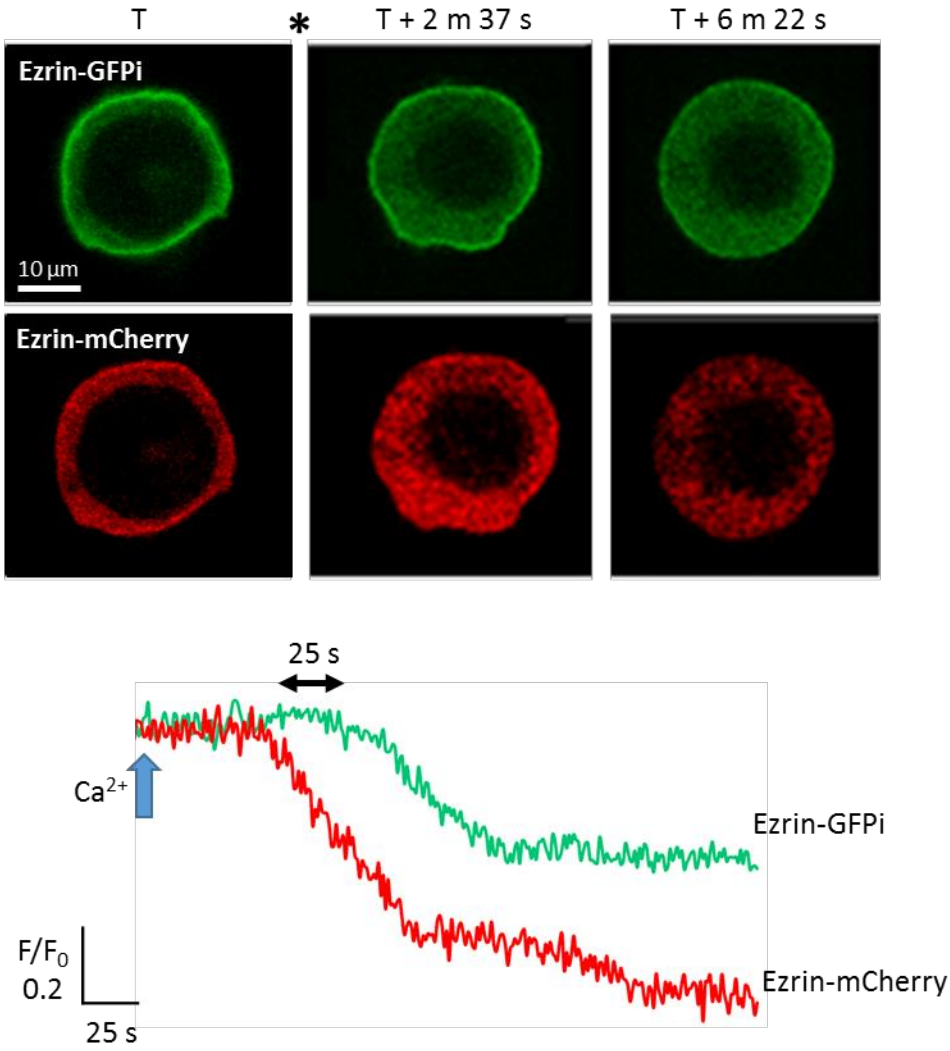

Figure 3.3.6ii: Delay in ezrin N-FERM domain release from cell edge

RAW 264.7 cell co-expressing ezrin-GFPi and ezrin-mCherry. A high Ca^{2+} cocktail (40 µM thapsigargin, 20 µM ionomycin and 65 mM Ca^{2+}) was added at the (* and blue arrow). C-terminal ezrin (red) is lost from the cell edge concurrent with cell bloating. N-terminal domain ezrin is also lost with a delay of 25 s. Scale bar 10 µm.

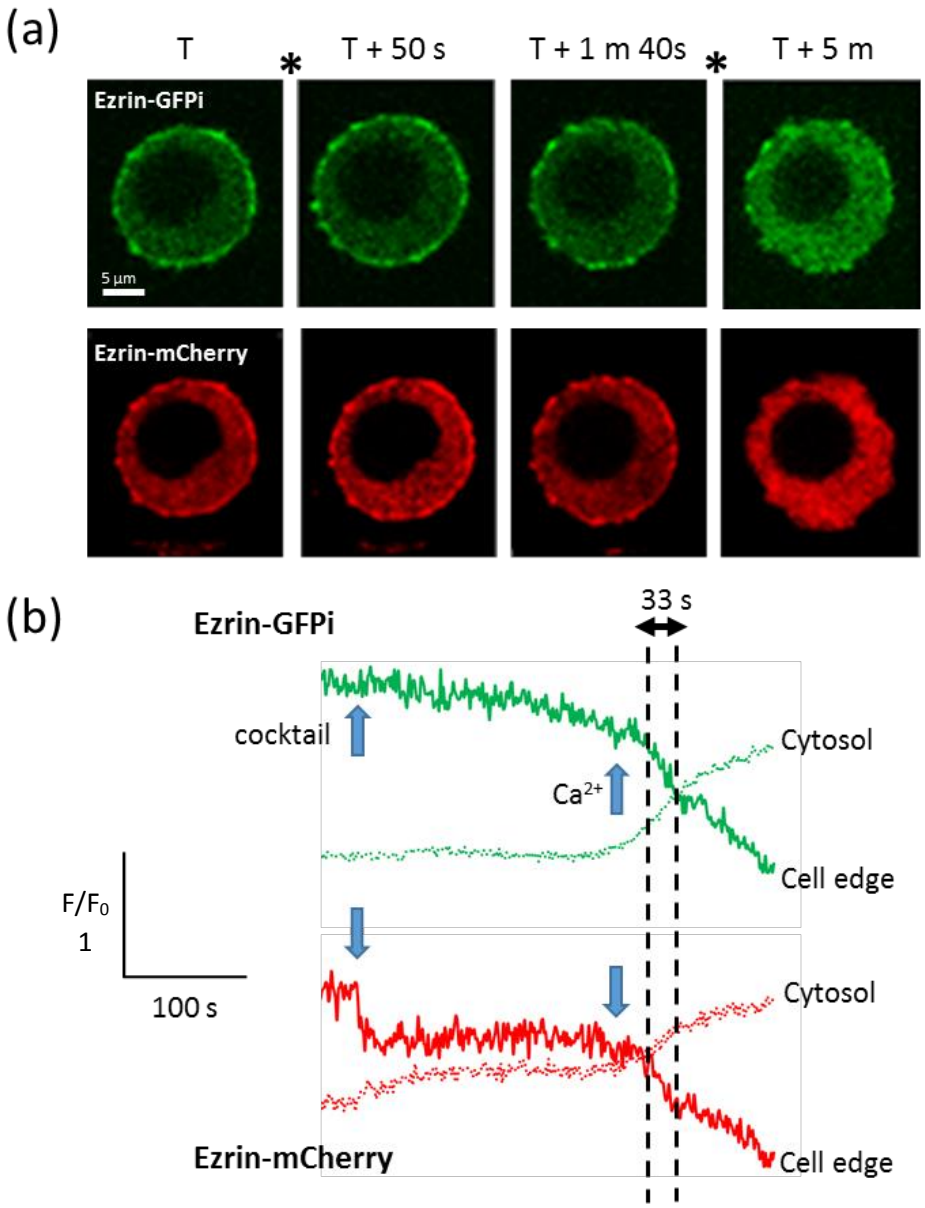

Figure 3.3.6iii: Differential release of ezrin-GFPi and ezrin-mCherry after Ca^{2+} elevation **(a)** RAW 264.7 cell co-expressing ezrin-GFPi and ezrin-mCherry, with addition of the high Ca^{2+} cocktail, and subsequent additional Ca^{2+} at the (*). **(b)** Ezrin-GFPi (green traces) and ezrin-mCherry (red traces) fluorescence intensity measured from the cell periphery (solid line) and the cytosol (dashed line) during the elevation of Ca^{2+} influx. At the first arrow, a Ca^{2+} elevating 'cocktail' (40 µM thapsigargin, 20 µM ionomycin and 65 mM Ca^{2+}) was added; at the second arrow, the extracellular Ca^{2+} was stepped up by a second addition of 65 mM Ca^{2+}.

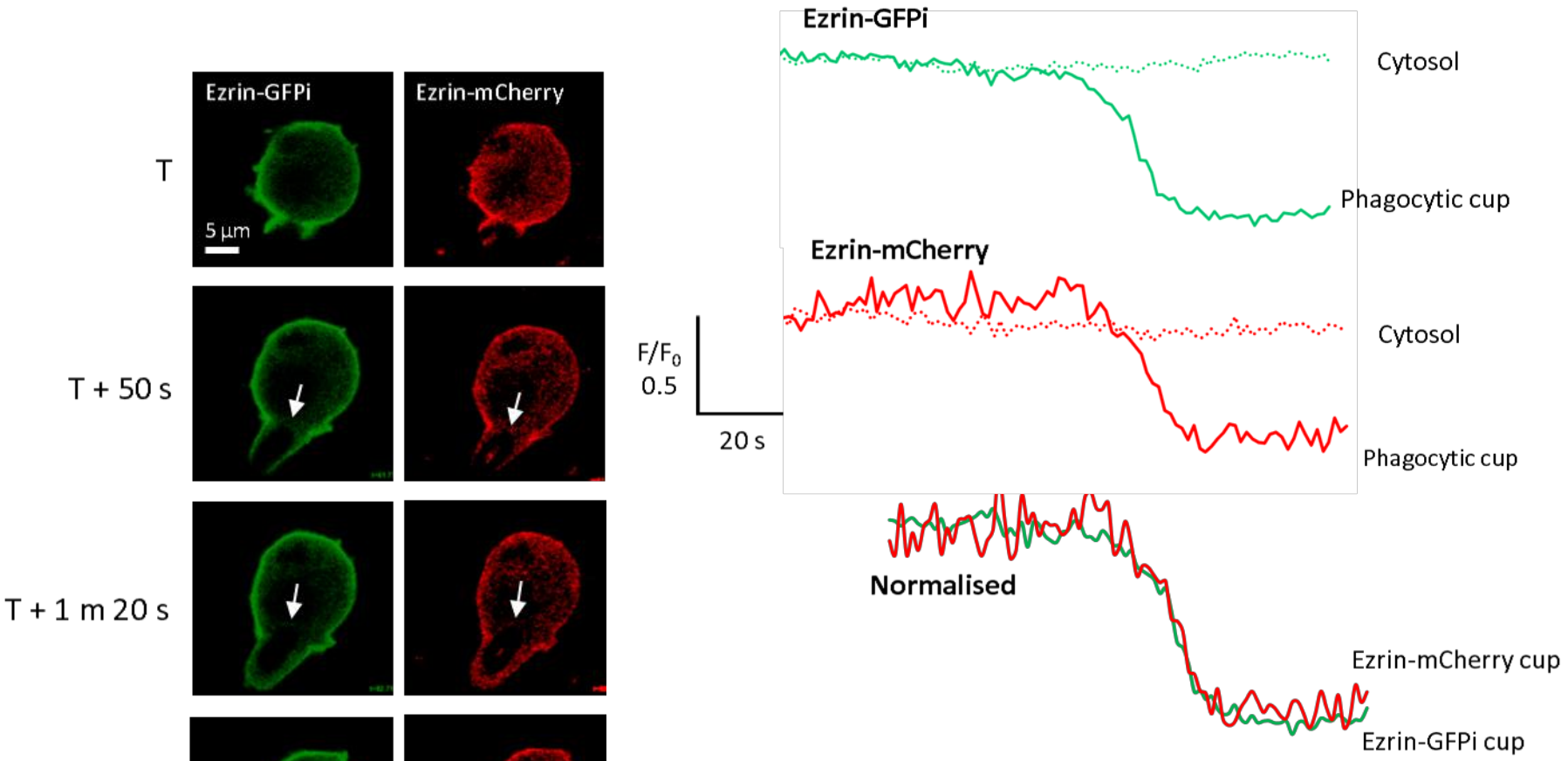

Figure 3.3.7i: Ezrin location in RAW 264.7 cells during phagocytosis
RAW 264.7 cell co-expressing ezrin-GFPi and ezrin-mCherry performing phagocytosis of a C3bi-opsonised zymosan particle. Both ezrin constructs were lost from the phagocytic cup during phagocytosis, and neither were present at the newly formed phagosome (white arrows). Ezrin was recovered at the cell edge following particle internalisation (grey arrows). Scale bar 5 µm.

cleavage events (therefore unable to be time-resolved, due to their rapid nature), or (ii) that the entire ezrin molecules was lost from the membrane intact.

However, when cells attempted more complex phagocytosis (i.e. of multiple zymosan particles) the mCherry fragment could be lost without concomitant loss of the GFPi fragment. Occasionally, RAW 264.7 cells attempt to generate two phagocytic cups at once, and under these conditions, phagocytosis of one cup is able to pause while the other progresses (Dewitt et al., 2002; Dewitt et al., 2006). In these experiments, during such a pause, the signature of ezrin cleavage at the linker region was observed. There was a small release of the C-terminal fluorophore (mCherry), while the N-terminal fluorophore (GFPi) remained attached to the base of the phagocytic cup (fig. 3.3.7ii). However, this was a temporary situation; within 30 s there was a decrease in GFPi fluorescence at the cup, and after 60 s both fluorophores were lost. It was concluded that during phagocytosis, the loss of ezrin from the base of the forming phagocytic cup involved at least two steps: (i) rapid cleavage of ezrin at the linker site, and (ii) a high Ca^{2+} influx signal.

3.4 Discussion

The work presented in this chapter has progressed our understanding of the role of ezrin in myeloid shape change, and especially during the process of phagocytosis. The loss of localised ezrin at the phagocytic cup was observed in both fixed human neutrophils, and dynamically in RAW 264.7 cells. The data here have shown that a similar loss of ezrin from the cell edge can be triggered over the entire cell surface by artificially inducing Ca^{2+} influx. Using a novel method, whereby two fluorophores are attached to ezrin molecules either side of the μ-calpain sensitive linker region, it was shown that cleavage of ezrin is involved in this mechanism. A second mechanism for the release of ezrin has also been established, which occurs at higher Ca^{2+} influx levels. This may also involve μ-calpain activation and cleavage of ezrin at loci other than the linker

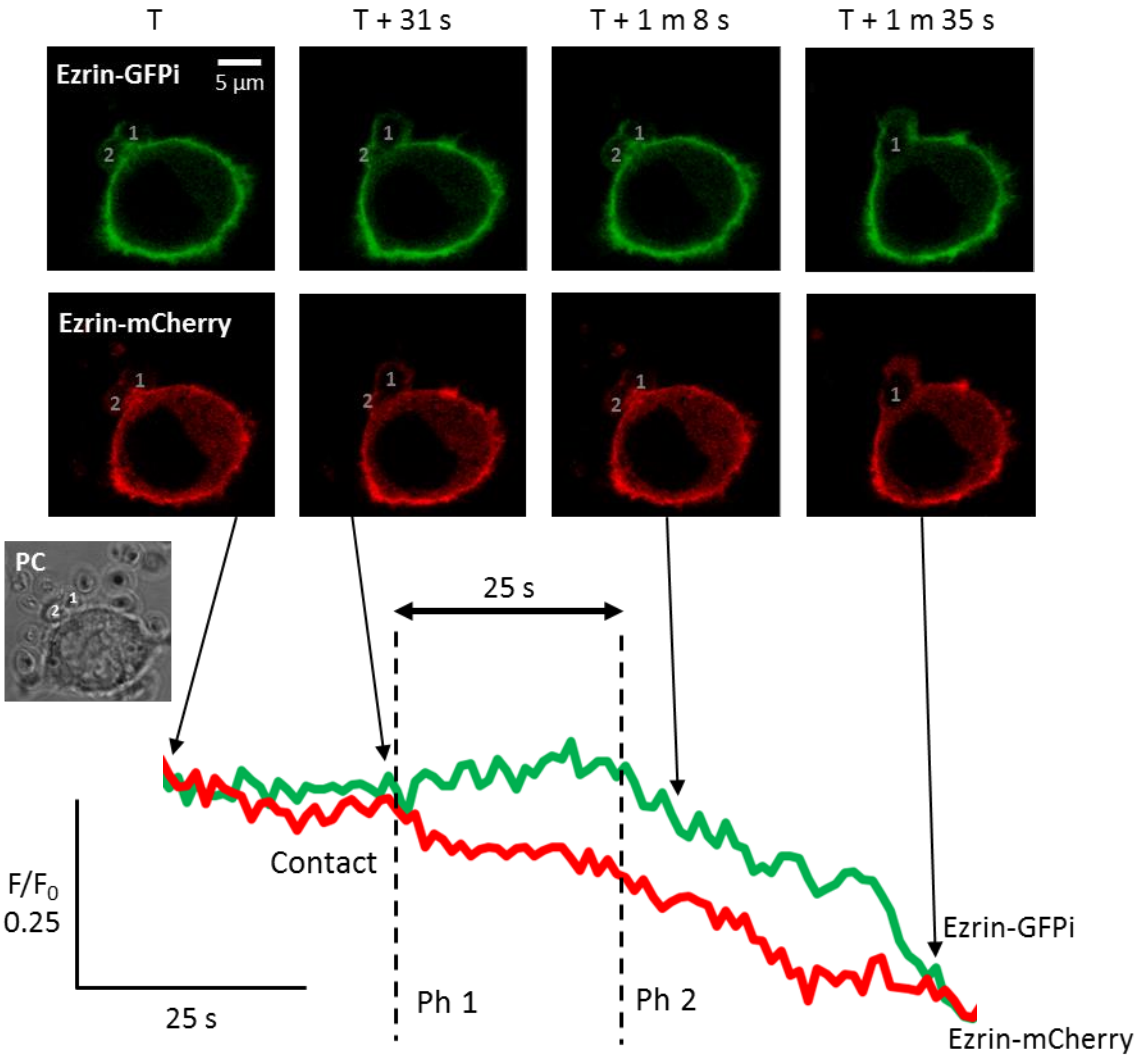

Figure 3.3.7ii: The N-FERM domain of ezrin persists at the phagocytic cup
RAW 264.7 cell co-expressing ezrin-GFPi and ezrin-mCherry, attempting complex phagocytosis of two zymosan particles (1 and 2). Insert: Phase contrast (PC) image shows location of two targeted zymosan. In phase 1 (Ph1) immediately following particle contact, ezrin-mCherry is released from the cup while ezrin-GFPi is retained. In phase 2 (Ph2) about 25 sec later, both fluorophores are released in parallel. Scale bar 5 µm.

region. Alternatively, it may be the result of mechanisms not involving μ-calpain cleavage or proteolysis. When applied to phagocytosis, a similar picture emerged. There was a specific localised and temporally precise release of ezrin from the base of the forming phagocytic cup, which involved ezrin cleavage at the linker site, followed by a second release mechanism which may be similar to that seen with artificially induced higher Ca^{2+} influx. Work presented in subsequent chapters of this thesis will show that Ca^{2+} influx, which occurs locally near the forming phagocytic cup, can exceed levels achieved using the global 'cocktail' approach.

3.4.1 Mechanisms of ezrin release

Before the work presented in this chapter, the hypothetical relationship between ezrin and μ-calpain activation, through Ca^{2+} influx, was simply that cleavage of ezrin occurred. In neutrophils this has been shown to occur when the cells were stimulated with the Ca^{2+} influx inducing agonist, fMLP (Shcherbina et al., 1999; This thesis Chapter 6). Although, this earlier report was a biochemical study and could not localise the event within the cell, or provide single cell dynamics. Western blot analysis has showed that the major ezrin fragment size was 56KDa (Yao et al., 1993; Shuster and Herman, 1995; Elumalai, 2012), which is consistent with cleavage of ezrin at the linker region between the N-terminal FERM plasma membrane binding domain, and the C-terminal actin binding domain. However, in our lab, neutrophil ezrin often presents with multiple smaller degradation bands of varying size (Yao et al., 1993; Elumalai, 2012). This would suggest that other μ-calpain cleavage sites also exist in ezrin. We have also found that hexa-peptides, from the linear linker region are *in vitro* substrates for μ-calpain proteolysis. This may not be unexpected as, when presented with a substrate *in vitro*, μ-calpain has little selectively. However, mass spectrum analysis of the resultant degradation of the ezrin derived peptides showed that while this region was prone to μ-calpain degradation, other sites were not cleaved by μ-calpain. Clearly, in the 'dual fluor' ezrin

approach, where the two ends of the ezrin molecule were separated in the cell, cleavage must have occurred somewhere in the linker region. This is the first demonstration of this event in a living cell.

Additional issues arose when both the N- and C-terminal ends of ezrin were released. It was not possible to distinguish between cleavage at another non-linker region site from another other non-proteolytic mechanism. The computational prediction of μ-calpain cleavage sites software, Multiple Kernel learning software (duVerle et al., 2011 – available at www.calpain.org), points to several high probability cleavage sites. These include loci within both the linker region, and outside; including loci which would liberate both fluorophores (fig. 3.4.1).

The possibility that other mechanisms which release ezrin exist, must also be considered as a result of this work. As ezrin binds to F-actin, conditions which depolymerise actin may cause ezrin to be released. For example, gelsolin which depolymerises F-actin by capping the growing ends, is a Ca^{2+} dependent protein with a Ca^{2+} binding EF hand (Kinosian et al., 1998), similarly to μ-calpain (see Chapter 1). However, the N-terminus and C-terminus binding states are clearly of different importance for maintaining ezrin at the cell edge. Whether the fluorophore is at the N- or C-termini has a profound influence on the localisation of ezrin, and shows that the FERM domain binding is far more important for maintaining ezrin at the cell periphery. Also, since the fluorophore on the actin binding domain probably interferes with its ability to bind to F-actin, ezrin-mCherry may have no actin binding activity, and was found to be located at the plasma membrane simply by virtue of its intact FERM domain. In which case, any Ca^{2+}-induced changes to actin polymerization would have no effect.

If there is a non-μ-calpain effect, it is more likely to be through reduction of the FERM domain binding. The FERM domain binds to the plasma membrane, mainly via PIP_2 (Barret et al., 2000; Gautreau et al., 2002). While initially

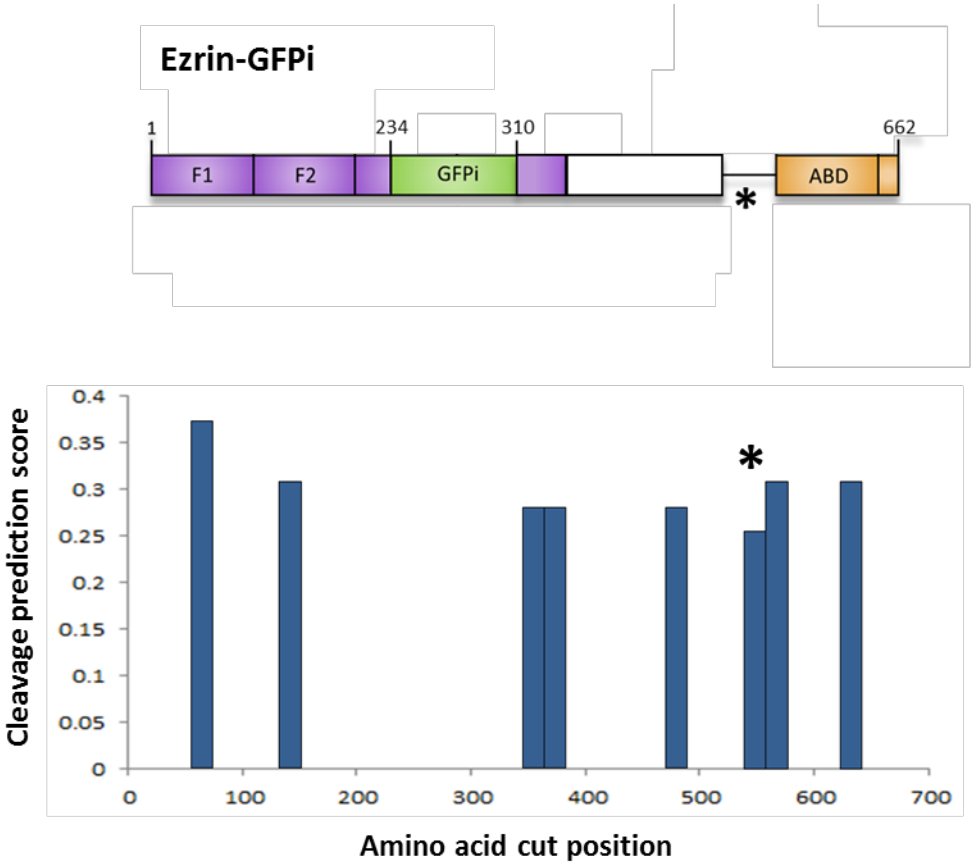

Figure 3.4.1: The most probable μ-calpain cleavage sites in ezrin Cleavage sites predicted by the Multiple Kernel learning (duVerle et al, 2011) provided online by http://calpain.org/predict (re-mapped onto ezrin-GFPi). The (*) indicates the region in the linker which differs between ezrin and moesin (which is not a μ-calpain substrate *in vivo*).

activated by GPCRs, PLCβ has a feed-forward loop whereby elevated Ca^{2+} activates it further (Horowitz et al., 2005); therefore artificially elevating cytosolic Ca^{2+} could activate PLCβ, and thereby temporarily deplete the inner leaflet of the plasma membrane of PIP_2. However, it might be expected that intact ezrin would relocate to the membrane once the homeostatic mechanism for regenerating PIP_2 (PI kinase) had restored PIP_2. In these experiments, such a return of ezrin to the cell edge after its global loss following 'cocktail' treatment was not seen. The global release of ezrin from the cell periphery, after experimentally induced Ca^{2+} influx, was an irreversible step, as were the global cell shape changes such as cell bloating. During phagocytosis, PLCβ may also be activated locally and so deplete PIP_2 and similarly underlie the release of ezrin. Once the phagosome has closed, this shuts off the possibility of PIP_2 diffusing into the phagosomal membrane and may thus lead to a persistent reduction of PIP_2. During phagocytosis there is a large production of PIP_3 localised to the phagocytic cup (Dewitt et al., 2006; Ellson et al., 2001), caused by PI(3)kinase activity, which would also result in locally depleting the membrane of PIP_2. Once formed, PIP_3 stays associated with the phagosomal membrane (Dewitt et al., 2006; Swanson, 2008; Blin et al., 2008; Maniti et al., 2012). While this could be a mechanism for ezrin release during phagocytosis, it should be remembered that the N-terminal FERM domain may also have an affinity for PIP_3 in addition to PIP_2, since both phospholipids have a charged head group. The FERM domain is also reported to bind to another charged phospholipid, phosphatidyl serine (PS), the concentration of which is unlikely to change (Yeung et al., 2009) unless PS is externalised, which occurs during apoptosis.

3.4.2 Ca^{2+} hotspots in wrinkles and during phagocytosis

The difference in the mechanism of ezrin release between the experimentally induced Ca^{2+} influx, and the physiological Ca^{2+} influx during phagocytosis, may be due to the extent of the Ca^{2+} signal. It has been shown by mathematical modelling that the cell surface topography is responsible for generating microdomains of high Ca^{2+} (Brasen et al., 2010). These domains are within

wrinkled microridge regions of the cell surface. The experimentally induced Ca^{2+} influx is a blunt instrument which would open Ca^{2+} channels at all locations on the cell surface. In contrast, the physiological route to phagocytosis is likely to be tuned to open channels where required in the microridge structures. In fact, the distribution of CD18 on human neutrophils (the binding partner for C3bi) may preferentially couple the Ca^{2+} channels at microridge structures (Erlandsen et al., 1993). It is therefore likely that during phagocytosis the local Ca^{2+} concentration rises to higher levels, when release of ezrin by μ-calpain-mediated cleavage of the linker region, and other routes of ezrin release, are almost synchronous. Later in this thesis, work is presented which supports this supposition (Chapter 5). Nunes and colleagues have also reported that hot spots of high Ca^{2+} concentration are generated near the phagosome (Nunes et al., 2012). Although it is difficult to quantify the Ca^{2+} concentration reached within these hotspots, since they are extremely localised and result from Ca^{2+} influx through open channels in the phagosomal membrane, it is likely to also be very high.

Chapter 4:

Generation of a novel genetically encoded Ca^{2+} indicator

4.1 Introduction

The cytosolic cysteine protease μ-calpain has many different substrates. As previously described, there is no commonly recognised cleavage site among its substrates in different cell types. The lack of preference for a specific sequence suggests that other factors, such as its activation by Ca^{2+}, are critical in directing μ-calpain activity to where it is required. Since Ca^{2+} is a ubiquitous secondary messenger in cells, the Ca^{2+}-mediated activation of μ-calpain activation must be tightly regulated both spatially and temporally, because any unregulated μ-calpain activity could result in the cleavage of many off-target proteins, with potentially disastrous downstream consequences for the cell. Establishing the nature of the Ca^{2+}-regulation of μ-calpain cleavage of ezrin is thus crucial for a full understanding of the mechanism of changing neutrophil and myeloid cell morphology, for example during extravasation and phagocytosis.

An important feature of μ-calpain is the concentration of Ca^{2+} required for its activation. The K_d for μ-calpain activation is in the range 20-60 μM Ca^{2+}, and purified μ-calpain is active and able to cleave purified ezrin in assays when the Ca^{2+} concentration exceeds 30 μM (Michetti et al., 1997; Shcherbina, 1999). Although there have been significant obstacles in the quest to achieve accurate measurements of sub-plasma membrane Ca^{2+} fluctuations experimentally, high Ca^{2+} concentrations of at least 30 μM have been previously reported beneath the plasma membrane in neutrophil populations, using the membrane associated probe FFP-18 (Davies and Hallett, 1998). FFP-18 loaded neutrophils reported that the Ca^{2+} concentration within 0.1 μm of the plasma membrane increased much more rapidly than that of the global cytosol when stimulated with fMLP. This correlates with areas of proposed μ-calpain activity.

Subsequently, there was an observed elevation of Ca^{2+} in the bulk cytosol, which coincided with subsidence of the cortical Ca^{2+} signal. However, limited by the relatively low fluorescent signal produced by FFP-18, these data could only be

calculated from populations, rather than measured in single cells. Furthermore, the optical resolution of membrane-associated FFP-18 and cytosolic Ca^{2+} indicators was not achievable in the same cell populations. Thus, the reconstructed data incorporate the accumulated micro-delays of individual neutrophil responses (Pettit and Hallett, 1995). At the single cell level, Ca^{2+} fluctuations in the bulk and the peripheral cytosol are likely to be faster than the rate suggested by population studies with FFP-18 (Pettit and Hallett, 1995). There is also speculation about whether the reported Ca^{2+} concentrations would actually be sufficient to activate μ-calpain (Goll et al., 2003). Interestingly, computer model simulations have predicted that microridges in the plasma membrane may provide the suitable microenvironments to foster Ca^{2+} concentrations in the higher micromolar range, up to 80 μM, and thus be capable of activating μ-calpain (Brasen et al., 2010). However, these modelling predictions have so far not been corroborated with experimental data obtained from single cell investigations.

Cytosolic Ca^{2+} distribution is complex, and involved in many cellular processes. The Ca^{2+}-dependent regulation of μ-calpain is likely a crucial regulator of neutrophil cell spreading, however, the Ca^{2+} signalling properties of this process are still not fully understood. The complexity of the mechanism, regarding the spatiotemporal organisation and the transient nature of the signal, mean that novel techniques are required to further investigate this phenomenon.

4.1.2 CEPIA (calcium-measuring organelle-entrapped protein indicators)

The calcium-measuring organelle-entrapped protein indicators (CEPIA) family (Suzuki et al., 2014) are genetically encoded Ca^{2+} indicators (GECIs) (Sun et al., 2013), with specific targeting sequences which localise them to intracellular organelles. The CEPIA family was developed by Suzuki and colleagues (2014), based on the GCaMP family of Ca^{2+} sensing probes, to measure intraorganellar Ca^{2+} concentrations much higher than those achieved in the global cytosol.

Unlike small molecule Ca^{2+} indicators, which are dispersed throughout the cell cytosol, GECIs can be engineered to orientate themselves to specific locations within the cell. Thus, this family of GECIs represent new possibilities for high resolution Ca^{2+} imaging.

CEPIA2 and CEPIA3 are based on the popular and robust Ca^{2+} indicating protein GCaMP2 (Nakai et al., 2001). At physiological temperatures, Ca^{2+} signalling via GCaMP2 proteins occurs within 100 ms, which is sufficient to detect many intracellular Ca^{2+} signalling processes. CEPIA proteins are made up of three functional domains; a cyclically permuted enhanced green fluorescent protein (cpEGFP), which is attached to the light chain of myosin kinase M13, and also the Ca^{2+} binding calmodulin domain (CaM) (fig. 4.1.2i). Fluorescence of cpEGFP is achieved through interactions between the CaM and cpEGFP domains, which arise when CaM binds Ca^{2+}. This reorganisation of domains stabilises the deprotonated state of cpEGFP, allowing it to fluoresce under a 488 nm laser (Wang et al., 2008). The Ca^{2+} dependency of the domain interactions provide the basis for GECIs with different affinities for Ca^{2+}. CEPIA2 and CEPIA3 were generated by site directed mutagenesis in the CaM domain, in order to reduce the binding affinity of the moiety, and therefore reduce the CaM/cpEGFP interactions at lower concentrations of Ca^{2+} (Suzuki et al., 2014). The CEPIAs were developed to have Ca^{2+} affinities specifically in the micromolar range, to be suitable for measuring Ca^{2+} within intracellular organelles.

The specific features of the CEPIA family which make them relevant to this project, are their variability in sub-cellular localisation, the high spatiotemporal resolution which they can achieve, and their relatively low affinity for Ca^{2+}. By adding a mitochondrial localisation sequence to the CEPIA coding sequences, they have been expressed in HeLa cells to report mitochondrial Ca^{2+} signalling, revealing heterogeneous Ca^{2+} dynamics (Suzuki et al., 2014). Therefore, addition of an alternative localisation sequence could repurpose the probe to measure Ca^{2+} concentrations at various distinct subcellular locations. Furthermore their high spatiotemporal resolution enables multiple simultaneous Ca^{2+}

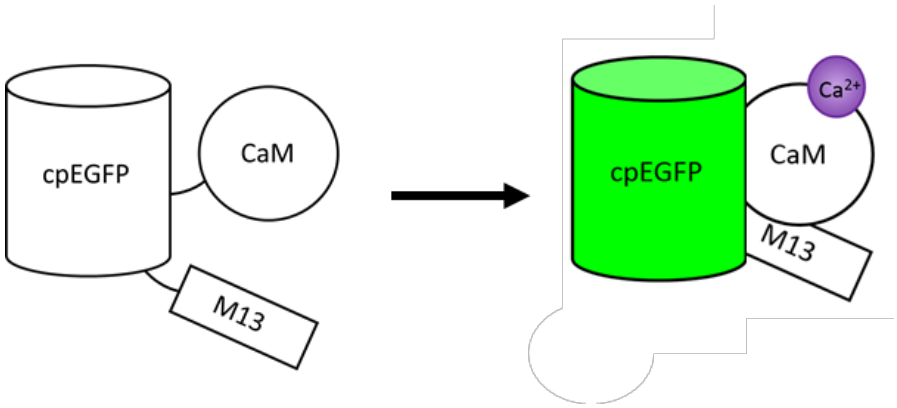

Figure 4.1.2i: Activation of CEPIA upon binding Ca^{2+}

CaM is attached to the cpEGFP via a new terminus in the centre, created by the fusing of the N- and C-termini. Ca^{2+} binding to calmodulin (CaM) causes a conformational change which brings cyclically permuted enhanced green fluorescent protein (cpEGFP), CaM and the light chain of myosin (M13) into contact, stabilising cpEGFP in the deprotonated state where it fluoresces.

measurements to be taken from different organelles/subcellular locations at the same time. Among the CEPIA family of proteins, two members have Ca^{2+} binding characteristics that would be capable of detecting Ca^{2+} fluctuations in the μ-calpain activating Ca^{2+} concentration range observed *in vitro*; CEPIA2 and CEPIA3. CEPIA2 has a Ca^{2+}-binding K_d of 0.16 μM, and CEPIA3 has a K_d of 11 μM. I hypothesised that by manipulating the targeting sequence of the CEPIA proteins, I could utilise their Ca^{2+} binding properties to detect Ca^{2+} in the micromolar range, at sub-plasma membrane/ezrin-rich locations (fig. 4.1.2ii).

4.2 Aims of this chapter

The aim of the work reported in this chapter was to generate a novel GECI, capable of measuring high Ca^{2+} concentration in ezrin-rich regions of the cell.

The objectives were:

1. To isolate the Ca^{2+} sensing domain of CEPIA2 and CEPIA3 using molecular biology techniques.
2. To conjugate the Ca^{2+} sensing domains to the C-terminal domain of ezrin, and clone the novel GECIs into pcDNA3.1(-) expression vectors.
3. To amplify and then purify the novel ezrin-GECI plasmids for further experiments investigating Ca^{2+} elevation events localised to ezrin rich regions of the cell, such as the plasma membrane and within surface microridges.

4.2.1 Cardiff-KU Leuven bilateral agreement

The work reported in this chapter was carried out under a bilateral agreement between Cardiff University and the Katholieke Universiteit (KU) Leuven, Belgium. The inspiration for the collaboration came from a small conference held between the Inter-school Calcium Signalling Group at Cardiff and the Calcium Signalling group in Leuven. The conference, held in Cardiff (October 2015), was

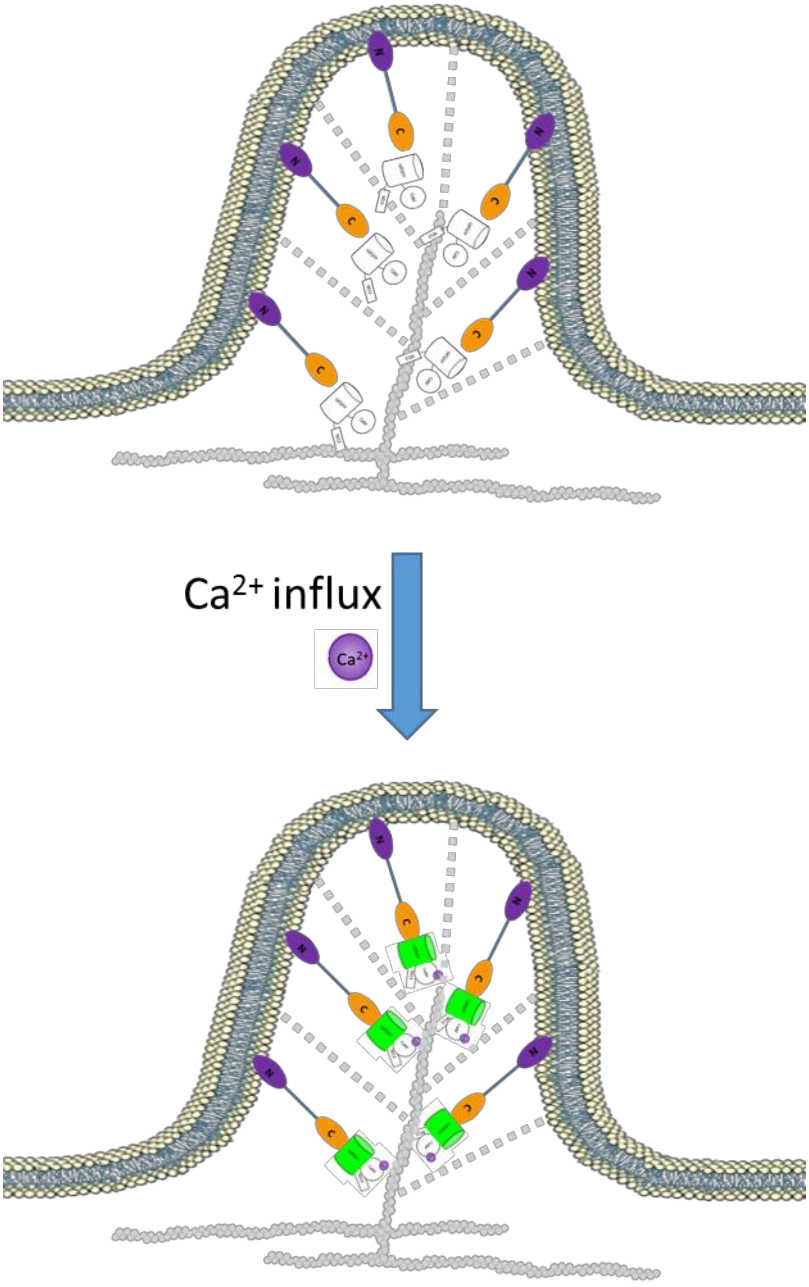

Figure 4.1.2:ii Ezrin-mCherry and EPIC fluorescence

EPIC fluorescence intensity under a 488 nm laser is related to Ca^{2+} binding. As Ca^{2+} concentration increases, reorganisation of the CEPIA domains causes the cpEGFP moiety to fluoresce.

independently organised between the two groups and funded though sponsorships.

Prof. Jan Parys, from KU Leuven, presented his group's recent work on localised GECIs; namely the CEPIA family of Ca^{2+} sensors, developed by Suzuki and colleagues (2014). I hypothesised that we could use the same idea to generate a Ca^{2+} sensing probe that would localise to the ezrin-rich regions of the plasma membrane, and crucially within the microridges at the plasma membrane of myeloid cells. I discussed the idea with Prof. Parys and submitted an application for funding to the Cardiff University selection panel. The application was successful and I secured funding to spend four weeks over March-April 2016 in Prof. Parys' Laboratory of Molecular and Cellular Signalling in the Department of Cellular and Molecular Medicine, at the KU Leuven in Belgium. During this visit, I generated two new GECIs: EPIC2 and EPIC3, which I brought back to Cardiff for further experiments investigating Ca^{2+} concentrations in ezrin-rich cytosolic microdomains of myeloid cells.

4.3 Specific Materials and Methods

4.3.1 Generation of Ezrin-CEPIA conjugates for detection of localised calcium signalling

The work in this chapter was carried out in Prof. Jan Parys' Laboratory of Molecular and Cellular Signalling in the Department of Cellular and Molecular Medicine, KU Leuven (Leuven, Belgium).

4.3.1.1 Primer design

Plasmid vectors pCMV CEPIA2mt and CEPIA3mt were gifts from Masamitsu Lino (Addgene plasmid # 58218, 58219 and 58220). Plasmid vector mCherry-Ezrin-N-14 was a gift from Michael Davidson (Addgene plasmid # 55043).

PCR primers were designed to amplify ezrin and CEPIA2 and CEPIA3, using the CLC Sequence Viewer (Qiagen), to include complementary restriction sites for the ligation of ezrin-CEPIA conjugates. The protein sequences were searched using SnapGene® and any restriction sites flagged within the protein sequences were not used. NotI and EcoRV were identified as suitable restriction sites for ezrin, and EcoRV and HindIII were suitable for the CEPIA variants. The pcDNA3.1(-) vector was a gift from Jan Parys, and has restriction sites for NotI and HindIII in its multiple cloning site (fig. 4.3.1.1).

Approximately 20 bases from the beginning or end of each sequence to be amplified were incorporated in the Forward and Reverse primers respectively, each ending in either a C or G. Restriction sites for the appropriate restriction enzymes were incorporated, and a leader sequence of 6 non-coding C and G bases was added at the beginning of each primer to increase primer annealing, since C and G base pairs form 3 hydrogen bonds, making them stronger binding partners than A and T, with only 2 hydrogen bonds. The bespoke primers were ordered from Integrated DNA Technologies (IDT) (Leuven, Belgium).

For Ezrin the primer designs were:
Forward: CTAATAGCGGCCGCATGCCGAAACCAATCAATGTC NotI
Reverse: GTAATAGATATCCAGGGCCTCGAACTCGTCG EcoRV

For CEPIA2 and 3 the primer designs were (based on the GCaMP2 sequence):
CEPIA forward: GCGGCGGATATCGGTTCTCATCATCATCATCATC EcoRV
CEPIA reverse: GCGGCGAAGCTTTTACTTCGCTGTCATCATTTG HindIII

4.3.1.2 PCR

PCR was performed for two purposes: (i) to remove existing tags from the gifted ezrin and CEPIA variants, and (ii) to amplify DNA fragments for molecular cloning.

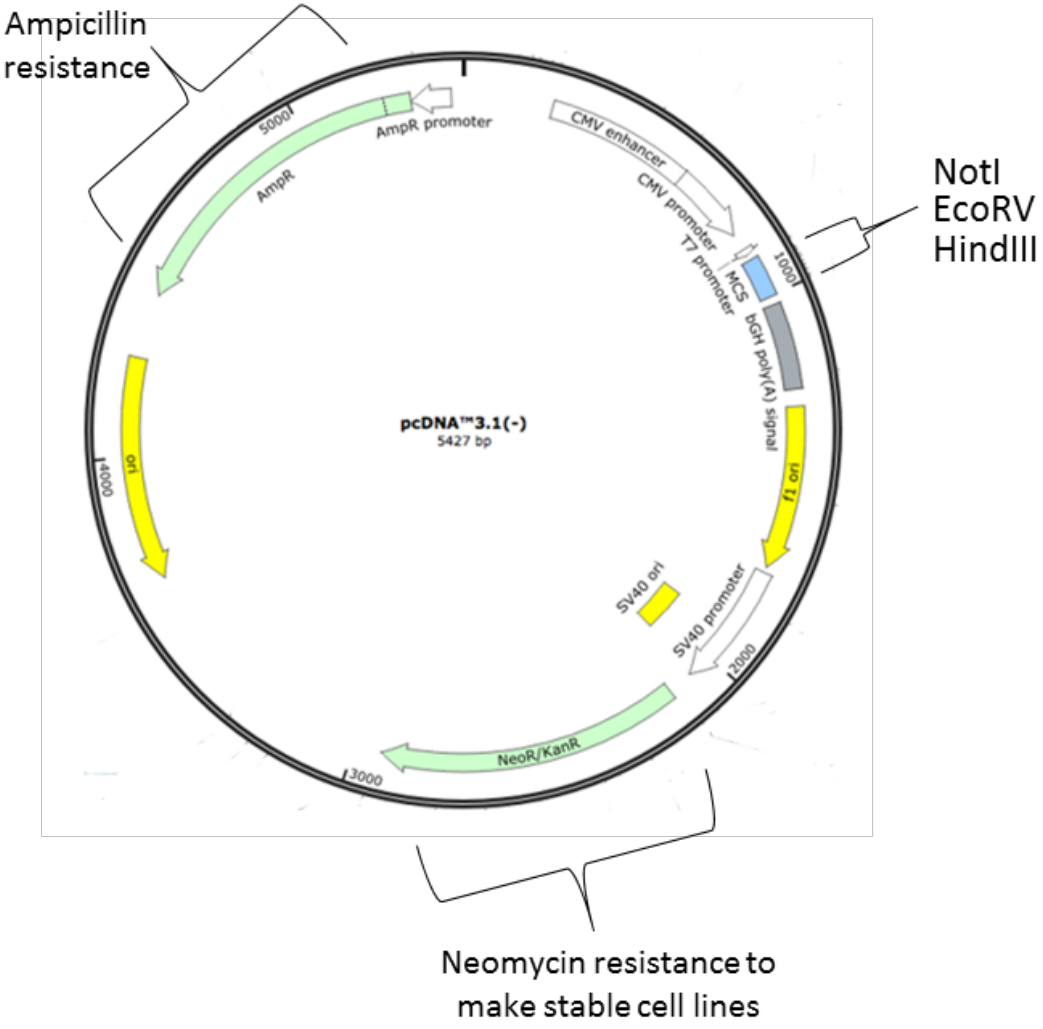

Figure 4.3.1.1: pcDNA3.1(-) plasmid map

With ampicillin resistance gene.

The quantities of template DNA, primers and dNTPs are listed in table 4.3.1.2i, and the PCR program is detailed in table 4.3.1.2ii.

4.3.1.3 PCR clean-up

DNA from the PCR products and was purified using the GenElute™ PCR Clean-Up Kit (Sigma-Aldrich), to remove excess dNTPs and primers, and again after the restriction digests to remove DNA fragments. The PCR clean-up was performed according to the manufacturer's protocol, and the DNA was recovered in ddH_2O.

4.3.1.4 Restriction and ligation of PCR products and pcDNA3.1(-) vector

Ezrin PCR product was digested by NotI and EcoRV restriction enzymes. CEPIA2 and CEPIA3 PCR products were digested with EcoRV and HindIII. The vector pcDNA3.1(-) was digested with NotI and HindIII. The quantities of PCR products and restriction enzymes are shown in table 4.3.1.4i. 1 µL of alkaline phosphatase was added to the vector samples, to prevent re-annealing of the sticky ends. The reaction was left to incubate for 30 mins at 37°C with gentle mixing after 15 mins to ensure complete digestion. The PCR clean-up procedure was then repeated (as described in section 4.3.1.3).

Ligation reactions were carried out using the fast acting enzymes from ThermoScientific. Digested pcDNA3.1(-) vector was incubated with ezrin and CEPIA2/3 for 10 mins at 22°C in a heat block. The reaction volumes are listed in table 4.3.1.4ii. For the negative control the digested pcDNA3.1(-) was ligated without the PCR products, to test the likelihood of the vector re-annealing without the inserts.

4.3.1.5 Agarose gel electrophoresis

Mini-preps were re-digested with NotI and HindIII to check for correct ezrin-CEPIA insertion. Reaction volumes are described in table 4.3.1.5. The reaction

Table 4.3.1.2i: PCR set-up

Reagent	Quantity
Template DNA	10-50 ng
Forward Primer (25 µM)	1.5 µL
Reverse Primer (25 µM)	1.5 µL
dNTPs	1 µL
PfuUltra II (Agilent Technologies)	1 µL
10x PfuUltra II Reaction Buffer (Aglient Technologies)	5 µL
$MgCl_2$	2.5 µL
H_2O	To total 50 µL

Table 4.3.1.2ii: PCR program

Cycle 1		Cycle 2		Cycle 3	
Temperature (°C)	Time (mins)	Temperature (°C)	Time (mins)	Temperature (°C)	Time (mins)
95	1	95	1	95	1
45	0.5	50	0.5	55	0.5
68	1/1000 bp	68	1/1000 bp	68	1/1000 bp

Table 4.3.1.4i: Restriction digest

Reagent	Quantity
DNA	pcDNA3.1(-) 0.8 µg OR PCR product 50 µL
Enzyme 1	1 µL
Enzyme 2	1 µL
Buffer 10x	7 µL
H_2O	To total 70 µL

Table 4.3.1.4ii: Ligation reaction

Reagent	Negative control	Ligation
Vector	1 µL	1 µL
Insert	-	2 µL of each PCR product
Buffer (10x)	2 µL	2 µL
T4 DNA ligase	1 µL	1 µL
H_2O	16 µL	14 µL

Table 4.3.1.5: Re-digest

Reagent	Quantity
Mini-prep DNA	500 ng
NotI	0.5 µL
HindIII	0.5 µL
Buffer 10x	7 µL
H_2O	To total 70 µL

was performed in a water bath at 37°C for 10 minutes, so that the reaction did not go to completion, and was stopped by transferring the samples to ice.

Agarose gels were prepared by heating 1.25 g agarose in 125 mL TAE buffer (for a 1% gel) in a conical flask in the microwave on full power for 1-3 minutes, until the agarose was completely dissolved. Care was taken not to over boil the solution, which would affect the gel composition. The dissolved agarose was cooled, to approximately 60°C, and 6.25 µL ethidium bromide was added. After pouring, the gel was left to set for at least 30 mins at room temperature, before the comb was removed.

To perform electrophoresis, the gel was submerged in 1 x TAE buffer (4.84 g Tris-base, 1.142 mL acetic acid (100%), 2 mL 0.5 M EDTA in I L ddH_2O) plus 1-2 % ethidium bromide for even staining. 10 µL of ready-to-use DNA ladder was loaded in the first and last wells as a reference. DNA samples (10 µL) were prepared with loading buffer (4 µL) and ddH_20 (6 µL). 10 µL of each prepared sample was loaded into wells. The gel was run at a constant 120 V for 30 mins, at which point the migration distance was assessed and the run time was extended if necessary.

4.3.1.6 Transformation of DH5α cells

50 µL of DH5α cells (gifts from Jan Parys) were thawed on ice and carefully mixed with 4 µL of ligation reaction and incubated on ice for 30 mins. The mixture was heat-shocked for 2 mins at 42°C in a heat block, followed by 2 mins on ice. 400 µL of sterile LB medium was added and the cells were incubated in a rotating incubator (225 rpm) for 1 hour at 37°C. The cells were then spread onto agar plates containing ampicillin, and incubated overnight at 37°C.

4.3.1.7 Mini-preps

Mini-preps were carried out using the GenEluteTM Plasmid Miniprep Kit (Sigma Aldrich) as per the manufacturer's instructions, but the final plasmid was

recovered in dH_2O, instead of the supplied Elution Solution (10 mM Tris-HCl, 1 mM EDTA, pH approx. 8.0) because the DNA was immediately sent for sequencing (LGCgenomics), to confirm the correct insertion of the ezrin/CEPIA conjugates. Five colonies were picked from each agar plate and used to inoculate 5x2 mL LB broth overnight cultures (37°C, 225 rpm). The purified plasmid DNA was stored on ice prior to quantification. Long-term storage was at -20°C.

4.3.1.8 Quantification of plasmid DNA

Purified DNA from the mini and maxi-preps was assessed using the Qubit dsDNA BR Assay Kit® and Qubit® Fluorometer (Life Technologies), according to manufacturer's instructions.

4.3.2 Transfection of HeLa cells

24 hrs post-seeding the novel GECI constructs were introduced into HeLa cells (gifts from Jan Parys) using the X-tremeGENE™ HP DNA Transfection Reagent (Sigma Aldrich), as per the manufacturer's instructions. A ratio of 1:1.5 X-tremeGENE™ to DNA was used.

4.4 Results

4.4.1 Generation of EPIC2 and EPIC3

In order to generate a GECI-ezrin conjugate, the Ca^{2+} sensing-domain of CEPIA2 and CEPIA3 first had to be removed from the organelle targeting sequence, to which it was attached. The mCherry domain of ezrin-mCherry was also removed to provide the ezrin sequence, for conjugation to the CEPIA sequence. PCR primers to the CEPIA2/3 and ezrin sequences were generated using CLC sequence viewer, and PCR was performed to isolate the genes of interest. Following the PCR clean-up procedure, the DNA fragments were digested with restriction enzymes NotI, EcoRV and HindIII, to generate appropriate sticky ends

for ligation with a pcDNA3.1(-) plasmid vector. The ezrin-CEPIA2/3 conjugate (fig. 4.4.1i) was cloned into the pcDNA3.1(-) plasmid vector and transformed into chemically competent DH5α *E. coli*, before being plated onto agar plates containing ampicillin. Only bacteria which had been successfully transformed with the pcDNA3.1(-) plasmid vector were able to grow, because they had acquired the gene for ampicillin antibiotic resistance. Five colonies were selected from each plate for further amplification. Cultures with the correct ezrin-CEPIA conjugate inserted into the plasmid vector were identified by agarose gel electrophoresis, after re-digestion with the restriction enzymes NotI and HindIII (fig. 4.4.1ii). Several colonies were identified as having successfully incorporated the new conjugate. Ezrin-CEPIA2a and ezrin-CEPIA3d had the strongest 'insert' bands, and therefore these mini-preps contained more plasmid DNA. Sequencing analysis confirmed the correct orientation of the ezrin-CEPIA2a and ezrin-CEPIA3d conjugates (figs. 4.4.1iii-vi), and the novel GECIs were named EPIC (Ezrin Peripheral Indicator of Ca^{2+}) 2 and EPIC3, on account of their CEPIA2 and CEPIA3-like properties respectively. EPIC2 and EPIC3 were successfully amplified via expansion of the broth culture and subsequent maxi-preps.

4.5 Discussion

This work has produced the first ezrin-associated GECIs, with Ca^{2+} binding affinities 0.16 µM and 11 µM (based on the Ca^{2+} titrations carried out by Suzuki and colleagues on the CEPIA2 and 3 GECIs (Suzuki et al.,2014) (fig. 4.5); named EPIC2 and EPIC3 respectively. The Ca^{2+} binding properties of the novel probes will be used in experiments investigating Ca^{2+} signalling and the relationship with ezrin activity during changes in myeloid cell morphology, during specific events such as phagocytosis. The assumption will be made that the Ca^{2+} binding properties of EPIC2 and 3 are akin to those of CEPIA2 and 3, as detailed by Suzuki and colleagues (2014) (fig. 4.5), based on their common GCaMP2-like domains. All estimations of Ca^{2+} concentrations in this thesis that are taken using the EPIC probes will be made with this assumption.

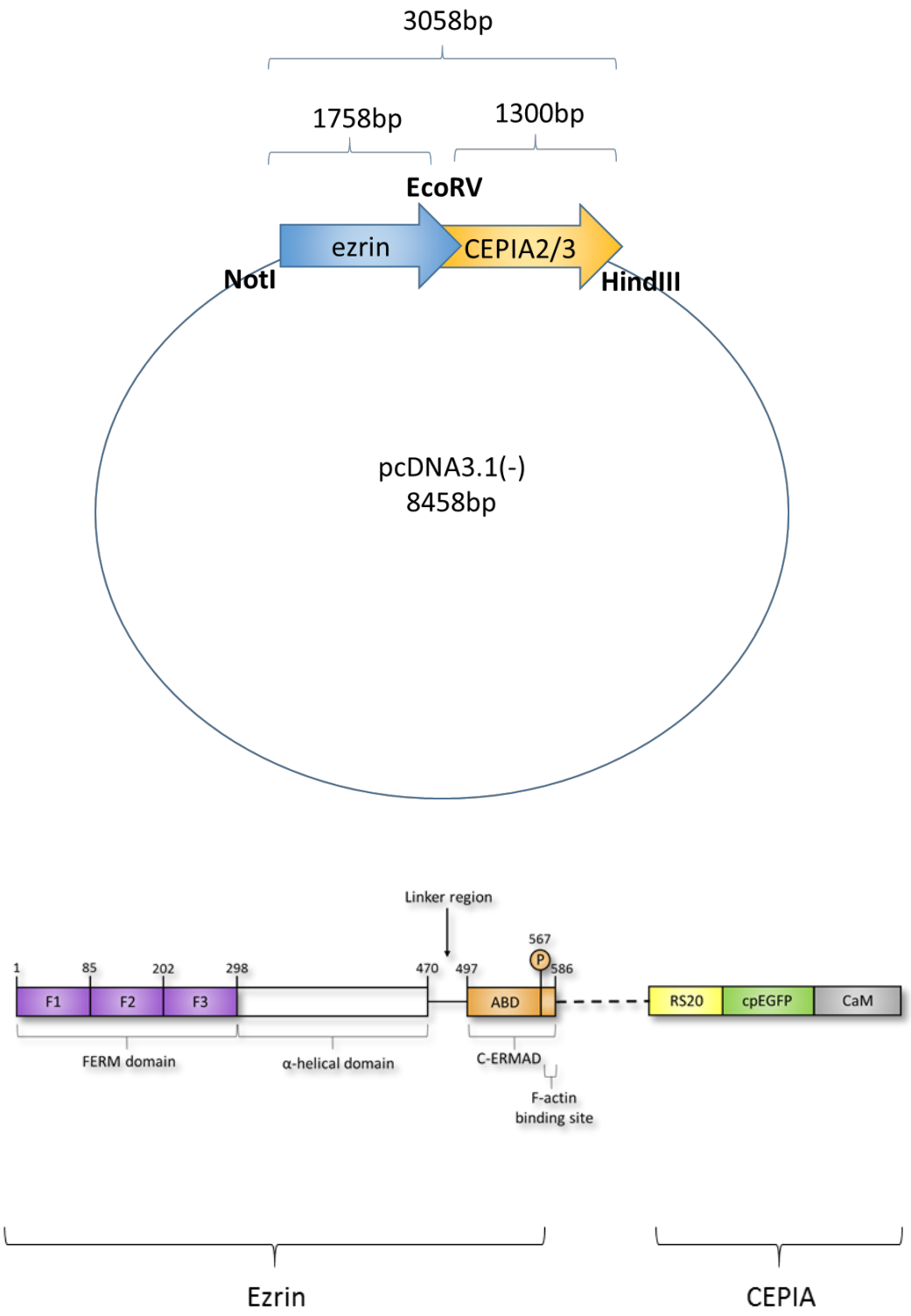

Figure 4.4.1i: Scheme of molecular cloning novel EPIC

Ezrin and CEPIA2/3 were cloned into the pcDNA3.1(-) plasmid vector with restriction sites NotI and HindIII.

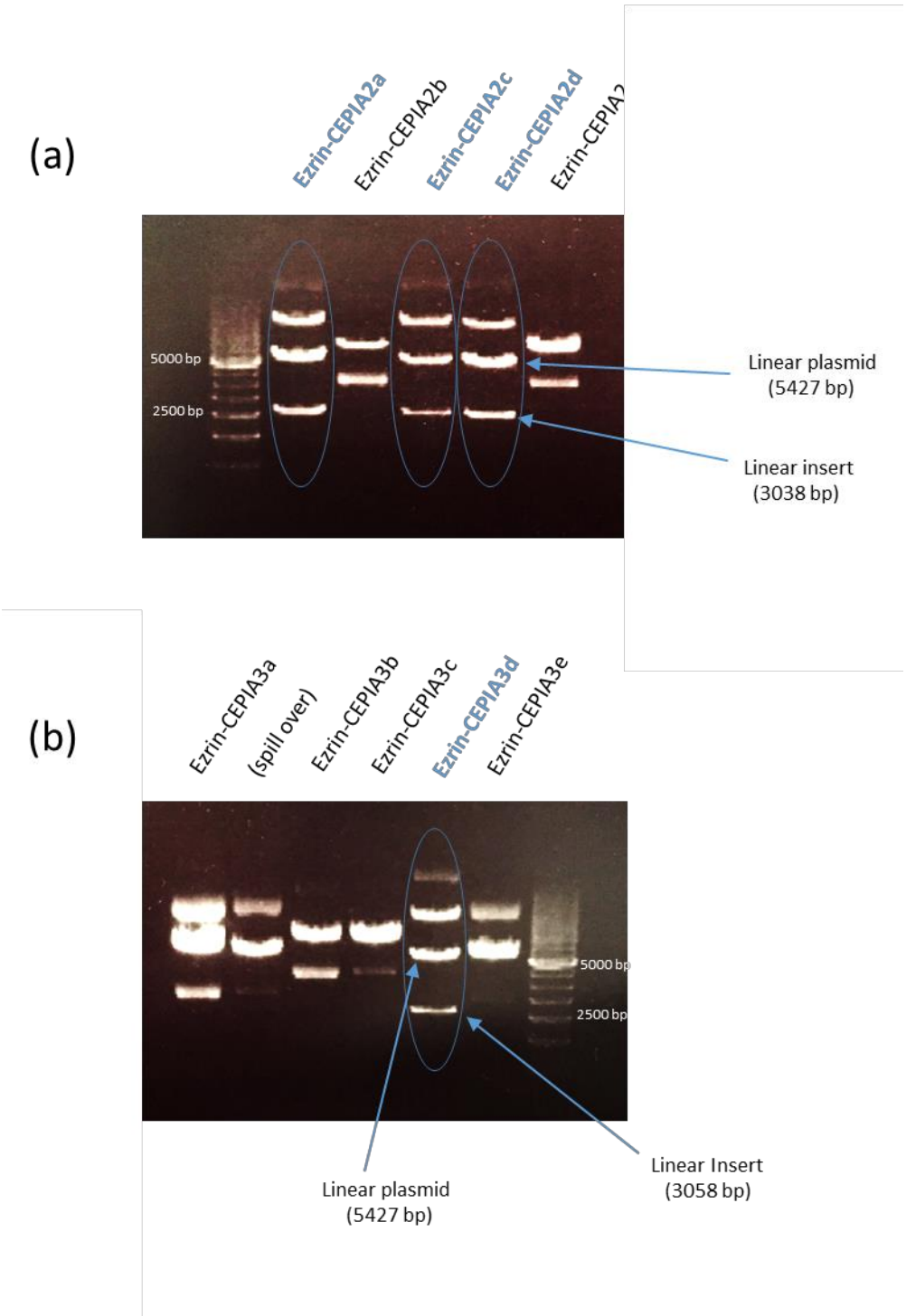

Figure 4.4.1ii: Agarose gel electrophoresis to identify successful vector ligations
Samples were re-digested with NotI and HindIII and the resultant DNA bands were analysed for bands correlating with the molecular weight of the ezrin-CEPIA conjugate (3058bp). **(a)** Ezrin-CEPIA2a/c/d and **(b)** Ezrin-CEPIA3d, contained the correct size insert and were sent for further sequencing.

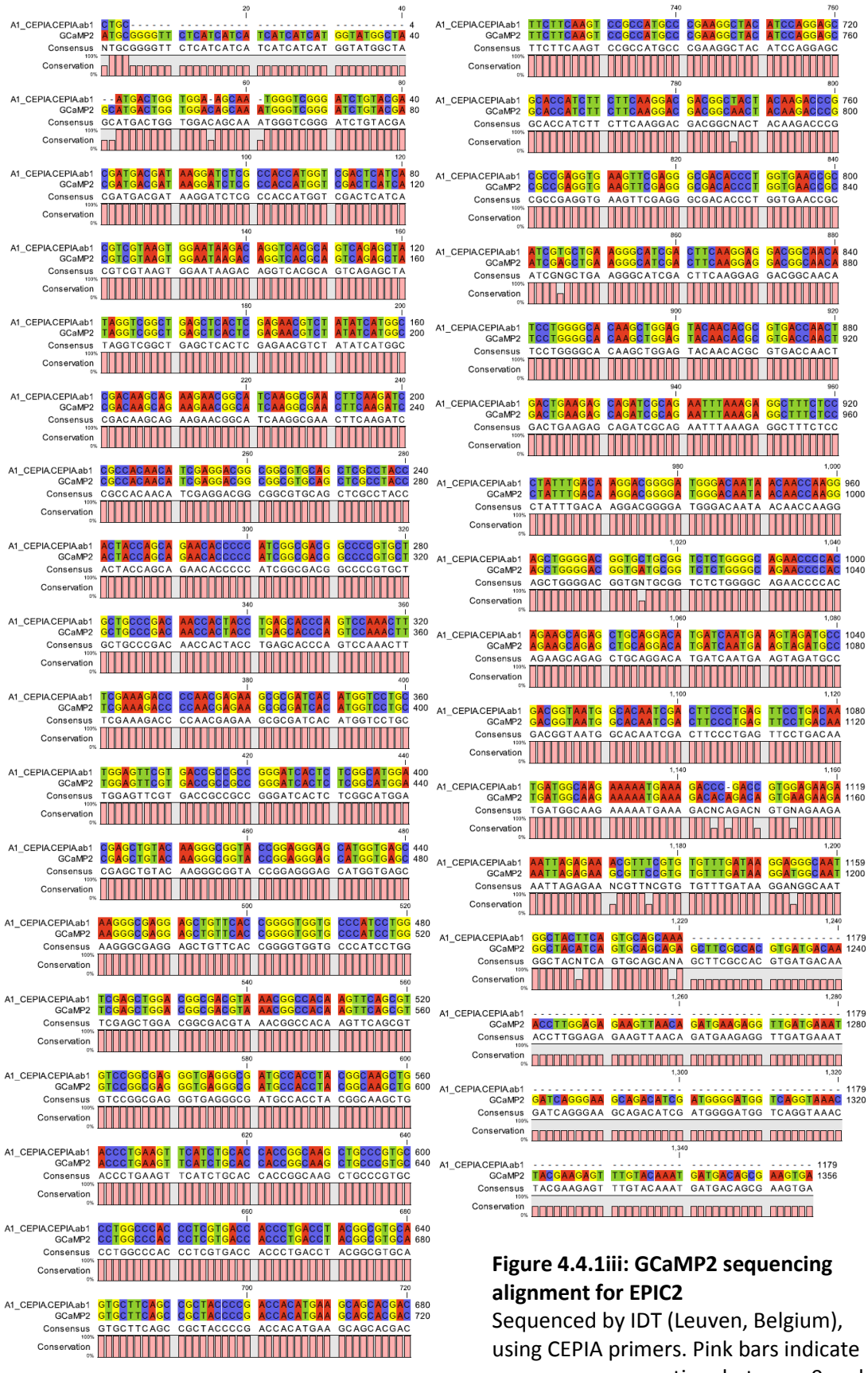

Figure 4.4.1iii: GCaMP2 sequencing alignment for EPIC2
Sequenced by IDT (Leuven, Belgium), using CEPIA primers. Pink bars indicate sequence conservation, between 0 and 100%.

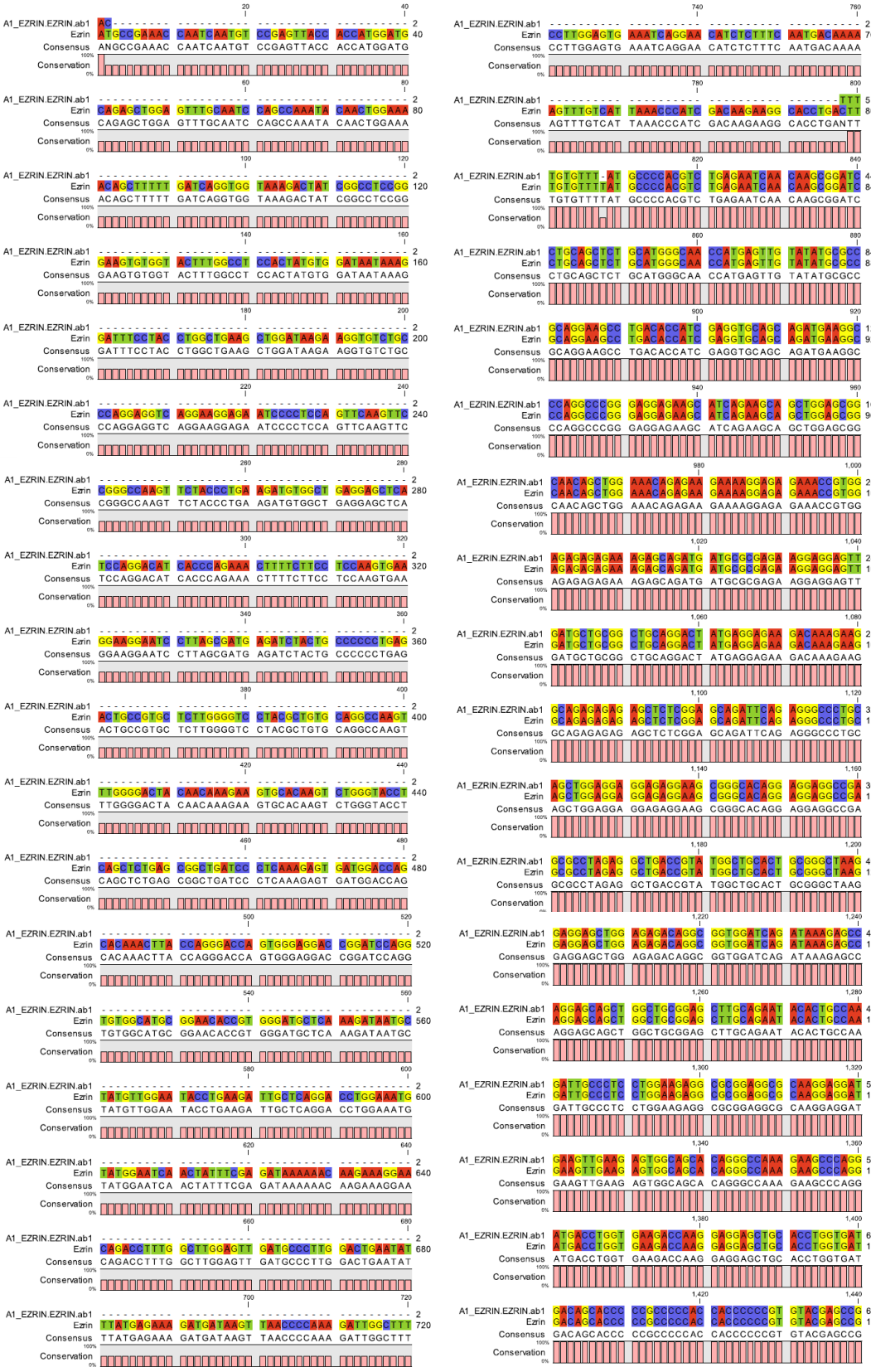
A1_EZRIN.EZRIN.ab1
Ezrin
Consensus
Conservation

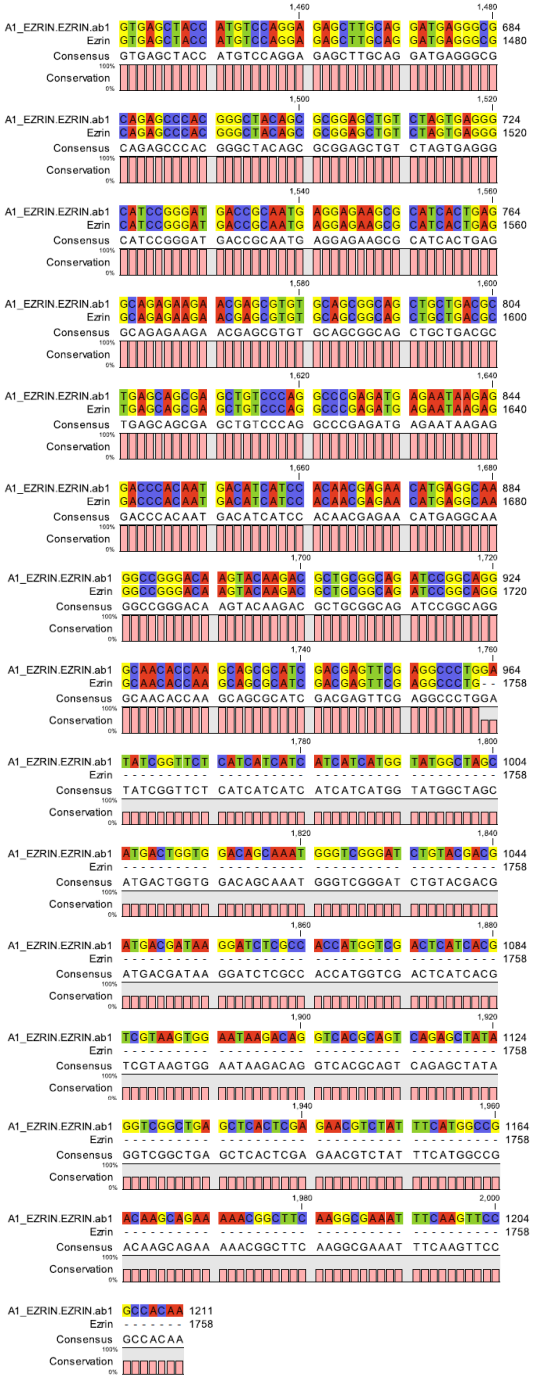

Figure 4.4.1iv: Ezrin sequencing alignment for EPIC2
Sequenced by IDT (Leuven, Belgium), using ezrin primers. Pink bars indicate sequence conservation, between 0 and 100%.

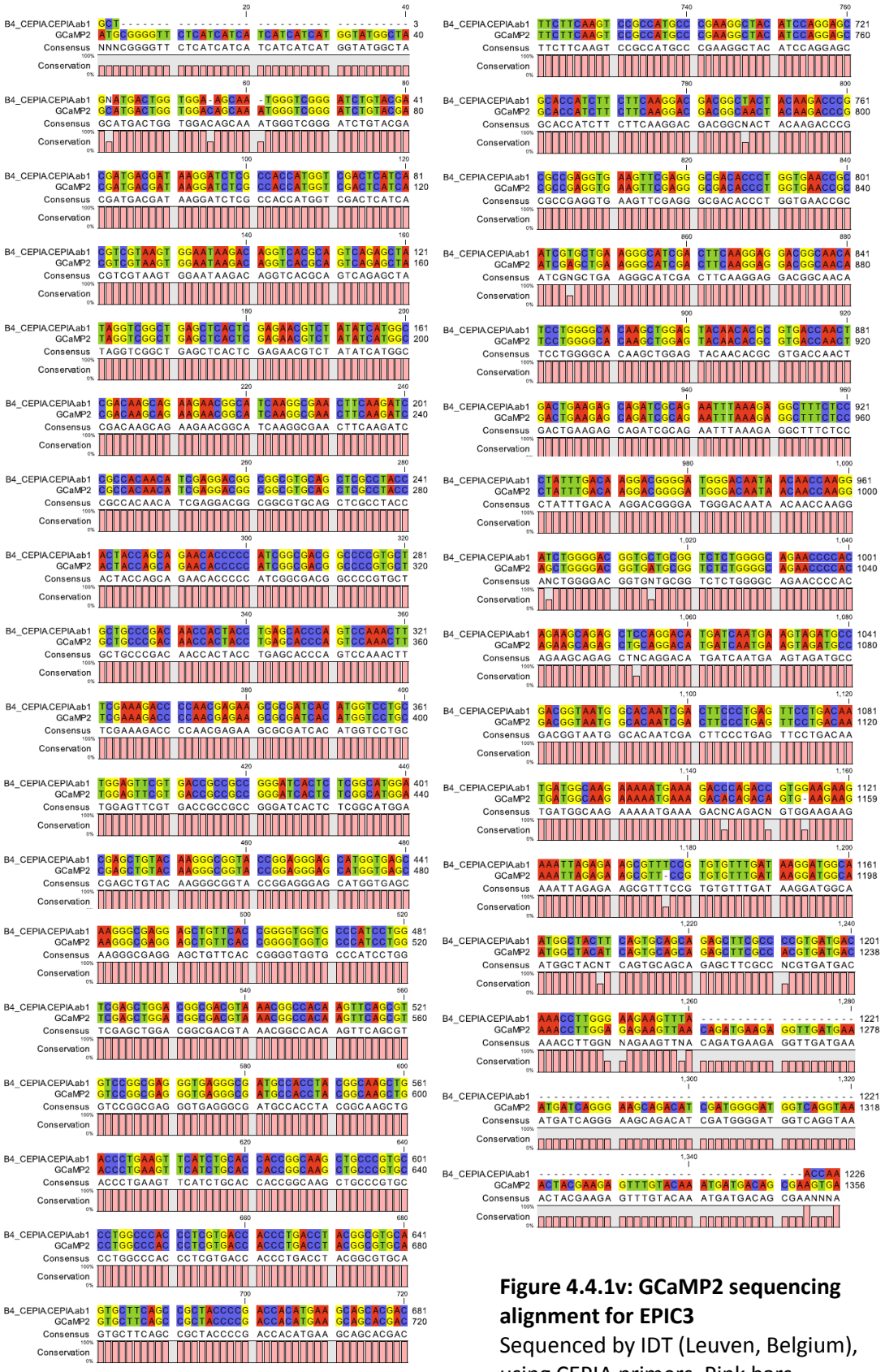

Figure 4.4.1v: GCaMP2 sequencing alignment for EPIC3
Sequenced by IDT (Leuven, Belgium), using CEPIA primers. Pink bars indicate sequence conservation, between 0 and 100%.

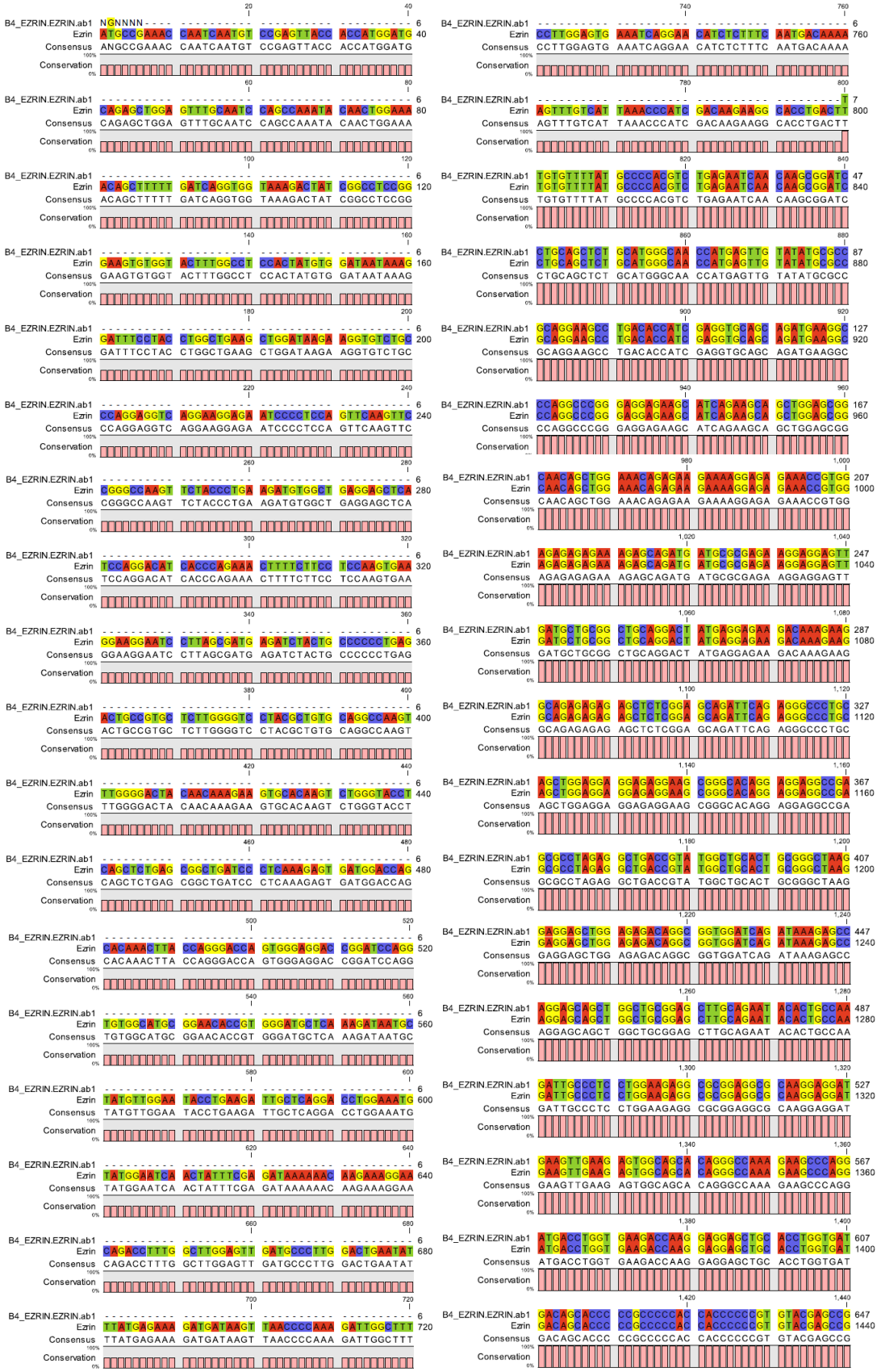
B4_EZRIN.EZRIN.ab1
Ezrin
Consensus
Conservation

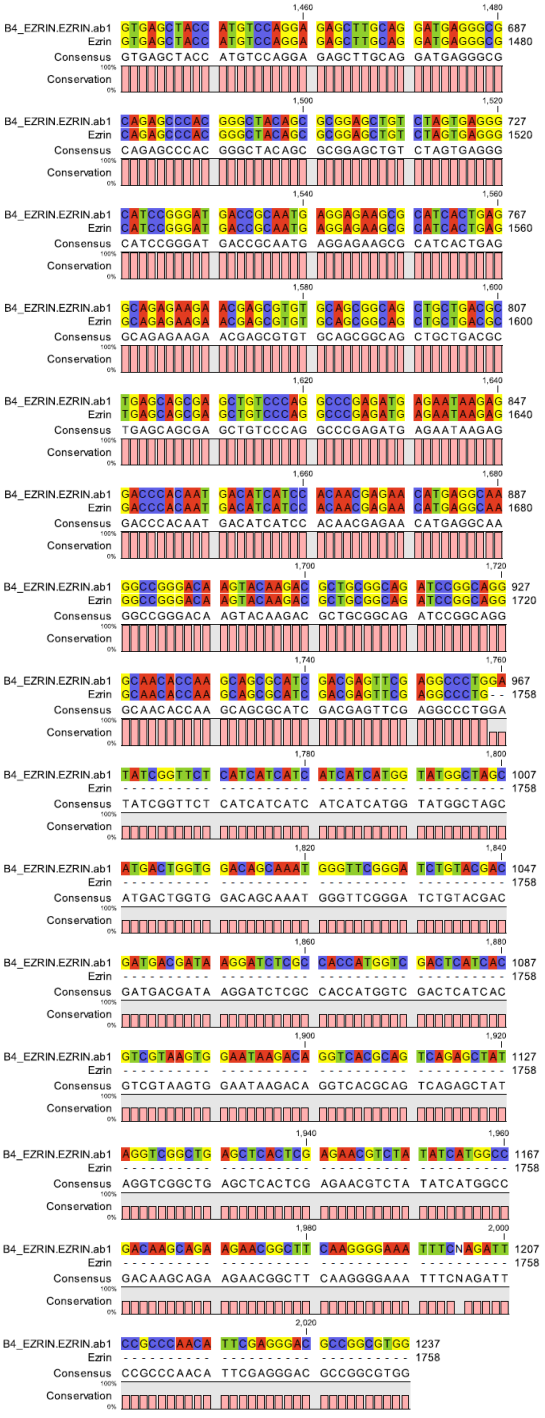

Figure 4.4.1vi: Ezrin sequencing alignment for EPIC3
Sequenced by IDT (Leuven, Belgium), using ezrin primers. Pink bars indicate sequence conservation, between 0 and 100%.

The relationship between ezrin and Ca^{2+} localisation is complex. It is important to recognise that the fluorescent activity of EPIC2 and EPIC3 is coupled to their Ca^{2+} sensing activities (0.16 µM and 11 µM respectively). Therefore, the fluorescent signal produced by intracellular EPIC3 would not be maximal in resting cells, when there is no net Ca^{2+} influx/efflux event. Furthermore, a cytosolic pool of free, unbound and unphosphorylated inactive ezrin exists. Therefore EPIC2 and EPIC3 should also be distributed in the cytosol. EPIC2, with a lower K_d of 0.16 µM Ca^{2+}, would also be reporting the cytosolic free Ca^{2+} concentration in the resting cell (approx. 0.10 µM Ca^{2+}). It is therefore likely that EPIC2 would become saturated at the cell edge upon Ca^{2+} influx, much faster than the imaging capacity of the confocal resonance scanner (high resolution imaging requires at least 4 seconds/frame). EPIC3 was selected for further immediate analysis, because of its 11 µM K_d for binding Ca^{2+}, in the range of µ-calpain activation. These Ca^{2+}-binding properties were considered to be more useful for further Ca^{2+} measuring experiments in myeloid cells undergoing, for example, localised morphological changes such as phagocytosis.

Furthermore, since ezrin is a substrate of µ-calpain, it is presumed that the EPIC ezrin variants will also be susceptible to Ca^{2+}-mediated µ-calpain cleavage. Since it is predicted that the ezrin cleavage site lies somewhere between the two terminal functional domains (Dewitt and Hallett, 2007), ezrin cleavage would result in the GECI dissociating from the plasma membrane. In this way, the novel probes report both localised Ca^{2+} concentrations, and also ezrin cleavage events at the cell edge. This may be useful in single cell experiments, where the EPIC can act as both an indicator of localised elevations of Ca^{2+} concentration, and also as a secondary diffusible Ca^{2+} indicator in the global cytosol.

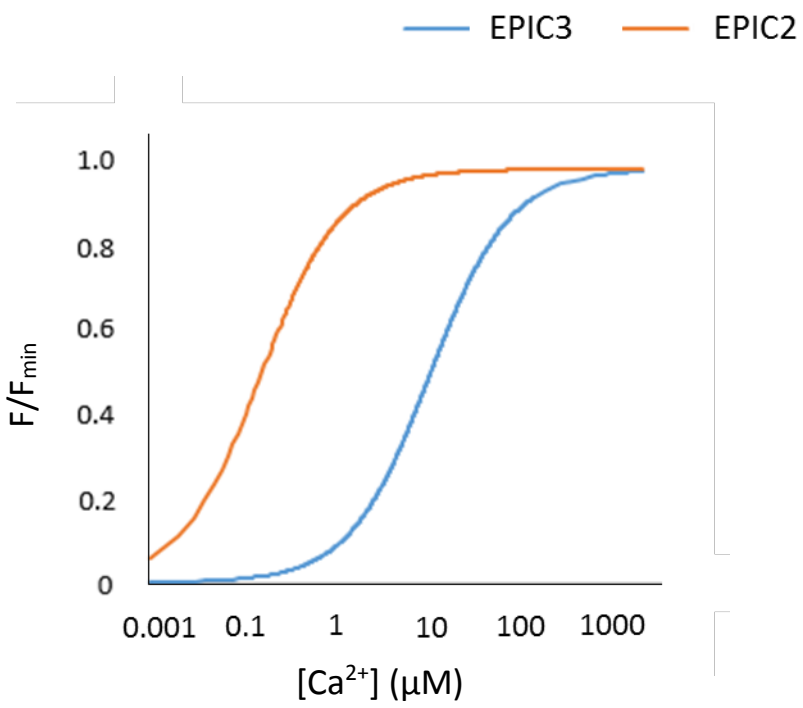

Figure 4.5: Assumed EPIC2 and EPIC3 titration curves

Ca^{2+} titration curves for EPIC2 and 3 (based on calculations performed by Suzuki and colleagues (2014)). With the assumption that EPIC2 and 3 will have the same Ca^{2+} binding affinities as CEPIA2 and 3 respectively, EPIC2 will have a K_d of 0.16 µM and EPIC3 will have a K_d of 11 µM. Under physiological conditions EPIC2 will be at half maximal fluorescent activity, whilst EPIC3 will have minimal fluorescence activity.

Chapter 5:

Cytosolic microdomains of high Ca^{2+} concentration

5.1. Introduction

The biphasic Ca^{2+} response in neutrophils undergoing cell spreading, such as during extravasation or during the process of phagocytosis, is similar. Both processes demand an apparent expansion of the cell surface area. In the spreading neutrophil, this is up to 200% (Hallett and Dewitt, 2007), which is far greater than the stretching capacity of the resting cell membrane of 4% (Hamill and Martinac, 2001). The force required to expand the plasma membrane is reduced during phagocytosis (Herant et al., 2003), a mechanism which would enable the membrane to expand into fillopodia (Atilgan et al., 2006). In this thesis, μ-calpain and ezrin have both been implicated as key players in the remodelling of the cytoskeletal and plasma membrane relationship. The Ca^{2+}-mediated activation of μ-calpain, in ezrin-rich regions at the plasma membrane, is proposed to disrupt the cross-linking role of ezrin. Cleavage of this tether between the cortical actin cytoskeleton and the plasma membrane would release the 'reservoir' of trapped membrane from within microridge structures, and provide both additional membrane for the increase in cell surface area, and also reduce the membrane tension which allows actin polymerisation to proceed (Cordova et al., 1992; Peskin et al., 1993), and so enable cell spreading.

As previously discussed, the K_d of μ-calpain is in the range 20-60 μM Ca^{2+}, and as such is higher than the physiological Ca^{2+} concentrations in the bulk cytosol. It is for this reason that we propose that the plasma membrane microridges serve a dual purpose. Not only do they provide (i) a storage mechanism for plasma membrane to be released when required, but they also provide (ii) a suitable microenvironment where localised cytosolic concentrations of Ca^{2+} in the mid-decade micromolar range are attainable. This therefore provides a 'safe' and contained microenvironment for appropriate μ-calpain activation, where it can cleave ezrin cross-links to release tension in the plasma membrane.

5.1.1 Microridge Ca^{2+} domains

Many cell types have microridge structures in their plasma membranes, serving a variety of different purposes. In neutrophils, as previously discussed, it is understood that the plasma membrane microridges provide the stored excess plasma membrane required for cell shape change events; specifically spreading and phagocytosis (fig. 5.1.1i).

Computer simulations of neutrophil plasma membrane microridges have modelled the size of microridge structures on the neutrophil surface which are capable of generating Ca^{2+} microenvironments, with transient Ca^{2+} concentrations which are higher than that of the global cytosol. Brasen and colleagues have predicted that the Ca^{2+} concentrations in plasma membrane microridges could reach up to 80 µM in a 1 µm long microridge, upon Ca^{2+} influx during cell stimulation (fig. 5.1.1ii) (Brasen et al., 2010). This calculation is approximately 100-fold higher than the Ca^{2+} levels typically thought to be achievable in the global cytosol. It is also out of the range of detection by most conventional small molecule Ca^{2+} indicators.

Total internal reflection fluorescence microscopy (TIRF) has measured intracellular Ca^{2+} signals within 100 nm of the plasma membrane, using the fluorescent Ca^{2+} indicator Fluo3, but the increase at the plasma membrane was small compared to the bulk cytosolic Ca^{2+} signal, at 20-60% (Omann et al., 1996). However, the Fluo3 signal becomes saturated at Ca^{2+} concentrations above approximately 3 µM, thereby giving a gross underestimate of the peak Ca^{2+} concentrations reached at the plasma membrane. Moreover, the TIRF technique requires the plasma membrane to be closely positioned to an adherent surface (i.e. within 100 nm of the reflection beam), thus this approach would only be capable of measuring the Ca^{2+} concentration beneath a flattened, and non-wrinkled membrane. TIRF was therefore not able to measure the Ca^{2+} concentration in the microridge structures of the plasma membrane.

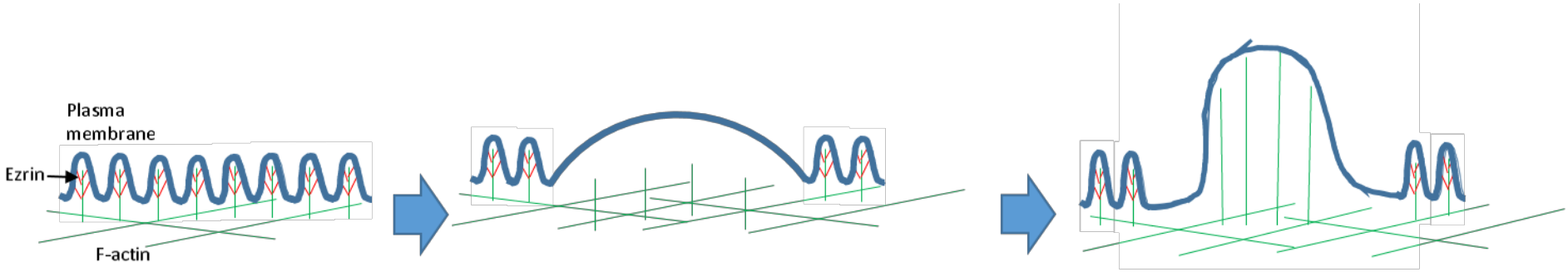

Figure 5.1.1: Schematic of relaxing microridges
Myeloid cell microridges are supported by a scaffold of cortical F-actin (green) bound to the plasma membrane (blue) via ezrin crosslinks (red). When the crosslinks are broken, the F-actin polymerisation is no longer inhibited and continues to grow via the Brownian Ratchet mechanism, in the direction of the now slackened cell membrane. F-actin extension continues, and forces the plasma membrane to protrude from the cell, until the point at which the Brownian Ratchet motion is again inhibited by plasma membrane tension, or the cell regains ezrin-crosslinking activity.

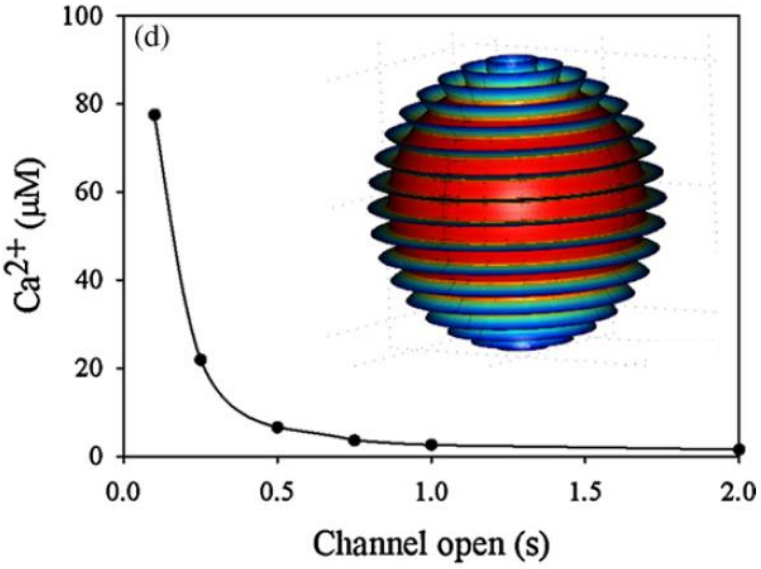

Figure 5.1.1ii: Estimation of Ca^{2+} concentration attainable beneath a wrinkled membrane

The Ca^{2+} influx periods in a model cell with microridge structures. When the channel is open for 0.1 s, the Ca^{2+} beneath the membrane microridges is estimated to reach 80 μM. (Figure reproduced with permission from Brasen et al., 2010.)

In an attempt to measure the Ca^{2+} concentration beneath the wrinkled plasma membrane of neutrophils, live cells in suspension have been loaded with FFP-18, a membrane-targeting fluorescent probe with a lower Ca^{2+} affinity (Davies and Hallett, 1998). This approach reported higher than global Ca^{2+} concentrations at the plasma membrane, of up to 30 µM (Davies and Hallett, 1998). However, these experiments were unable to produce data from individual cells during Ca^{2+} influx, due to the fluorescent signals being too weak. At the time of writing this thesis it is understood that no single cell experiments have been performed to measure the Ca^{2+} concentrations in sub-plasma membrane domains, formed by folds of the plasma membrane, in any cell type. Furthermore, this has never been achieved within the specific compartment of ezrin-rich microridge structures, in stimulated myeloid cells.

5.1.2 Ezrin peripheral indicator of Ca^{2+} (EPIC)

In the previous chapter, generation of a novel GECI, EPIC3, was reported, which has both ezrin localising properties and a low Ca^{2+} binding affinity K_d of 11 µM. This novel probe thus provides the opportunity to report Ca^{2+} concentrations in the higher micromolar range, feasible only during cytosolic Ca^{2+} elevation, as a result of Ca^{2+} influx. Because the Ca^{2+} sensing domain is conjugated to the C-terminal domain of ezrin, it was anticipated that the probe would have the same plasma membrane interactions as native ezrin (fig. 5.1.2). This would place the Ca^{2+} sensor in the precise location where µ-calpain is postulated to be activated, and cleave ezrin to permit relaxation of the plasma membrane microridges.

Furthermore, as shown in Chapter 3, ezrin is lost from the cell edge during Ca^{2+} influx (e.g. ezrin is lost from the phagocytic cup during phagocytosis, and almost uniformly from the cell edge during artificial Ca^{2+} influx stimulated by a high Ca^{2+} cocktail containing, thapsigargin and ionomycin). As EPIC is essentially a modified ezrin, it is also expected to be a substrate for µ-calpain. In this way,

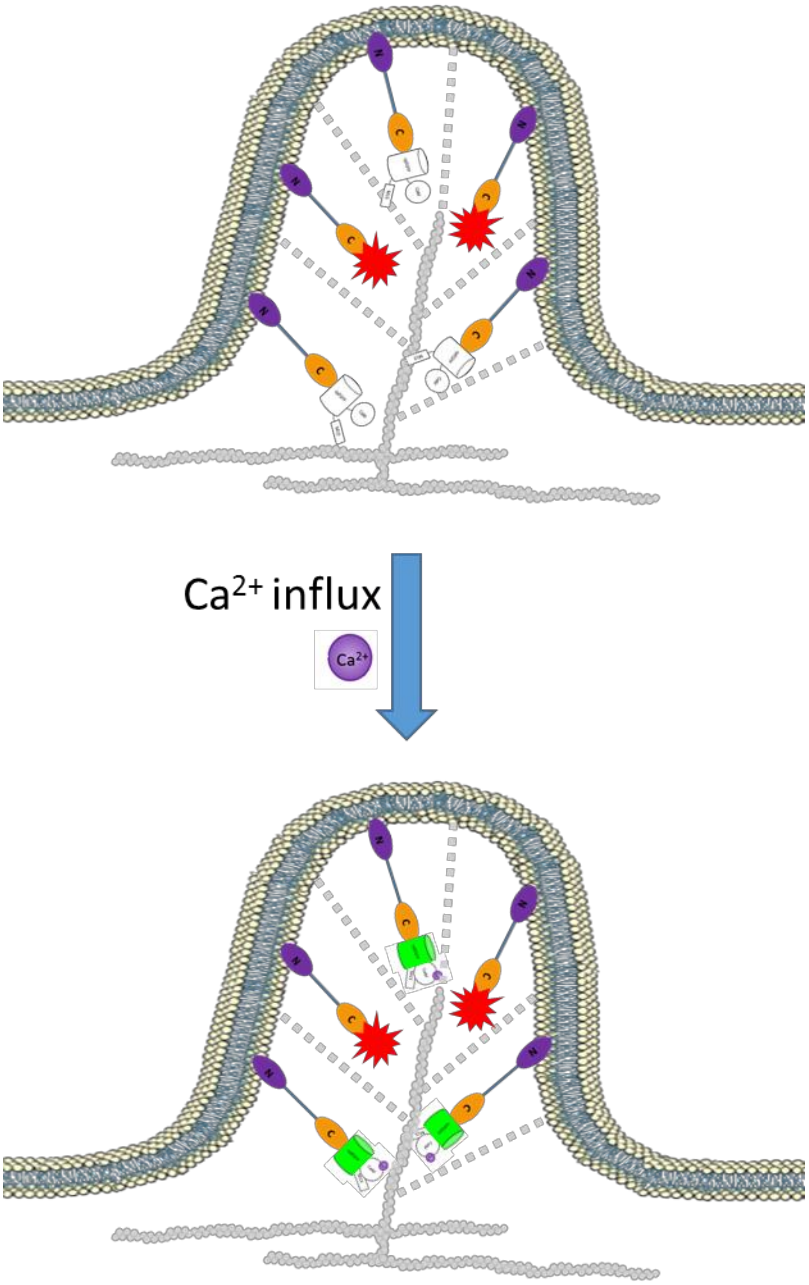

Figure 5.1.2: EPIC3 signalling
Ezrin-mCherry is constitutively fluorescent under a 587 nm laser. EPIC3 fluorescence intensity increases with elevated Ca^{2+} concentration. Both ezrin-mCherry and EPIC3 have the same ezrin localising properties, which means that ezrin-mCherry can be used as a location marker for EPIC3, when Ca^{2+} concentration is below EPIC3 sensitivity and fluorescence is low.

EPIC would both indicate the intra-microridge Ca^{2+} concentration, and be a marker of μ-calpain activity by ezrin cleavage.

5.1.3 Aims of this chapter

The activity of μ-calpain must be highly controlled, because of its lack of substrate specificity, and having many different potential substrates. Untimely or poorly restricted activation of μ-calpain could result in off target protein cleavage, and the potential disruption of multiple cellular processes. It is for these reasons we hypothesise that during morphological rearrangements of the plasma membrane and cortical actin cytoskeleton, μ-calpain is transiently and locally activated specifically beneath microridges in the plasma membrane, which provide a microenvironment in which the Ca^{2+} concentration is capable of transiently reaching higher micromolar Ca^{2+} concentrations; within the range required to activate μ-calpain.

The aim of this chapter, therefore, was to use the novel probe developed in Chapter 4, in order to experimentally measure the intra-microridge Ca^{2+} concentration in myeloid cells, specifically at the point of Ca^{2+} influx, where μ-calpain is thought to be activated.

The objectives were:

1. To express the novel EPIC3 in RAW 264.7 cells by nucleofection.
2. To measure localised EPIC3 signal within ezrin-rich cytosolic microdomains beneath plasma membrane microridges, during Ca^{2+} influx events.
3. To quantify changes in Ca^{2+} concentration using the Ca^{2+} binding properties of EPIC3.

5.2 Specific Materials and Methods

5.2.1 Transfection of RAW 264.7 cells

RAW 264.7 cells ($2x10^6$) were transfected with 3 µg of ezrin-mCherry, and 3 µg EPIC3 plasmid DNA, using programme D-032 on the Cell Line Nucleofector™ Device (Lonza), as previously described in Chapter 2.

5.2.2 Artificial elevation of Ca^{2+} concentration in RAW 264.7 cells

Transfected RAW 264.7 cells were seeded onto glass-bottomed petri dishes (approx. $6x10^5$ cells) and incubated for 3-4 hrs at 37°C with 5% CO_2, to allow for EPIC3 and ezrin-mCherry protein expression. Artificial Ca^{2+} influx was stimulated by extracellular addition of a high Ca^{2+} cocktail of thapsigargin (40 µM), ionomycin (20 µM) and Ca^{2+} (65-130 mM).

5.2.3 Physiological stimulation of RAW 264.7 cells (phagocytosis)

Zymosan particles (1 mg) were opsonised with mouse C3bi as previously described (Chapter 2). RAW 264.7 cells, transfected with EPIC3 and ezrin-mCherry, were seeded into glass-bottomed petri dishes, and kept at 4°C for 15 mins prior to the addition of excess C3bi-opsonised zymosan (200 µL). The cold RAW 264.7 cells were then left at 4°C for a further 15 mins, to allow the zymosan particles to sediment and bind to the adherent RAW 264.7 cells, without triggering phagocytosis. The chilled media was then aspirated and replaced with 200 µL of pre-warmed DMEM (37°C), to allow for phagocytosis to proceed. The cells were then imaged by confocal microscopy.

5.2.4 Measurement of dynamic changes in cytosolic Ca^{2+} as reported by novel EPIC3

5.2.4.1 Confocal microscopy

Confocal images were taken using the Leica SP5 confocal inverted microscope (Leica Microsystems, Heidelberg) with resonance scanner, laser scanning [63x objective; 633 nm and 488 nm argon laser] in a perfusion chamber at 37°C. Images were acquired from the two lasers by sequentially scanning alternate lines with each laser. In this way, each image line was the result of a single laser excitation, and there was no possibility of cross-talk (i.e. the inadvertent excitation of both fluorophores at the same time). Sequential line imaging also gave simultaneous images from each laser excitation, as previously described in Chapter 2.

5.2.4.2 ImageJ EPIC3 image processing

Two approaches have been used to process the image files: (A) a ratio calculated of EPIC3 and ezrin-mCherry to give a Ca^{2+} dependent ratio image, at each time point; (B) a dynamic mask of the cell edge applied to exclude cytosolic signals, and so allow only imaging of fluorescent signals from the ezrin rich periphery of the cell.

The dynamic masks were generated using ImageJ, in order to automate the image processing, and acquire data from the same region of a cell over several minutes of a time series. This was beneficial because the software was able to calculate the perimeter of the mask between frames, which was more efficient than manually adjusting the region of interest by eye, and between frames. The dynamic mask was used to process the EPIC3 signal from co-transfected cells. This enabled a more accurate description of changes in EPIC3 fluorescence.

A. EPIC3/ezrin-mCherry ratio

Avi. files of the EPIC3 and ezrin-mCherry were imported as gray scale. The image was smoothed twice ('Process' > 'Smooth') and image brightness was improved using the controls in the 'Image' > 'Adjust' menu (e.g. 15 min: 82 max). A ratio of the EPIC3 signal by the ezrin-mCherry signal was calculated using the 'Ratio Plus' plugin (*https://imagej.nih.gov/ij/plugins*), with clipping and threshold values set to approximately background level. A look up table (LUT) was applied and the file was smoothed as necessary. Changes in the EPIC3 signal were quantified using the 'Measure Stacks' function, as before. When the cell was moving it was sometimes also necessary to also use a dynamic mask, so that only the phagocytic cup was above the threshold of the mask, and therefore visible. Data were exported to Microsoft Excel for further analysis.

B. Dynamic mask using ezrin-mCherry and EPIC3 ratio

Avi files of the ezrin-mCherry signal were created and converted into binary masks. Avi fles were created from the ezrin-mCherry Leica .lif files. Files were imported into ImageJ as gray scale, smoothed, and brightness adjusted as described, then converted to binary ('Process' > 'Binary' > 'Make Binary'; calculated individually for each image in a series, with a black background). The binary images were dilated up to five times, if necessary to fill the mask ('Process' > 'Binary' > 'Dilate'), and the 'Fill Holes' function was applied ('Process' > 'Binary' > 'Fill Holes'). The 'Find Edge' function was selected ('Process' > 'Find Edge') and the mask was dilated a further three times and adjusted as necessary. Image files containing the EPIC3 signal data and ezrin-mCherry signal data were imported into ImageJ as gray scale, then smoothed and brightness adjusted. A ratio of the EPIC3 file by the ezrin-mCherry file was calculated using the 'Ratio Plus' plugin. The clipping and threshold values were set to approximately background level, and the ratio file was smoothed. The resultant mask was then multiplied by the ratio data image ('Process' > 'Image Calculator'), in 32 bit floating format, and a LUT was selected. Changes in EPIC3 signal were quantified using the 'Measure Stacks' function. A region of interest

was drawn around the cell (or region of cell) being analysed. Data were exported to Microsoft Excel for further analysis.

5.2.4.3 Calculating the Ca^{2+} concentration reported by EPIC3

EPIC3 fluorescence intensity was converted into approximate Ca^{2+} concentration by observing the following equations.

A. The relationship between free Ca^{2+} + EPIC3 ↔ (Ca^{2+}EPIC3)

a) The fraction of EPIC3 with Ca^{2+} bound (***f***) is given by the standard Law of Mass Action equation for binding:

$$f = 1/(1+(K_d/Ca^{2+}))$$

b) Note when $Ca^{2+} = K_d$ the equation is:

$f = 1/(1+1)$ i.e. $f = 0.5$ (that is half maximal binding)

c) This can be rearranged to give:

$$Ca^{2+} = K_d/((1/f)-1) \quad \text{.....} \quad \textbf{Equation 1}$$

B. The relationship between EPIC3 fluorescence and f

a) The minimum fluorescence of EPIC3 (in the absence of Ca^{2+}, or 0.1 µM Ca^{2+}) is F_{min}.

b) The max fluorescence of EPIC3 (in the presence of saturating Ca^{2+} e.g. > 200 µM Ca^{2+}) is F_{max}.

c) The dynamic range of EPIC3 fluorescence is 2.6 (Suzuki et al., 2014). Thus the maximum fluorescence attainable with EPIC3, under saturating Ca^{2+}, is 2.6 times greater than F_{min}. Therefore Equation 2 is:

$$F_{max} = approx.\ 2.6F_{min} \quad \text{.....} \quad \textbf{Equation 2}$$

C. The relationship between measured EPIC3 intensity and Ca^{2+} concentration

a) The ***f*** (fractional binding) is between zero and 1 as Ca^{2+} changes from the resting cytosolic level to saturating.

b) The intensity of EPIC3 at any time or in any location is ***F***. So:

$$f = (F-F_{min})/(F_{max}-F_{min})$$

c) However as F_{max} is 2.6 times F_{min}. Equation 3 can be derived as follows:

$$f = (F-F_{min})/(2.6F_{min}-F_{min})$$

⇨ $$f = (F-F_{min})/(1.6F_{min})$$

⇨ $$f = F/1.6F_{min} - F_{min}/1.6F_{min}$$

⇨ $$f = 1/1.6\ ((F/F_{min})-1)$$

⇨ $$f = (F/F_{min})-1)/1.6$$ …… **Equation 3**

e) The value of f from Equation 3, was inserted into Equation 1, to give the Ca^{2+} concentration reported by EPIC3.

5.2.5 Calculating the cell footprint (2D area)

Avi. fles were created from the ezrin-mCherry Leica .lif files, imported into ImageJ as gray scale, and converted into binary masks. The image was smoothed twice ('Process' > 'Smooth') and image brightness was improved using the controls in the 'Image' > 'Adjust' menu. Files were converted to binary ('Process' > 'Binary' > 'Make Binary'). It was important that the binary images corresponded to the cell outline and, if necessary the 'Fill Holes' function was applied ('Process' > 'Binary' > 'Fill Holes'). In the binary image, all pixels within the cells had a value of 1 and all pixels outside the cell had a value of zero. Consequently, the number of non-zero pixels in each image of the time series corresponded to the cell footprint, or 2D area. This was measured using the 'Measure Stacks' function, which gave the mean pixel number in each frame. The data were exported to Microsoft Excel for further analysis, and processed using the formula: $N_{x\neq 0} = \frac{\bar{x}}{255} \times n$. Where $N_{x\neq 0}$ is the number of non-zero pixels, *n* is the total number of pixels and 255 is the value of a pixel.

5.2.6 Calibrating the LUTs

The LUTs were individually calibrated by hand for each cell, by first observing Equation 1 (section 5.2.4.3), rearranged to give:

$$f = 1/(1+(K_d/Ca^{2+}))$$

Where the $\mathbf{K_d}$ is 11 µM. For defined Ca^{2+} concentrations (e.g. 0.1 µM – 200 µM) the **F** was then calculated using Equation 3, rearranged to give:

$$\mathbf{F = F_{min}(1.6}\boldsymbol{f}\mathbf{ + 1)}$$

Where **F** is the pixel value on the LUT (in gray scale). This was converted in to pixel distance (from 0-255) along the LUT, and Ca^{2+} concentration was labelled accordingly.

5.3 Results

5.3.1 EPIC3 reports Ca^{2+} activity at the cell edge in myeloid cells

Due to the limitations of working with human neutrophils, in that they cannot be transfected to produce novel proteins in sufficient quantities for these experiments, a RAW 264.7 cell line was used to model the behaviour of microridge domains in myeloid cells. RAW 264.7 cells are a suitable model for these experiments because they are capable of changing morphology and performing phagocytosis of C3bi-opsonised zymosan particles; and are also able to undergo cell spreading, involving an apparent expansion of the cell membrane, similar to neutrophils.

Initially, the novel EPIC3 alone was transfected into RAW 264.7 cells, using nucleofection. Artificial Ca^{2+} elevation was stimulated by addition of a cocktail containing thapsigargin (40 µM), to inhibit intracellular store re-filling via the SERCA pump, ionomycin (20 µM) to transport Ca^{2+} across the cell membrane, in combination with or followed by a Ca^{2+} concentration step-up (Δ 65-130 mM) to provide a temporally-defined and rapid Ca^{2+} influx.

EPIC3 fluorescence intensity is Ca^{2+} dependent, and minimal (i.e. F_{min}) at the cytosolic Ca^{2+} levels in a resting cell. However, even in unstimulated conditions, 25% of the cells had an elevated EPIC3 signal at the cell edge. This may indicate that even at rest, sub-plasma membrane Ca^{2+} is sufficiently high to cause detectable EPIC3 fluorescence in some cells. In 94% of cells in which EPIC3 was

detected, EPIC3 intensity increased following artificial elevation of cytosolic Ca^{2+} (fig. 5.3.1i). 87% of cells that responded to Ca^{2+} influx changed morphology, often becoming round, concomitantly with an increase in cell footprint (fig. 5.3.1ii).

The intensity of EPIC3 fluorescence increased, reporting elevated global Ca^{2+} concentrations within 10 s of extracellular Ca^{2+} elevation (15/16 cells). Peak EPIC3 intensity typically occurred within 30s of extracellular Ca^{2+} addition (fig. 5.3.1ii). Cell imaging by confocal microscopy revealed the EPIC3 signal was transiently higher at regions of the cell edge (fig. 5.3.1iii; blue=low Ca^{2+}, green=high Ca^{2+}). The Ca^{2+} concentration at the cell edge was estimated to reach 19.2 ±5.3 µM (SEM) at 10 s after Ca^{2+} elevation. Despite the morphological changes which accompanied the Ca^{2+} increase, and which are indicative of µ-calpain activation and ezrin cleavage, the sub-plasma membrane Ca^{2+} estimated by these measurements may not be sufficient to fully activate µ-calpain (K_d=20-60 µM). However, as ezrin cleavage occurs at the cells edge, as a result of Ca^{2+} elevation (discussed in Chapter 3), EPIC3 would be progressively lost from the cell edge under these conditions, giving a lower fluorescent signal from that location, regardless of the Ca^{2+} concentration reached. Also, the Ca^{2+} sensing domain of EPIC3 would move away from the areas of high Ca^{2+}, at the cell edge, and into the relatively lower Ca^{2+} concentration of the bulk cytosol. This approach is therefore likely to underestimate the Ca^{2+} concentrations within high Ca^{2+} microdomains. The initial estimate of 19.2 ±5.3 µM, should therefore be taken as a minimum value of Ca^{2+} concentration within the ezrin-rich sub-membranous microdomain, with the expectation that a more refined estimate would yield a higher value.

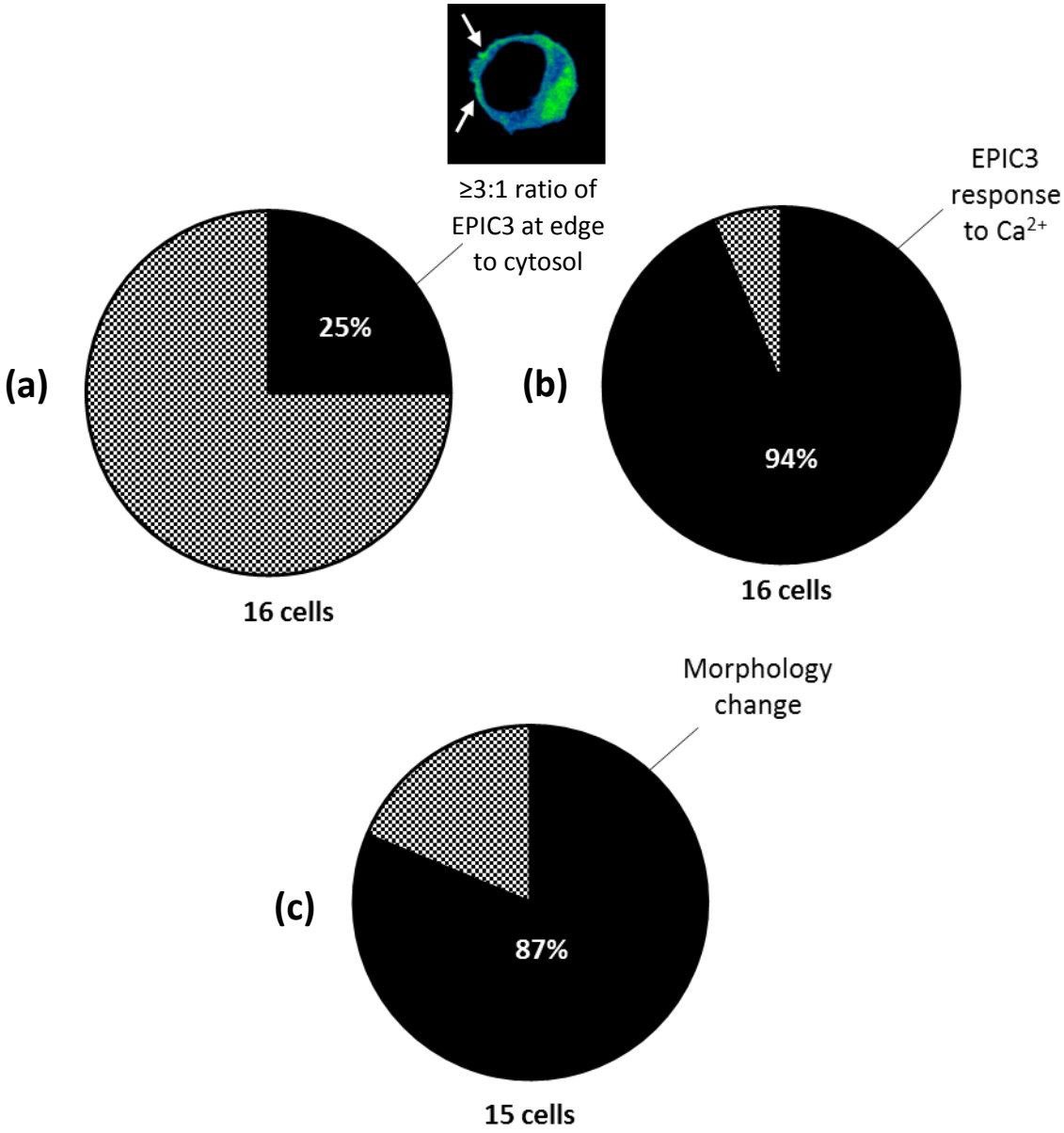

Fig 5.3.1i: RAW 264.7 cells expressing EPIC3
Of 16 cells expressing EPIC3 **(a)** only 4 had a elevated signal at the cell edge under resting conditions. **(b)** In 94% of the cells measured (15/16) EPIC3 reported a rise in overall cell Ca^{2+} concentration. **(c)** 87 % of cells (13/15) had a morphological change, bloated and rounded up.

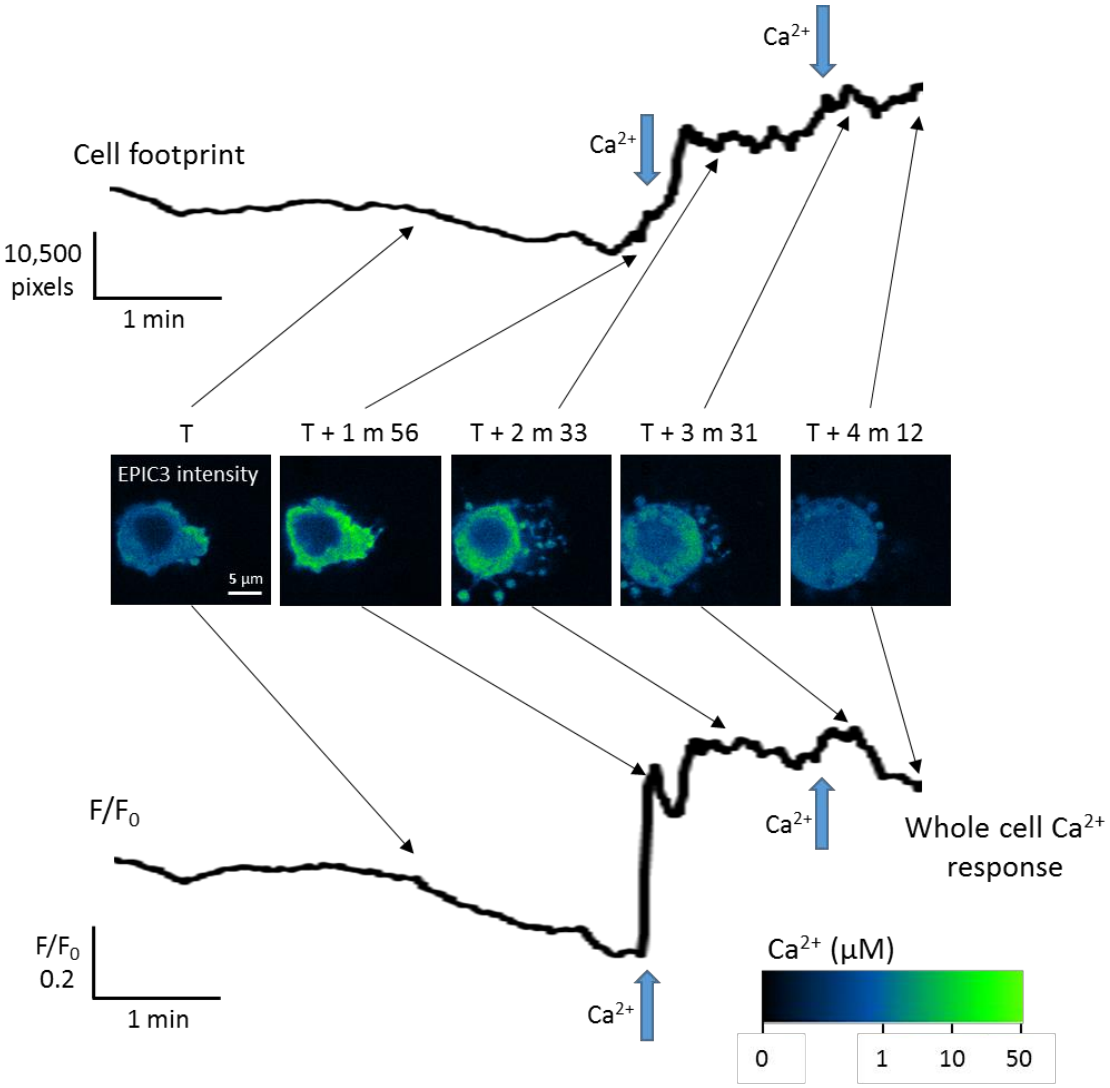

Figure 5.3.1ii: EPIC3 reports elevation in Ca^{2+} prior to cell spreading
RAW 264.7 cell transfected with EPIC3 and pre-treated with thapsigargin (40 µM). Before addition of Ca^{2+} the cell had a large diameter of 14.5 µm and a smaller diameter of 11.6 µm. Ca^{2+} (65 mM) was added at the blue arrows. EPIC3 reports elevated Ca^{2+} at the cell edge (estimated to reach 19.2 ±5.3 µM) within 10 s after elevation of extracellular Ca^{2+}. Within 40 s the cell begins to bleb and Ca^{2+} is elevated in the cytosol. At T + 3 m 31 s (8 s after the second Ca2+ addition) the cell has rounded up (approx. 26% larger) and continues to increase in size whilst Ca^{2+} levels remain elevated. At T + 4 m 12 s EPIC3 signal is cytosolic, the cell is round and has expanded to a diameter of 13 µm. Scale bar 5 µm.

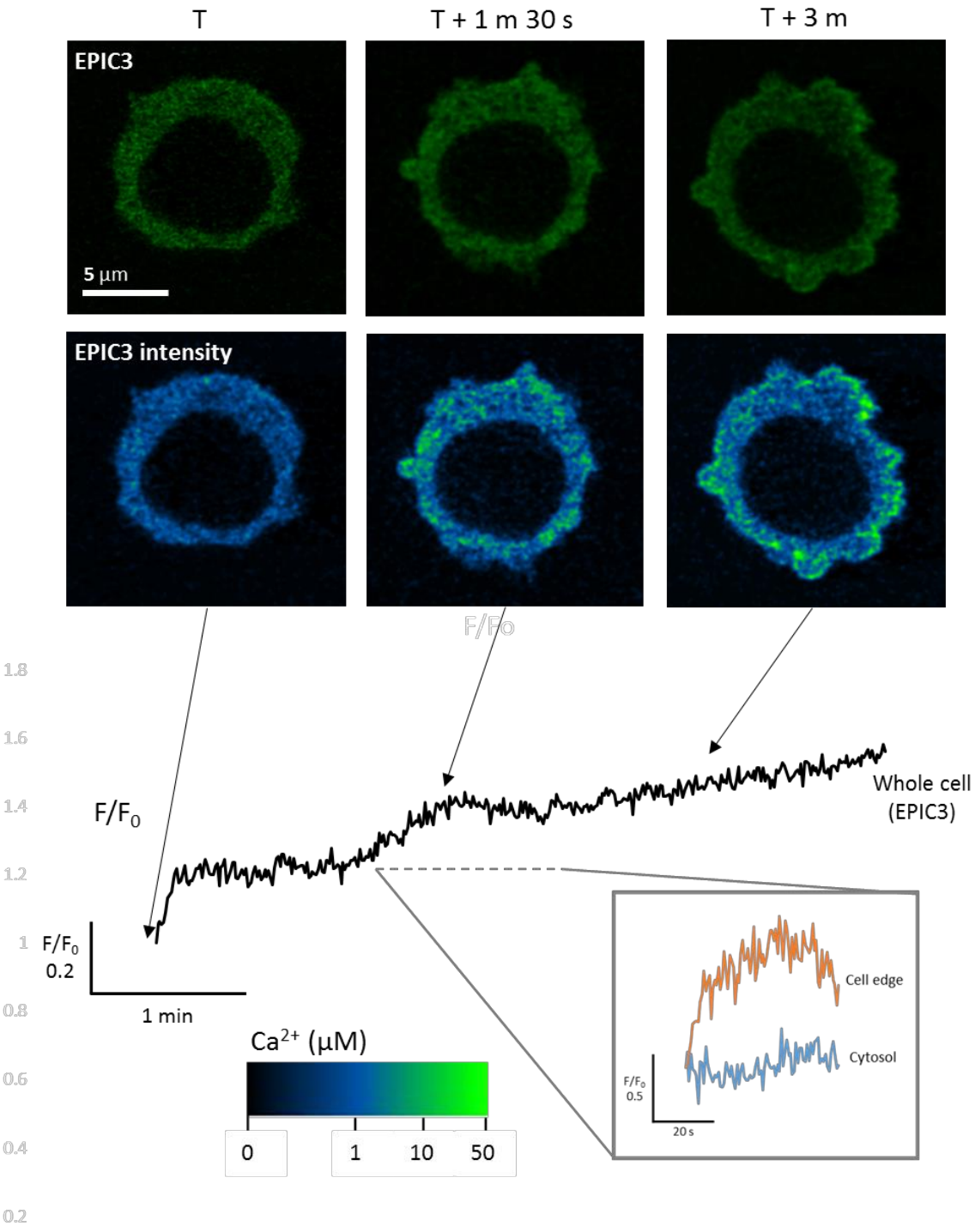

Figure 5.3.1iii: EPIC3 reports elevated Ca^{2+} at the cell edge

RAW 264.7 cell transfected with EPIC3, shown after treatment with a high Ca^{2+} cocktail containing thapsigargin (40 µM), ionomycin (20 µM) and Ca^{2+} (65 mM). Top panels: Raw data. Bottom panels: Green-fire-blue LUT identifies Ca^{2+} hotspots at the cell edge. Ca^{2+} concentration at the cell edge was estimated to reach 9.4 ±2.4 µM, 3 mins post stimulation with the cocktail. A global rise in cytosolic Ca^{2+} (estimated from 0.4 µM to 6.3 µM) was seen in cells expressing EPIC3 (alone), after treatment with the high Ca^{2+} cocktail. Insert: 30 s snapshot of Ca^{2+} concentration at the cell edge rising more rapidly and reaching 3 µM higher than in the cytosol. Scale bar 5 µm.

Secondary to Ca^{2+} influx, cells were observed to undergo morphological rearrangements, involving an increase in cell area. The cell footprint was defined as the number of non-zero pixels in frame. Cells typically began to round-up within 10-15 s after the observed Ca^{2+} influx (approx. 30 s post extracellular Ca^{2+} elevation), and some cells began to bleb (fig. 5.3.1ii). In spreading cells, the EPIC3 signal was lost from the cell edge concurrent with cell expansion, the EPIC3 signal becoming dispersed in the global cytosol. A similar response was previously described in RAW 264.7 cells expressing ezrin-mEmerald, post Ca^{2+} influx (Chapter 3), and so probably represented loss of EPIC3 binding at the cell edge, rather than lowering of Ca^{2+} concentration. Therefore, these estimates of Ca^{2+} concentration from EPIC3 may be lower than the true value. Rounding-up and a detectable increase in cell footprint was observed in 13/15 cells expressing EPIC3, which responded to artificial elevation of cytosolic Ca^{2+} concentration. This response is indicative of μ-calpain activation, and cleavage of the ezrin cross-links.

The global Ca^{2+} response in RAW 264.7 cells expressing EPIC3 typically reported an increase in Ca^{2+} over the first 90 s, followed by a secondary rise in Ca^{2+} which was less steep, and continued to increase gradually over the next 90 s (fig. 5.3.1iii). However, it was often difficult to obtain accurate measurements of EPIC3 intensity at the cell edge, as the cellular response to Ca^{2+} influx resulted in morphological changes. However, in at least 4 cells, it was possible to take accurate measurements at defined cellular regions over 20-30 s intervals. These revealed diverging Ca^{2+} responses at the cell edge, compared to the cell cytosol, post treatment with the stimulating cocktail (fig. 5.3.1iii). EPIC3 reported rising Ca^{2+} concentration at the cell edge, when cytosolic signal was decreasing, and the global Ca^{2+} response appeared to plateau (fig. 5.3.1iii). The maximum Ca^{2+} concentration measured at the cell edge ranged from 5.4 – 34.4 μM between individual cells. In the example shown in figure 5.3.2iii the global Ca^{2+} concentration was estimated to reach 6.3 μM, and the concentration at the cell edge was estimated to reach 9.4 ±2.4 μM. Although, these values are again not in the range capable of activating μ-calpain, they should as previously stated, be

considered minimum estimates, which are artefactually decreased by the re-distribution of ezrin into the bulk cytosol.

The Ca^{2+} traces recorded in these experiments were shallower than typical intracellular Ca^{2+} measurements, which can be achieved using probes with a physiological range, because the K_d of EPIC3 is 11 μM Ca^{2+}. The Ca^{2+} estimates recorded at the cell edge in these experiments were significantly higher than in the cell cytosol, but lower than expected for the full activation of μ-calpain (K_d 20-60 μM). However, the morphological changes in the cell, and the loss of ezrin at the cell edge both suggested that μ-calpain activation had occurred. Taken together this suggested that the present methodology of measuring the EPIC3 signal was not sufficient to capture the full Ca^{2+} activity at the cell edge. It was obviously important to take into account any changes in fluorescence which were due to fluctuations in EPIC3 distribution, rather than changes in Ca^{2+}.

5.3.2 Dual expression ratio imaging of EPIC3 and ezrin-mCherry

In order to provide a non Ca^{2+}-sensing control probe with excitation and emission properties which allowed it to be used in conjugation with the Ca^{2+}-sensing probes, ezrin conjugated to an mCherry fluorophore, at the C-terminal end, was used. RAW 264.7 cells were transfected with both EPIC3 and ezrin-mCherry (fig. 5.3.2i). A ratio of the two fluorescence intensities was taken, so that EPIC3 fluorescence could be normalised to exclude changes due to ezrin movement, and LUTs were applied to visualise the gradient of cytosolic Ca^{2+} concentration at the cell edge (fig. 5.3.2ii).

ALL RAW 264.7 cells co-transfected with EPIC3 and ezrin-mCherry had a detectable ezrin-mCherry signal at the cell edge, but only 50% of cells had a detectable peripheral EPIC3 signal. This lack of correlation between the subcellular distributions of intensities of the non-Ca^{2+}-sensing ezrin, and the

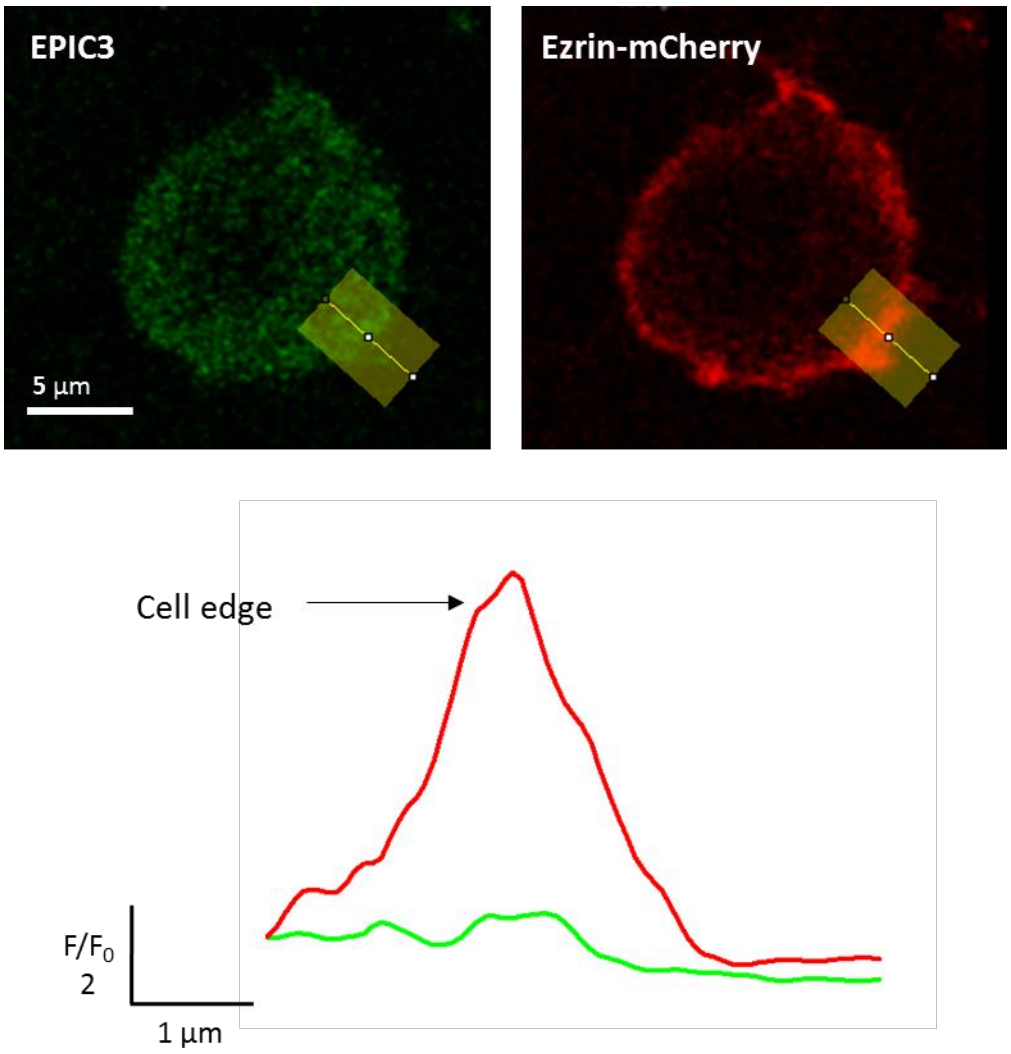

Figure 5.3.2i: EPIC3 and ezrin-mCherry co-transfected RAW 264.7 cells
In unstimulated cells the ezrin-mCherry reports ezrin location at the cell edge, where there is no detectable EPIC3 signal. Representative of 8 cells. Scale bar 5 µm.

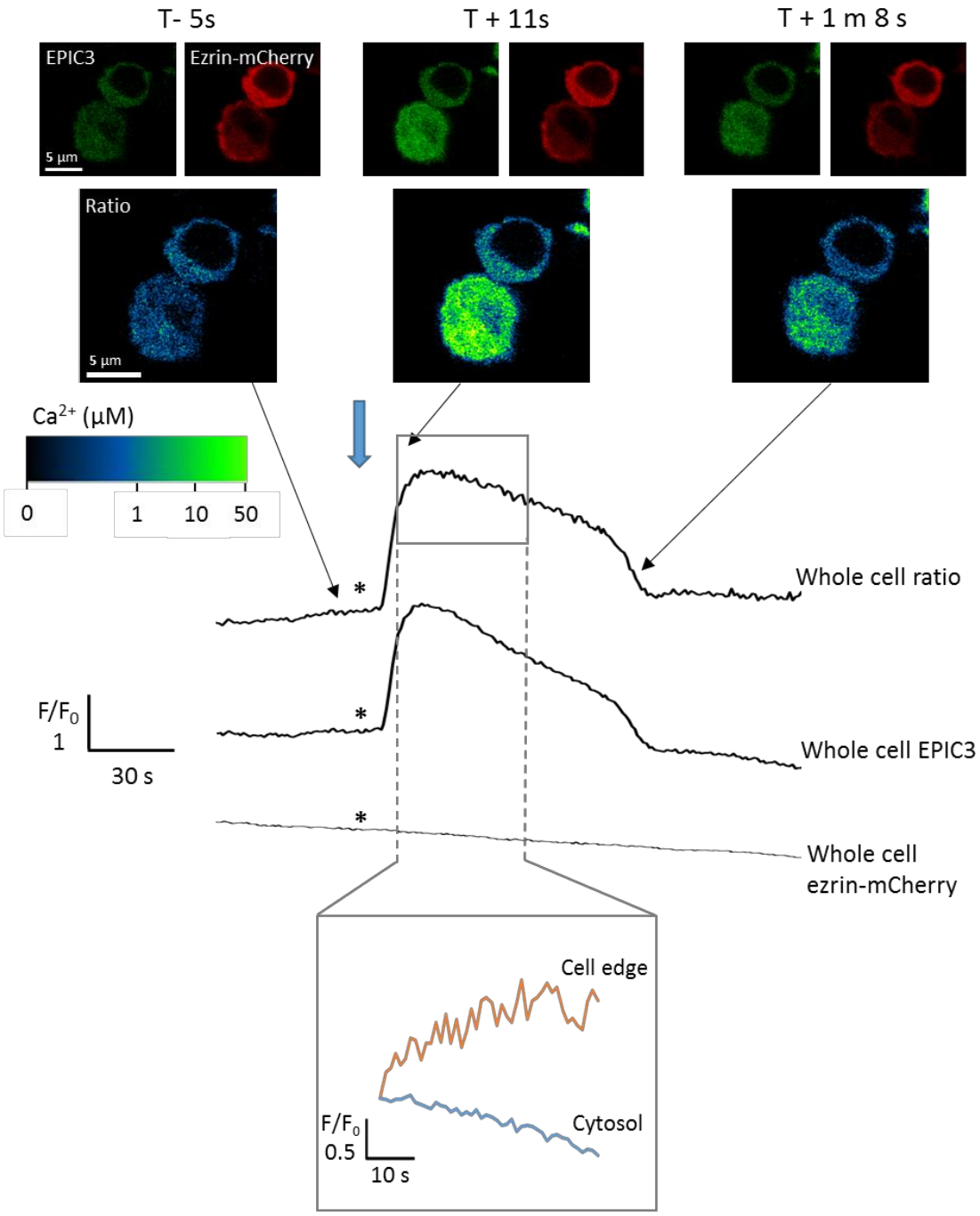

Figure 5.3.2ii: EPIC3 and ezrin-mCherry co-transfected RAW 264.7 cells report differential Ca^{2+} concentration at the cell edge and cytosol

Both the raw EPIC3 signal and the ratio of the two probes reported a global rise in Ca^{2+} concentration following addition of the high Ca^{2+} cocktail, added at the blue arrow (*). Insert: 20 s snapshot of rising Ca^{2+} concentration at the cell edge, concurrent with falling Ca^{2+} concentration in the cytosol (estimated difference of 5.95 µM). Scale bars both 5 µm.

Ca^{2+}-sensing ezrin, provided good evidence that (i) EPIC3 intensity was not simply reporting ezrin location, but also included information about local Ca^{2+} concentrations, and (ii) some cells had low level sub-plasma membrane Ca^{2+}, while in other cells the elevation of sub-plasma membrane Ca^{2+} was apparent, and upon Ca^{2+} influx.

Co-transfected cells mostly behaved in a similar way to singly-transfected cells. In 88% of cells, artificially induced Ca^{2+} influx resulted in an increase in EPIC3 intensity. 71% of cells responded to the Ca^{2+} influx by changing morphology. However, no cells were seen to bloat, bleb or spread, as with the singly-transfected cells (fig. 5.3.2iii). It is possible that the introduction of multiple ezrin constructs may have reduced the ability of the cell to change morphology in response to Ca^{2+}, by complementing endogenous ezrin. The extra F-actin-plasma membrane cross-links provided by the additional ezrin would also have to be cleaved in addition to the endogenous proteins.

By taking a ratio of the EPIC3 and ezrin-mCherry signals, it became apparent that rises in EPIC3 fluorescence intensity were masked by ezrin redistribution, and the true signal was typically higher (fig. 5.3.2ii). Furthermore, it was again possible to obtain data from the cell edge. In 4/6 cells the ratio of the EPIC3/ezrin-mCherry signal at the cell edge diverged from the cytosolic signal, and reported higher peripheral Ca^{2+} concentrations, of up to 30.4 ±7.6 µM, when the overall cell ratio appeared to plateau and then decrease (fig. 5.3.2ii). The total ezrin-mCherry signal decreased over time in all cells, which may have been a result of extended laser exposure and fluorophore bleaching.

By taking ratios (EPIC3/ezrin-mCherry) of all images within a time series, it was possible to visualise regions of high EPIC3 signal in the tips of cell protrusions, microridges and pseudopodia (fig. 5.3.2iv). The Ca^{2+} concentration in these microdomains after artificial stimulation of Ca^{2+} influx was estimated to reach up to 61 µM (fig. 5.3.2ivb), which would be capable of activating µ-calpain (K_d 20-60 µM).

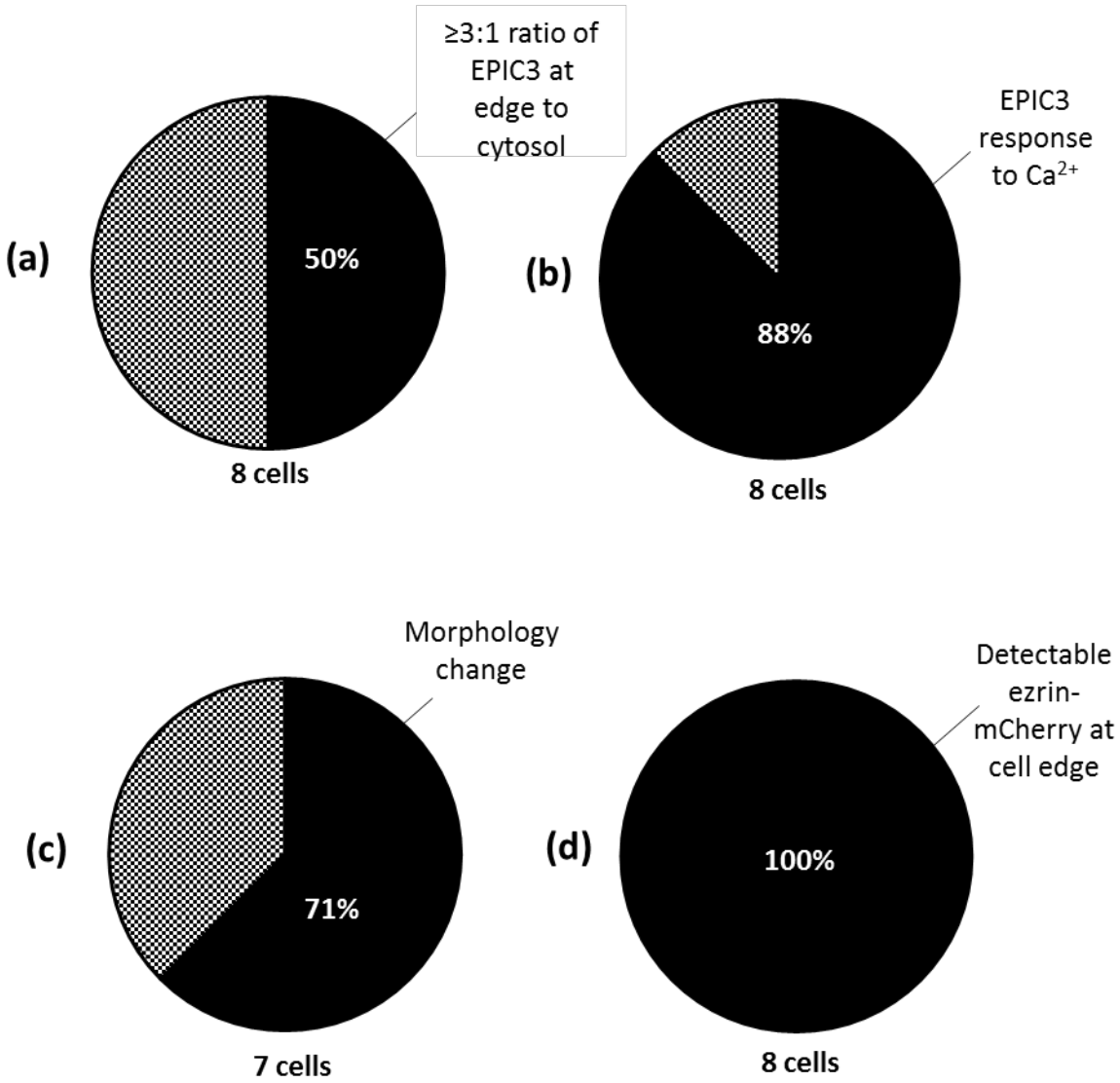

Fig 5.3.2iii: RAW 264.7 cells co- expressing EPIC3 and ezrin-mCherry
Of 8 cells expressing EPIC3 and ezrin-mCherry, **(a)** 4 had a elevated EPIC3 signal at the cell edge under resting conditions. **(b)** In 88% of the cells measured (7/8) EPIC3 reported a rise in overall Ca^{2+} concentration, and **(c)** 71 % of those cells (5/7) had a morphological change, bloated and rounded-up. **(d)** All of the cells expressing EPIC3 and ezrin-mCherry had a detectable ezrin-mCherry signal at the cell edge.

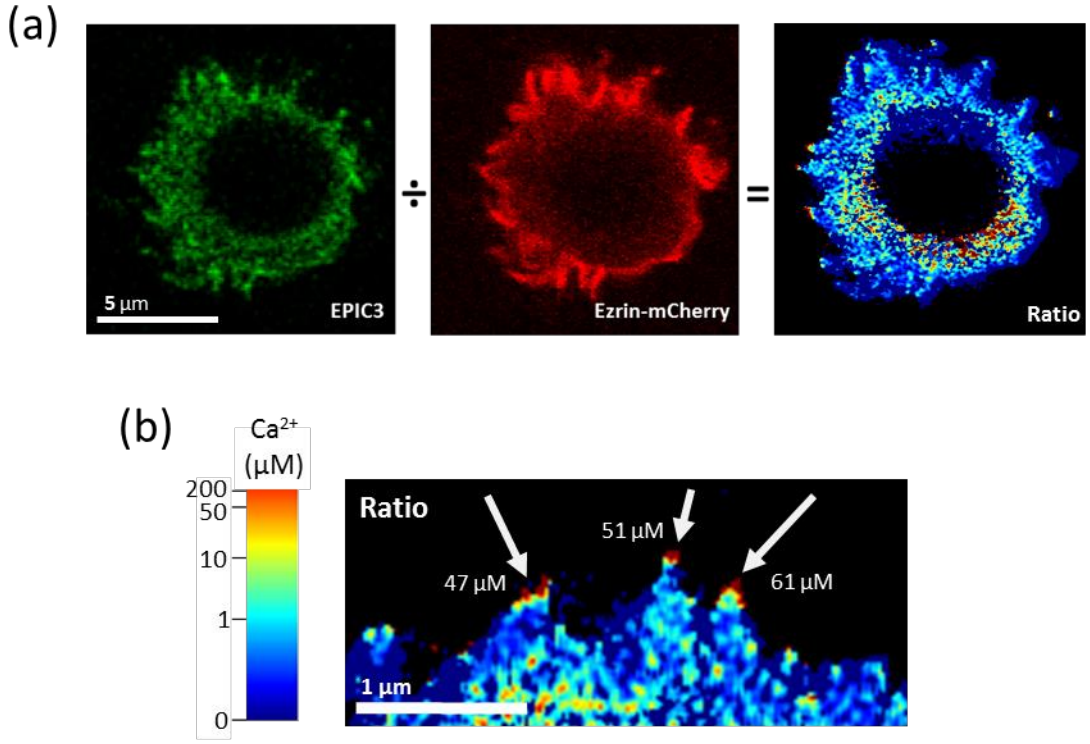

Figure 5.3.2iv: Ratio of EPIC3 and ezrin-mCherry signals

RAW 264.7 cell co-transfected with EPIC3 and ezrin-mCherry, treated with a high Ca^{2+} cocktail containing thapsigargin and ionomycin. **(a)** A ratio of the EPIC3 and ezrin-mCherry signals was taken using ImageJ, and the LUT JET was applied. Scale bar 5 µm. **(b)** Ca^{2+} hotspots (yellow-red) can be seen at the tips of microridge, estimated to reach 61 µM. Scale bar 1 µm

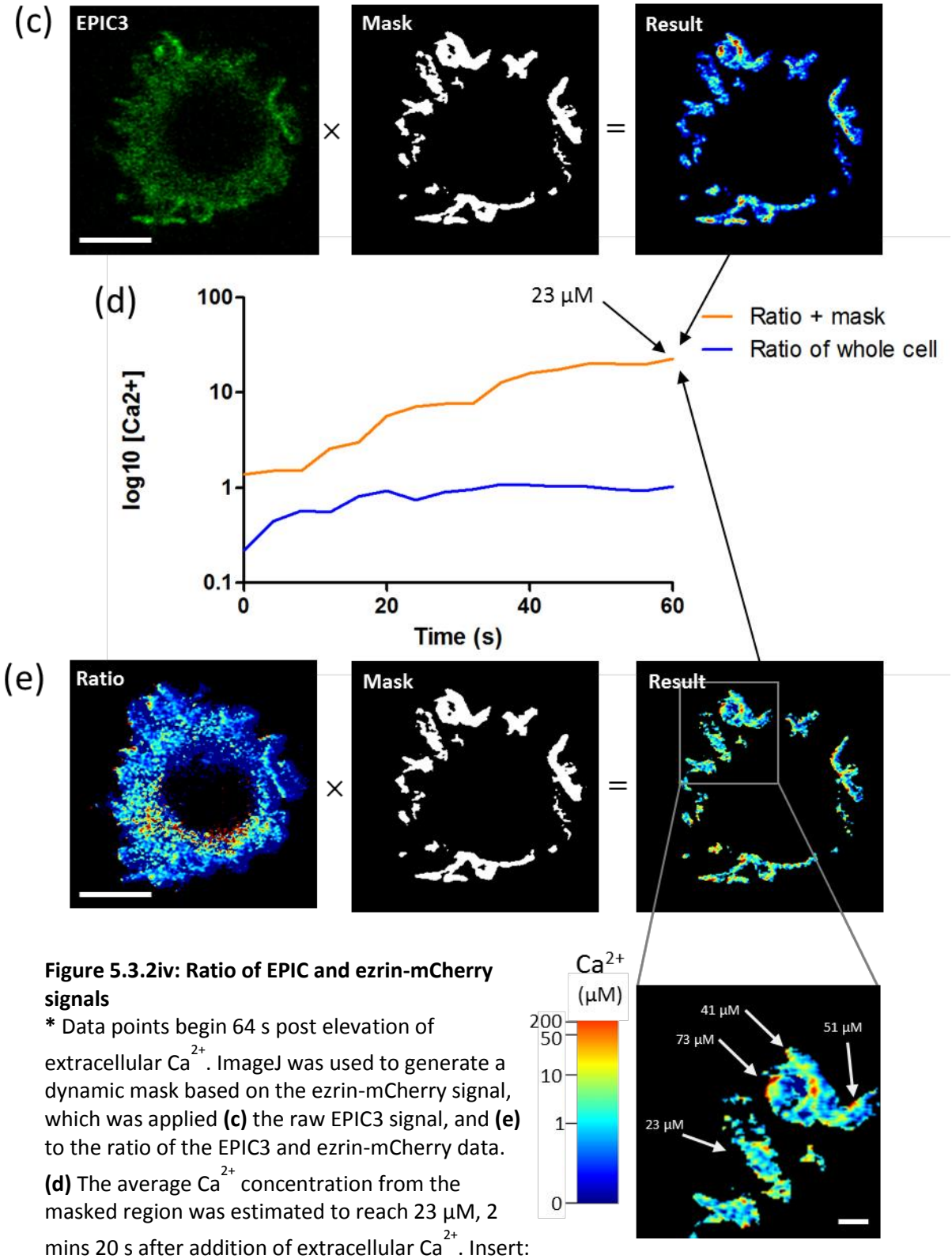

Figure 5.3.2iv: Ratio of EPIC and ezrin-mCherry signals

***** Data points begin 64 s post elevation of extracellular Ca^{2+}. ImageJ was used to generate a dynamic mask based on the ezrin-mCherry signal, which was applied **(c)** the raw EPIC3 signal, and **(e)** to the ratio of the EPIC3 and ezrin-mCherry data. **(d)** The average Ca^{2+} concentration from the masked region was estimated to reach 23 µM, 2 mins 20 s after addition of extracellular Ca^{2+}. Insert: regions of high Ca^{2+} concentration, estimated to reach 73 µM, can be seen at the peaks of microridges. Scale bars 5 µm, and insert 1 µm.

However, while the ezrin-mCherry probe is useful and important in accounting for any signal fluctuation caused by ezrin re-distribution, it also produces two artefacts. Firstly, the total ezrin-mCherry signal decreased over time in all cells, which may have been a result of extended laser exposure and fluorophore bleaching. Without any changes in the EPIC3 signal intensity, the ratio would therefore increase. This problem was negated by only taking reliable data from short time periods of laser exposure, typically 0-50s. Secondly, the ratio calculated when the cytosolic ezrin-mCherry signal is very low (i.e. before cleavage, when the majority of active ezrin is located at the cell edge), can be over-estimated. This is evident in the cytosol of the cell shown in figures 5.3.2ii & 5.3.2iva. To overcome this, and also the problem of measuring fluorescence intensity at the edge of a moving cell across an image stack of up to one thousand frames, a dynamic mask was generated. ImageJ was used to record fluctuating fluorescence intensity within a region of the cell edge defined by a dynamic mask, based on the ezrin-mCherry signal (fig. 5.3.2ivc). When the mask was applied to the whole cell ratio data (EPIC3/ezrin-mCherry), only the signal coming from the regions of highest ezrin intensity was recorded (fig. 5.3.2ivd,e). In this way, the ezrin-mCherry was used to define a threshold ezrin intensity, through which to measure changes in Ca^{2+} concentration, in ezrin-rich sub-membrane cytosolic microdomains.

In cells artificially stimulated to elevate cytosolic Ca^{2+} concentration, the ratio of EPIC3 and ezrin-mCherry reported a higher average Ca^{2+} concentration in the peripheral cytosol, at the cell edge, increasing up to 23 µM over 60 s post stimulation (fig. 5.3.2iv), which is in the µ-calpain-activating range. Whereas data from the whole cell ratio, without application of the high intensity ezrin mask as a threshold, reported a maximum Ca^{2+} concentration of 1 µM, which is consistent with previous cytosolic measurements (Demaurex et al., 1992). The data from the cell edge and the global Ca^{2+} signals were significantly different at all time points (Two-tailed, paired, T-test; $p < 0.0001$).

Further application of the dynamic mask in an inverse manner – so that only cytosolic signal was being measured – made it possible to compare changes in both the bulk and peripheral cytosol, with the same probe (fig. 5.3.2va,b). From such measurements, the average Ca^{2+} concentration in the bulk cytosol was found to rise steadily after the Ca^{2+} injection, up to an estimated 8 μM (fig. 5.3.2vc) before slowing, and then gradually decreasing. The signal at the cell edge also rose steadily, and up to a maximum 26 μM, before decreasing rapidly. The point at which both signals stopped rising is perhaps linked to the threshold Ca^{2+} concentration required for μ-calpain activation and ezrin cleavage. Since both EPIC3 and the control ezrin-mCherry are susceptible to calpain cleavage, both will also be lost from the cell edge upon μ-calpain activation (as discussed in Chapter 3). Therefore, EPIC3 reports not only the Ca^{2+} concentration achieved in cytosolic microdomains during Ca^{2+} influx, and bulk cytosol, but also the Ca^{2+} concentration at which μ-calpain-activated cleavage of ezrin occurs.

It was decided that using the dynamic mask was a suitable way to measure EPIC3 fluorescence at the cell edge in moving cells, and cells undergoing morphological changes. The Ca^{2+} estimations generated using the 'ratio + mask' method suggested that peripheral cytosolic Ca^{2+} reached mid-decade micromolar concentrations, capable of activating μ-calpain.

5.3.3 Ca^{2+} responses during phagocytosis

It was previously observed that doubly-transfected cells were less able to undertake dramatic shape changes, following Ca^{2+} influx. The morphological response of the transfected RAW 264.7 cell line may have been compromised by the introduction of extra ezrin constructs. The activity of μ-calpain and elevated Ca^{2+} concentration were instead investigated in localised membrane expansion events, such as phagocytosis. This approach also provided a more physiological method to stimulate Ca^{2+} influx. Zymosan particles were C3bi-opsonised by incubation with mouse serum, and introduced to glass-bottomed petri dishes

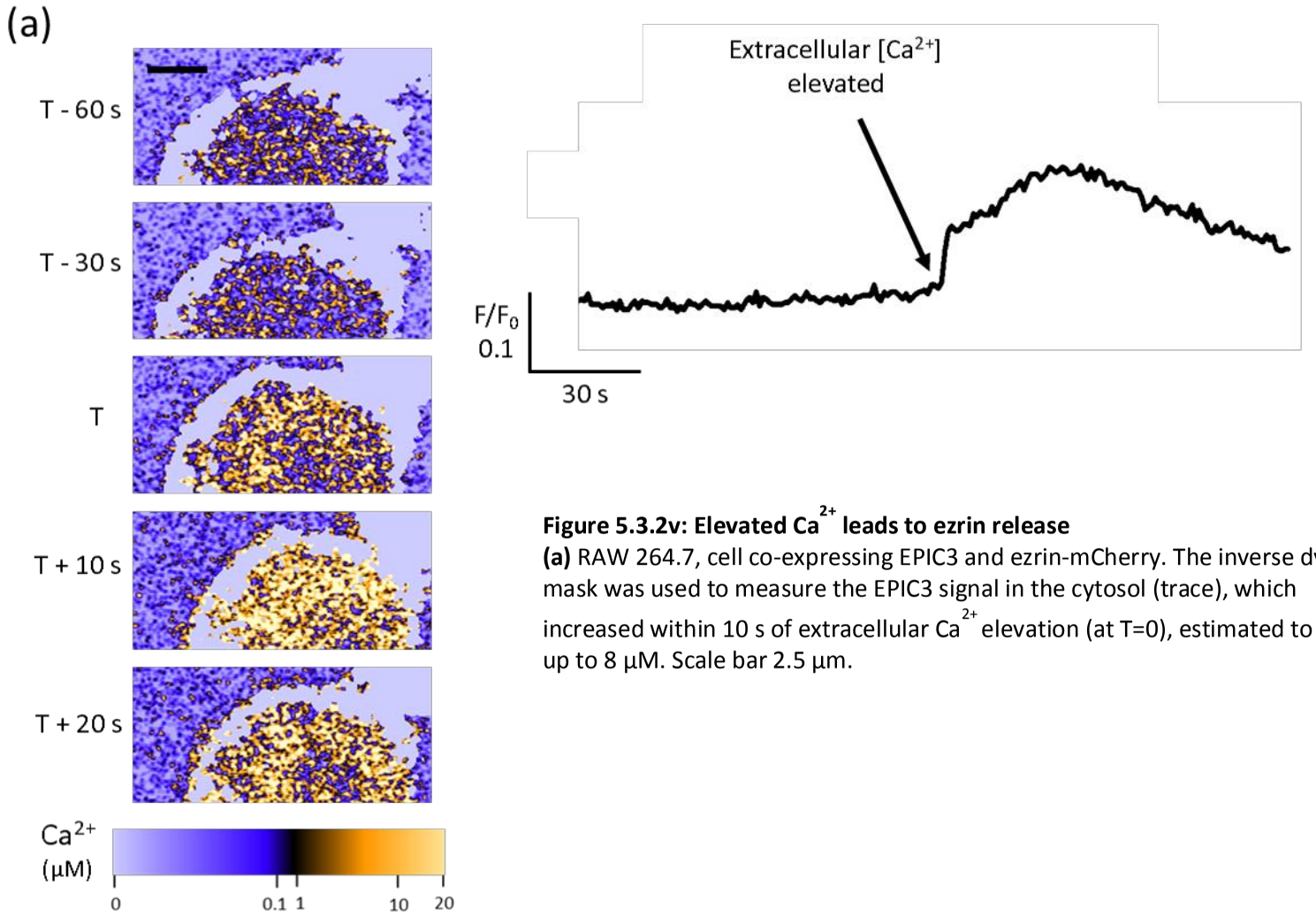

Figure 5.3.2v: Elevated Ca^{2+} leads to ezrin release
(a) RAW 264.7, cell co-expressing EPIC3 and ezrin-mCherry. The inverse dynamic mask was used to measure the EPIC3 signal in the cytosol (trace), which increased within 10 s of extracellular Ca^{2+} elevation (at T=0), estimated to reach up to 8 μM. Scale bar 2.5 μm.

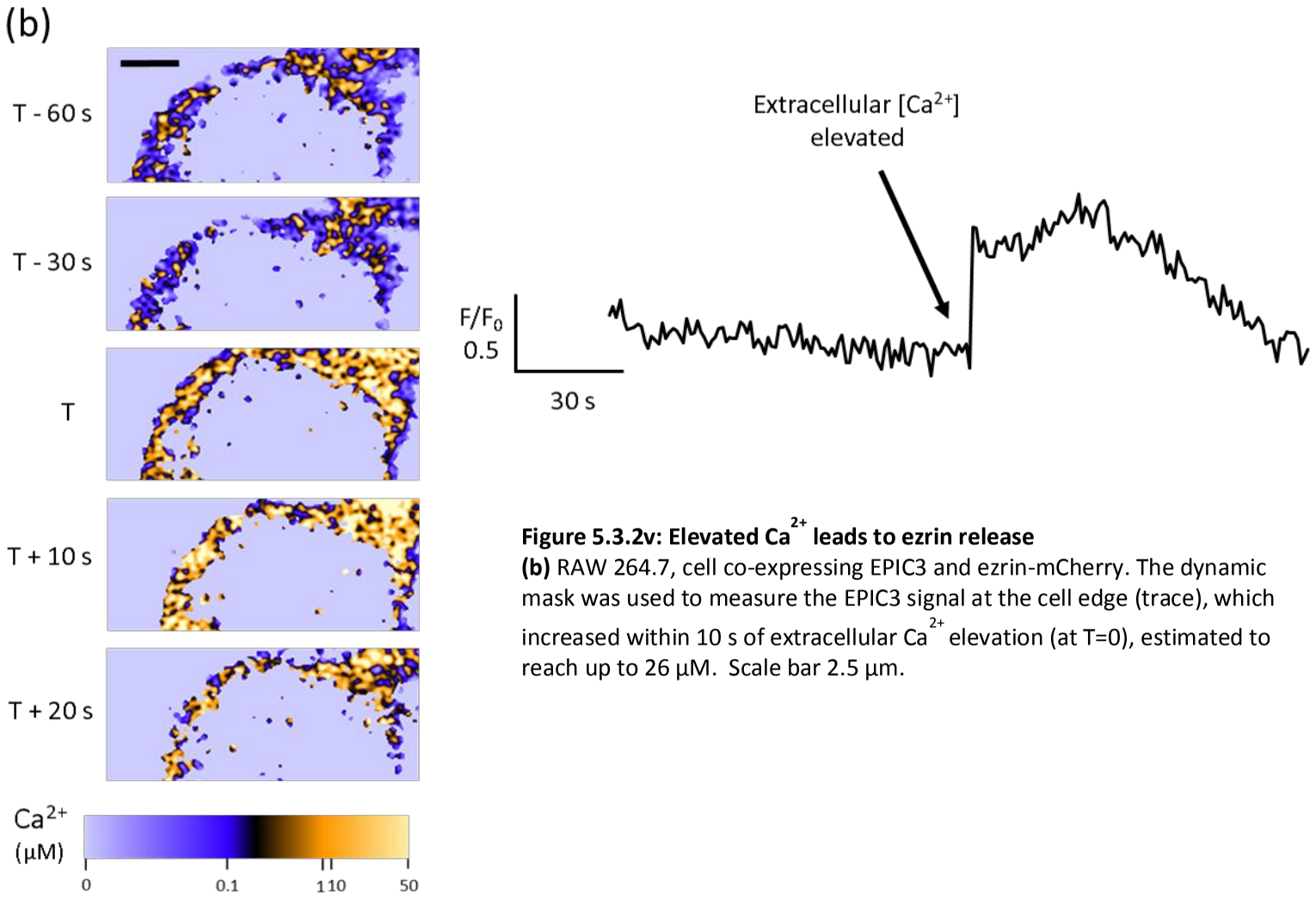

Figure 5.3.2v: Elevated Ca^{2+} leads to ezrin release
(b) RAW 264.7, cell co-expressing EPIC3 and ezrin-mCherry. The dynamic mask was used to measure the EPIC3 signal at the cell edge (trace), which increased within 10 s of extracellular Ca^{2+} elevation (at T=0), estimated to reach up to 26 µM. Scale bar 2.5 µm.

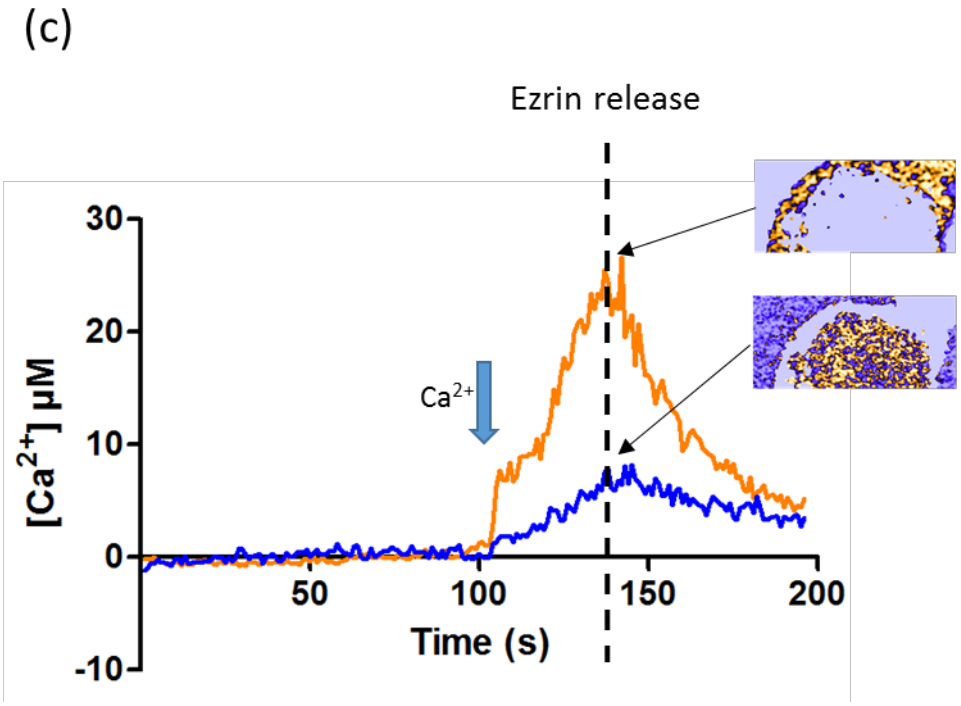

Figure 5.3.2v: Elevated Ca^{2+} leads to ezrin release

(c) Estimated Ca^{2+} concentration at the cell edge (orange), and in the cytosol (blue). The point of ezrin release is suggested at 2 mins 18 s (dashed line), when Ca^{2+} concentration at the cell edge is estimated to be 23 µM.

containing the transfected RAW 264.7 cells. Phagocytosis events were captured on the Leica SP5, at 63x magnification.

As before, cells were initially assessed for their phagocytic activity when expressing EPIC3 alone. Transfection with the EPIC3 probe did not inhibit phagocytosis, and areas of high EPIC3 intensity were identified at the forming phagocytic cup (fig. 5.3.3i). The Ca^{2+} concentration in these regions near the site of active phagocytosis, were estimated to reach between 29.3 ±16.9 μM – capable of activating μ-calpain to cleave ezrin, and so facilitate localised expansions of the plasma membrane (fig. 5.3.3i and ii).

RAW 264.7 cells co-expressing both EPIC3 and ezrin-mCherry were then assessed. A ratio of the two signals was taken and a dynamic mask based on the ezrin-mCherry signal was applied, as previously described. Similarly to the co-transfected cells which were artificially stimulated to elevate cytosolic Ca^{2+} levels, a non-typical morphological behaviour was again observed. Of the 106 cells co-expressing EPIC3 and ezrin-mCherry, which were considered capable of performing phagocytosis (i.e. touching or <2 μm away from a zymosan particle), only 22% of cells successfully completed phagocytosis (fig. 5.3.3iii). In addition, a further 29% of the cells 'attempted' phagocytosis, by the extension of pseudopodia towards, and/or encircling of proximal zymosan, and the formation but then retraction of phagocytic cups. It is likely that similarly to disrupting whole cell spreading, the transfection with multiple ezrin constructs interfered with typical morphological outcomes.

Out of the 23 cells which had internalised zymosan within their cytosols, occasions of only 6 dynamic phagocytosis events were captured in motion. The 'ratio + mask' technique was applied to Avi. files, and Ca^{2+} concentration was estimated to reach up to 55 μM in distinct regions of peripheral cytosol, at sites of phagocytic cup formation (fig. 5.3.3iv). This is in keeping with the hypothesis that Ca^{2+} is locally elevated to activate μ-calpain and release the ezrin bridges at

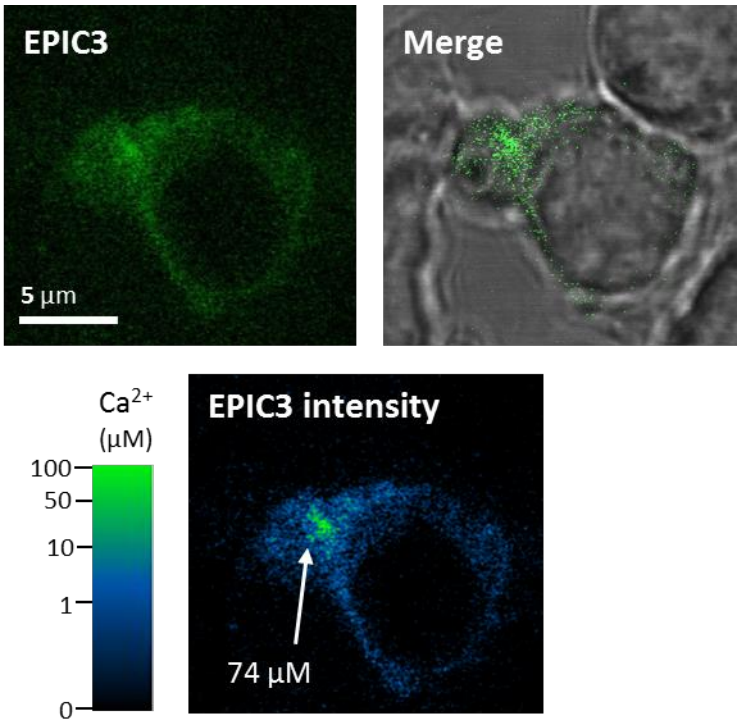

Figure 5.3.3i: Ca^{2+} hotspots at phagocytic cup
RAW 264.7, cell expressing EPIC3, performing phagocytosis of an opsonised zymosan particle. Areas of high Ca^{2+} estimated to reach up to 74 µM at the phagocytic cup. Scale bar 5 µm.

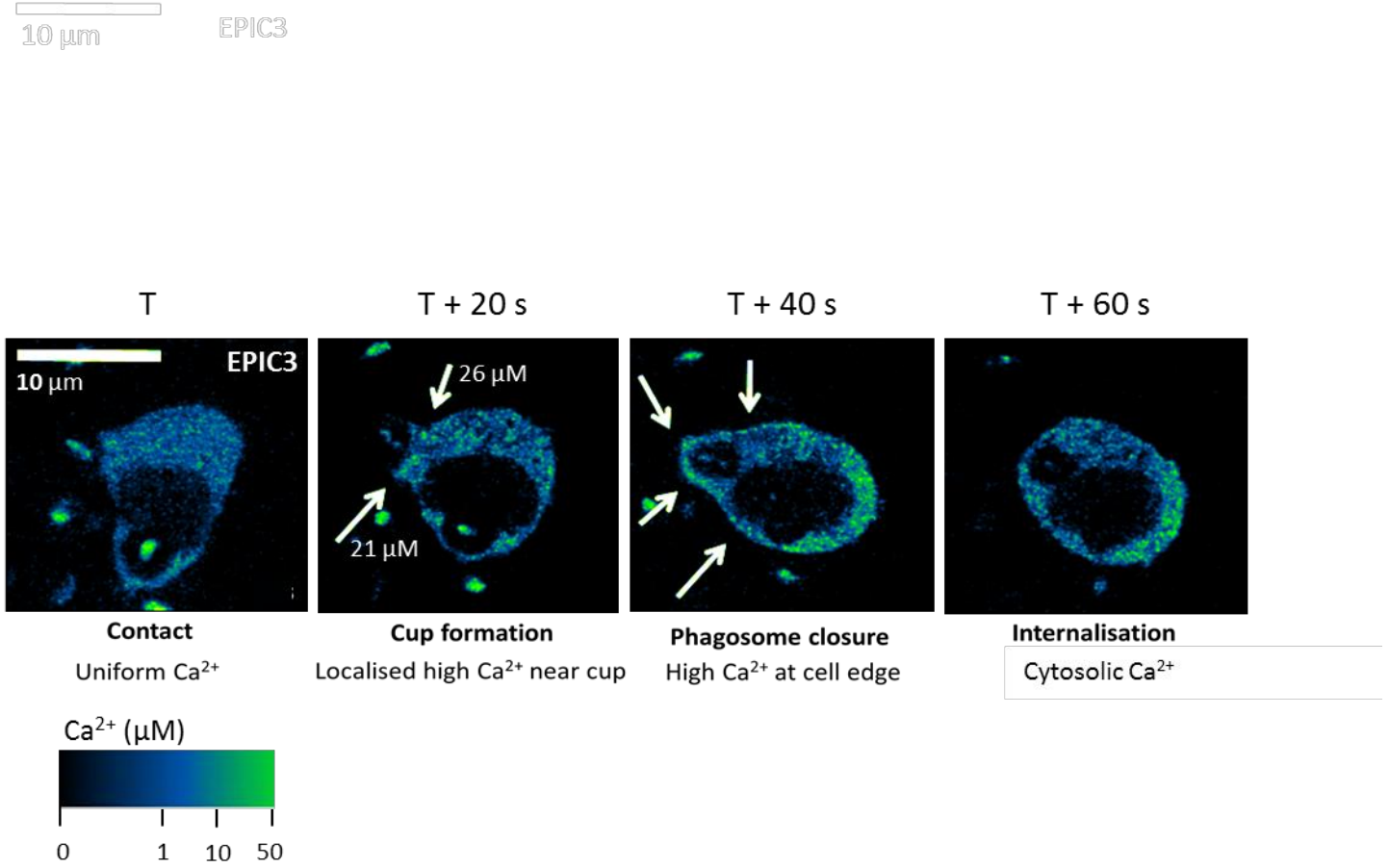

Figure 5.3.3ii: EPIC3 reports Ca^{2+} hotspots at phagocytic cup
RAW 264.7, cell expressing EPIC3, performing phagocytosis of an opsonised zymosan particle. Green Fire Blue LUT applied. Areas of high Ca^{2+} estimated to reach up to 26 µM at the phagocytic cup. Scale bar 10 µm.

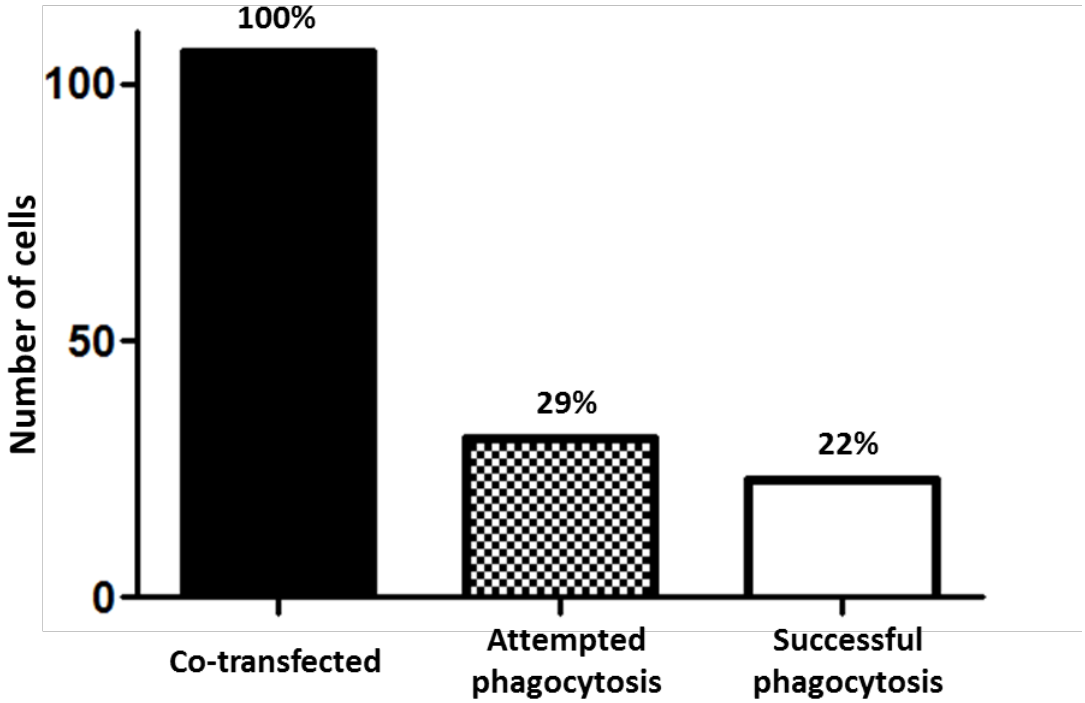

Figure 5.3.3iii: Phagocytosis by co-transfected RAW 264.7 cells
Of the cells co-expressing EPIC3 and ezrin-mCherry, 106 were considered capable of performing phagocytosis i.e. touching or in close proximity (<2 µm from an opsonised zymosan). Of these 31 cells attempted phagocytosis, but were unsuccessful. Only 23 cells had evidence of zymosan in the cytosol.

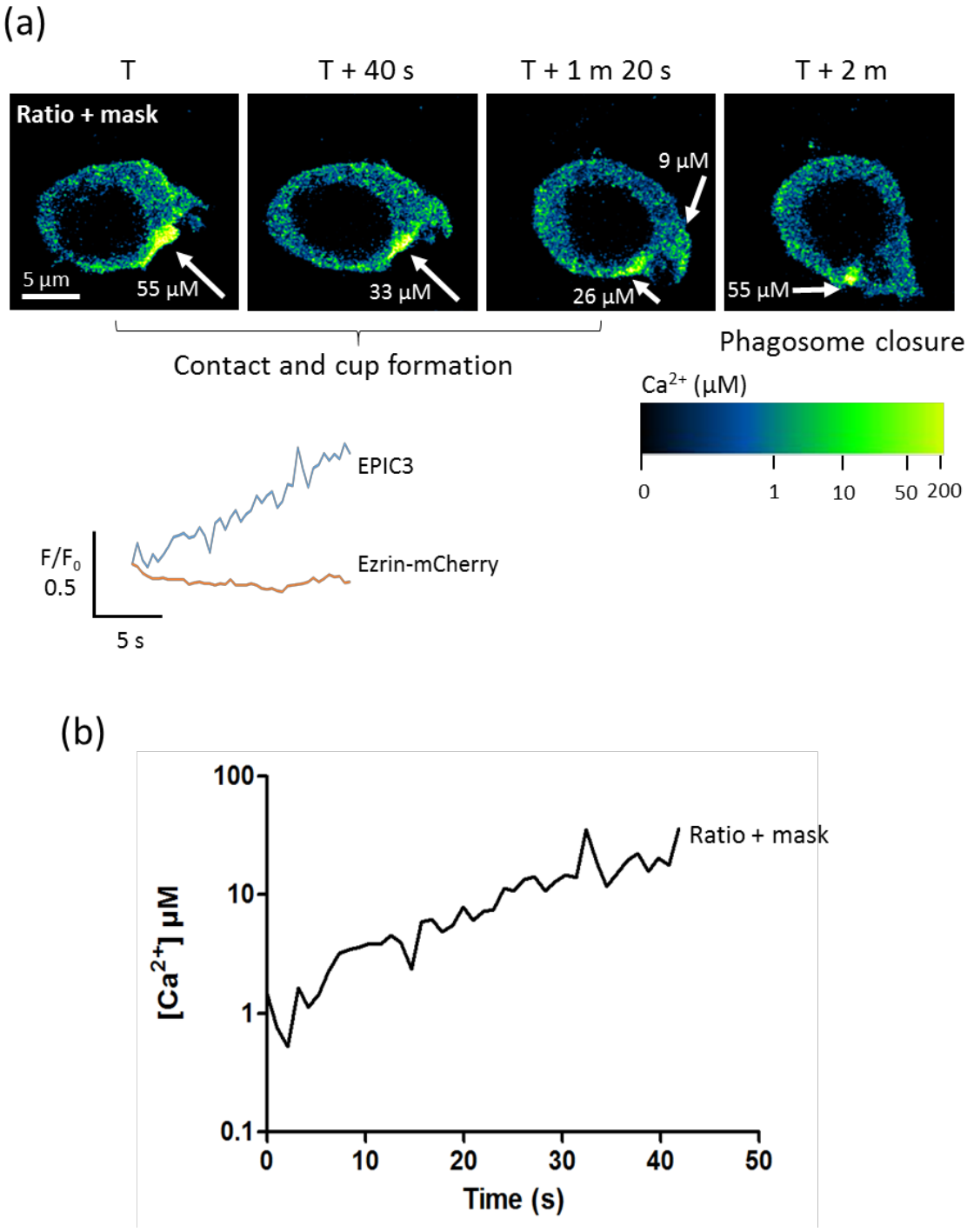

Figure 5.3.3iv: Ca^{2+} hotspots at phagocytic cup
RAW 264.7, cell co-expressing EPIC3 and ezrin-mCherry, performing phagocytosis of an opsonised zymosan particle. **(a)** Image processed (EPIC3/ezrin-mCherry ratio, with applied dynamic mask) and Green Fire Blue LUT applied. High Ca^{2+} hotspots at the phagocytic cup estimated to reach up to 55 µM. Scale bar 5 µm. Insert: EPIC3 signal increase at the phagocytic cup. Ezrin-mCherry remains constant. **(b)** Estimated Ca^{2+} concentration at the phagocytic cup rises to 36 µM.

the phagocytic cup, to enable localised membrane expansion and facilitate phagocytosis.

RAW 264.7 cells co-expressing EPIC3 and ezrin-mCherry were also assessed for other localised shape change events, such as the extension of pseudopodia and local membrane expansion at the leading edge of moving cells (fig. 5.3.3v). Cells attempting to perform phagocytosis of proximal zymosan particles produced pseudopodia extensions, and often had a defined leading edge. In these regions of active morphology change, the Ca^{2+} concentration in ezrin-rich domains (i.e. in plasma membrane microridges) was estimated to reach 94 ±54.3 μM, in the range sufficient to fully activate μ-calpain.

5.4 Discussion

The work in this chapter represents the first ever measurements of sub-membranous cytosolic Ca^{2+} concentrations, within microridge structures at the plasma membrane of live myeloid cells. These estimations were achieved by transfecting RAW 264.7 cells with the novel probe EPIC3, with a Ca^{2+} binding K_d of 11 μM. RAW 264.7 cells were used to model the effect of elevating cytosolic Ca^{2+} in myeloid cells on the subsequent morphological changes, akin to those experienced by neutrophils during cell spreading and extravasation.

In RAW 264.7 cells both artificially stimulated to produce a Ca^{2+} influx, and those performing phagocytosis of C3bi-opsonised zymosan, EPIC3 reported elevated Ca^{2+} concentrations at the cell edge in the mid-decade micromolar range, capable of activating μ-calpain (K_d 20-60 μM). However, whilst the ezrin-like properties of EPIC3 make it a useful and suitable tool to measure the Ca^{2+} concentrations achieved in ezrin-rich areas of sub-membranous cytosol, they also make it vulnerable to other properties of ezrin; namely cleavage by μ-calapin, and re-distribution in the cytosol. Therefore, using EPIC3 alone typically reported lower estimates of Ca^{2+} at the cell edge, where the reduced signal was probably a result of ezrin re-distribution, rather than falling Ca^{2+} concentration.

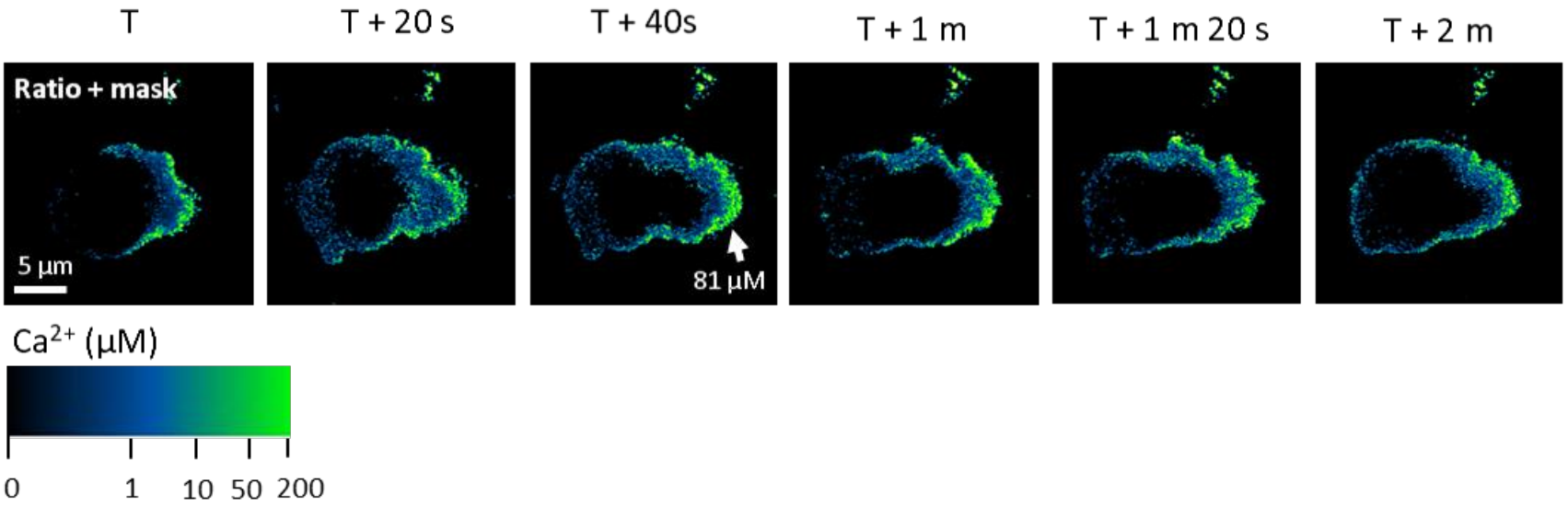

Figure 5.3.3v: High Ca^{2+} at the leading edge
RAW 264.7 cell co-expressing EPIC3 and ezrin-mCherry. After taking a ratio of the two probes and applying the dynamic mask, regions of high Ca^{2+} concentration, estimated to reach up to 81 µM, can be seen at the leading edge. Scale bar 5 µm.

To overcome this problem, the ezrin-mCherry probe was introduced into cells at the same time as the EPIC3 probe. This provided a non Ca^{2+}-sensing control, to account for cellular re-distribution of ezrin during the Ca^{2+} signal – an expected and physiological response. Taking a ratio of these two probes revealed that elevation of Ca^{2+} concentration was sustained at the cell edge during stimulated Ca^{2+} influx, and was estimated to reach the mid-decade micromolar range, capable of activating μ-calpain.

Since the nature of the Ca^{2+} influx in myeloid cells is to evoke a change in cell morphology, measuring distinct regions of interest in moving cells was a problem. This was overcome by employing advanced imaging techniques, and generating bespoke dynamic masks (in ImageJ) for individual cells. In this way, the EPIC3 response to Ca^{2+} was only reported in ezrin-rich areas, at the cell edge. This technique also corrected for the artefact produced by taking a ratio of the whole cell, which included the pool of dormant cytosolic ezrin. By recording only the ratio of EPIC3/ezrin-mCherry, through the ezrin-mCherry rich defined dynamic mask (referred to as the 'ratio + mask' method), the Ca^{2+} concentration at the cell edge was found to readily exceed that of the global cytosol, and reach upwards of 50 μM.

It is worth noting that some cells expressing EPIC3 (13/15) some cells expressing both EPIC3 and ezrin-mCherry (5/7) had reduced ability to perform morphological rearrangements. This may be because the introduction of additional ezrin into the cell also strengthened the ezrin cross-linking activity. This meant that the morphological changes such as cell bloating, spreading and phagocytosis, were not always evident, even when cytosolic Ca^{2+} concentrations at the cell edge were estimated to be capable of activating μ-calpain. Another limitation in these experiments, was the relative transfection efficiency of both EPIC3 and ezrin-mCherry (fig. 5.4). The percentage of co-transfected cells among the populations was typically around 10-20 %, often favouring ezrin-mCherry expression over EPIC3.

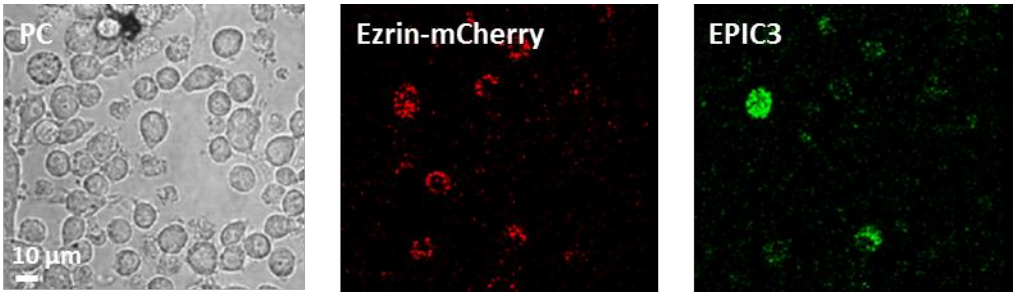

Figure 5.4: Co-transfection efficiency
The percentage of co-transfected cells among the populations was typically around 10%. Scale bar 10 µm.

The Ca^{2+} concentrations reported here are estimations, based on the Ca^{2+} binding affinity of EPIC3, and the ratio of two fluorescently-tagged ezrin probes, to account for ezrin redistribution. However, the findings are in line with previous estimations by Brasen and colleagues, based on computer models of cells with defined microridge structures (Brasen et al., 2010). Since ezrin is an important cross-linking protein, and important in the architecture and regulation of plasma membrane microridge structures, measuring the Ca^{2+} concentration in ezrin-rich regions of the cell gives important insight into the mechanism of membrane expansion and the μ-calpain-ezrin axis.

Chapter 6:

Molecular and cellular effects of ezrin phosphorylation inhibition

6.1 Introduction

In neutrophils and other myeloid cells, ezrin forms crucial cross-links between the plasma membrane and cortical F-actin (Algrain et al., 1993; Bretscher, 1983; Gould et al., 1989). It is thought to play an important role in maintaining the structure of cell surface microridges, which act as a reservoir of stored plasma membrane for release upon cell spreading. A key step in regulating its activity is the phosphorylation of ezrin at Thr567 (Gautreau et al., 2000). Recently, a small molecule inhibitor of ezrin phosphorylation, NSC668394 (10 µM), has been shown to inhibit this step (Bulut et al., 2012; Prentice-Mott et al., 2016). As explored in previous chapters, there is also evidence that another key regulatory step in breaking the ezrin cross-link in neutrophils, is its cleavage by the neutral Ca^{2+}-activated cysteine-protease, µ-calpain. Since ezrin is a known substrate of Ca^{2+}-activated µ-calpain (Shcherbina et al., 1999), it is suggested that µ-calpain activation upon Ca^{2+} influx, as a consequence of cell stimulation, severs the ezrin tether between the actin cytoskeleton and the plasma membrane; releasing the stored membrane and enabling cell spreading (Dewitt et al., 2013).

In epithelial cells, NSC668394 has recently been shown to reduce membrane tension (Bruckner et al., 2015), maintained by the ezrin-regulated strength of cell surface wrinkles (Bruckner et al., 2015). These two factors offer the possibility that NSC668394 may interfere with morphological changes in neutrophils, and this activity may be beneficial in an anti-inflammatory agent. Furthermore, using NSC668394 to manipulate the phosphorylation status of ezrin in neutrophils and myeloid cells enables experimental investigations of the interplay between the Ca^{2+}-mediated regulation of ezrin cleavage and ezrin phosphorylation.

In many cell types, ezrin exists as a pool of dormant protein in the cytosol, but as active protein where it functions at the cell cortex. It was hypothesised that preventing ezrin activation, and therefore inhibiting its function as a cross-link at

the cell cortex, may have a consequential effect on the ability of the cell to maintain, or indeed change, its morphology. To test this hypothesis, the inhibitor of ezrin phosphorylation NSC668394 was used in neutrophils for the first time, as an experimental tool to probe the μ-calpain-ezrin axis, and investigate the interplay between these two steps in regulating neutrophil shape change.

6.1.1 Conformational states of ezrin

Ezrin exists in two conformational states (Bretscher et al., 1997); an un-phosphorylated closed, inactive conformation where the N-terminal ERM domain self-associates with the C-terminal actin binding domain (ABD), and an open, active conformation where phosphorylation at Thr567 facilitates ezrin self-dissociation and enables F-actin binding (Viswanatha et al., 2013).

Ezrin cross-linking of the cortical actin network to the plasma membrane is achieved through binding of the N terminal FERM domain (N-ERMAD) to the plasma membrane, and the C-terminal (C-ERMAD) binding to polymerized actin at the cell cortex (Gould et al. 1989; Shuster and Herman, 1995). The two domains are connected by a μ-calpain sensitive linker region. This cross-linking ability is thus lost by Ca^{2+}-activation of μ-calpain and cleavage of ezrin at the cell periphery (Shuster and Herman, 1995; Yao et al., 1993). Ezrin, but not the structurally similar ERM family protein moesin, is susceptible to cleavage by μ-calpain (Shcherbina et al., 1999), and as such ezrin is implicated as a key protein in the reorganisation of the neutrophil cell membrane.

Phosphorylation of ezrin at Thr567 disrupts the self-association of the N-ERMAD and C-ERMAD ends of the inert molecule to allow it to participate in cortical binding (Bretscher et al. 1997; Shuster and Herman, 1995). This latter event can be disrupted by the inhibition of ezrin phosphorylation at Thr567.

6.1.2 The ezrin inhibitor NSC668394

NSC668394 is a reversible inhibitor of PKC_I-mediated phosphorylation of Thr567 on ezrin, inhibiting ezrin-F-actin binding. It is a cell permeable quinoline derivative, with a K_d of 12.6 μM. The compound has a red-orange colour in DMSO, and when prepared in this way is capable of freely diffusing across the phospholipid bilayer of cell membranes. Bulut and colleagues have shown that NSC668394 reduces motility and metastasis in osteosarcoma cells with high ezrin expression (Bulut et al., 2012). NSC668394 activity prevents endogenous ezrin binding to actin without altering cellular levels of actin (Bulut et al., 2012).

6.1.3 Aims of this chapter

1. To use molecular biology techniques to analyse the subcellular localisation of ezrin in neutrophils and RAW 264.7 cells that have been incubated with the ezrin inhibitor of phosphorylation, NSC668394.
2. To investigate the effect of the ezrin inhibitor NSC668394 on the behaviour of live neutrophils, when stimulated to undergo phagocytosis and chemotaxis.

6.2 Specific Materials and Methods

6.2.1 Immunocytochemistry

Human neutrophils were isolated from healthy donor blood, as previously described in Chapter 2. Fixed and permeabilised neutrophils were stained with mouse anti-ezrin primary antibody (Santa Cruz (3C12)) and goat anti-mouse FITC conjugated secondary antibody (Santa Cruz IgG1-FITC). Cell staining was analysed using the Leica SP5 confocal microscope with 488 nm argon laser.

6.2.2 Plasmid amplification

The ezrin-mEmerald (mEmerald-Ezrin-N-14, #54090) high copy number plasmid was a gift from Michael Davidson (Addgene). Plasmid DNA was amplified as described in Chapter 2. Kanamycin was added to both the agar plates and the LB culture medium to select for transformed E. coli, because the vector backbone of ezrin-mEmerald contains the gene for selective Kanamycin resistance. 1 L of LB culture was inoculated as a compromise between the high copy number of the plasmids and the volume of culture which could be suitably processed by maxi prep. The plasmids were purified by maxi prep, as described in Chapter 2.

6.2.3 RAW 264.7 cell transfection

RAW 264.7 cells ($2x10^6$), were harvested by scraping and were then electroporated to introduce ezrin-mEmerald plasmid DNA (2-4 µg/100 µL) using the Cell Line Nucleofector™ Device (Lonza) as previously described (Chapter 2). Cells were incubated at 37°C in 5% CO_2 for 3-4 hours before imaging on the Leica SP5 confocal microscope.

6.2.4 Pre-treatment with NSC6683934 inhibitor of ezrin phosphorylation

A 10 mM stock of NSC668394 was made by dissolving in DMSO. Neutrophils and RAW 264.7 cells were pre-treated with 10 µM NSC668394 (1 µL in 1 mL cell suspension), or an equal volume of DMSO (i.e. 1 µL), for 10 mins at 37°.

6.2.5 Confocal microscopy

Transfected RAW 264.7 cells were imaged on the Leica SP5 confocal inverted microscope (Leica Microsystems, Heidelberg) with resonance scanner and perfusion chamber at 37°C. The 488 nm argon laser was used.

6.2.6 Protein extraction and preparation of cell lysates and Western blotting

Isolated human neutrophils (Chapter 2) were spun down and re-suspended in neutrophil lysis buffer (50 mM HEPES, 150 mM NaCl, 10% Glycerol, 1% Triton X100, 5 mM EDTA, 5 mM EGTA, 1 mM Na_3VO_4, 1.5 mM NaF, 0.1% SDS, 1.5 mM $MgCl_2$) and PIC was added at 1:1000. Samples were incubated on ice for 1 hour and vortexed every 15 minutes to increase the efficacy of cell lysis, before being boiled for 10 minutes and then centrifuged for 5 minutes at 14,000 rpm. Band densitometry analysis was performed using ImageJ (Analyse>Gels), migration distances were calculated using ImageJ and the molecular weights were calculated using the formulas:

$$Rf = distance\ migrated\ (pixels)/gel\ length\ (pixels)$$

$$MW = e^{(gradient\ of\ line\ x\ Rf)\ +\ y\ intercept}$$

6.2.7 Neutrophil Phagocytosis

Isolated human neutrophils (Chapter 2) were loaded with Fluo4 (1µM in $1x10^6$ cells/mL) for 30 mins at room temperature. 100 µL of isolated neutrophils, in Krebs-BSA, were pipetted onto glass slides and placed on the Leica SP5 confocal stage in a perfusion chamber at 37°C. The cells were left to adhere for 2 mins, then the medium was aspirated and replaced with fresh Krebs-BSA, to leave only adherent neutrophils.

Zymosan were opsonised by incubation with excess NHS (prepared as described in Chapter 2), at 37°C for 30 mins. The zymosan were then spun down and re-suspended in 1 mL Krebs-BSA. 100 µL zymosan suspension was added to the neutrophils on the cover slide and allowed to 'rain down' onto the cells. Cells within proximity of the opsonised zymosan (i.e. <5 µm) were imaged on the Leica SP5 confocal inverted microscope, using the 488 nm laser to record changes in Ca^{2+} concentration.

6.2.8 Preparation of zymosan filled collagen beads

Glass micropipettes were pulled from 10 cm borosilicate glass capillaries, with an outer diameter of 1 mm and an inner lumen diameter of 0.5 mm, using the P-2000 laser micropipette puller, pre-set programme 11 (Sutter Instrument, California, US) and loaded with 15 µL of zymosan in BSS (1: 10 dilution). The micropipettes were manoeuvred using the InjectMan (Eppendorf, Hamburg, Germany) and suitable collagen beads (2BScientific) were injected using the Eppendorf® InjectMan®, with a counter pressure of >120ppi.

6.2.9 Neutrophil chemotaxis experiments

100 µL isolated neutrophils (Chapter 2) at $3x10^6$ cell/mL in Krebs-BSA were loaded with CellTrace™ Calcein Green, AM (Life Technologies) and 10 µM ezrin inhibitor NSC668394, or equal volume of a DMSO control, and pipetted onto glass slides with 8 µL of NHS (diluted 1:20 in BSS) and 60 µL of pre-prepared zymosan injected collagen beads. A cover slip was applied with some pressure, to immobilise the collagen beads on the slide, and maintain a fixed point of C5a stimulus. The 'chamber' was sealed by applying grease around the seal between the cover slip and the glass slide, to hold the cover slip in place and prevent evaporation during the experiment. Chemotaxis was monitored using the Leica SP5 confocal inverted microscope (Leica Microsystems, Heidelberg) with resonance scanner, laser scanning [10x objective; 488 nm argon laser; 64 frame average; 1 frame/4 seconds; 90 mins] in a perfusion chamber at 37°C.

6.2.10 Imagestream

Human neutrophils from healthy donors were isolated from whole blood (Chapter 2), and immunocytochemistry was performed as previously described (Chapter 2) using the anti-ezrin Cy5-conjugated antibody (1:100) (Bioss Antibodies) and the anti-CD18 FITC-conjugated antibody (1:100) (BD Biosciences Pharmingen). Cells were loaded onto the AMNIS® ImageStream®X Mark II Imaging Flow Cytometer (Merck), at approximately $5x10^6$ cells/mL. Cells were

imaged using Channels 1, 2, 6 and 11 (bright field, 480-560 nm, 745-800 nm (side scatter) and 642-745 nm wavelengths respectively). Data were acquired at 60x magnification, and laser intensities were adjusted relative to individually stained controls for compensation. The data were analysed using the IDEAS® software.

6.3 Results

6.3.1 Effect of NSC668394 on ezrin distribution at the plasma membrane in neutrophils

As previously discussed in Chapter 3, fluorescent ezrin constructs have been expressed in the model myeloid cell line (RAW 264.7) in order to visualise the subcellular location of ezrin. Cells were transfected by nucleofection with the Cell Line Nucleofector™ Device (Lonza), as before, and imaged on the Leica SP5 confocal microscope. From the results in Chapter 3, we know that C-terminally-tagged fluorescent ezrin displays typical ezrin localising properties. To see if the ezrin inhibitor of phosphorylation, NSC668394, has any effect on ezrin distribution in the cell, RAW264.7 cells were incubated with the inhibitor (10 µM) before being transfected with ezrin-mEmerald. This meant that all ezrin-mEmerald was expressed under the influence of the phosphorylation inhibitor.

There was no effect of NSC668394 on the peripheral location of expressed ezrin-mEmerald either after expression, or in RAW 267.4 cells pre-treated with NSC668394 before transfection and maintained during the subsequent 3 hours (fig. 6.3.1i). As under these latter conditions, phosphorylation of newly synthesised ezrin-mEmerald would be suppressed, it was concluded that constructs with the fluorophore at the actin-binding C-terminus did not require phosphorylation to activate them for peripheral binding. Thus, ezrin constructs would not be useful models in which to test the effects of NSC668394.

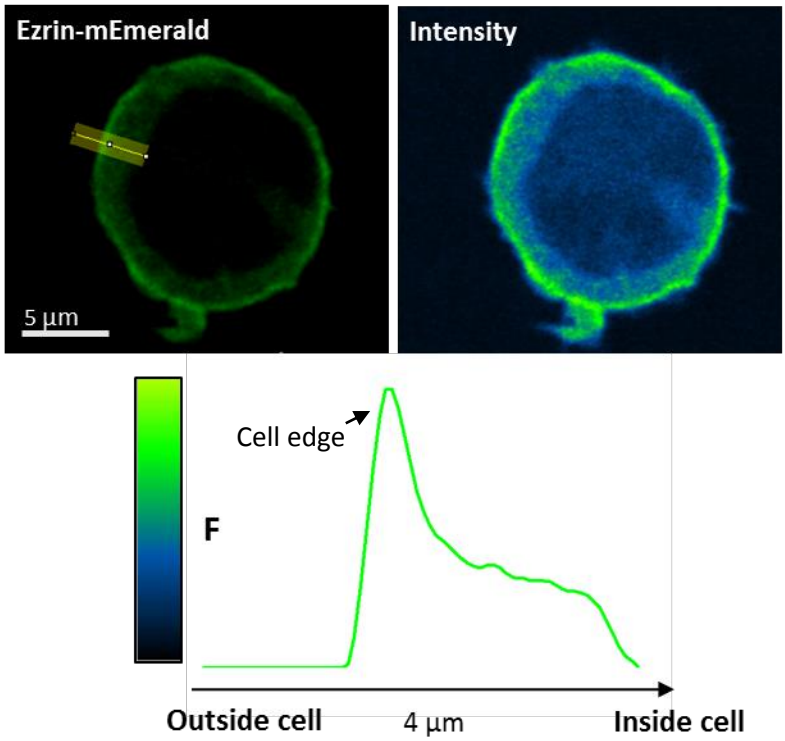

Figure 6.3.1i: Ezrin-mEmerald expression in RAW 264.7 cell treated with NSC668394 before transfection
First panel: A single RAW 264.7 cell expressing ezrin-mEmerald (green) at the cell edge, pre-treated with NSC668394 (10 µM). The relative fluorescence trace of ezrin-mEmerald distribution within a defined ROI (yellow shaded box; 4 µm) at the cell edge is shown. Fluorescence intensity remains highest at the cell edge, decreasing towards the cytosol. Second panel: Pseudo-coloured look-up table (LUT) applied to the same cell. Ezrin is primarily located at the cell edge. Scale bar 5 µm. Representative of at least 10 cells.

The subcellular location of ezrin was therefore established in human neutrophils by immunocytochemistry. Ideally, the distribution of ezrin in large populations of neutrophils would be quantified using Imagestream technology. This is a relatively new technology, and was used in this project as a means of generating larger data sets about ezrin distribution in neutrophils. This entailed fixing and staining neutrophils in suspension for quantitation by Imagestream. A Cy5-conjugated anti-ezrin antibody was used in conjugation with an anti-CD18 FITC-conjugated antibody as a marker for the cell edge. Analysis of the data from 20,000 cells in the IDEAS software suite did not indicate a marked loss of peripheral ezrin, post incubation with the inhibitor of ezrin phosphorylation, NSC668394 (fig. 6.3.1ii). However, inspection of the cells by confocal microscopy revealed that ezrin staining with the Cy5 conjugated antibody did not report strong peripheral staining (fig. 6.3.1iii). This prevented accurate quantitation of peripheral ezrin in the cells. It was concluded that the immunocytochemistry protocol for staining ezrin in neutrophils in suspension should be further optimised before useful data sets could be generated using this technique. Therefore, although the technology offers enormous potential for experimental upscaling and high-throughput data acquisition, it was concluded that the further optimisation necessary was not suitable for this work.

However, using the immunocytochemistry on loosely adherent cells, the peripheral location of ezrin was easily observed (fig. 6.3.1iv). Ezrin was located at the cell periphery of 65.7 % ± 8.8 % (SEM) cells (n=41). After neutrophils were pre-treated with NSC668394 this was reduced to only 11.7 % ± 5.7 % (n=39) and was significantly different from untreated cells ($P<0.001$) (fig. 6.3.1v).

Using a blind scoring system for peripheral ezrin (0=no peripheral ezrin; 1=peripheral ezrin at less than 75% of cortex; 2=peripheral ezrin at more than 75% of cortex), 16.1 ± 4.9 % of the control population scored 0, compared to 70.3 ± 10.5 % of the NSC668394 pre-treated population ($P<0.001$). Within the control population, significantly more neutrophils ranked the highest score 2,

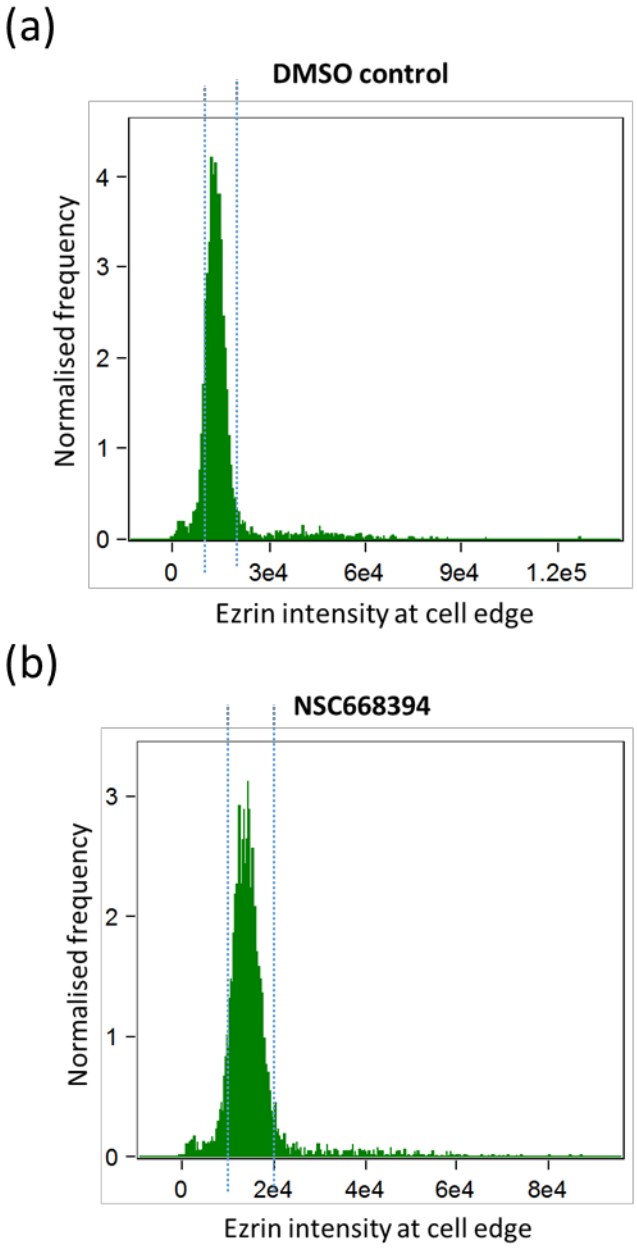

Figure 6.3.1ii: Imagestream analysis of ezrin distribution in neutrophils
There was no significant difference in the ezrin distribution between **(a)** DMSO control cells and **(b)** NSC668394 pre-treated cells (10 µM, 10 mins, 37°C).

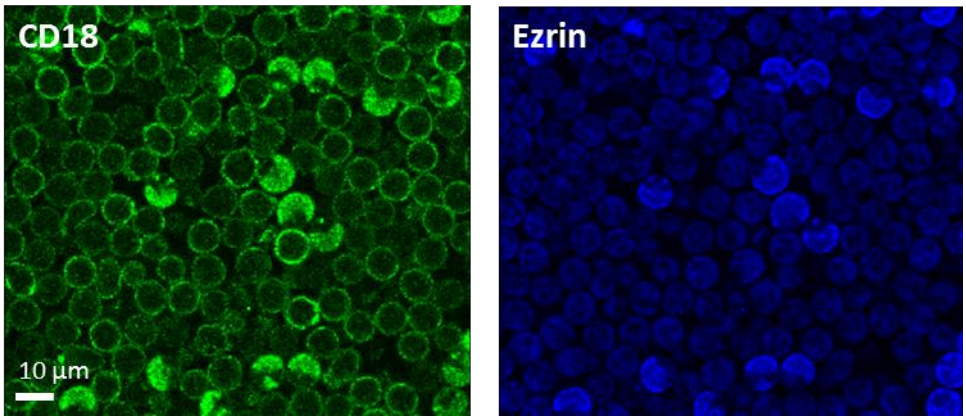

Figure 6.3.1iii: Confocal microscopy inspection of ezrin distribution in neutrophils
Confocal images of neutrophil populations that were run on the Imagestream. CD18 staining marks the cell edge. Ezrin staining with the Cy5-conjugated anti-ezrin antibody is largely cytosolic and shows less peripheral staining of ezrin in the control sample.

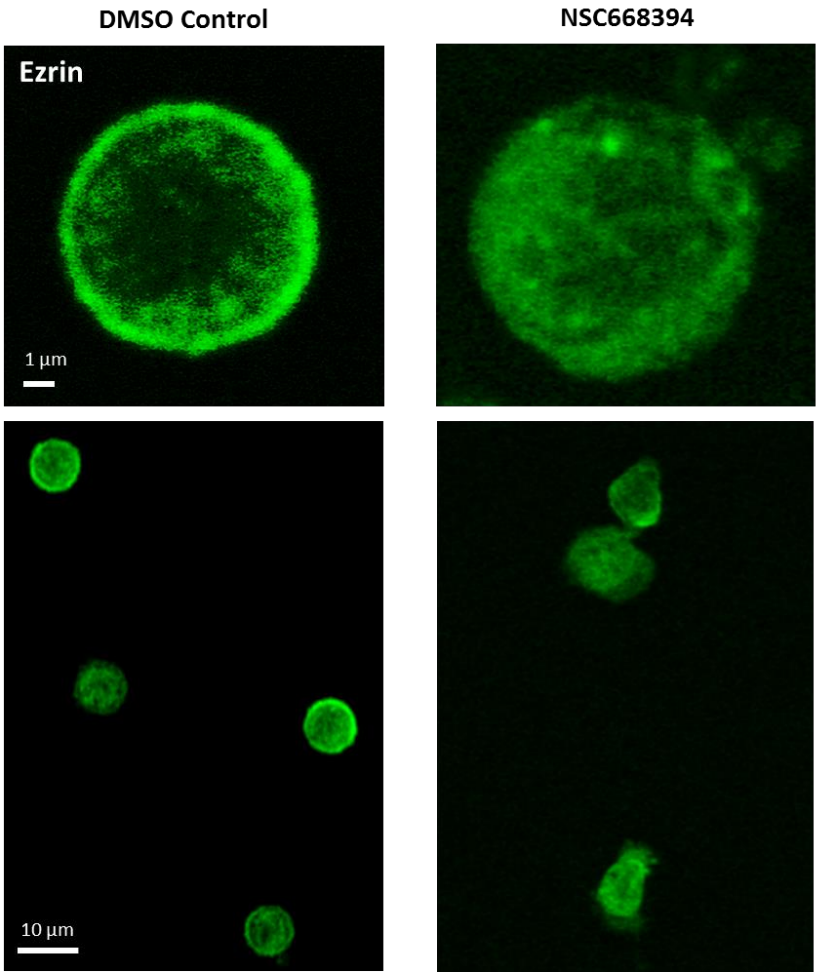

Figure 6.3.1iv: Ezrin subcellular location in myeloid cells
Immunocytochemistry of unstimulated neutrophils pre-treated with (left) DMSO control); (right) NSC668394 (10 µM). Scale bar top panels: 1 µm, lower panels: 10 µm.

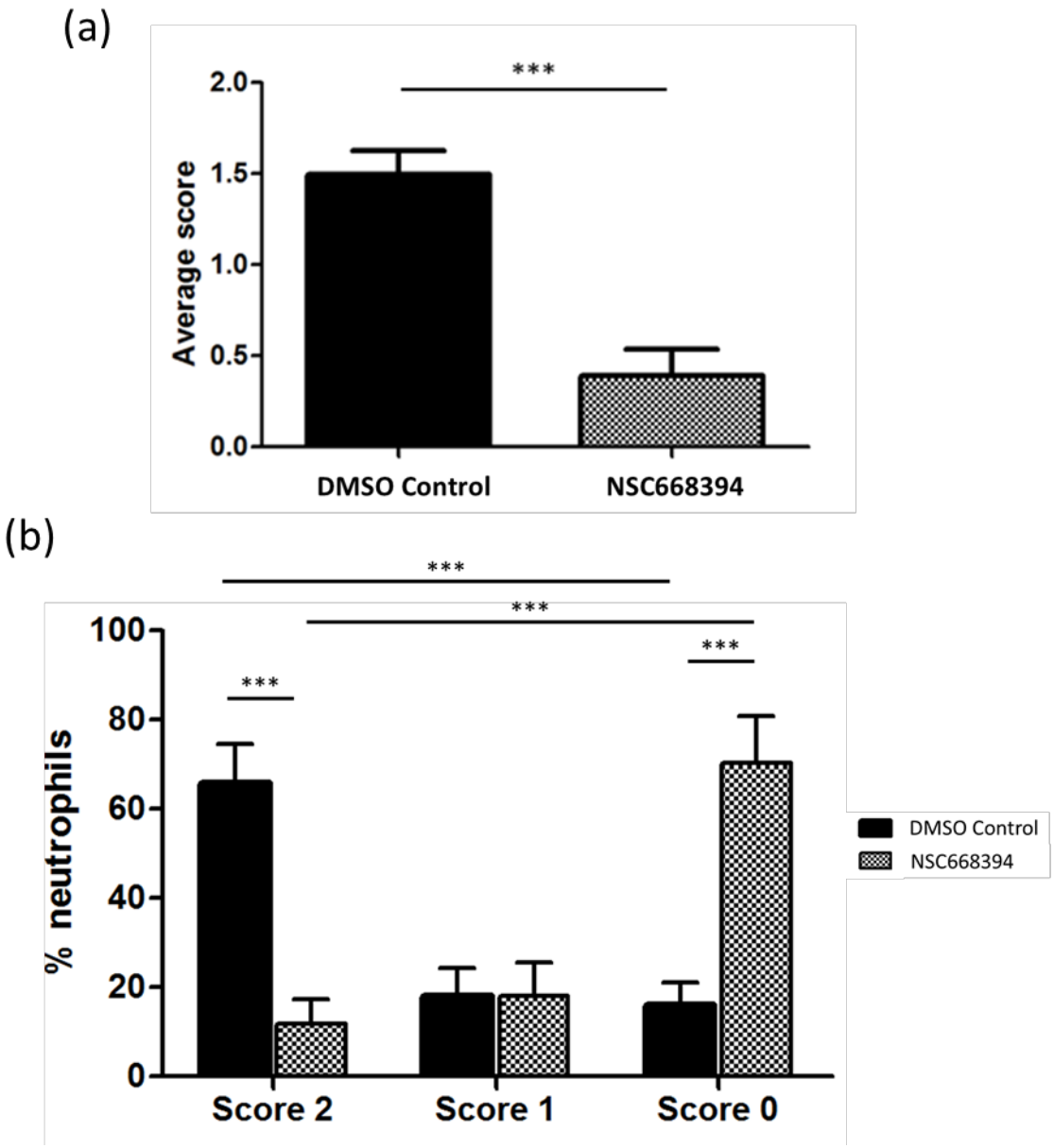

Figure 6.3.1v: Ezrin subcellular location in myeloid cells
(a) Mean scores of peripheral ezrin (from lowest score 0, to highest score 2) in neutrophils pre-treated with DMSO control, and NSC668394 (10 µM) (n=41 and n=39 respectively). *** = P<0.0001 (Two-tailed unpaired t-test). **(b)** Percentage of neutrophils in either DMSO control or NSC668394 (10 µM) pre-treated populations ranked with scores 0, 1 or 2. *** = P<0.0001 (Two-way ANOVA with Bonferroni post-test).

than the lowest score 0 ($P<0.001$). In the NSC668394 treated population significantly more neutrophils ranked the lowest score 0, than highest score 2 ($P<0.001$). The control cells had a mean score of 1.5 ± 0.13 whereas NSC66394 pre-treated neutrophils had a mean score of only 0.4 ± 0.14, which was significantly different ($P<0.0001$). Inadvertent activation of some neutrophils in the untreated population may account for cells which had no peripheral ezrin, as neutrophils lacking cytochemically detectable peripheral ezrin often had larger diameters (fig. 6.3.1iv). Thus, these cells may represent a subpopulation of activated and spreading cells. However, the effect of NSC668394 in further reducing the percentage of neutrophils with peripheral ezrin suggested that in human neutrophils, phosphorylation of ezrin was responsible for maintaining its location at the cell periphery.

6.3.2 Effect of NSC668394 on ezrin cleavage

Having shown that, in neutrophils, an NSC668394-sensitive step was important for locating ezrin at the cell periphery, the molecular consequences on ezrin in NSC668394 pre-treated neutrophils were investigated.

It was not possible to directly monitor ezrin phosphorylation at Thr567 because antibodies specific for this site also detected the identical site around Thr558 of moesin, a related and more abundant protein in neutrophils. Instead, ezrin was detected with a monoclonal antibody for amino acid residues 362-585 of human ezrin (abcam [3C12] ab4069). In human neutrophils, full length ezrin runs at a molecular size close to the predicted amino acid weight (72 KDa). This is different from in other cell types, where ezrin was called p81 because it runs near to 81kDa (fig. 6.3.2i). In these experiments in neutrophils, Ca^{2+}-activated μ-calpain cleavage generated detectable ezrin fragments of approx 55-62 KDa (fig6.3.2ii). This suggests that in other cell lines there is significant post-translation modification which is absent in neutrophils. It is unclear whether this difference explains the reliance on phosphorylation for activation or effectivenes of the ezrin inhibitor.

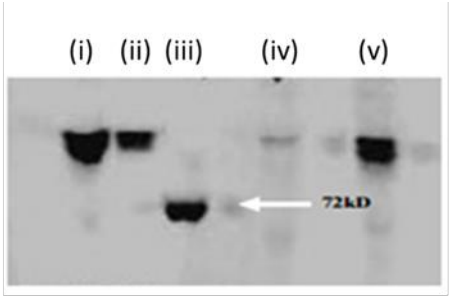

(i) HL60 cells
(ii) RAW 264.7 cells
(iii) **Human neutrophils**
(iv) PZHPV7 cells
(v) 3T3 cells

Figure 6.3.2i: Molecular weights of ezrin
Various cell types have been found to have different molecular weight ezrin. Human neutrophils showed the lowest molecular weight ezrin, at 72 kDa. (Roberts et al., 2017 – unpublished data).

(a)

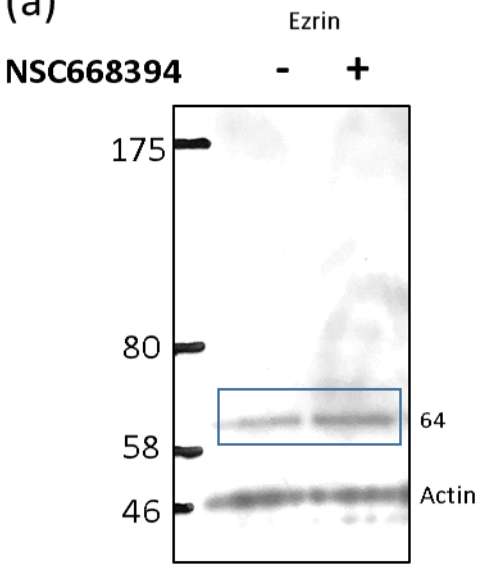

(b)

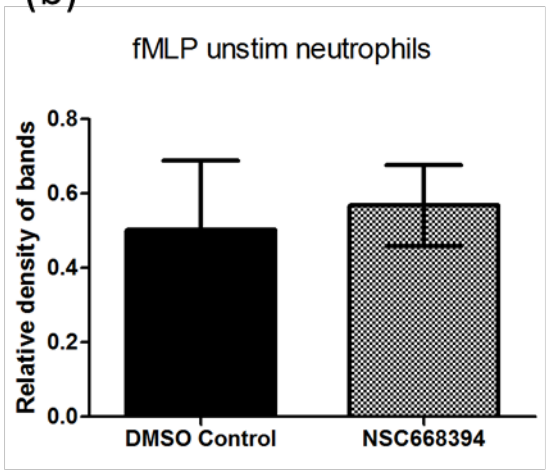

(c)

MW	$Log_{10}MW$	Distance (pixels)	Rf value
175	2.243038	0	0
80	1.90309	160	0.557491
58	1.763428	242	0.843206
46	1.662758	287	1

$$Rf = \frac{distance\ migrated\ (pixels)}{gel\ length\ (pixels)}$$

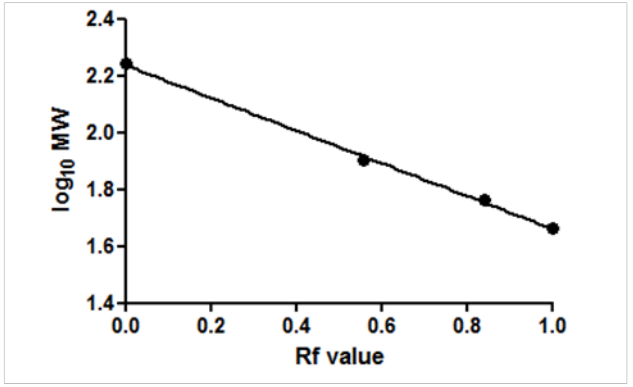

$$MW = e^{(gradient\ of\ line \times Rf) + y\ intercept}$$

Distance (pixels)	Rf value	MW
216	0.752613	63.86272
217	0.756098	63.56878378
275	0.958188	48.6454037

Figure 6.3.2ii: Immunodetection of ezrin and ezrin fragments in un-stimulated neutrophils

(a) Western blot of human neutrophil extracts without (-) or with (+) pre-treatment with NSC668394 (10 µM). **(b)** Densitometry analysis of western blots, with SEM. Data from 3 independent experiments. **(c)** The MW were identified by calculating the line of regression.

Unstimulated neutrophils treated with NSC668394 showed no significant increase in detectable ezrin (fig. 6.3.2ii). Although in resting neutrophils where there is no great demand for ezrin turnover, it is likely that the inhibition of phosphorylation in the ezrin pool did not have opportunity to impact the phosphorylation status of peripheral ezrin, because of the slow turnover rate. We have therefore used the Ca^{2+}-stimulated generation of the ezrin fragment as an 'inverse surrogate' measure of Thr567 phosphorylation within neutrophils. After physiological elevation of cytosolic Ca^{2+}, triggered by the neutrophil agonist fMLP, there was no significant increase in ezrin of 62 kDa, however ezrin fragments of 50-55 kDa were detectable (fig.6.3.2iii), as expected from activation of μ-calpain. These data do not conflict with the effect of NSC668394 reducing phosphorylation of ezrin within treated neutrophils, and may suggest an increased vulnerability to Ca^{2+}-dependent cleavage.

6.3.3 Effect of NSC668394 on neutrophil phagocytic ability

Since NSC668394 was found to have an effect on neutrophil ezrin subcellular localisation, and on its sensitivity to Ca^{2+}-activated cleavage within neutrophils, the impact of these biochemical events on two neutrophil behaviours, phagocytosis and chemotaxis, was examined.

Neutrophils treated with NSC668394 were able to undertake phagocytosis of C3bi-opsinised zymosan particles (fig. 6.3.3b) with a phagocytic index of 1.972 ±0.588 (n=20), which was not significantly different from in control cells, 2.417 ±1 .003 (n=10) (fig. 6.3.3c). Ca^{2+} signalling upon zymosan binding was intact after treatment with NSC668394 (fig. 6.3.3b,c) with similar characteristics at the individual cell level. The times between cell-particle contact, phagocytic cup formation and phagosome closure were not different in untreated and drug treated cells (fig. 6.3.3d,e). As each phagocytic event takes only ~100s from initial contact to internalisation (Campbell and Hallett, 2015), there may be no requirement for additional recruitment of ezrin by phosphorylation of cytosolic ezrin over this timescale.

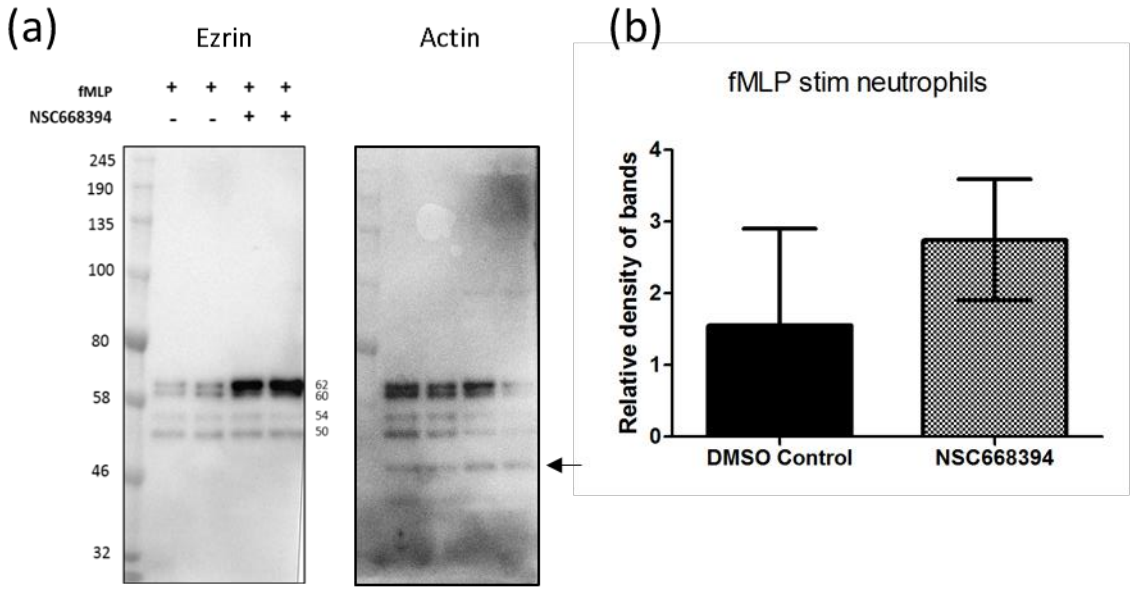

(c)

MW	Log_{10} MW	Distance (pixels)	Rf value
100	2	0	0
80	1.90309	86	0.242938
58	1.763428	151	0.426554
46	1.662758	242	0.683616
32	1.50515	327	0.923729
25	1.39794	354	1

$$Rf = \frac{distance\ migrated\ (pixels)}{gel\ length\ (pixels)}$$

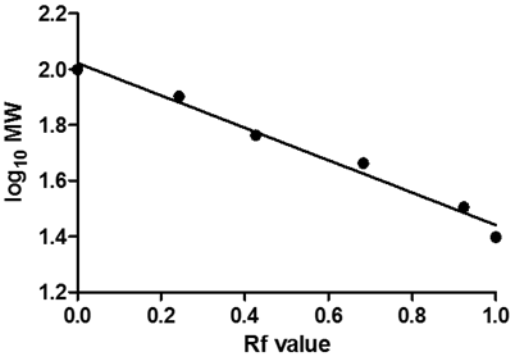

$$MW = e^{(gradient\ of\ line \times Rf) + y\ intercept}$$

Distance (pixels)	Rf value	MW
126	0.355932	62.09562704
136	0.384181	59.79120253
163	0.460452	53.98750041
184	0.519774	49.86586878

Figure 6.3.2iii: Immunodetection of ezrin and ezrin fragments in fMLP stimulated neutrophils

(a) Western blot of human neutrophil extracts stimulated with fMLP (1 µM) either without (-) or with (+) pre-treatment with NSC668394 (10 µM). **(b)** Densitometry analysis of western blots, with SEM. Data from 3 independent experiments. **(c)** The MW were identified by calculating the line of regression.

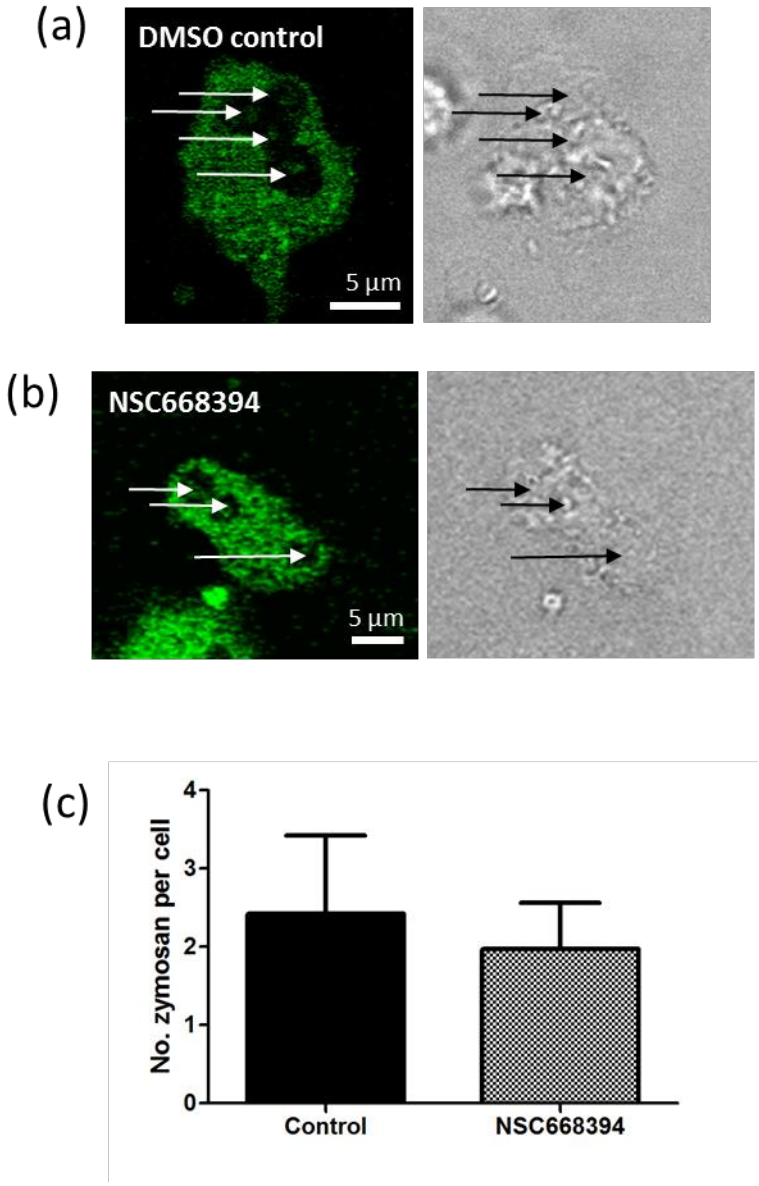

Figure 6.3.3: Phagocytosis of opsonised zymosan by neutrophils pre-treated with NSC668394

Confocal (left) and phase contrast (right) images of neutrophils loaded with Fluo-4 performing phagocytosis of opsonised zymosan particles (indicated by arrows), pre-treated with **(a)** DMSO control or **(b)** NSC668394 (10 µM). **(c)** The phagocytic index of neutrophils that were pre-treated with DMSO (n=10) control or NSC668394 (n=20) at 10, 50 and 100 µM.

(d)

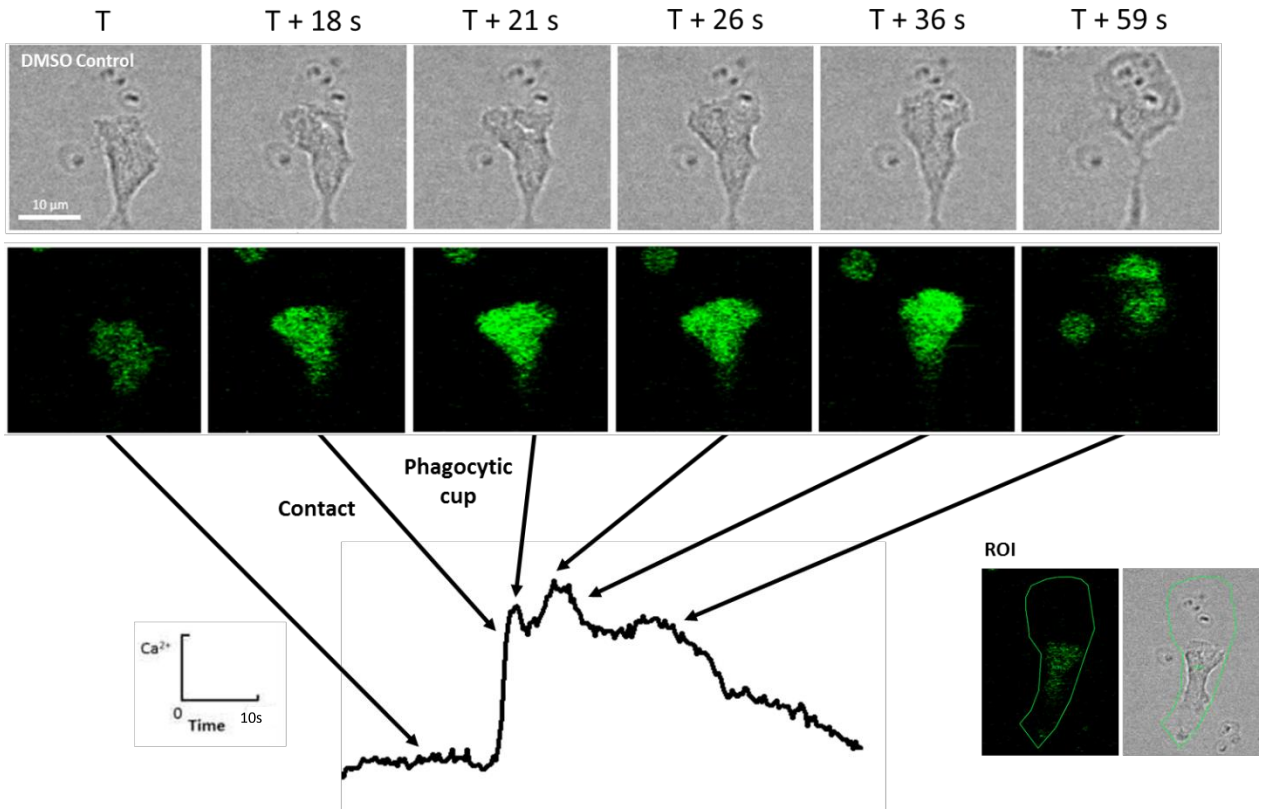

Figure 6.3.3: Phagocytosis of opsonised zymosan by neutrophils
(d) Time series images of Fluo-4 loaded neutrophils, pre-treated with DMSO control, performing phagocytosis of opsonised zymosan particles. Ca^{2+} trace (from defined region; insert) shows typical Ca^{2+} response.

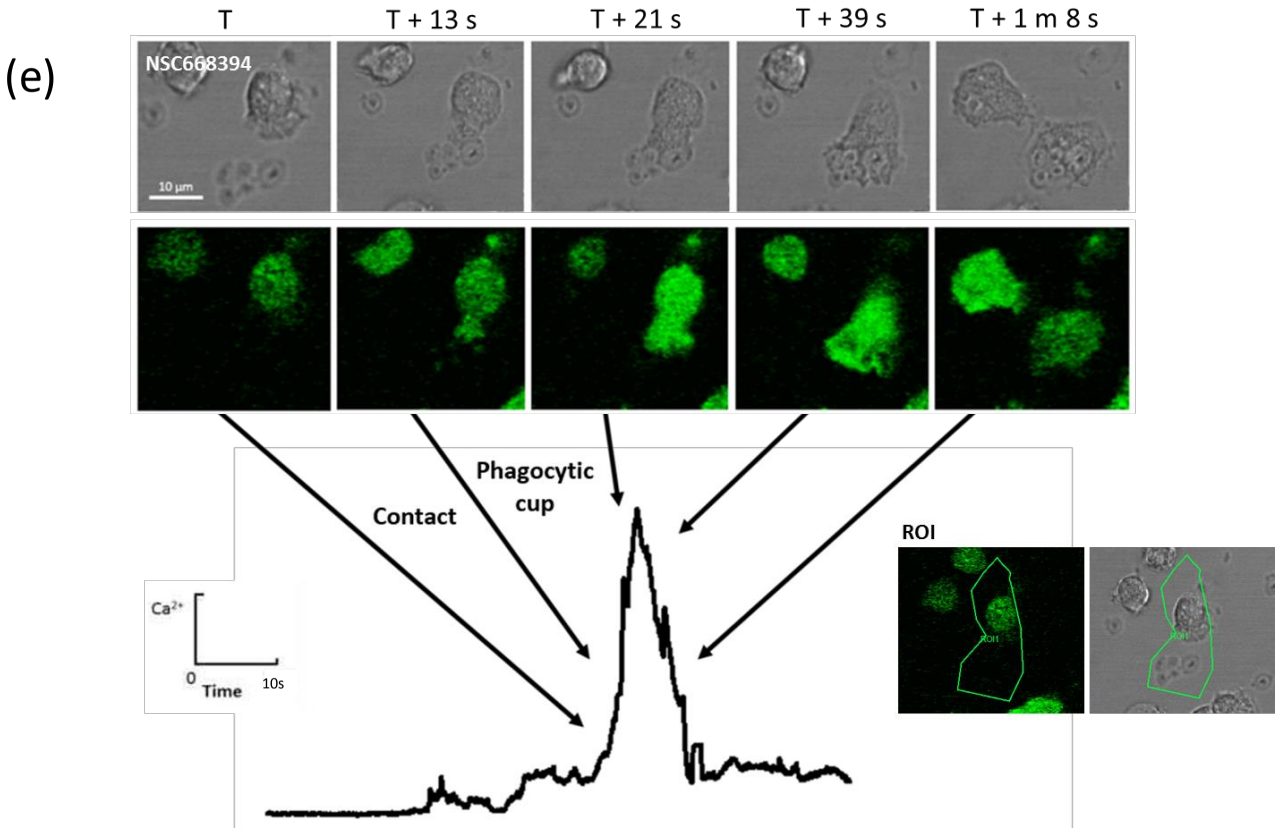

Figure 6.3.3: Phagocytosis of opsonised zymosan by neutrophils
(e) Time series images of Fluo-4 loaded neutrophils, pre-treated with NSC668394 (10 mins), performing phagocytosis of opsonised zymosan particles. Ca^{2+} trace (from defined region; insert) shows typical Ca^{2+} response.

6.3.4 Effect of ezrin phosphorylation inhibition on neutrophil chemotactic ability

In order to test whether ezrin phosphorylation may be required over longer timescales, chemotaxis over several hours was investigated. Previous members of our laboratory have identified cavities in some collagen beads (from 2BScientific), and found that these can be exploited for the purpose of generating focal points of stimuli in neutrophil chemotaxis experiments. The collagen bead cavities were injected with zymosan particles, so that when serum is added, they generate a gradient of C5a chemoattractant around the beads. 3-4 beads were loaded onto each slide. Prior to the experiment, beads were located on the slide using a Bright-field microscope, and their position was marked at the edge of the slide with a marker pen. If beads were at sufficient distance from each other (i.e. more than 5mm), to not produce conflicting gradients of C5a which may have confused the path of the neutrophils, then the experiment proceeded. The 10x objective was chosen because it was necessary to image the volume of the chamber, and a large field of view was beneficial, in order to record neutrophils migrating from some distance towards the stimulus.

Chemotaxis of neutrophils towards the single focal point of C5a generation in either the continued presence of NSC668394 (10 μM), or an equal volume of DMSO, was assessed in fluorescently labelled neutrophils by quantitation of the increase in fluorescence intensity at the target. The NSC668394 treated cells initially migrated towards C5a with a similar speed to the untreated cells, but the recruitment of further cells declined. After 90 minutes, 34% fewer treated cells than untreated cells had accumulated around the bead (fig. 6.3.4a). This was the result of cessation of chemotaxis of a significant number of treated neutrophils, as can be seen from tracking individual cells. Immediately before the cells stopped moving, they acquired an elongated and abnormal shape (fig. 6.3.4b). The neutrophils which travelled to the target were not significantly different in the speed of chemotaxis or in their overall directional persistence (as defined by Petrie and colleagues (2009)) from untreated neutrophils (fig. 6.3.4c).

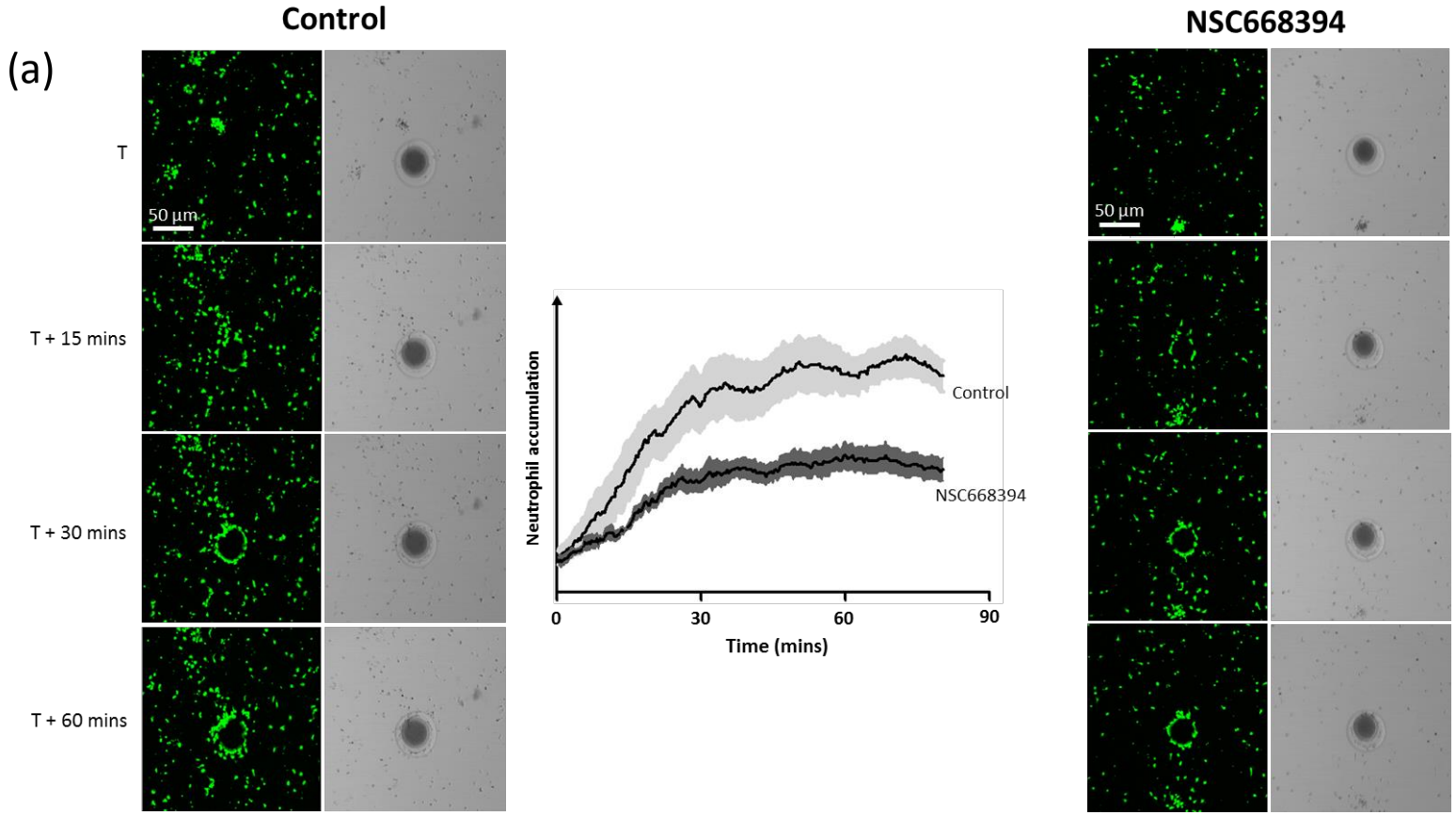

Figure 6.3.4: Chemotaxis of neutrophils pre-treated with NSC668394

(a) Time series snapshots of human neutrophils loaded with CellTrace Calcein AM, and **(c)** pre-treated with NSC668394 (10 µM), in the proximity of a source of C5a (dark circle in phase contrast image) at T=0, 15, 30 and 90 mins. **(b)** Neutrophil accumulation at collagen bead. N=4 determinations, from more than 20 cells. All differences were significant at T=15 mins ($P<0.05$).

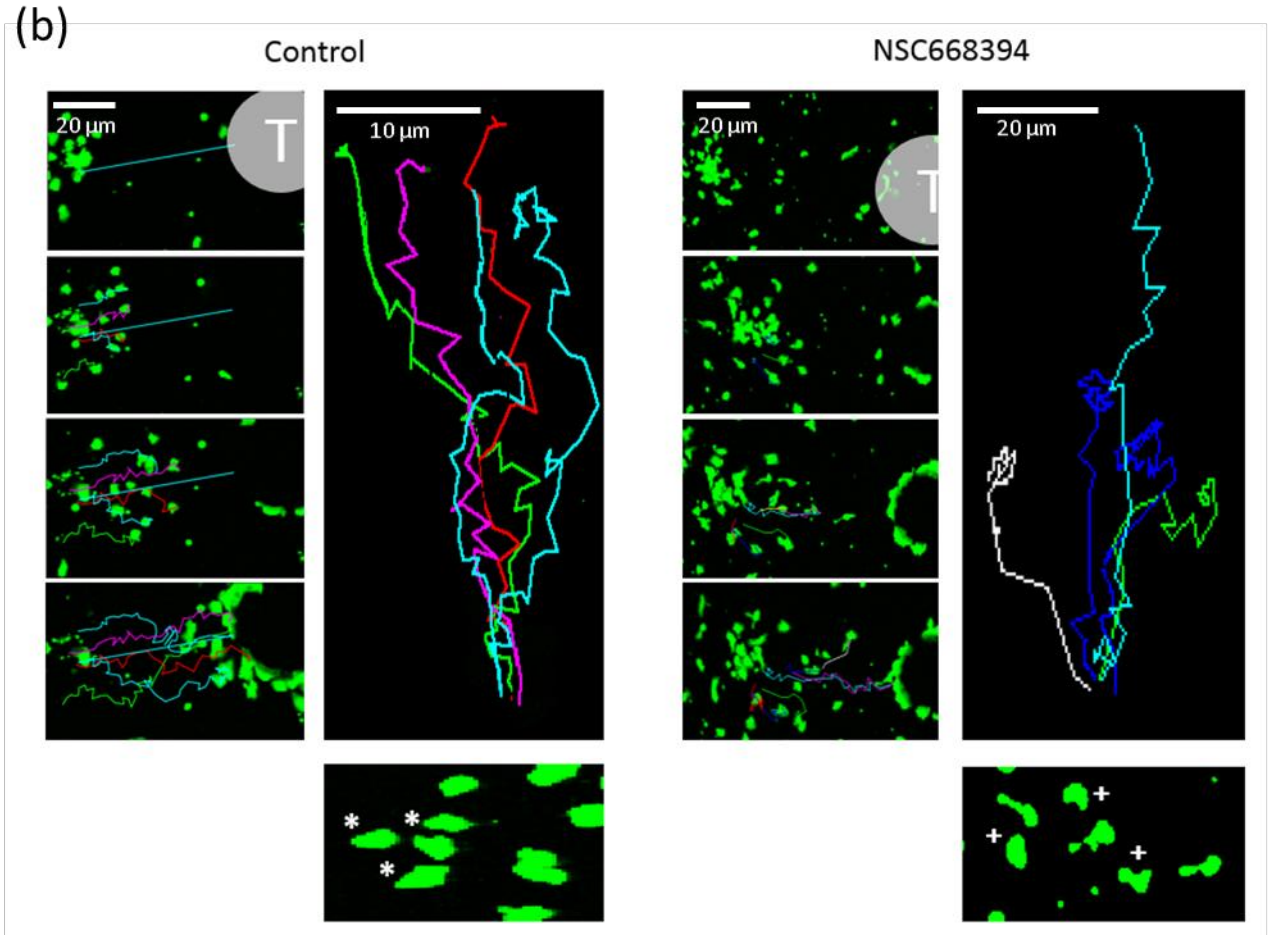

Figure 6.3.4: Chemotaxis of neutrophils pre-treated with NSC668394
(b) Examples of cell tracks, from 5 randomly chosen cells in each population, towards the source of C5a (ROI = T). Asterisks (*) indicate characteristically elongated cells and plus signs (+) indicate rounded-up cells.

(c)

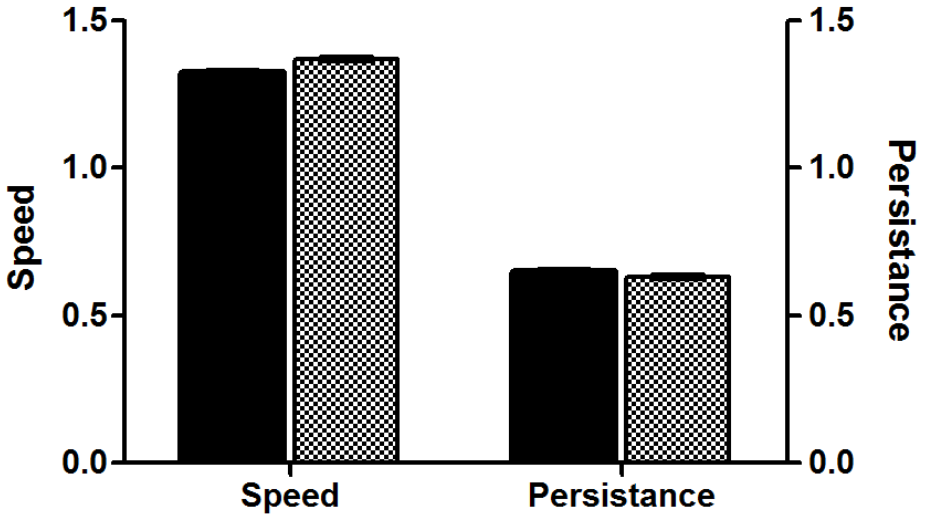

Figure 6.3.4: Chemotaxis of neutrophils pre-treated with NSC668394
(c) The average speed and persistence of neutrophils pre-treated with either the DMSO control or NSC668394 (10 µM) (n=210 and 170 respectively).

6.4 Discussion

Because of the important structural role of ezrin in neutrophils, in linking the cortical F-actin to the plasma membrane, and its involvement in the architectural maintenance and rearrangement of neutrophil microridges (during extravasation) (Herant et al., 2005; Herant et al., 2006; Dewitt et al., 2013), the pharmacological inhibition of ezrin activation (through phosphorylation at Thr567) was investigated. The work reported here has shown that inhibition of ezrin phosphorylation by NSC668394 increases the detectable amount of cleaved ezrin, but does not totally inhibit either neutrophil phagocytosis, or the initial ability of neutrophils to undergo chemotaxis. However, it was clear that prolonged chemotaxis by neutrophils was restricted.

The Imagestream technology provides the possibility of high throughput large data sets, combined with the imaging capabilities that provide details comparable to confocal imaging (fig. 6.4). In this work the technology was trialled to see if it was capable of differentiating between different subcellular locations of ezrin, predicted by the previous single-cell immunocytochemistry investigations. The quality of the captured images was impressive, and sufficient to show peripheral ezrin staining in some cells. However, only a minority of cells displayed specific staining at the cell edge. Further confocal investigation found that among the population of neutrophils only a few cells displayed peripheral ezrin staining. Therefore it was concluded that the limiting factor was not the Imagestream technology, but the immunocytochemistry step. It was decided that further optimisation of the staining protocol was required, but the information this would provide did not justify further exploration

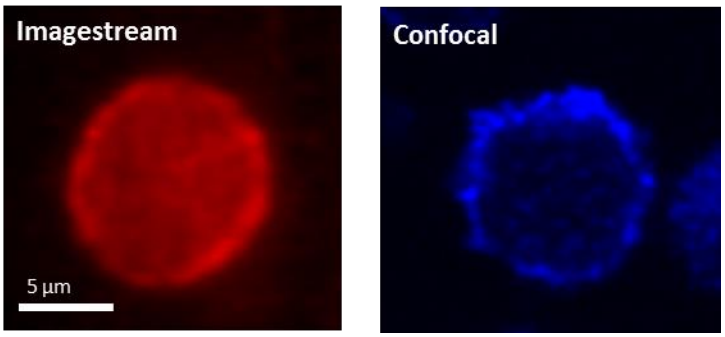

Figure 6.4: Comparison of Imagestream and confocal imaging
Neutrophils stained with Cy5-conjugated anti-ezrin antibody. Left: Image acquired by Imagestream shows peripheral ezrin staining. Right: Confocal image also shows ezrin at the cell edge. Scale bar 10 µm.

in this project. However, Imagestream remains an innovative technology for achieving larger data sets to support the conclusions drawn from smaller scale immunocytochemistry experiments.

The data reported here show that NSC668394 reduced the amount of ezrin at the neutrophil periphery. It was not clear that NSC668394 had an effect on the sensitivity of unphosphorylated ezrin to cytosolic Ca^{2+}-signalled cleavage. Although, stimulation with fMLP did generate detectable ezrin fragments of 50-62 kDa, suggesting unphosphorylated ezrin was a substrate for cytosolic Ca^{2+}-signalled cleavage. These events may be related, as both the lack of Thr567 phosphorylation of ezrin in the cytosol or cleavage of ezrin at the periphery would result in a decrease in peripheral ezrin. Cleavage of ezrin between the N- and C- termini would therefore destabilise the binding by separating the high affinity and low affinity components, and ezrin fragments would be released.

Despite these changes in ezrin handling within neutrophils, phagocytosis and short term chemotaxis was able to continue. An explanation for this may be that phosphorylation at Thr567 of ezrin is initially required to unfold ezrin for cross-linking of the cortical actin to the plasma membrane, and for maintaining ezrin in a μ-calpain-insensitive state (Bretscher et al., 1997). This would provide a mechanism for maintaining a static and stable cell surface morphology in microvilli, in cells types such as intestinal epithelial cells (Saotome et al., 2004). Moreover, mutation of the ezrin at Thr567 to a phosphomimetic active Thr567D or to an unphosphorylatable inactive Thr567A (Ruppelt et al., 2007) has a profound effect on sensitivity to μ-calpain cleavage, and demonstrates that phosphorylation at this site is strongly protective against cleavage (McRobert et al., 2012). In neutrophils, the role of ezrin in regulating rapid cell shape may be achieved through a pool of peripheral ezrin which is susceptible to Ca^{2+}-activated μ-calpain cleavage, and so can release a membrane reservoir rapidly on demand in response to localised elevation of Ca^{2+} (Dewitt et al., 2013). Ezrin in this pool may have become un-phosphorylated, but is retained at the cell periphery within surface microridges, and so becomes the releasable pool of

ezrin which facilitates rapid shape change, due to the acquisition of sensitivity to μ-calpain cleavage.

Perhaps the most interesting finding in this study was that neutrophils treated with NSC668394 were unable to maintain the normal chemotactic morphology required for continued chemotaxis. This effect is similar to that reported recently (Prentice-Mott et al., 2016), in which it was found that NSC668394 reduced 'directional memory' of neutrophil-like HL-60 cells from 90% to 60%. In our study, it was seen that human neutrophils treated with NSC668394 could not maintain the polarised morphology over long periods and this resulted in rounding up of the neutrophils. This is the minimum surface area to volume configuration that is expected if the cell surface topography is unregulated due to lack of peripheral ezrin to maintain cell surface micro-ridges. It was observed that neutrophils that lack peripheral ezrin adopt this spherical configuration with a larger diameter. Presumably the presence of the inhibitor and the continued demand for replacement of ezrin at the cell edge, as a result of either μ-calpain cleavage or the slow depletion of the regulatory pool of periphery ezrin, which occurred over this time period, meant that lost ezrin could not be replaced by unphosphorylated folded ezrin from the cytosol. This latter effect may be beneficial in the treatment of chronic inflammatory disease, by slowing the influx of neutrophils into chronic inflammatory sites without inhibition of phagocytosis and acute inflammation.

It was therefore concluded from the work reported here, that phosphorylation of ezrin plays only a minor role in ezrin-regulation of rapid cell shape change in neutrophils. However, when multiple and prolonged cell shape changes are required, such as during prolonged chemotaxis, the dependency on the pool of unphosphorylated ezrin was evident and inhibition was observed. Although, NSC668394 did not abolish neutrophil chemotaxis towards a focal stimulus, the number of neutrophils able to continue movement over a long range was reduced. This suggested that there was a role of peripheral ezrin turnover for maintaining prolonged shape change activity. It has been postulated that peripheral ezrin is cleaved by elevated μ-calpain activity (Shuster and Herman, 1995). If this is prolonged, it may be necessary for the replacement of ezrin from

the cytosolic pool which may require activation of ‘inactive’ ezrin, phosphorylation. This phenomenon, and its susceptibility to inhibition, may prove a useful target for anti-inflammatory therapy. Inhibition of neutrophil chemotaxis towards chronically inflamed sites, without compromising their ability to undergo phagocytosis, would be a beneficially selective effect on neutrophil behaviours.

Chapter 7:

General discussion: synopsis, hypothesis, future work

7. General Discussion

The work presented in this thesis has aimed to shed light on the μ-calpain-ezrin axis, in the regulation of myeloid cell morphology changes, and in response to elevated cytosolic Ca^{2+} concentrations. This mechanism is particularly relevant to neutrophils at the point of extravasation from the bloodstream, where their transition to a flattened and adherent cell morphology requires an apparent membrane expansion of approximately 200% (Dewitt and Hallett, 2007).

The accumulation and infiltration of neutrophils in tissues is a somewhat double-edged sword. On the one hand, the process is entirely necessary, and appropriate recruitment of neutrophils at sites of infection protect the body via phagocytosis of invasive pathogens, and resolution of inflammation. On the other hand, the unregulated recruitment of neutrophils to tissues presenting with chronic inflammation only contributes to the propagation of the inflammatory state; leading to further tissue damage. Autoimmune diseases, such as rheumatoid arthritis, fall into this latter category. Excessive neutrophil infiltration into the joints leads to cartilage erosion and propagation of the inflammatory state, which causes pain upon movement, architectural rearrangement of the joint and ultimately fusion of the joints. This joint destruction is irreversible, and current therapies are insufficient at preventing the onset of the disease. There is therefore a need for further research in this area, in order to design more appropriate and effective treatments.

Despite the obvious hurdle that changing morphology presents to the migrating neutrophil, very little is known about the molecular mechanisms governing it. With further understanding of this mechanism, and the relationship between μ-calpain, ezrin and Ca^{2+} concentration, we would be better placed to inform and guide the development of targeted therapies for autoimmune conditions, such as rheumatoid arthritis. Such therapies may specifically interfere with the mechanism of changing neutrophil morphology, with the aim of reducing

extravasation, and therefore also inappropriate accumulation of inflammatory cells during chronic inflammation.

7.1 Overall research strategy

Primary scientific research with neutrophils poses a number of challenges, not least because the cells are terminally differentiated, have a short lifespan and easily become activated. All of these factors make conducting experiments to investigate intracellular molecular processes challenging. Previous work by this lab has found the RAW 264.7 myeloid cell line a suitable compromise between amenability of experimental approach, and information output (e.g. limited ability to perform phagocytosis).

7.2 Summary of progress made by this work

In this thesis, it was shown that elevating cytosolic Ca^{2+} had a large effect on ezrin distribution in RAW 264.7 cells expressing fluorescently-tagged ezrin constructs. Since ezrin is a crucial cross-linking protein which maintains the structure of plasma membrane microridges, this work points to a key role for Ca^{2+} influx in regulating cell surface topography. Furthermore, these microridges are proposed to provide the mechanism for apparent membrane expansion, by acting as 'reservoirs' of extra membrane; amenable to release when the cell requires a change in morphology (Dewitt and Hallett, 2007). Ca^{2+} influx is implicated as the switch that releases this stored excess membrane, and it is suggested to act via the Ca^{2+}-mediated activation of the ubiquitous cytosolic protease, μ-calpain. Since the *in vitro* Ca^{2+} concentrations required to activate μ-calpain exceed those which can be achieved in the global cytosol (Goll et al., 2003), there is an obvious need for careful regulation of the both the Ca^{2+} signal and the activated μ-calpain response.

The data presented in this thesis have also provided evidence of ezrin loss from the cell edge in myeloid cells, in agreement with ezrin cleavage by μ-calpain

upon elevation of cytosolic Ca^{2+} (fig. 7.2); be it via artificial stimulation of Ca^{2+} influx via SOCE, or via physiological activation through receptor-mediated phagocytosis. The precise cleavage site in ezrin is not known, however this thesis has investigated potential cleavage sites (using the CaMPDB algorithm) in ezrin, which differs from moesin (another structurally similar ERM protein) in its sensitivity to μ-calpain cleavage (Shcherbina et al., 1999). In myeloid cells ezrin was found to be cleaved by μ-calpain, at least once, in the linker region between the two functional domains; the N-ERMAD and C-ERMAD domains respectively. Cleavage of ezrin in this region would sever its cross-linking activity between the plasma membrane and the cortical F-actin cytoskeleton, thereby releasing the constraints which maintain cell surface microridges (fig. 7.2). This provision of additional plasma membrane, from 'reservoirs' would also transiently reduce membrane tension, which is rapidly restored due to remodelling of the sub-membranous F-actin network (Pietuch and Janshoff, 2013). Thus the provision of additional membrane for events requiring a change in cell shape, e.g. phagocytosis or extravasation, is in cooperation with interactions between the plasma membrane and the actin cytoskeleton; where ezrin provides important structural cross-links. Consequently, a decrease in active ezrin at the cell edge leads to a reduction in membrane tension, and a loss of cell height (Brückner et al., 2015), similar to those observed in a neutrophil undergoing a morphological change such a s cell spreading (Dewitt et al., 2013).

The question of μ-calpain activation *in vivo* then arose, since its K_d is in the range 20-60 μM Ca^{2+}. Whilst the Ca^{2+} concentration within cytosolic microdomains beneath plasma membrane microridge structures has been predicted to reach within this μ-calpain activating range, such measurements have, to date, never been achieved in live single cells. This thesis reports the development of a new methodology, specifically to measure the Ca^{2+} concentration within these ezrin-rich cytosolic microdomains. EPIC3 was generated, because of its ezrin localising properties, and its GCaMP2-like Ca^{2+}-sensing domain. By expressing EPIC3 in a model myeloid cell line (RAW 264.7), cytosolic Ca^{2+} was recorded within ezrin-rich cytosolic microdomains, beneath plasma membrane microridges, during

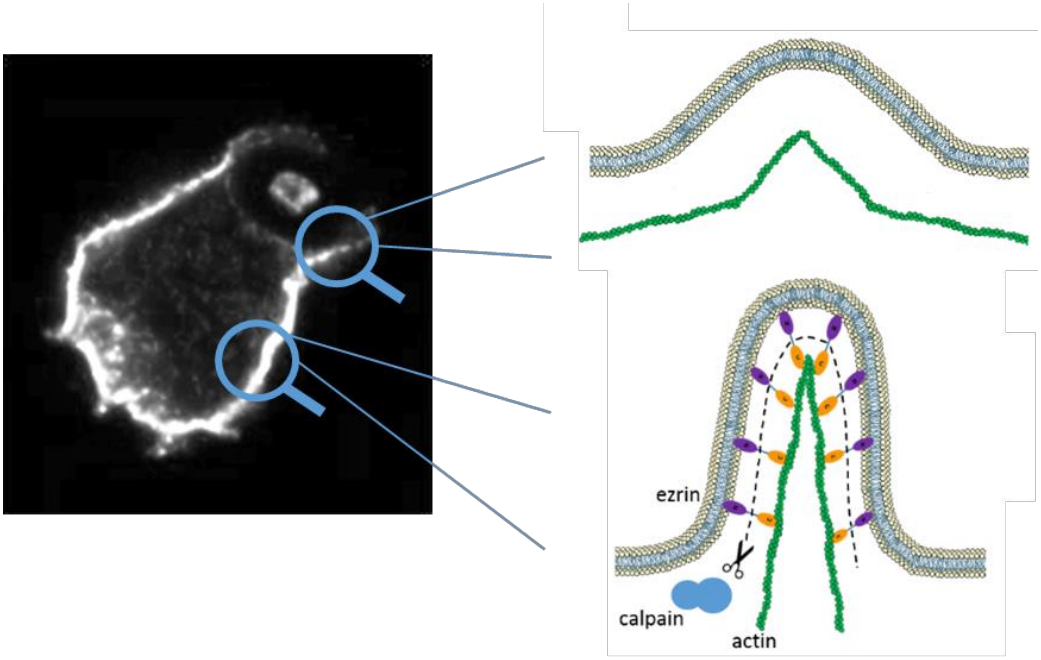

Figure 7.2: Neutrophil microridge plasma membrane reservoirs
A neutrophil with localised membrane expansion at the point of phagocytosis. Microridges in the neutrophil plasma membrane are released during elevations of cytosolic Ca^{2+}, via activity of the Ca^{2+}-activated protease μ-calpain, which cleaves the cross-linker ezrin.

SOCE Ca^{2+} influx events. Within these sub-membranous cytosolic domains, the Ca^{2+} concentration was recorded to reach mid-decade micromolar levels – capable of activating μ-calpain.

The cross-linking activity of ezrin is dependent on its activation, by phosphorylation. Therefore, the effect of inhibiting ezrin phosphorylation in neutrophils was also investigated. The small molecule inhibitor of ezrin phosphorylation at Thr567, NSC668394, was used in neutrophils, for the first time, as an experimental tool to probe the μ-calpain-ezrin axis, and investigate the interplay between ezrin phosphorylation and Ca^{2+}-mediated μ-calpain activation in regulating neutrophil shape change. The phosphorylation status of ezrin did not dictate localised membrane reorganisations, for the purpose of phagocytosis, and inhibition of ezrin phosphorylation was found to have only a limiting effect on neutrophil migration. However, this latter event may be useful for the design of future pharmacological interventions to reduce neutrophil migration in chronic inflammatory conditions.

7.3 Hypothesis

It is therefore interesting to postulate that, in myeloid cells at least, ezrin exerts its cross-linking activity between the plasma membrane and the actin cytoskeleton via the "molecular clutch" (Mitchison and Kirschner, 1988; Case and Waterman, 2015). In this model, ezrin provides the crucial connection between the actin cytoskeleton and integrin-containing focal adhesions at the plasma membrane when the clutch is engaged. Disengagement of the clutch, perhaps via μ-calpain-mediated ezrin cleavage (Dewitt and Hallett, 2002), would decrease the retrograde cytoskeletal flow (Mitchison and Kirschner, 1988; Case and Waterman, 2015), thereby reducing the forces generated by actin polymerisation on the cell edge and causing a transient decrease in membrane tension (Brückner et al., 2015); whereby the release of stored plasma membrane from cell surface microridges would be possible, for the purpose of cell spreading, extravasation and phagocytosis (fig. 7.2). Inhibition of μ-calpain

activity has also been to shown to limit pseudopodia extension in neutrophils performing phagocytosis (Dewitt and Hallett, 2002), reinforcing the concept that ezrin release from the molecular clutch is the trigger for release of stored plasma membrane reservoirs.

7.4 Future work

There are three lines of future research which could be followed from the progress reported here. The first two involve modifying and refining the probes reported in Chapters 3 and 4. The third line of investigation is a novel approach which has not been tried here.

7.4.1 Refined probe for *in vivo* ezrin cleavage

The use of ezrin with attached fluorescent tags, either before or after the μ-calpain-sensitive linker region, provided the evidence for μ-calpain-mediated cleavage of ezrin *in vivo*. However, there were three problems with this approach: (i) two probes had to be co-expressed in the same cell, in order to obtain simultaneous data signals, which formed the basis of the ratio determination; (ii) the percentage of cells displaying dual expression of both probes was low, therefore the number of cells which could be used from each transfection event was low, also the ratio technique assumed that both probes were equally distributed at identical loci within the cell; (iii) cells expressing more than one ezrin variant often failed to perform phagocytosis, which may have been an inhibitory result of excessive ezrin competing with or complementing endogenous ezrin cross-links, thereby stabilising microridge structures in the face of high Ca^{2+} and activated μ-calpain. All three of these concerns could be overcome by amalgamating the concept of the probes used in this work into one single ezrin construct; by generating a plasmid to express ezrin with two fluorescent tags: (i) GFPi at the intra-FERM domain position, which doesn't interfere with N-terminal interactions with the plasma membrane, and (ii) an mCherry fluorophore attached to the C-terminus. In this

way, a single successfully transfected cell would provide information about both the N- and C-functional domains of ezrin, from exactly the same loci inside the cell, and without the need for expression of multiple ezrin constructs, as long as the two fluorophores in the single ezrin construct have fluorophores with excitation/emission wavelengths at opposing sides of the spectrum.

7.4.2 Refined probe for intra-microridge Ca^{2+} measurement and imaging

The novel approach of linking a low affinity Ca^{2+}-sensing probe to ezrin was successful in this work (Chapters 4 and 5). However, further investigation into the μ-calpain-ezrin axis in the context of neutrophil morphology change, for the purpose of extravasation, may seek to refine the cytosolic Ca^{2+} measurements obtained from ezrin-rich microdomains. As discussed in this thesis (Chapter 3), the addition of a fluorophore at the N-terminus of ezrin prevented localisation to the plasma membrane. Whilst C-terminally tagged ezrin appeared to behave as endogenous protein, it is not unreasonable to speculate that a fluorophore on the C-terminus, such as EPIC3, may also limit some typical ezrin interactions, e.g. firm binding with the F-actin cytoskeleton. The intra-tagged ezrin construct, ezrin-GFPi (Marion et al., 2011) has been used to successfully report typical ezrin behaviours in the live cell. This thesis has found evidence that the N-FERM domain of ezrin persists at the cell edge, presumably through firmer interactions with the plasma membrane (Fritzsche et al., 2014), typically 25 s longer than C-terminally tagged ezrin fragments, generated by μ-calpain-mediated cleavage.

Therefore, future efforts may aim to introduce a Ca^{2+}-sensing domain at the intra-FERM domain position, as has been achieved with ezrin-GFPi. This would also overcome the problem of the Ca^{2+}-sensing domain being released during the crucial 25 s after initial μ-calpain activation and ezrin linker cleavage (where the N-ERMAD was found to persist at the cell edge, but the C-ERMAD became cytosolic). Furthermore, new generations of EPIC with different affinities for Ca^{2+} would also provide more information about the Ca^{2+} concentrations which can

be achieved in these ezrin-rich cytosolic microdomains. One such probe may incorporate the Ca^{2+} sensing domain of CEPIA4, with a K_d of 54 μM Ca^{2+} (Suzuki et al., 2014). It is predicted that this would report the elevated Ca^{2+} concentrations achieved in the microridges (estimated here to be typically between 30-100 μM), but would be insensitive to the global cytosolic free Ca^{2+} concentration, even at several micromolar; thus giving an enhancement between the signals from beneath the cell surface, and elsewhere in the cell.

7.4.3 Interference of ezrin cleavage as a test of the hypothesis

In order to test the μ-calpain-ezrin cleavage hypothesis, it would be necessary to generate fluorescently tagged ezrin constructs which were insensitive to μ-calpain proteolysis. The hypothesis would be that without severing of the ezrin cross-link, the "molecular clutch" would remain engaged; stored plasma membrane would not be released from surface microridges, and the cell would be unable to respond to Ca^{2+} influx and signals to change morphology. The main limitation to this approach is that the exact μ-calpain cleavage site in ezrin is unknown. This thesis has speculated that cleavage occurs primarily within the linker region, where the sequence of ezrin differs from its μ-calpain insensitive cousin, moesin. However, it has also been acknowledged that ezrin is likely cleaved by Ca^{2+}-activated μ-calpain at multiple sites. Therefore, development of a μ-calpain insensitive ezrin would require further optimisation.

However, the effect of point mutations altering single amino acids in the ezrin specific sequence of the linker region would in itself produce crucial information about the μ-calpain-mediated mechanism of ezrin cleavage *in vivo*. Also, such a non-cleavable ezrin construct would be ideal for the basis of designing a further peripheral Ca^{2+}-sensing probe; one which would not be released by μ-calpain activity, and therefore faithfully report the Ca^{2+} concentrations in the peripheral cytosol, beneath plasma membrane microridges, throughout elevation of Ca^{2+} and the activation of μ-calpain.

7.5 Conclusions

In conclusion, the μ-calpain-ezrin axis is clearly important in the mechanism by which myeloid cells, including neutrophils, carry out effector functions which require changes in cell morphology, with a dramatic increase in available plasma membrane. This apparent membrane expansion required by neutrophils to perform cell spreading, the necessary prelude to extravasation, may be a common hurdle in the exit of leukocytes from the bloodstream during excessive recruitment in chronic inflammatory conditions. Disruption of this mechanism, at the μ-calpain-ezrin axis, may be a useful target for the development of novel pharmacological therapies, aimed at reducing propagation of the inflammatory response in chronic immune disease.

8. References

Abbassi, O., Kishimoto, T.K., Mcintire, L.V., and Smith, C.W. (1993). Neutrophil Adhesion to Endothelial-Cells. Blood Cells 19, 245-260.

Abramson, J.S. and **Wheeler** J.G. (1993). Maturation of neutrophil. In: The neutrophil. IRL Press, Oxford, pp 9–11.

Adams, S, E. (2013). The Synthesis and Evaluation of Novel Calpain-I Inhibitors PhD Thesis, Cardiff University.

Alamanos, Y., and **Drosos**, A.A. (2005). Epidemiology of adult rheumatoid arthritis. Autoimmun Rev 4, 130-136.

Algrain, M., Turunen, O., Vaheri, A., Louvard, D., and Arpin, M. (1993). Ezrin contains cytoskeleton and membrane binding domains accounting for its proposed role as a membrane-cytoskeletal linker. J Cell Biol 120, 129-139.

Al-Mohanna, F.A., Pettit, E.J., and Hallett, M.B. (1997). Does actin polymerization status modulate Ca^{2+} storage in human neutrophils? Release and coalescence of Ca^{2+} stores by cytochalasins. Exp Cell Res 234, 379-387.

Anderson, C.L., and **Looney**, R.J. (1986). Human-Leukocyte Igg Fc-Receptors. Immunol Today 7, 264-266.

Anderson, D.C., and **Springer**, T.A. (1987). Leukocyte adhesion deficiency: an inherited defect in the Mac-1, LFA-1, and p150,95 glycoproteins. Annu Rev Med 38, 175-194.

Aoki, K., Imajoh, S., Ohno, S., Emori, Y., Koike, M., Kosaki, G., and Suzuki, K. (1986). Complete amino acid sequence of the large subunit of the low-Ca^{2+}-requiring form of human Ca^{2+}-activated neutral protease (muCANP) deduced from its cDNA sequence. Febs Lett 205, 313-317.

Arif, S. and Mufti, A. (1998). Immune, blood and lymphatic system. Mosby's Crash course. Mosby International Ltd, Barcelona, Spain.

Athens, J.W., Wintrobe, M.M., Ashenbrucker, H., Cartwright, G.E., Mauer, A.M., Haab, O.P., and Raab, S.O. (1961). Leukokinetic Studies .4. Total Blood, Circulating and Marginal Granulocyte Pools and Granulocyte Turnover Rate in Normal Subjects. J Clin Invest 40, 989.

Atilgan, E., Wirtz, D., and Sun, S.X. (2006). Mechanics and dynamics of actin-driven thin membrane protrusions. Biophys J 90, 65-76.

Babior, B.M. (1984). The Respiratory Burst of Phagocytes. J Clin Invest 73, 599-601.

Badour, K., Zhang, J., and Siminovitch, K.A. (2003). The Wiskott-Aldrich syndrome protein: forging the link between actin and cell activation. Immunol Rev 192, 98-112.

Baggiolini, M., and Wymann, M.P. (1990). Turning on the Respiratory Burst. Trends Biochem Sci 15, 69-72.

Barret, C., Roy, C., Montcourrier, P., Mangeat, P., and Niggli, V. (2000). Mutagenesis of the phosphatidylinositol 4,5-bisphosphate (PIP_2) binding site in the NH_2-terminal

domain of ezrin correlates with its altered cellular distribution. J Cell Biol 151, 1067-1080.

Berryman, M., Gary, R., and Bretscher, A. (1995). Ezrin oligomers are major cytoskeletal components of placental microvilli: a proposal for their involvement in cortical morphogenesis. J Cell Biol 131, 1231-1242.

Berti, P.J., and **Storer**, A.C. (1995). Alignment/phylogeny of the papain superfamily of cysteine proteases. J Mol Biol 246, 273-283.

Bessis, M. (1973). Living Blood Cells and Their Ultrastructure. Springer, Berlin.

Bevilacqua, M., Butcher, E., Furie, B., Furie, B., Gallatin, M., Gimbrone, M., Harlan, J., Kishimoto, K., Lasky, L., Mcever, R., et al. (1991). Selectins - a Family of Adhesion Receptors. Cell 67, 233-233.

Bigger, C.H and **Hildemann**, W.H. (1982). Cellular Defense Systems of the Coelenterata. Phylogeny and Ontogeny 59, pp 59-87

Blanchard, H., Grochulski, P., Li, Y., Arthur, J.S., Davies, P.L., Elce, J.S., and Cygler, M. (1997). Structure of a calpain Ca^{2+}-binding domain reveals a novel EF-hand and Ca^{2+}-induced conformational changes. Nat Struct Biol 4, 532-538.

Blaustein, M.P., and **Hodgkin**, A.L. (1968). Effect of Cyanide on Calcium Efflux in Squid Axons. J Physiol-London 198, P46-+.

Borregaard N, Miller L, Springer TA. (1987). Chemoattractant-regulated mobilization of a novel intracellular compartment in human neutrophils. Science 237, 1204-1206.

Borregaard, N., and **Cowland**, J.B. (1997). Granules of the human neutrophilic polymorphonuclear leukocyte. Blood 89, 3503-3521.

Boxer, L.A., and **Smolen**, J.E. (1988). Neutrophil Granule Constituents and Their Release in Health and Disease. Hematol Oncol Clin N 2, 101-134.

Brasen, J.C., Olsen, L.F., and Hallett, M.B. (2010). Cell surface topology creates high Ca^{2+} signalling microdomains. Cell Calcium 47, 339-349.

Bretscher, A. (1983). Purification of an 80,000-dalton protein that is a component of the isolated microvillus cytoskeleton, and its localization in nonmuscle cells. J Cell Biol 97, 425-432.

Bretscher, A. (1991). Microfilament structure and function in the cortical cytoskeleton. Annual review of cell biology 7, 337-374.

Bretscher, A., Edwards, K., and Fehon, R.G. (2002). ERM proteins and merlin: integrators at the cell cortex. Nature reviews Molecular cell biology 3, 586-599.

Bretscher, A., Reczek, D., and Berryman, M. (1997). Ezrin: a protein requiring conformational activation to link microfilaments to the plasma membrane in the assembly of cell surface structures. J Cell Sci 110 (Pt 24), 3011-3018.

Bretz, U., and **Baggiolini**, M. (1974). Biochemical and Morphological Characterization of Azurophil and Specific Granules of Human Neutrophilic Polymorphonuclear Leukocytes. J Cell Biol 63, 251-269.

Brinckerhoff, C.E. (1991). Joint Destruction in Arthritis - Metalloproteinases in the Spotlight. Arthritis Rheum 34, 1073-1075.

British Society for Immunology (https://www.immunology.org/thorn-tangerine-tree-1882) retrieved 10th September 2017.

Bruckner, B.R., Pietuch, A., Nehls, S., Rother, J., and Janshoff, A. (2015). Ezrin is a Major Regulator of Membrane Tension in Epithelial Cells. Scientific reports 5, 14700.

Bruhns, P. (2012). Properties of mouse and human IgG receptors and their contribution to disease models. Blood 119, 5640-5649.

Bulut, G., Hong, S.H., Chen, K., Beauchamp, E.M., Rahim, S., Kosturko, G.W., Glasgow, E., Dakshanamurthy, S., Lee, H.S., Daar, I., et al. (2012). Small molecule inhibitors of ezrin inhibit the invasive phenotype of osteosarcoma cells. Oncogene 31, 269-281.

Campbell, J.S., and **Hallett**, M.B. (2015). Active calpain in phagocytically competent human neutrophils: electroinjection of fluorogenic calpain substrate. Biochem Biophys Res Commun 457, 341-346.

Campbell, M.S., Lovell, M.A., and Gorbsky, G.J. (1995). Stability of nuclear segments in human neutrophils and evidence against a role for microfilaments or microtubules in their genesis during differentiation of HL60 myelocytes. J Leukocyte Biol 58, 659-666.

Cao, X., Ding, X., Guo, Z., Zhou, R., Wang, F., Long, F., Wu, F., Bi, F., Wang, Q., Fan, D., et al. (2005). PALS1 specifies the localization of ezrin to the apical membrane of gastric parietal cells. J Biol Chem 280, 13584-13592.

Carafoli, E., and **Molinari**, M. (1998). Calpain: a protease in search of a function? Biochem Biophys Res Commun 247, 193-203.

Carvalho, L.O., Aquino, E.N., Neves, A.C.D., and Fontes, W. (2015). The Neutrophil Nucleus and Its Role in Neutrophilic Function. J Cell Biochem 116, 1831-1836.

Case, R.M., Eisner, D., Gurney, A., Jones, O., Muallem, S., and Verkhratsky, A. (2007). Evolution of calcium homeostasis: From birth of the first cell to an omnipresent signalling system. Cell Calcium 42, 345-350.

Case, L.B. and **Waterman**, C.M. (2015). Integration of actin dynamics and cell adhesion by a three-dimensional, mechanosensitive molecular clutch. Nat Cell Biol 17(8), 955-963.

Caswell, A.H. (1979). Methods of measuring intracellular calcium. International review of cytology 56, 145-181.

Clark, R.A. and **Nauseef**, W.M. (2001). Isolation and functional analysis of neutrophils. Curr Protoc Immunol. 2001 May; Chapter 7: Unit 7.23.

Clemens, R.A., and **Lowell**, C.A. (2015). Store-operated calcium signaling in neutrophils. J Leukoc Biol 98, 497-502.

Cohnheim, J. (1867a) Entendung und Eitung. Virchow's Arch Pathol Anat, 40,1-

25.

Cohnheim, J. (1867b). Ueber Entzündung und Eiterung. Archiv für Pathologische Anatomie und Physiologie und für Klinische Medizin.

Cohnheim, J. (1967) Inflammation in Lectures in General Pathology. Syndenham

Society of London, 1, 242-254.

Coico, R. and **Sunshine, G.** (2009). "Immunology: A Short Course." Wiley-Blackwell Sixth Edition.

Cong, J., Thompson, V.F., and Goll, D.E. (1993). Effect of monoclonal antibodies specific for the 28-kDa subunit on catalytic properties of the calpains. J Biol Chem 268, 25740-25747.

Cordova, N.J., Ermentrout, B., and Oster, G.F. (1992). Dynamics of single-motor molecules: the thermal ratchet model. Proc Natl Acad Sci U S A 89, 339-343.

Cornillon, S., Gebbie, L., Benghezal, M., Nair, P., Keller, S., Wehrle-Haller, B., Charette, S.J., Bruckert, F., Letourneur, F., and Cosson, P. (2006). An adhesion molecule in free-living Dictyostelium amoebae with integrin beta features. Embo Rep 7, 617-621.

Correas, I., Leto, T.L., Speicher, D.W., and Marchesi, V.T. (1986). Identification of the functional site of erythrocyte protein 4.1 involved in spectrin-actin associations. J Biol Chem 261, 3310-3315.

Cosson, P., and **Soldati**, T. (2008). Eat, kill or die: when amoeba meets bacteria. Curr Opin Microbiol 11, 271-276.

Cramer, E.B., and **Gallin**, J.I. (1979). Localization of submembranous cations to the leading end of human neutrophils during chemotaxis. J Cell Biol 82, 369-379.

Dasilva, F.M., Massartleen, A.M., and Burvenich, C. (1994). Development and Maturation of Neutrophils. Vet Quart 16, 220-225.

Davies, E.V., and **Hallett**, M.B. (1995a). A novel pathway for Ca^{2+} signalling in neutrophils by immune complexes. Immunology 85, 538-543.

Davies, E.V., and **Hallett**, M.B. (1995b). A soluble cellular factor directly stimulates Ca^{2+} entry in neutrophils. Biochem Biophys Res Commun 206, 348-354.

Davies, E.V., and **Hallett**, M.B. (1998). High micromolar Ca^{2+} beneath the plasma membrane in stimulated neutrophils. Biochem Biophys Res Commun 248, 679-683.

Demaurex, N., Monod, A., Lew, D.P., and Krause, K.H. (1994). Characterization of receptor-mediated and store-regulated Ca^{2+} influx in human neutrophils. Biochem J 297 (Pt 3), 595-601.

Demaurex, N., and **Nunes**, P. (2016). The role of STIM and ORAI proteins in phagocytic immune cells. American journal of physiology Cell physiology 310, C496-508.

Demaurex, N., Schlegel, W., Varnai, P., Mayr, G., Lew, D.P., and Krause, K.H. (1992). Regulation of Ca^{2+} Influx in Myeloid Cells - Role of Plasma-Membrane Potential, Inositol Phosphates, Cytosolic Free [Ca^{2+}], and Filling State of Intracellular Ca^{2+} Stores. J Clin Invest 90, 830-839.

Desowitz, R.S. (1988). Thorn In The Starfish: Immune System and How It Works, Penguin Books Canada. Chapter 3, p. 4.

Dewitt, S., Francis, R.J., and Hallett, M.B. (2013). Ca^{2+} and calpain control membrane expansion during the rapid cell spreading of neutrophils. J Cell Sci 126, 4627-4635.

Dewitt, S., and **Hallett**, M. (2007). Leukocyte membrane "expansion": a central mechanism for leukocyte extravasation. J Leukoc Biol 81, 1160-1164.

Dewitt, S., and **Hallett**, M.B. (2002). Cytosolic free Ca^{2+} changes and calpain activation are required for beta integrin-accelerated phagocytosis by human neutrophils. J Cell Biol 159, 181-189.

Dewitt, S., Tian, W. and Hallett, M. (2006). Localised PtdIns(3,4,5)P-3 or Ptdns(3,4)P-2 at the phagocytic cup is required for both phagosome closure and Ca^{2+} signalling in HL60 neutrophils. J Cell Sci 119, 443-451.

Di, A., Kiya, T., Gong, H., Gao, X., and Malik, A.B. (2017). Role of the phagosomal redox-sensitive TRP channel TRPM2 in regulating bactericidal activity of macrophages. J Cell Sci 130, 735-744.

Ding, Z.M., Babensee, J.E., Simon, S.I., Lu, H.F., Perrard, J.L., Bullard, D.C., Dai, X.Y., Dustin, M.L., Smith, W.C., and Ballantyne, C.M. (1999). Relative contribution of LFA-1 and Mac-1 to neutrophil adhesion and migration. Circulation 100, 333-333.

Du, J., Xie, J., and **Yue**, L. (2009). Intracellular calcium activates TRPM2 and its alternative spliced isoforms. Proc Natl Acad Sci U S A 106, 7239-7244.

Dustin, M.L., Olszowy, M.W., Holdorf, A.D., Li, J., Bromley, S., Desai, N., Widder, P., Rosenberger, F., van der Merwe, P.A., Allen, P.M., et al. (1998). A novel adaptor protein orchestrates receptor patterning and cytoskeletal polarity in T-cell contacts. Cell 94, 667-677.

duVerle, D.A., Ono, Y., Sorimachi, H. and Mamitsuka, H. (2011). Calpain cleavage prediction using multiple kernel learning. PLOS ONE, 6 e19035.

Dwir, O., Kansas, G.S., and Alon, R. (2001). Cytoplasmic anchorage of L-selectin controls leukocyte capture and rolling by increasing the mechanical stability of the selectin tether. J Cell Biol 155, 145-156.

Ellson, C., Anderson, K., Morgan, G., Chilvers, E., Lipp, P., Stephens, L. and Hawkins, P. (2001). Phosphatidylinositol 3-phosphate is generated in phagosomal membranes. Curr Biol 11, 201-213.

Elumalai, G.L. (2012). Cytosolic signalling and behaviour of oral neutrophils “Search for biochemical memory”. PhD Thesis, Cardiff University.

Edwards, S.W., and **Hallett**, M.B. (1997). Seeing the wood for the trees: The forgotten role of neutrophils in rheumatoid arthritis. Immunol Today 18, 320-324.

Eggleton, P., Wang, L., Penhallow, J., Crawford, N., and Brown, K.A. (1995). Differences in Oxidative Response of Subpopulations of Neutrophils from Healthy-Subjects and Patients with Rheumatoid-Arthritis. Ann Rheum Dis 54, 916-923.

Ehrlich, P.L.E. (1898) Die Anaemie. Wein. Kessinger Publishing Company.

Elling, R., Keller, B., Weidinger, C., Haffner, M., Deshmukh, S.D., Zee, I., Speckmann, C., Ehl, S., Schwarz, K., Feske, S., et al. (2016). Preserved effector functions of human ORAI1- and STIM1-deficient neutrophils. The Journal of allergy and clinical immunology 137, 1587-1591 e1587.

Erlandsen, S.L., Hasslen, S.R. and Nelson, R.D. (1993). Detection and spatial distribution of the β_2 integrin (Mac-1) and L-selectin (LECAM-1) adherence receptors on human neutrophils by high-resolution field emission SEM. J Histochem Cytochem 41, 327-333.

Evans, E., Leung, A., and Zhelev, D. (1993). Synchrony of cell spreading and contraction force as phagocytes engulf large pathogens. J Cell Biol 122, 1295-1300.

Favre, C.J., Jerstrom, P., Foti, M., Stendhal, O., Huggler, E., Lew, D.P., and Krause, K.H. (1996a). Organization of Ca^{2+} stores in myeloid cells: association of SERCA2b and the type-1 inositol-1,4,5-trisphosphate receptor. Biochem J 316 (Pt 1), 137-142.

Favre, C.J., Nusse, O., Lew, D.P., and Krause, K.H. (1996b). Store-operated Ca^{2+} influx: what is the message from the stores to the membrane? J Lab Clin Med 128, 19-26.

Fehon, R.G., McClatchey, A.I and Bretscher, A. (2010). Organising the cell cortex: the role of ERM proteins. Nat Rev Mol Cell Biol 11, 276-287.

Feske, S. (2007). Calcium signalling in lymphocyte activation and disease. Nat Rev Immunol 7, 690-702.

Fievet, B. T., Gautreau, A., Roy, C., Del Maestro, L., Mangeat, P., Louvard, D. and Arpin, M. (2004). Phosphoinositide binding and phosphorylation act sequentially in the activation mechanism of ezrin. J. Cell Biol. 164, 653- 659.

Fossati, G., Bucknall, R.C., and Edwards, S.W. (2001). Fc gamma receptors in autoimmune diseases. Eur J Clin Invest 31, 821-831.

Fossati, G., Bucknall, R.C., and Edwards, S.W. (2002). Insoluble and soluble immune complexes activate neutrophils by distinct activation mechanisms: changes in functional responses induced by priming with cytokines. Ann Rheum Dis 61, 13-19.

Fossati, G., Moulding, D.A., Spiller, D.G., Moots, R.J., White, M.R.H., and Edwards, S.W. (2003). The mitochondrial network of human neutrophils: Role in chemotaxis, phagocytosis, respiratory burst activation, and commitment to apoptosis. J Immunol 170, 1964-1972.

Franco, S.J., and **Huttenlocher**, A. (2005). Regulating cell migration: calpains make the cut. J Cell Sci 118, 3829-3838.

Fritzche, M., Thorogate, R. and Charras, G. (2014). Quantitative analysis of ezrin turnover dynamics in the actin cortex. Biophys J 106, 343-353.

Fuchs, T.A., Abed, U., Goosmann, C., Hurwitz, R., Schulze, I., Wahn, V., Weinrauch, Y., Brinkmann, V., and Zychlinsky, A. (2007). Novel cell death program leads to neutrophil extracellular traps. J Cell Biol 176, 231-241.

Futosi, K., Fodor, S., and Mocsai, A. (2013). Neutrophil cell surface receptors and their intracellular signal transduction pathways. Int Immunopharmacol 17, 638-650.

Futosi, K., Fodor, S., and Mocsai, A. (2013). Reprint of Neutrophil cell surface receptors and their intracellular signal transduction pathways. Int Immunopharmacol 17, 1185-1197.

Gagnon, E., Duclos, S., Rondeau, C., Chevet, E., Cameron, P.H., Steele-Mortimer, O., Paiement, J., Bergeron, J.J.M., and Desjardins, M. (2002). Endoplasmic reticulum-mediated phagocytosis is a mechanism of entry into macrophages. Cell 110, 119-131.

Gary, R., and **Bretscher**, A. (1993). Heterotypic and homotypic associations between ezrin and moesin, two putative membrane-cytoskeletal linking proteins. Proc Natl Acad Sci U S A 90, 10846-10850.

Gary, R., and **Bretscher**, A. (1995). Ezrin self-association involves binding of an N-terminal domain to a normally masked C-terminal domain that includes the F-actin binding site. Mol Biol Cell 6, 1061-1075.

Gautreau, A., Louvard, D., and Arpin, M. (2000). Morphogenic effects of ezrin require a phosphorylation-induced transition from oligomers to monomers at the plasma membrane. J Cell Biol 150, 193-203.

Gautreau, A., Louvard, D., and Arpin, M. (2002). ERM proteins and NF2 tumor suppressor: the Yin and Yang of cortical actin organization and cell growth signaling. Curr Opin Cell Biol 14, 104-109.

Gee, K.R., Brown, K.A., Chen, W.N., Bishop-Stewart, J., Gray, D. and Johnson, I. (2000). Chemical and physiological characterization of fluo-4 Ca^{2+}-indicator dyes. Cell Calcium 27(2), 97-106.

Gerard, C. and **Gerard**, N.P. (1994) C5a and its receptor. Ann Rev Immunol 12: 775-888.

Gil-Parrado, S., Popp, O., Knoch, T.A., Zahler, S., Bestvater, F., Felgentrager, M., Holloschi, A., Fernandez-Montalvan, A., Auerswald, E.A., Fritz, H., et al. (2003). Subcellular localization and in vivo subunit interactions of ubiquitous mu-calpain. J Biol Chem 278, 16336-16346.

Goll, D.E., Thompson, V.F., Li, H., Wei, W. and Cong, J. (2003) The calpain system. Physiol Rev, 83, 731-801.

Gordon, S.M. (2008). Elie Metchnikoff: Father of natural immunity. Eur J Immunol 38, 3257-3264.

Gould, K.L., Bretscher, A., Esch, F.S., and Hunter, T. (1989). cDNA cloning and sequencing of the protein-tyrosine kinase substrate, ezrin, reveals homology to band 4.1. Embo J 8, 4133-4142.

Grune, T., Reinheckel, T., North, J. A., Li, R., Bescos, P. B., Shringarpure, R. and Davies, K. J. (2002). Ezrin turnover and cell shape changes catalyzed by proteasome in oxidatively stressed cells. FASEB J. 16, 1602-1610.

Guroff, G. (1964). A Neutral, Calcium-Activated Proteinase from the Soluble Fraction of Rat Brain. J Biol Chem 239, 149-155.

Guttmann, R.P., Elce, J.S., Bell, P.D., Isbell, J.C., and Johnson, G.V. (1997). Oxidation inhibits substrate proteolysis by calpain I but not autolysis. J Biol Chem 272, 2005-2012.

Hallett, M.B. (1989) The Neutrophil: cellular biochemistry and physiology / editor, Maurice B. Hallett. Boca Raton, Fla.: CRC Press, c1989.

Hallett, M.B. (1989). The Unpredictability of Cellular Behaviour - Trivial or of Fundamental Importance to Cell Biology. Perspect Biol Med 33, 110-119.

Hallett, M.B., and **Campbell**, A.K. (1983). Two distinct mechanisms for stimulation of oxygen-radical production by polymorphonuclear leucocytes. Biochem J 216, 459-465.

Hallett, M.B., and **Campbell**, A.K. (1984). Is intracellular Ca^{2+} the trigger for oxygen radical production by polymorphonuclear leucocytes? Cell Calcium 5, 1-19.

Hallett, M.B., and **Dewitt**, S. (2007). Ironing out the wrinkles of neutrophil phagocytosis. Trends Cell Biol 17, 209-214.

Hallett, M.B., and **Lloyds**, D. (1995). Neutrophil Priming - the Cellular Signals That Say Amber but Not Green. Immunol Today 16, 264-268.

Hallett, M.B. and **Lloyds**, D. (1997). Molecular and Ionic Signalling of Neutrophils. Springer-Verlag, Heidelberg & Chapman & Hall, New York, Landes Bioscience Publications, Austin.

Hallett, M.B., von Ruhland, C.J., and Dewitt, S. (2008). Chemotaxis and the cell surface-area problem. Nature reviews Molecular cell biology 9, 662; author reply 662.

Hamada, K., Shimizu, T., Matsui, T., Tsukita, S., and Hakoshima, T. (2000). Structural basis of the membrane-targeting and unmasking mechanisms of the radixin FERM domain. Embo J 19, 4449-4462.

Hamill, O.P., and **Martinac**, B. (2001). Molecular basis of mechanotransduction in living cells. Physiol Rev 81, 685-740.

Haslett, C. (1992). Resolution of Acute-Inflammation and the Role of Apoptosis in the Tissue Fate of Granulocytes. Clin Sci 83, 639-648.

Haslett, C. (1997). Granulocyte apoptosis and inflammatory disease. Brit Med Bull 53, 669-683.

Haslett, C. (1999). Granulocyte apoptosis and its role in the resolution and control of lung inflammation. Am J Resp Crit Care 160, S5-S11.

Hayashi, M., Suzuki, H., Kawashima, S., Saido, T.C. and Inomata, M. (1999). The Behavior of Calpain-Generated N- And C-Terminal Fragments of Talin in Integrin-Mediated Signaling Pathways. Arch Biochem Biophys 371(2), 133-141.

Hellberg, C., Molony, L., Zheng, L., and Andersson, T. (1996). Ca^{2+} signalling mechanisms of the beta 2 integrin on neutrophils: involvement of phospholipase C gamma 2 and Ins(1,4,5)P3. Biochem J 317 (Pt 2), 403-409.

Henderson, L.M., Chappell, J.B., and Jones, O.T. (1987). The superoxide-generating NADPH oxidase of human neutrophils is electrogenic and associated with an H^+ channel. Biochem J 246, 325-329.

Herant, M., Heinrich, V., and Dembo, M. (2005). Mechanics of neutrophil phagocytosis: behavior of the cortical tension. J Cell Sci 118, 1789-1797.

Herant, M., Heinrich, V., and Dembo, M. (2006). Mechanics of neutrophil phagocytosis: experiments and quantitative models. J Cell Sci 119, 1903-1913.

Herant, M., Marganski, W.A., and Dembo, M. (2003). The mechanics of neutrophils: synthetic modeling of three experiments. Biophys J 84, 3389-3413.

Hirsch, J.G. and Cohn, Z.A. (1960). Degranulation of polymorphonuclear leukocytes following phagocytosis of microorganisms. J Exp Med 112, 1005.

Hogan, P.G., Lewis, R.S. and Rao, A. (2010). Molecular basis of calcium signalling in lymphocytes: STIM1 and ORAI. Annu Rev Immunol 28, 491-533.

Hoffmann, K., Sperling, K., Olins, A.L. and Olins, D.E. (2007). The granulocyte nucleus and lamin B receptor: Avoiding the ovoid. Chromosoma 116(3):227–35.

Hoffstein, S.T. (1979). Ultrastructural demonstration of calcium loss from local regions of the plasma membrane of surface-stimulated human granulocytes. J Immunol 123, 1395-1402.

Hogg, J.C. (1987). Neutrophil kinetics and lung injury. Physiol Rev 67, 1249-1295.

Horowitz, L.F., Hirdes, W., Suh, B.C., Higemann, D.W., Mackie, K. and Hille, B. (2005). Phospholipase C in living cells: activation, inhibition, Ca^{2+} requirement, and regulation of M current. J Gen Physiol 126(3), 243-262.

Hosfield, C.M., Elce, J.S., Davies, P.L., and Jia, Z. (1999a). Crystal structure of calpain reveals the structural basis for Ca^{2+}-dependent protease activity and a novel mode of enzyme activation. Embo J 18, 6880-6889.

Hosfield, C.M., Ye, Q., Arthur, J.S., Hegadorn, C., Croall, D.E., Elce, J.S., and Jia, Z. (1999b). Crystallization and X-ray crystallographic analysis of m-calpain, a Ca^{2+}-dependent protease. Acta crystallographica Section D, Biological crystallography 55, 1484-1486.

Hughes, V., Humphreys, J.M., and Edwards, S.W. (1987). Protein-Synthesis Is Activated in Primed Neutrophils - a Possible Role in Inflammation. Bioscience Rep 7, 881-890.

Humphreys, J.M., Hughes, V., and Edwards, S.W. (1989). Stimulation of Protein-Synthesis in Human-Neutrophils by Gamma-Interferon. Biochem Pharmacol 38, 1241-1246.

Hynes, R.O. (1992). Integrins – Versatility, modulation, and signalling in cell adhesion. Cell 69, 11-25.

Imajoh, S., Aoki, K., Ohno, S., Emori, Y., Kawasaki, H., Sugihara, H., and Suzuki, K. (1988). Molecular cloning of the cDNA for the large subunit of the high-Ca^{2+}-requiring form of human Ca^{2+}-activated neutral protease. Biochemistry-Us 27, 8122-8128.

Itagaki, K., Kannan, K.B., Livingston, D.H., Deitch, E.A., Fekete, Z., and Hauser, C.J. (2002). Store-operated calcium entry in human neutrophils reflects multiple contributions from independently regulated pathways. J Immunol 168, 4063-4069.

Ivetic, A., Deka, J., Ridley, A., and Ager, A. (2002). The cytoplasmic tail of L-selectin interacts with members of the Ezrin-Radixin-Moesin (ERM) family of proteins: cell activation-dependent binding of Moesin but not Ezrin. J Biol Chem 277, 2321-2329.

Ivetic, A. and Ridley, A. J. (2004). Ezrin/radixin/moesin proteins and Rho GTPase signalling in leucocytes. Immunology 112, 165-176.

Jaconi, M.E., Theler, J.M., Schlegel, W., Appel, R.D., Wright, S.D., and Lew, P.D. (1991). Multiple elevations of cytosolic-free Ca^{2+} in human neutrophils: initiation by adherence receptors of the integrin family. J Cell Biol 112, 1249-1257.

Jaiswal, J.K. (2001). Calcium - how and why? J Bioscience 26, 357-363.

Jakus, Z., Simon, E., Frommhold, D., Sperandio, M., and Mocsai, A. (2009). Critical role of phospholipase Cgamma2 in integrin and Fc receptor-mediated neutrophil functions and the effector phase of autoimmune arthritis. J Exp Med 206, 577-593.

Jilma, B., Hergovich, N., Homoncik, M., Jilma-Stohlawetz, P., Kreuzer, C., Eichler, H.G., Zellner, M., and Pugin, J. (2000). Granulocyte colony-stimulating factor (G-CSF)

downregulates its receptor (CD114) on neutrophils and induces gelatinase B release in humans. Brit J Haematol 111, 314-320.

Johnson, P. (1990). Calpains (intracellular calcium-activated cysteine proteinases): Structure-activity relationships and involvement in normal and abnormal cellular metabolism. International Journal of Biochemistry 22(8), 811-822.

Kansas, G.S., Ley, K., Munro, J.M., and Tedder, T.F. (1993). Regulation of leukocyte rolling and adhesion to high endothelial venules through the cytoplasmic domain of L-selectin. J Exp Med 177, 833-838.

Kannwar, V.S. and **Cairo**, M.S. (1993). Neonatal neutrophil maturation, kinetics, and function. In The neutrophil (ed. Abramson JS, Wheeler JG), pp. 1–16 Oxford University Press, New York.

Kay, A.B., Glass, E.J., and Salter, D.M. (1979). Leucoattractants Enhance Complement Receptors on Human Phagocytic-Cells. Clin Exp Immunol 38, 294-299.

Kay, B.A. (2016). Paul Ehrlich and the Early History of Granulocytes Microbiol Spectrum 4(4): pp. 1-13.

Kay, R.R., Langridge, P., Traynor, D., and Hoeller, O. (2008). Changing directions in the study of chemotaxis. Nature reviews Molecular cell biology 9, 455-463.

Khorchid, A., and **Ikura**, M. (2002). How calpain is activated by calcium. Nat Struct Biol 9, 239-241.

Kinosian, H.J., Newman, J., Lincoln, B., Selden, L.A., Gershman, L.C. and Estes, J.E. (1998). Ca^{2+} regulation of gelsolin activity: Binding and severing of F-actin. Biophys J 75, 3101-3109.

Klebanoff, S.J., Kettle, A.J., Rosen, H., Winterbourn, C.C., and Nauseef, W.M. (2013). Myeloperoxidase: a front-line defender against phagocytosed microorganisms. J Leukocyte Biol 93, 185-198.

Krause, K.H., Pittet, D., Volpe, P., Pozzan, T., Meldolesi, J., and Lew, D.P. (1989). Calciosome, a sarcoplasmic reticulum-like organelle involved in intracellular Ca^{2+}-handling by non-muscle cells: studies in human neutrophils and HL-60 cells. Cell Calcium 10, 351-361.

Kruskal, B.A., Shak, S., and Maxfield, F.R. (1986). Spreading of human neutrophils is immediately preceded by a large increase in cytoplasmic free calcium. Proc Natl Acad Sci U S A 83, 2919-2923.

Kulkarni, S., Sitaru, C., Jakus, Z., Anderson, K.E., Damoulakis, G., Davidson, K., Hirose, M., Juss, J., Oxley, D., Chessa, T.A., et al. (2011). PI3Kbeta plays a critical role in neutrophil activation by immune complexes. Sci Signal 4, ra23.

Larsen, F.L., and Vincenzi, F.F. (1979). Calcium-Transport across the Plasma-Membrane - Stimulation by Calmodulin. Science 204, 306-309.

Lawrence, M.B., and **Springer**, T.A. (1991). Leukocytes Roll on a Selectin at Physiological Flow-Rates - Distinction from and Prerequisite for Adhesion through Integrins. Cell 65, 859-873.

Lebart, M.C., and Benyamin, Y. (2006). Calpain involvement in the remodeling of cytoskeletal anchorage complexes. Febs J 273, 3415-3426.

Lee, W.L., Harrison, R.E., and Grinstein, S. (2003). Phagocytosis by neutrophils. Microbes Infect 5, 1299-1306.

Leitinger, B., McDowall, A., Stanley, P., and Hogg, N. (2000). The regulation of integrin function by Ca^{2+}. Biochim Biophys Acta 1498, 91-98.

Ley, K., Laudanna, C., Cybulsky, M.I., and Nourshargh, S. (2007). Getting to the site of inflammation: the leukocyte adhesion cascade updated. Nat Rev Immunol 7, 678-689.

Lewis, Bain & Bates. (2006). Dacie and Lewis Practical Haematology,

Churchill Livingstone Elsevier.

Liao, Y., Erxleben, C., Yildirim, E., Abramowitz, J., Armstrong, D.L., and Birnbaumer, L. (2007). Orai proteins interact with TRPC channels and confer responsiveness to store depletion. Proc Natl Acad Sci U S A 104, 4682-4687.

Lloyds, D., Brindle, N.P.J., and Hallett, M.B. (1995). Priming of Human Neutrophils by Tumor-Necrosis-Factor-Alpha and Substance-P Is Associated with Tyrosine Phosphorylation. Immunology 84, 220-226.

Lominadze, G., Powell, D.W., Luerman, G.C., Link, A.J., Ward, R.A., and McLeish, K.R. (2005). Proteomic analysis of human neutrophil granules. Mol Cell Proteomics 4, 1503-1521.

Lorani, D.E., Zimmerman, G.A., Mcintyre, T.M., and Prescott, S.M. (1995). Platelet-Activating-Factor Mediates Procoagulant Activity on the Surface of Endothelial-Cells by Promoting Leukocyte Adhesion. Semin Cell Biol 6, 295-303.

Luik, R.M., Wu, M.M., Buchanan, J. and Lewis, R.S. (2006). The elementary unit of store-operated Ca^{2+} entry: local activation of CRAC channels by STIM1 at ER-plasma membrane junctions. J Cell Biol 174(6), 815-825.

Macconi, D., Foppolo, M., Paris, S., Noris, M., Aiello, S., Remuzzi, G., and Remuzzi, A. (1995). Paf Mediates Neutrophil Adhesion to Thrombin or Tnf-Stimulated Endothelial-Cells under Shear-Stress. Am J Physiol-Cell Ph 269, C42-C47.

Mackay, D.J., Esch, F., Furthmayr, H., and Hall, A. (1997). Rho- and rac-dependent assembly of focal adhesion complexes and actin filaments in permeabilized fibroblasts: an essential role for ezrin/radixin/moesin proteins. J Cell Biol 138, 927-938.

Mak, T.W. and **Saunders**, M.E. (2006). The Immune Response. Basic and Clinical Principals. San Diego: Elsevier Academic Press. Cytokines and Cytokine Receptors; pp. 464–516.

Mancarella, S., Wang, Y. and Gill, D.L. (20011). Signal transduction: STIM1 senses both Ca^{2+} and heat. Nat Chem Biol 7, 344-345.

Mantovani, A., Cassatella, M.A., Costantini, C., and Jaillon, S. (2011). Neutrophils in the activation and regulation of innate and adaptive immunity. Nat Rev Immunol 11, 519-531.

Marion, S., Hoffmann, E., Holzer, D., Le Clainche, C. Martin, M. Sachse, M., Ganeva, I, Mangeat, P. and Griffiths, G. (2011). Ezrin promotes actin assembly at the phagosome membrane and regulates phago-lysosomal fusion. Traffic 12(4), 421-437.

Marks, P.W., and Maxfield, F.R. (1990a). Local and global changes in cytosolic free calcium in neutrophils during chemotaxis and phagocytosis. Cell Calcium 11, 181-190.

Marks, P.W., and Maxfield, F.R. (1990b). Transient increases in cytosolic free calcium appear to be required for the migration of adherent human neutrophils. J Cell Biol 110, 43-52.

Martin, M., Roy, C., Montcourrier, P., Sahuquet, A., and Mangeat, P. (1997). Three determinants in ezrin are responsible for cell extension activity. Mol Biol Cell 8, 1543-1557.

Matsui, T., Maeda, M., Doi, Y., Yonemura, S., Amano, M., Kaibuchi, K., Tsukita, S., and Tsukita, S. (1998). Rho-kinase phosphorylates COOH-terminal threonines of ezrin/radixin/moesin (ERM) proteins and regulates their head-to-tail association. J Cell Biol 140, 647-657.

McCachren, S.S., Haynes, B.F., and Niedel, J.E. (1990). Localization of Collagenase Messenger-Rna in Rheumatoid-Arthritis Synovium by Insitu Hybridization Histochemistry. J Clin Immunol 10, 19-27.

McEver, R.P. (1991). Selectins - Novel Receptors That Mediate Leukocyte Adhesion during Inflammation. Thromb Haemostasis 65, 223-228.

McNeil, P.L. (1981). Mechanisms of Nutritive Endocytosis .1. Phagocytic Versatility and Cellular Recognition in Chlorohydra Digestive Cells, a Scanning Electron-Microscope Study. J Cell Sci 49, 311-339.

McRobert, E.A., Young, A.N., and Bach, L.A. (2012). Advanced glycation end-products induce calpain-mediated degradation of ezrin. Febs J 279, 3240-3250.

Metchnikoff (1893). Leçon sur la pathologie comparée d'inflammation.

Ann I'lnstiture Pasteur, 7, 348-357.

Metchnikoff (1901). Lectures on the Comparative Physiology of

Inflammation, Kegan Paul: London.

Metchnikoff (1905). Immunity in Infectious Disease, Cambridge University:

London.

Michetti, M., Salamino, F., Minafra, R., Melloni, E., and Pontremoli, S. (1997). Calcium-binding properties of human erythrocyte calpain. Biochem J 325 (Pt 3), 721-726.

Mitchison, T. and Kirschner, M. (1988). Cytoskeletal dynamics and nerve growth. Neuron 1, 761-772.

Mocsai, A., Ruland, J., and Tybulewicz, V.L. (2010). The SYK tyrosine kinase: a crucial player in diverse biological functions. Nat Rev Immunol 10, 387-402.

Mocsai, A., Zhou, M., Meng, F., Tybulewicz, V.L., and Lowell, C.A. (2002). Syk is required for integrin signaling in neutrophils. Immunity 16, 547-558.

Monsel, A., Lécart, S., Roquilly, A., Broquet, A., Jacqueline, C., Mirault, T., Troude, T., Fontaine-Aupart, M. and Asehnoune, K. (2014). Analysis of Autofluorescence in Polymorphonuclear Neutrophils: A New Tool for Early Infection Diagnosis. PLOSONE 9, 1-10.

Montero, M., Lobaton, C.D., Gutierrez-Fernandez, S., Moreno, A., and Alvarez, J. (2004). Calcineurin-independent inhibition of mitochondrial Ca^{2+} uptake by cyclosporin A. Br J Pharmacol 141, 263-268.

Morales, F.C., Takahashi, Y., Kreimann, E.L. and Georgescu, M.M. (2004). Ezrin-radixin-moesin (ERM)-binding phosphoprotein 50 organises ERM proteins at the apical membrane of polarised epithelia. Proc Acad Sci (USA) 101, 17705-17710.

Morgan, B.P., van den Berg, C.W., Davies, E.V., Hallett, M.B., and Horejsi, V. (1993). Cross-linking of CD59 and of other glycosyl phosphatidylinositol-anchored molecules on neutrophils triggers cell activation via tyrosine kinase. Eur J Immunol 23, 2841-2850.

Murachi, T., Tanaka, K., Hatanaka, M., and Murakami, T. (1980). Intracellular Ca^{2+}-dependent protease (calpain) and its high-molecular-weight endogenous inhibitor (calpastatin). Adv Enzyme Regul 19, 407-424.

Murphy, G., and Nagase, H. (2008). Reappraising metalloproteinases in rheumatoid arthritis and osteoarthritis: destruction or repair? Nat Clin Pract Rheum 4, 128-135.

Murphy, P.M. (1994). The Molecular-Biology of Leukocyte Chemoattractant Receptors. Annu Rev Immunol 12, 593-633.

Nadel, J.A. (2000). Role of neutrophil elastase in hypersecretion during COPD exacerbations, and proposed therapies. Chest 117, 386s-389s.

Nakai, J., Ohkura, M., and Imoto, K. (2001). A high signal-to-noise Ca^{2+} probe composed of a single green fluorescent protein. Nature biotechnology 19, 137-141.

Nakamura, K., Fujita, A., Murata, T., Watanabe, G., Mori, C., Fujita, J., Watanabe, N., Ishizaki, T., Yoshida, O., and Narumiya, S. (1999). Rhophilin, a small GTPase Rho-binding protein, is abundantly expressed in the mouse testis and localized in the principal piece of the sperm tail. Febs Lett 445, 9-13.

Nathan, C. (2006). Neutrophils and immunity: challenges and opportunities. Nat Rev Immunol 6, 173-182.

Nunes, P., Cornut, D., Bochet, V., Hasler, U., Oh-Hora, M., Waldburger, J.M. and Demaurex, N. (2012). STIM1 jusxtaposes to ER phagosomes, generating Ca^{2+} hotspots that boost phagocytosis. Curr Biol 22(21), 1990-1997.

Ohno, S., Emori, Y., and Suzuki, K. (1986). Nucleotide sequence of a cDNA coding for the small subunit of human calcium-dependent protease. Nucleic Acids Res 14, 5559.

Ohtani, K., Sakamoto, H., Rutherford, T., Chen, Z., Kikuchi, A., Yamamoto, T., Satoh, K., and Naftolin, F. (2002). Ezrin, a membrane-cytoskeletal linking protein, is highly expressed in atypical endometrial hyperplasia and uterine endometrioid adenocarcinoma. Cancer Lett 179, 79-86.

Okuda, K., Sanghera, J.S., Pelech, S.L., Kanakura, Y., Hallek, M., Griffin, J.D., and Druker, B.J. (1992). Granulocyte-Macrophage Colony-Stimulating Factor, Interleukin-3, and Steel Factor Induce Rapid Tyrosine Phosphorylation of P42 and P44 Map Kinase. Blood 79, 2880-2887.

Olins, D.E., and **Olins**, A.L. (2005). Granulocyte heterochromatin: defining the epigenome. Bmc Cell Biol 6.

Omann, G.M., and Axelrod, D. (1996). Membrane-proximal calcium transients in stimulated neutrophils detected by total internal reflection fluorescence. Biophys J 71, 2885-2891.

Ono, Y., and **Sorimachi**, H. (2012). Calpains: an elaborate proteolytic system. Biochim Biophys Acta 1824, 224-236.

Otsuka, Y., and **Goll**, D.E. (1987). Purification of the Ca^{2+}-dependent proteinase inhibitor from bovine cardiac muscle and its interaction with the millimolar Ca^{2+}-dependent proteinase. J Biol Chem 262, 5839-5851.

Peskin, C.S., Odell, G.M., and Oster, G.F. (1993). Cellular motions and thermal fluctuations: the Brownian ratchet. Biophys J 65, 316-324.

Petrie, R.J., Doyle, A.D., and Yamada, K.M. (2009). Random versus directionally persistent cell migration. Nature reviews Molecular cell biology 10, 538-549.

Pettit, E.J., and **Hallett**, M.B. (1995). Early Ca^{2+} signalling events in neutrophils detected by rapid confocal laser scanning. Biochem J 310 (Pt 2), 445-448.

Pettit, E.J., and **Hallett**, M.B. (1996a). Localised and global cytosolic Ca^{2+} changes in neutrophils during engagement of Cd11b/CD18 integrin visualised using confocal laser scanning reconstruction. J Cell Sci 109 (Pt 7), 1689-1694.

Pettit, E.J., and **Hallett**, M.B. (1996b). Temporal and spatial resolution of Ca^{2+} release and influx in human neutrophils using a novel confocal laser scanning mode. Biochem Biophys Res Commun 229, 109-113.

Pettit, E.J., and **Hallett**, M.B. (1998a). Ca^{2+} signalling delays in neutrophils: Effects of prior exposure to platelet activating factor or formyl-met-leu-phe. Cell Signal 10, 49-53.

Pettit, E.J., and **Hallett**, M.B. (1998b). Release of 'caged' cytosolic Ca^{2+} triggers rapid spreading of human neutrophils adherent via integrin engagement. J Cell Sci 111, 2209-2215.

Pettit, E.J., and **Hallett**, M.B. (1998c). Two distinct Ca^{2+} storage and release sites in human neutrophils. J Leukocyte Biol 63, 225-232.

Pfaff, M., Du, X., and Ginsberg, M.H. (1999). Calpain cleavage of integrin beta cytoplasmic domains. Febs Lett 460, 17-22.

Pietrobon, D., Di Virgilio, F., and Pozzan, T. (1990). Structural and functional aspects of calcium homeostasis in eukaryotic cells. Eur J Biochem 193, 599-622.

Pietuch, A. and Janshoff, A. (2013). Mechanics of spreading cells probed by atomic force microscopy. Open Biol 3: 130084.

Pivot-Pajot, C., Chouinard, F.C., El Azreq, M.A., Harbour, D. and Bourgoin, S.G. (2010). Characterisation of degranulation and phagocytic capacity of human neutrophilic cellular model, PLB-985 cells. Immunobio 215, 38-52.

Plow, E.F., Haas, T.A., Zhang, L., Loftus, J., and Smith, J.W. (2000). Ligand binding to integrins. J Biol Chem 275, 21785-21788.

Polgar, L. (1989). Transition state stabilization and enzymic rate acceleration. Acta biochimica et biophysica Hungarica 24, 25-32.

Prakriya, M., Feske, S., Gwack, Y., Srikanth, S., Rao, A., and Hogan, P.G. (2006). Orai1 is an essential pore subunit of the CRAC channel. Nature 443, 230-233.

Prentice-Mott, H.V., Meroz, Y., Carlson, A., Levine, M.A., Davidson, M.W., Irimia, D., Charras, G.T., Mahadevan, L., and Shah, J.V. (2016). Directional memory arises from long-lived cytoskeletal asymmetries in polarized chemotactic cells. Proc Natl Acad Sci U S A 113, 1267-1272.

Pryzwansky, K.B., Macrae, E.K., Spitznagel, J.K., and Cooney, M.H. (1979). Early Degranulation of Human-Neutrophils - Immunocytochemical Studies of Surface and Intracellular Phagocytic Events. Cell 18, 1025-1033.

Rabinovitch, M. (1995). Professional and Nonprofessional Phagocytes - an Introduction. Trends Cell Biol 5, 85-87.

Raza, K., Scheel-Toellner, D., Lee, C.Y., Pilling, D., Curnow, S.J., Falciani, F., Trevino, V., Kumar, K., Assi, L.K., Lord, J.M., et al. (2006). Synovial fluid leukocyte apoptosis is inhibited in patients with very early rheumatoid arthritis. Arthritis Res Ther 8.

Reuter, H., and **Seitz**, N. (1968). Dependence of Calcium Efflux from Cardiac Muscle on Temperature and External Ion Composition. J Physiol-London 195, 451.

Roberts, G.M., Davies, E.V., Pettit, E.J., and Hallett, M.B. (1997). The timing and magnitude of Ca2+ signalling by CD32 depends on its redistribution on the cell surface. Exp Cell Res 230, 303-309.

Rooney, T.A., and **Thomas**, A.P. (1993). Intracellular calcium waves generated by Ins(1,4,5)P3-dependent mechanisms. Cell Calcium 14, 674-690.

Roos, J., DiGregorio, P.J., Yeromin, A.V., Ohlsen, K., Lioudyno, M., Zhang, S., Safrina, O., Kozak, J.A., Wagner, S.L., Cahalan, M.D., et al. (2005). STIM1, an essential and conserved component of store-operated Ca2+ channel function. J Cell Biol 169, 435-445.

Rosales, C., Jones, S.L., McCourt, D., and Brown, E.J. (1994). Bromophenacyl bromide binding to the actin-bundling protein l-plastin inhibits inositol trisphosphate-independent increase in Ca^{2+} in human neutrophils. Proc Natl Acad Sci U S A 91, 3534-3538.

Roy, C., Martin, M., and Mangeat, P. (1997). A dual involvement of the amino-terminal domain of ezrin in F- and G-actin binding. J Biol Chem 272, 20088-20095.

Ruppelt, A., Mosenden, R., Gronholm, M., Aandahl, E.M., Tobin, D., Carlson, C.R., Abrahamsen, H., Herberg, F.W., Carpen, O., and Tasken, K. (2007). Inhibition of T cell activation by cyclic adenosine 5'-monophosphate requires lipid raft targeting of protein kinase A type I by the A-kinase anchoring protein ezrin. J Immunol 179, 5159-5168.

Saez, M.E., Ramirez-Lorca, R., Moron, F.J., and Ruiz, A. (2006). The therapeutic potential of the calpain family: new aspects. Drug discovery today 11, 917-923.

Saotome, I., Curto, M., and McClatchey, A.I. (2004). Ezrin is essential for epithelial organization and villus morphogenesis in the developing intestine. Developmental cell 6, 855-864.

Saris, N.E.L., and **Carafoli**, E. (2005). A historical review of cellular calcium handling, with emphasis on mitochondria. Biochemistry-Moscow+ 70, 187-194.

Savill, J.S., Henson, P.M., and Haslett, C. (1989). Phagocytosis of Aged Human-Neutrophils by Macrophages Is Mediated by a Novel Charge-Sensitive Recognition Mechanism. J Clin Invest 84, 1518-1527.

Schaff, U.Y., Dixit, N., Procyk, E., Yamayoshi, I., Tse, T., and Simon, S.I. (2010). Orai1 regulates intracellular calcium, arrest, and shape polarization during neutrophil recruitment in shear flow. Blood 115, 657-666.

Schatzmann, H.J. (1966). Atp-Dependent Ca++-Extrusion from Human Red Cells. Experientia 22, 364-+.

Schmid-Schönbein, G.W., Usami, S., Skalak, R. and Chien, S. (1980). The interaction of leukocytes and erythrocytes in capillary and postcapillary vessels. Microvascular Research 19(1), pp. 45-70.

Segal, A.W. (1987). Absence of Both Cytochrome-B-245 Subunits from Neutrophils in X-Linked Chronic Granulomatous-Disease. Nature 326, 88-91.

Segal, A.W. (1996). The NADPH oxidase and chronic granulomatous disease. Mol Med Today 2, 129-135.

Segal, A.W., and **Jones**, O.T.G. (1978). Novel Cytochrome-B System in Phagocytic Vacuoles of Human Granulocytes. Nature 276, 515-517.

Serrador, J.M., Alonso-Lebrero, J.L., del Pozo, M.A., Furthmayr, H., Schwartz-Albiez, R., Calvo, J., Lozano, F., and Sanchez-Madrid, F. (1997). Moesin interacts with the cytoplasmic region of intercellular adhesion molecule-3 and is redistributed to the uropod of T lymphocytes during cell polarization. J Cell Biol 138, 1409-1423.

Shcherbina, A., Bretscher, A., Kenney, D.M., and Remold-O'Donnell, E. (1999). Moesin, the major ERM protein of lymphocytes and platelets, differs from ezrin in its insensitivity to calpain. Febs Lett 443, 31-36.

Shiozawa, S., Shiozawa, K., and Fujita, T. (1983). Morphologic Observations in the Early Phase of the Cartilage Pannus Junction - Light and Electron-Microscopic Studies of Active Cellular Pannus. Arthritis Rheum 26, 472-478.

Shiue, H., Musch, M. W., Wang, Y., Chang, E. B. and Turner, J. R. (2005). Akt2 phosphorylates ezrin to trigger NHE3 translocation and activation. J. Biol. Chem. 280, 1688-1695.

Shuster, C.B., and **Herman**, I.M. (1995). Indirect association of ezrin with F-actin: isoform specificity and calcium sensitivity. J Cell Biol 128, 837-848.

Smith, C.W., Marlin, S.D., Rothlein, R., Toman, C., and Anderson, D.C. (1989). Cooperative Interactions of Lfa-1 and Mac-1 with Intercellular-Adhesion Molecule-1 in Facilitating Adherence and Transendothelial Migration of Human-Neutrophils Invitro. J Clin Invest 83, 2008-2017.

Soboloff, J., Rothberg, B.S., Madesh, M., and Gill, D.L. (2012). STIM proteins: dynamic calcium signal transducers. Nature reviews Molecular cell biology 13, 549-565.

Sorimachi, H., Hata, S., and Ono, Y. (2011). Calpain chronicle--an enzyme family under multidisciplinary characterization. Proceedings of the Japan Academy Series B, Physical and biological sciences 87, 287-327.

Southwick, F.S., and **Stossel**, T.P. (1983). Contractile proteins in leukocyte function. Seminars in hematology 20, 305-321.

Squier, M.K., Miller, A.C., Malkinson, A.M., and Cohen, J.J. (1994). Calpain activation in apoptosis. J Cell Physiol 159, 229-237.

Steinckwich, N., Schenten, V., Melchior, C., Brechard, S., and Tschirhart, E.J. (2011). An essential role of STIM1, Orai1, and S100A8-A9 proteins for Ca^{2+} signaling and FcgammaR-mediated phagosomal oxidative activity. J Immunol 186, 2182-2191.

Stendahl, O., Krause, K.H., Krischer, J., Jerstrom, P., Theler, J.M., Clark, R.A., Carpentier, J.L., and Lew, D.P. (1994). Redistribution of intracellular Ca^{2+} stores during phagocytosis in human neutrophils. Science 265, 1439-1441.

Stewart, M., Roberts, T.M., Italiano, J.E., Jr., King, K.L., Hammel, R., Parathasathy, G., Bullock, T.L., McCoy, A.J., Kent, H., Haaf, A., et al. (1998). Amoeboid motility without actin: insights into the molecular mechanism of locomotion using the major sperm protein (MSP) of nematodes. Biol Bull 194, 342-343; discussion 343-344.

Stossel, T.P. (1989). From signal to pseudopod. How cells control cytoplasmic actin assembly. J Biol Chem 264, 18261-18264.

Summers, C., Rankin, S.M., Condliffe, A.M., Singh, N., Peters, A.M., and Chilvers, E.R. (2010). Neutrophil kinetics in health and disease. Trends Immunol 31, 318-324.

Sun, X.R., Badura, A., Pacheco, D.A., Lynch, L.A., Schneider, E.R., Taylor, M.P., Hogue, I.B., Enquist, L.W., Murthy, M., and Wang, S.S. (2013). Fast GCaMPs for improved tracking of neuronal activity. Nature communications 4, 2170.

Suzuki, J., Kanemaru, K., Ishii, K., Ohkura, M., Okubo, Y., and Iino, M. (2014). Imaging intraorganellar Ca^{2+} at subcellular resolution using CEPIA. Nature communications 5, 4153.

Suzuki, K., and **Sorimachi**, H. (1998). A novel aspect of calpain activation. Febs Lett 433, 1-4.

Takenawa, T., and **Miki**, H. (2001). WASP and WAVE family proteins: key molecules for rapid rearrangement of cortical actin filaments and cell movement. J Cell Sci 114, 1801-1809.

Tauber, A.I. (1991). The Immunological Self - a Centenary Perspective. Perspect Biol Med 35, 74-86.

Tauber, A.I. (2003). Metchnikoff and the phagocytosis theory. Nat Rev Mol Cell Bio 4, 897-901.

Thelen, M., Dewald, B., and Baggiolini, M. (1993). Neutrophil Signal-Transduction and Activation of the Respiratory Burst. Physiol Rev 73, 797-821.

Ting-Beall, H.P., Needham, D., and Hochmuth, R.M. (1993). Volume and osmotic properties of human neutrophils. Blood 81, 2774-2780.

Tohyama, Y. and Yamamura, H. (2006). Complement-mediated phagocytosis – The role of Syk. IUBMB Life 58(5-6), 304-308.

Tompa, P., Emori, Y., Sorimachi, H., Suzuki, K., and Friedrich, P. (2001). Domain III of calpain is a ca2+-regulated phospholipid-binding domain. Biochem Biophys Res Commun 280, 1333-1339.

Tran Quang, C., Gautreau, A., Arpin, M., and Treisman, R. (2000). Ezrin function is required for ROCK-mediated fibroblast transformation by the Net and Dbl oncogenes. Embo J 19, 4565-4576.

Tsein, R.Y. and **Poenie**, M. (1986). Fluorescence ratio imaging: a new window into intracellular ionic signalling. Trends Biochem Sci, 11,450-452.

van Spriel, A.B., Leusen, J.H.W., van Egmond, M., Dijkman, H.B.P.M., Assmann, K.J.M., Mayadas, T.N., and van de Winkel, J.G.J. (2001). Mac-1 (CD11b/CD18) is essential for Fc receptor-mediated neutrophil cytotoxicity and immunologic synapse formation. Blood 97, 2478-2486.

Vincenzi, F.F. (1979). Calmodulin in the Regulation of Intracellular Calcium. P W Pharmacol Soc 22, 289-294.

Viswanatha, R., Wayt, J., Ohouo, P.Y., Smolka, M.B., and Bretscher, A. (2013). Interactome analysis reveals ezrin can adopt multiple conformational states. J Biol Chem 288, 35437-35451.

Volpe, P., Krause, K.H., Hashimoto, S., Zorzato, F., Pozzan, T., Meldolesi, J., and Lew, D.P. (1988). "Calciosome," a cytoplasmic organelle: the inositol 1,4,5-trisphosphate-sensitive Ca^{2+} store of nonmuscle cells? Proc Natl Acad Sci U S A 85, 1091-1095.

Volpi, M., Naccache, P.H., and Shaafi, R.I. (1983). Calcium-Transport in inside-out Membrane-Vesicles Prepared from Rabbit Neutrophils by Phagocytosis. Fed Proc 42, 694-694.

von Tscharner, V., Deranleau, D.A., and Baggiolini, M. (1986). Calcium fluxes and calcium buffering in human neutrophils. J Biol Chem 261, 10163-10168.

Waller, A. (1846). Microscopic observation on the perforation of capaillaries by the corpuscles of blood and the origin of mucus and pus globules. The London, Edinburgh and Dublin Philosophical Magazine and Journal of Science, 29 pp 271-287.

Wang, Q., Shui, B., Kotlikoff, M.I., and Sondermann, H. (2008). Structural basis for calcium sensing by GCaMP2. Structure 16, 1817-1827.

Watson, R.W.G., Rotstein, O.D., Nathens, A.B., Parodo, J., and Marshall, J.C. (1997). Neutrophil apoptosis is modulated by endothelial transmigration and adhesion molecule engagement. J Immunol 158, 945-953.

Weinmann, P., Moura, R.A., Caetano-Lopes, J.R., Pereira, P.A., Canhao, H., Queiroz, M.V., and Fonseca, J.E. (2007). Delayed neutrophil apoptosis in very early rheumatoid arthritis patients is abrogated by methotrexate therapy. Clin Exp Rheumatol 25, 885-887.

Wendt, A., Thompson, V.F., and Goll, D.E. (2004). Interaction of calpastatin with calpain: a review. Biological chemistry 385, 465-472.

Wheeler, J.S.A. (1993). The neutrophils. IRL Press/Oxford University Press, Oxford.

Wingrave, J.M., Schaecher, K.E., Sribnick, E.A., Wilford, G.G., Ray, S.K., Hazen-Martin, D.J., Hogan, E.L., and Banik, N.L. (2003). Early induction of secondary injury factors

causing activation of calpain and mitochondria-mediated neuronal apoptosis following spinal cord injury in rats. J Neurosci Res 73, 95-104.

Wintrobe, M.W. (1967). A Hematological Odyssey 1926-1966. Johns Hopkins Med J 120, 287.

Wittkowski, H., Foell, D., af Klint, E., De Rycke, L., De Keyser, F., Frosch, M., Ulfgren, A.K., and Roth, J. (2007). Effects of intra-articular corticosteroids and anti-TNF therapy on neutrophil activation in rheumatoid arthritis. Ann Rheum Dis 66, 1020-1025.

Woodin, A.M., and **Wieneke**, A.A. (1963). The accumulation of calcium by the polymorphonuclear leucocyte treated with staphylococcal leucocidin and its significance in the extrusion of protein. Biochem J 87, 487-495.

Woodin, A.M., and **Wieneke**, A.A. (1964). The participation of calcium, adenosine triphosphate and adenosine triphosphatase in the extrusion of the granule proteins from the polymorphonuclear leucocyte. Biochem J 90, 498-509.

Wright, H.L., Moots, R.J., and Edwards, S.W. (2014). The multifactorial role of neutrophils in rheumatoid arthritis. Nat Rev Rheumatol 10, 593-601.

www.nobelprize.org. Retrieved 13 April 2017

Yao, X., Thibodeau, A., and Forte, J.G. (1993). Ezrin-calpain I interactions in gastric parietal cells. Am J Physiol 265, C36-46.

Yeung, T., Heit, B., Dubuisson, J.F., Fairn, G.D., Chiu, B., Inman, R., Kapus, A., Swanson, M. and Grinstein, S. (2009). Contribution of phosphatidylserine to membrane surface charge and protein targeting during phagosome maturation. J Cell Biol 185(5), 917.

Yonemura, S., Tsukita, S., and Tsukita, S. (1999). Direct involvement of ezrin/radixin/moesin (ERM)-binding membrane proteins in the organization of microvilli in collaboration with activated ERM proteins. J Cell Biol 145, 1497-1509.

Zarbock, A., and **Ley**, K. (2008). Mechanisms and consequences of neutrophil interaction with the endothelium. Am J Pathol 172, 1-7.

Zegkos, T., Kitas, G., and Dimitroulas, T. (2016). Cardiovascular risk in rheumatoid arthritis: assessment, management and next steps. Ther Adv Musculoskel 8, 86-101.

Zhang, H., Clemens, R.A., Liu, F., Hu, Y., Baba, Y., Theodore, P., Kurosaki, T., and Lowell, C.A. (2014). STIM1 calcium sensor is required for activation of the phagocyte oxidase during inflammation and host defense. Blood 123, 2238-2249.

Zhang, S.L., Yu, Y., Roos, J., Kozak, J.A., Deerinck, T.J., Ellisman, M.H., Stauderman, K.A., and Cahalan, M.D. (2005). STIM1 is a $Ca2^{+}$ sensor that activates CRAC channels and migrates from the Ca^{2+} store to the plasma membrane. Nature 437, 902-905.

Zhou, Y., Cai, X., Loktionova, N.A., Wang, X., Nwokonko, R.M., Wang, X., Wang, Y., Rothberg, B.S., Trebak, M., and Gill, D.L. (2016). The STIM1-binding site nexus remotely controls Orai1 channel gating. Nature communications 7, 13725.

Zhou, Y., Meraner, P., Kwon, H.T., Machnes, D., Oh-hora, M., Zimmer, J., Huang, Y., Stura, A., Rao, A., and Hogan, P.G. (2010). STIM1 gates the store-operated calcium channel ORAI1 in vitro. Nature structural & molecular biology 17, 112-116.

Zigmond, S.H. (1977). Ability of Polymorphonuclear Leukocytes to Orient in Gradients of Chemotactic Factors. J Cell Biol 75, 606-616.

Zuckerfranklin, D., and **Hirsch**, J.G. (1963). Degranulation of Polymorphonuclear Leukocytes Following Phagocytosis- an Electron Microscopic Study. Blood 22, 824.

Appendix I – Ezrin-GFPi sequencing results

FERM C-terminal PH-like domain

```
Query  1    KRRTDLWLGVDALGLNIYEKDDKF  24
            K+ TDLWLGVDALGLNIYEKDDK
Sbjct  211  KKGTDLWLGVDALGLNIYEKDDKL  234
```

Enhanced green fluorescent protein [synthetic construct]

```
Query  25   MVSKGEELFTGVVPILVELDGDVNGHKFSVSGEGEGDATYGKLTLKFICTTGKLPVPWPT  84
            MVSKGEELFTGVVPILVELDGDVNGHKFSVSGEGEGDATYGKLTLKFICTTGKLPVPWPT
Sbjct  1    MVSKGEELFTGVVPILVELDGDVNGHKFSVSGEGEGDATYGKLTLKFICTTGKLPVPWPT  60

Query  85   LVTTLTYGVQCFSRYPDHMKQHDFFKSAMPEGYVQERTIFFKDDGNYKTRAEVKFEGDTL  144
            LVTTLTYGVQCFSRYPDHMKQHDFFKSAMPEGYVQERTIFFKDDGNYKTRAEVKFEGDTL
Sbjct  61   LVTTLTYGVQCFSRYPDHMKQHDFFKSAMPEGYVQERTIFFKDDGNYKTRAEVKFEGDTL  120

Query  145  VNRIELKGIDFKEDGNILGHKLEYNYNSHNVYIMADKQKNGIKVNFKIRHNIEDGSVQLA  204
            VNRIELKGIDFKEDGNILGHKLEYNYNSHNVYIMADKQKNGIKVNFKIRHNIEDGSVQLA
Sbjct  121  VNRIELKGIDFKEDGNILGHKLEYNYNSHNVYIMADKQKNGIKVNFKIRHNIEDGSVQLA  180

Query  205  DHYQQNTPIGDGPVLLPDNHYLSTQSALSKDPNEKRDHMVLLEFVTAAGITLGMDELYKS  264
            DHYQQNTPIGDGPVLLPDNHYLSTQSALSKDPNEKRDHMVLLEFVTAAGITLGMDELYKS
Sbjct  181  DHYQQNTPIGDGPVLLPDNHYLSTQSALSKDPNEKRDHMVLLEFVTAAGITLGMDELYKS  240

Query  265  GLRS  268
            GLRS
```

FERM domain C-lobe/F3 of the ERM family

```
Query  254  ITLGMDEL----YKSGLRSTPKIGFPWSEIRNISFNDKKFVIKPIDKKAPDFVFYAPRLR  309
            + LG+D L    Y+   + TPKIGFPWSEIRNISFNDKKFVIKPIDKKAPDFVFYAPRLR
Sbjct  216  LWLGVDALGLNIYEKDDKLTPKIGFPWSEIRNISFNDKKFVIKPIDKKAPDFVFYAPRLR  275

Query  310  INKRILQLCMGNHELYMRRRKPDTIEVQQMKAQAREENYQNHLDRQQLQPNKKGRKPGKK  369
            INKRILQLCMGNHELYMRRRKPDTIEVQQMKAQAREE +Q  L+RQQL+  KK R+  ++
Sbjct  276  INKRILQLCMGNHELYMRRRKPDTIEVQQMKAQAREEKHQKQLERQQLETEKKRRETVER  335

Query  370  MKQ  372
              K+
Sbjct  336  EKE  338
```

Appendix I: Sequenced ezrin-GFPi

372 amino acids returned from Sanger sequencing results were entered as query in NCBI Protein Blast. Residues 4-24 align with FERM C-terminal PH-like domain (88% Identity, E-value 2.41e-03). Residues 31-252 align with GFP (E-value 3.72e-105). Residues 256-330 align with FERM domain C-lobe/F3 of the ERM family (76% Identity, E-value 4.72e-44).

Appendix II – Materials and Reagents

Reagent	Source
4x NuPAGE Novex LDS sample buffer	Invitrogen
7% NuPAGE® Tris-Acetate Gel	Life Technologies
Agar	Sigma-Aldrich, Poole, UK
Amaxa N ucleofector solution V Lonza	Cologne, Germany
Amersham™ Hybond™ P 0.45	GE Healthcare, 10600023
Ampicillin	Sigma-Aldrich, Poole, UK
Anti-mouse IgG-FITC conjugated antibody	Santa Cruz Biotechnology, inc. SC-2047
Anti-rabbit IgG peroxidase conjugated antibody	Santa Cruz Biotechnology, inc. SC-2004
Bovine Serum Album in (BSA)	Sigma-Aldrich, Poole, UK
$CaCl_2$	Sigma-Aldrich, Poole, UK
CellTraceTM Calcein Green, AM	Life Technologies
CEPIA2	Addgene: pCMV CEPIA2mt (Plasmid #58218)
CEPIA3	Addgene: pCMV CEPIA3mt (Plasmid #58219)
Collagen Microspheres	2BScientific, 516064
ECL developing film: Amersham Hyperfilm ECL	GE Healthcare Life Sciences, 28-9068-36
ECL detection reagent: Amersham ECL Western Blotting Detection Reagent	GE Healthcare Life Sciences, RPN2109
ECL developing film: Amersham Hyperfilm	GE Healthcare Life Sciences, 28-9068-36
ECL™ peroxidase labelled donkey anti-rabbit secondary antibody	GE healthcare
ECL Western Blotting Detection Reagent	GE Healthcare Life Sciences, RPN2109
Ezrin-mCherry	Addgene: mCherry-Ezrin-N-14 (Plasmid #55043)
Ezrin-mEmerald	Addgene: mEmerald-Ezrin-N-14 (Plasmid #54090)
Ezrin-GFPi	Gift from Sabrina Marion
Dextran (m ol. W t. 70,000)	Sigma-Aldrich, Poole, UK
DH5α cells	Gift from Prof. Jan Parys lab
Dimethyl sulphoxide (DMSO)	Sigma-Aldrich, Poole, UK
DMEM	
EDTA	Sigma-Aldrich, Poole, UK
EGTA	Sigma-Aldrich, Poole, UK
Ethanol	Fisher Scientific, Leicester, UK
Ethidium bromide	Sigma-Aldrich
Ezrin Polyclonal Antibody, Cy5 Conjugated	Bioss Antibody (bs-1343r-cy5)
Fetal Calf Serum (FCS)	Sigma-Aldrich, Poole, UK
FastDigest Eco32I (EcoRV)	Thermo Fisher Scientific, FD0303
FastDigest NotI	Thermo Fisher Scientific, FD0593

FastDigest HindIII	Thermo Fisher Scientific, FD0504
Fluo-4-AM	Invitrogen, Carlsbad, California, USA
fMLP	Sigma-Aldrich, Poole, UK
GeneElute™ PCR clean-up kit	Sigma-Aldrich, NA1020
GenElute™ Plasmid Miniprep Kit	Sigma-Aldrich, PLN350
Glycerol	Sigma-Aldrich, Poole, UK
HeLa cells	Gift from Prof. Jan Parys lab
Heparin	C P Pharmaceuticals Ltd, Wrexham , UK
Hepes	Fisher Scientific, Leicester, UK
Horse Serum	Sigma-Aldrich, Poole, UK
Ionomycin	Calbiochem, Nottingham, UK
Isopropanol	Sigma-Aldrich, Poole, UK
Kanamycin	Sigma-Aldrich, Poole, UK
KCl	Sigma-Aldrich, Poole, UK
KH_2PO_4	Sigma-Aldrich, Poole, UK
mCherry-ezrin	mCherry-Ezrin-C-14 (Plasmid #55042)
Milk powder	Marvel
$MgCl_2$	Sigma-Aldrich, Poole, UK
$MgS0_4$	Sigma-Aldrich, Poole, UK
NaCl	Sigma-Aldrich, Poole, UK
NaOH	Sigma-Aldrich, Poole, UK
NuPAGE Antioxidant reagent	Invitrogen
NuPAGE Reducing Agent 10x	Invitrogen
NuPAGE® Tris-Acetate SDS running buffer 20x	Invitrogen
Na_2HP0_4	Sigma-Aldrich, Poole, UK
NaOH	Sigma-Aldrich, Poole, UK
OneShot®Top10 *E.coli*	Invitrogen, Paisly, UK
Paraformaldehyde	Sigma-Aldrich, Poole, UK
pcDNA3.1(-)	Gift from Prof. Jan Parys lab
Penicillin	Sigma-Aldrich, Poole, UK
PfuUltra HF DNA polymerase (2.5 U/ µl)	Agilent, 600380
Pierce™ BCA Protein Assay Kit	Life Technologies
Pierce™ Co-Immunoprecipitation Kit	ThermoFisher Scientific, 26149
PureLink® HiPure Plasmid Filter Maxiprep Kit	Invitrogen (Thermo Fisher Scientific), K210017
Primers	Integrated DNA Technologies (IDT), bespoke
Protease Inhibitor Cocktail	Sigma-Aldrich, Poole, UK
Qubit dsDNA BR Assay Kit®	Life Technologies, Q32853
Rabbit anti-ezrin polyclonal antibody	Cell Signalling, 3145
Rabbit anti-ezrin monoclonal [EP924Y] antibody	Abcam, ab75840
Rabbit anti-phosphorylated ERM family monoclonal antibody (41A3)	Cell Signalling, 3149
Rabbit anti-moesin polyclonal antibody	Cell Signalling, 3146

Rat anti-CD18 (Integrin β2 chain) monoclonal antibody	BD Biosciences Pharmingen, 01661D
RAW 264.7 cells	American Type Culture Collection
Streptomycin	Sigma-Aldrich, Poole, UK
SuperSignalTM West Dura Extended Duration Substrate	Life Technologies
T4 DNA Ligase (5 U/µL)	Thermo Fisher Scientific, EL0014
Thapsigargin	Sigma-Aldrich, Poole, UK
Triton-X100	Sigma-Aldrich, Poole, UK
Tween-20	Sigma-Aldrich, Poole, UK
X-tremeGENE™ HP DNA Transfection Reagent	Sigma-Aldrich, 06366546001
Zymosan A	Sigma-Aldrich, Poole, UK

Appendix III – Buffers

Buffer	Reagents
Balanced salt solution (BSS)	130 mM NaCl, 2.65 mM KCl, 8 mM $Na_2HPO_{4,}$ adjusted to pH 7.4
Cell growth media	DMEM, 10% FBS, 1% PenStrep
Dextran	6 g/100 mL BSS
Electroblotting buffer	25 mM Tris, 182 mM Glcine, 20% methanol. Cooled to -20°C prior to use.
Hepes Buffered Krebs (HBK)	120 mM NaCl, 4.8 mM KCl, 1.2 mM KH_2PO_4, 1.2 mM $MgSO_4$, 1.3 mM CaCl2, 25 mM Hepes pH 7.4 and 0.1% BSA, adjusted to pH 7.4 with NaOH stored at 4°C
Neutrophil lysis Buffer	50 mM Hepes pH 7.4, 150 mM NaCl, 10% glycerol, 1% Triton X100, 1.5 mM $MgCl_2$, 5 mM EGTA, 5 mM EDTA, 1 mM Na_3VO_4, 1.5 mM NaF, 0.1% SDS, 1:10 PIC
Running Buffer for SDS-PAGE	25 mL NuPAGE Tris Acetate SDS running buffer (20x), 475 mL ddH_2O (0.5 mL NuPAGE Antioxidant added to 200 mL of prepared running buffer loaded in upper chamber of gel tank)
Running buffer for agarose gel electrophoresis	1 xTAE buffer, plus ethidium bromide (1-2 %)

Appendix IV – Equipment

Specific equipment	Source
Amaxa nulceofector device	Lonza, Cologne, Germany
BMG FLUOstar OPTIMA	BMG Labtech
CLSM Confocal microscope SP5	Leica, Milton Keynes, UK
Eppendorf FemtoJet® pressure controller	Eppendorf, Hamburg, Germany
Eppendorf Injectman micromanipulator	Eppendorf, Hamburg, Germany
Micropipette Puller P2000	Sutter Instruments, Novato, California, USA
Micropipette borosilicate glass capillaries	Sutter Instruments, Novato, California, USA
NanoDrop™ Lite spectrophotometer	Thermo Scientific
Nexcelom Cellometer	Nexcelom Bioscience, MA, USA
Filters, dichroic mirrors	Omega Optical Inc F ilters,, Stanmore, UK
Single 488nm line laser	Laser Physics, Milton Green, UK

Appendix V - Software

Software	Source
AMNIS® IDEAS®	Merck, UK
AMNIS® INSPIRE®	Merck, UK
CLC Sequence Viewer	Qiagen, California, USA
Chromas version 2.9.2	Technelysium, Australia
Gif Animator (32-bit)	Alchemy Mindworks Inc., Ontario, Canada
GraphPad Prism 5 for Windows, version 5.00	San Diego California USA
HyperCam version 2.29.01	Hyperionics Technology, USA
ImageJ	NIH, Bethesda, Pennsylvania, USA
Leica Applications Suite Advanced Fluorescence Lite	Leica Microsystems
Microsoft Excel 2013	Microsoft, Redmond, Washington, USA
Microsoft Word 2013	Microsoft, Redmond, Washington, USA
Microsoft PowerPoint 2013	Microsoft, Redmond, Washington, USA
SnapGene® Viewer	GSL Biotech, Chicago, USA